Behavioural Model Analysis of Active Harmonic Load-pull Measurements

A thesis Submitted to Cardiff University
in candidature for the degree of

Doctor of Philosophy

By

Simon P Woodington, BEng.

Division of Electronic Engineering
School of Engineering
Cardiff University
United Kingdom

DECLARATION

This work has not previously been accepted in substance for any degree and is not concurrently submitted in candidature for any degree.

Signed …… (Candidate)

Date ……

STATEMENT 1

This thesis is being submitted in partial fulfilment of the requirements for the degree of PhD.

Signed …… (Candidate)

Date ……

STATEMENT 2

This thesis is the result of my own independent work/investigation, except where otherwise stated. Other sources are acknowledged by explicit references.

Signed …… (Candidate)

Date ……

STATEMENT 3

I hereby give consent for my thesis, if accepted, to be available for photocopying and for inter-library loan, and for the title and summary to be made available to outside organisations.

Signed …… (Candidate)

Date ……

STATEMENT 4

I hereby give consent for my thesis, if accepted, to be available for photocopying and for inter-library loans after expiry of a bar on access approved by the Graduate Development Committee.

Signed …… (Candidate)

Date ……

Abstract

In this thesis, an investigation of the use of the poly-harmonic distortion model and related techniques is conducted, and applied to model fundamental and harmonic load-pull. Contained within the thesis is a detailed review of the development of the poly-harmonic distortion model and related methods.

This thesis shows that although the poly-harmonic distortion model improves on the prediction of fundamental load-pull, over Hot-S-Parameters it still has a limited range of application. To address this observation, higher order models have been investigated along with Fourier methods allowing rapid extraction of the behavioral models. These methods allow conclusions to be drawn on the accuracy of the extracted models, by the direct observation of the magnitudes of the model coefficients.

The thesis is concluded with the presentation of the results from third party, using a model extracted using the methods discussed in this thesis. The Model is of a 0.5W GaAs pHEMT at 9 GHz and is used within the design of a Class-J MMIC amplifier.

Summary

- Investigated and discussed the limitations of the Poly-Harmonic-Distortion model

- Developed a Lookup table model of phase polynomials that can be used to describe fundamental load-pull Contours

- Developed a model of simultaneous fundamental and second harmonic load-pull

- Demonstrated Models during the design process of a Class-J MMIC amplifier

Acknowledgements

I would like to thank my supervisor Prof. Paul Tasker for his fully committed supervision during my research work. For which I am grateful. It has been a privilege also to be supported by Prof. Johannes Benedikit

I would also like to thank my industrial sponsor MIMIX Europe Ltd. (now MACOM), Belfast, Northern Ireland for their support of my research, in particular David Williams, Andrew Paterson. Also the Engineering and Physical Sciences Research Council (EPSRC), QinetiQ Ltd., Malvern UK, and Selex Galileo. must also be acknowledged for their contributions during the course of my research.

I would like to thank Peter Wright, Aamir Sheikh, Chris Roff, Randeep Saini and Dr Jonathan Lees for there continuing support during my PhD.

Finally I would like to give a special thank you to my family, and all of my friends outside of university.

List of publications

Supporting publications

Woodington, S.; Williams, T.; Qi, H.; Williams, D.; Pattison, L.; Patterson, A.; Lees, J.; Benedikt, J.; Tasker, P.J.; , "A novel measurement based method enabling rapid extraction of a RF Waveform Look-Up table based behavioural model," Microwave Symposium Digest, 2008 IEEE MTT-S International , vol., no., pp.1453-1456, 15-20 June 2008
doi: 10.1109/MWSYM.2008.4633053
URL: http://ieeexplore.ieee.org/stamp/stamp.jsp?tp=&arnumber=4633053&isnumber=4632906

Woodington, S.; Saini, R.; Williams, D.; Lees, J.; Benedikt, J.; Tasker, P.J.; , "Behavioural model analysis of active harmonic load-pull measurements," Microwave Symposium Digest (MTT), 2010 IEEE MTT-S International , vol., no., pp.1688-1691, 23-28 May 2010
doi: 10.1109/MWSYM.2010.5517261
URL: http://ieeexplore.ieee.org/stamp/stamp.jsp?tp=&arnumber=5517261&isnumber=5514662

J.Powell, M. Uren, T. Martin, S. Cripps, P. Tasker, J. Benedikt, S.Woodington, A. Mclachlan
“Investigation of high efficiency amplifiers at X-band using GaAs p-HEMT and GaN HFET technologies”
QinetiQ Ltd, Malvern, Cardiff University, Selex Galileo, Edinburgh,
Electro-Magnetic Remote Sensing (EMRS) Defence Technology Centre (DTC), 7th Annual Technical Conference,13th -14th July 2010,Conference Proceedings

J. Horn, S. Woodington, R. Saini, J. Benedikt, P.J. Tasker, D.E. Root, "Harmonic Load Tuning Predictions from X-parameters,"
Agilent Technologies, Santa Rosa, CA, USA; Cardiff University, Cardiff, UK
http://pasymposium.ucsd.edu/papers2009_2/2009_PA_Symp_Final_Program.htm

Saini, R.S.; Woodington, S.; Lees, J.; Benedikt, J.; Tasker, P.J.; , "An intelligence driven active loadpull system," *Microwave Measurements Conference (ARFTG),*

2010 75th ARFTG , vol., no., pp.1-4, 28-28 May 2010
doi: 10.1109/ARFTG.2010.5496327
URL: http://ieeexplore.ieee.org/stamp/stamp.jsp?tp=&arnumber=5496327&isnumber=5496310

Other contributions

Williams, T.; Mojon, O.; Woodington, S.; Lees, J.; Barciela, M.F.; Benedikt, J.; Tasker, P.J.; , "A robust approach for comparison and validation of large signal measurement systems," Microwave Symposium Digest, 2008 IEEE MTT-S International , vol., no., pp.257-260, 15-20 June 2008
doi: 10.1109/MWSYM.2008.4633152
URL: http://ieeexplore.ieee.org/stamp/stamp.jsp?tp=&arnumber=4633152&isnumber=4632906

Hashmi, M.S.; Clarke, A.L.; Woodington, S.P.; Lees, J.; Benedikt, J.; Tasker, P.J.; , "An Accurate Calibrate-Able Multiharmonic Active Load–Pull System Based on the Envelope Load–Pull Concept," *Microwave Theory and Techniques, IEEE Transactions on* , vol.58, no.3, pp.656-664, March 2010
doi: 10.1109/TMTT.2010.2040403
URL: http://ieeexplore.ieee.org/stamp/stamp.jsp?tp=&arnumber=5409539&isnumber=5429083

Hashmi, M.S.; Clarke, A.L.; Woodington, S.P.; Lees, J.; Benedikt, J.; Tasker, P.J.; , "Electronic multi-harmonic load-pull system for experimentally driven power amplifier design optimization," *Microwave Symposium Digest, 2009. MTT '09. IEEE MTT-S International* , vol., no., pp.1549-1552, 7-12 June 2009
doi: 10.1109/MWSYM.2009.5166005
URL: http://ieeexplore.ieee.org/stamp/stamp.jsp?tp=&arnumber=5166005&isnumber=5165586

Lees, J.; Williams, T.; Woodington, S.; McGovern, P.; Cripps, S.; Benedikt, J.; Tasker, P.; , "Demystifying Device related Memory Effects using Waveform Engineering and Envelope Domain Analysis," *Microwave Conference, 2008. EuMC 2008. 38th European* , vol., no., pp.753-756, 27-31 Oct. 2008
doi: 10.1109/EUMC.2008.4751562
URL: http://ieeexplore.ieee.org/stamp/stamp.jsp?tp=&arnumber=4751562&isnumber=4751336

Contents

	Title Page	1
	Declaration	2
	Abstract	3
	Summary	4
	Acknowledgements	5
	List of Publications	6
	Contents	8
	List of Abbreviations	12
1	**Chapter 1- Introduction**	14
1.1	Thesis Orientation	14
1.2	Transistor Characterization Methodologies for the design of power Amplifiers	17
1.3	Microwave Circuit design	18
1.4	Transistor Modeling Strategies	19
1.5	Thesis Objectives	24
1.6	Synopsis of Main Chapters	25
1.7	References	27
2	**Chapter 2 – Large-Signal S-Parameters to the Poly-**	31

Harmonic-Distortion model

2.1 Introduction 31

2.2 Extension of Scattering-parameter measurement and modeling techniques for use with devices operating in Large-Signal regimes 32

2.2.1 Advantages of S-parameters as a high frequency measurement technique 34

2.2.2 The problem with S-Parameters for measuring Large-Signal device operation 36

2.2.3 Improving the relevance of the measurement of “S22” 39

2.2.4 Development of Hot S-Parameters 46

2.3 Development of the Poly-Harmonic-Distortion-Model 50

2.3.1 Conversion Matrices and mixer theory 50

2.3.2 Investigations into linearized models of large-signal data as extensions to S-parameters 54

2.3.3 Phase Normalization and time reference adjustment 55

2.3.4 The Poly-Harmonic-Distortion Model 57

2.3.5 Current trends In Poly-Harmonic Distortion-modeling 63

2.4 Discussion 67

2.5 References 70

3 **Chapter 3 – Modeling Device behavior at a Fundamental frequency** 76

3.1 Introduction 76

3.2 Detailed study of Hot-S-Parameters and PHD models when used to model fundamental load-pull 76

3.3	Development of generic models of fundamental load-Pull	87
3.4	Measurement and extraction of Model	96
3.4.1	Measurement system	96
3.4.2	Practical Considerations	97
3.4.3	Measurement Results	99
3.4.4	Amplitude Dependence of coefficients within model	107
3.5	Discussion	110
3.6	References	111
4	**Chapter 4 – Multi-Harmonic Device models in the frequency domain**	113
4.1	Introduction	113
4.2	Models of individual harmonic terminations	114
4.3	Multiple Harmonic Interactions	131
4.4	Measurements and observations	133
4.4.1	Comparison with the Poly-Harmonic Distortion model	135
4.4.2	Verification and Validation of modelling Techniques	138
4.5	Discussion	140
4.6	References	140
5	**Chapter 5 – Design of a Class-J, X-Band Monolithic Power Amplifier**	142
5.1	Introduction	142
5.2	Integration of modeling frameworks into CAD environments	143
5.3	Design and fabrication of a Class J MMIC Amplifier	145

5.3.1	Measurement And Modeling of a class-J MMIC amplifier	146
5.3.2	Results from measurement of Fabricated Amplifier	149
5.4	Discussion	152
5.5	References	152
6	**Chapter 6 – Conclusions**	154
6.1	Discussion	154
6.2	Future work	156
6.3	Conclusion	157
6.4	References	157
A.1	**Appendix 1 Mathematical Reference**	159
A.2	**Appendix 2 Supporting Publications**	186

List of Abbreviations

GaN	Gallium Nitride
GaAs	Gallium Arsenide
HBT	Hetro-Junction Bipolar Transistor
HEMT	High Electron Mobility Transistor
VNA	Vector-Network-Analyzer
NVNA	Non-Linear-Vector-Network-Analyzer some work uses VNNA
VNNA	Vector-Non-Linear-Network-Analyzer see NVNA
LSNA	Large-Signal-Network-Analyser a type of NVNA Originally sold by Agilent Technologies
MTA	Microwave Transition Analyser
S-Parameter(s)	Scattering Parameter(s)
PHD model	Poly-Harmonic-Distortion model
X-Parameter(s)	a parameterization of the Poly-Harmonic-Distortion model Trademarked by Agilent Technologies
S-function(s)	a parameterization of the Poly-Harmonic-Distortion model
D.U.T.	Device-Under-Test
RF or R.F.	Radio Frequency
IP or I.P.	Intellectual Property

Small-Signal	Operation of a non-linear device in a state where its response can be considered entirely linear
Large-Signal	Operation of a non-linear device in a state where its response cannot be approximated as linear
MMIC	Monolithic-Microwave-Integrated-Circuit
CAD	Computer Aided Design (tools)
PDK	Process Design Kit
DRC	Design-Rule-Checker
AM-AM	Amplitude to Amplitude distortion
AM-PM	Amplitude to Phase Distortion
P, p	Used in most equations to refer to device under test port index
H, h	Used in most equations to refer to device under test harmonic index also used for the Hermation Conjugate
LUT	Look-Up-Table
DFT	Discrete-Fourier-Transform
FFT	Fast-Fourier-Transform
ALP	Active Load-pull

Chapter 1 – Introduction

1.1 Thesis Orientation

Radio Frequency (RF) communications have become the standard method for communicating voice and data information when physical wired connections are not desirable or possible. The advantages of modern RF communications networks are made possible thanks to the commercial availability of low cost mobile or cellular telephony equipment. The first hand-held cellular phone was demonstrated on April 3, 1973, by Martin Cooper, a Motorola researcher who first called his rival at Bell Labs using his new invention [1]. The popularity of these cellular networks has also been aided by the increasingly sophisticated portable small computing devices which utilize RF communications and are now almost ubiquitous in the modern home. Other applications of radio transmission have also grown including military and commercial radar, remote detection products and satellite communications.

The expansion in RF communications has been enabled by the development of affordable solid state semiconductor based transistor and integrated circuit technologies. The first transistor was demonstrated by John Bardeen, Walter Brattain working under William Shockley in 1948 [2] this work can also be partially

attributed to a patent by J. E. Lilienfeld in 1934 [3], since then the development and advancement of semiconductor growth and processing technologies has lead to the development of Integrated Circuits (ICs) [4] and the subset of ICs Monolithic Microwave Integrated Circuits (MMICs) for use at RF frequencies.

As the complexity of the RF circuits used to power these systems has increased, so the need for Computer Aided Design CAD packages has arisen to allow the complex products to be successfully designed in a timely fashion. The first freely available computer based circuit simulation tool, capable of simulating networks containing non-linear elements, was the SPICE circuit simulator an acronym for "**S**imulation **P**rogram with **I**ntegrated **C**ircuit **E**mphasis". Its first version was announced at the Sixteenth Midwest Symposium on Circuit Theory on April 12, 1973 [5]. SPICE itself has gone through many revisions and modifications since its first release and has been integrated into the commercial electronic CAD Tools for Integrated circuits like Cadence®.

The two most popular CAD tools for microwave engineers are Advanced Wave Research's "Microwave Office ^{TM}", and Agilent Technologies' "Advanced Design System ^{TM}". Such modern CAD tools provide the ability to rapidly design and simulate RF systems including the layout of the artwork used to manufacture MMIC cells and RF circuit boards with great success. However, the simulation tools have struggled to gain acceptance for use in accurately simulating RF active transistor devices operating under large signal conditions necessary for the design of Power Amplifiers (PAs). It should be noted that the author believes that this is not due to the availability of accurate modeling strategies but rather the ability to collect and

process the data necessary to successfully implement them which has lead to a widespread mistrust in their use among PA designers. This impasse, as stated in [6], has meant that complex high frequency non-linear measurement systems designed for measuring large-signal, high frequency power transistors have not disappeared even with the growth and availability of CAD tools aimed at designers of high-frequency and microwave systems.

Recently high frequency non-linear measurement systems have gained increased market interest with the release of a few key instruments. It remains to be seen whether they will gain popularity within the industry at large. As well as the availability of new instruments, the recent introduction of X-parameters[1] [7], which are a re-parameterization of the Poly-Harmonic-Distortion (PHD) model [8], along with specific packaged measurement routines have given further interest to the problems associated with the handling and usefulness of data collected by Non-Linear-Vector-Network-Analysers (NVNA) and load-pull systems. With these advances it is hoped that the collection of suitable datasets and their conversion into functional parameterized data blocks for use in simulation packages suitable for the design of large signal power amplifiers will become the default design flow.

In this thesis the author has set out to further investigate modelling approaches related to the PHD model and the PHD model itself to see if there is a modelling structure and a measurement method that is best suited to data produced by NVNA systems augmented by active load-pull. Such a measurement system is available at the Centre for High Frequency Engineering in Cardiff University. The following

[1] X-Parameters are a registered trade mark of Agilent Technologies Inc.

section discusses current methods for the characterization of high frequency devices for the design of Power Amplifiers.

1.2 Transistor Characterization Methodologies for the design of power amplifiers

Present methodologies for characterization of high frequency transistors include scalar power measurements using Power Meters or measurements with Spectrum Analyzers which provide information about power, oscillations and spurious signals. Vector Network Analyzers are also used, providing measurement of s-parameters, input reflection coefficient and complex transmission gain; allowing the calculation of Amplitude Modulation to Amplitude Modulation (AM-AM) and Amplitude Modulation to Phase Modulation (AM-PM). Often, Vector Network Analyzer and/or scalar power measurements are combined with passive impedance tuners allowing source-pull and load-pull measurements to be performed.

Load-Pull measurements started as a technique to investigate oscillators. The frequency of oscillation could be “pulled” by systematically altering the terminating load at the oscillator’s output [6]. These techniques were later found to be useful when measuring the performance of active devices driven under large signal conditions.

Load-pull systems are generally used to measure performance at all relevant and safe impedances that can be reached by the particular tuning mechanism. The

resulting design data is usually plotted as contours against impedance or reflection coefficient or against swept power for each impedance point, usually high-lighting an optimized set of conditions for an amplifier designer to use.

1.3 Microwave circuit design

Microwave circuit design is a challenging process and may contain multiple stages. For Amplifier design these depend on the size of devices to be used, the availability of samples or accurate reliable models. Two main distinctions however can be drawn; these are between designs of Monolithic-Microwave-Integrated-Circuits (MMIC) and designs based on discrete packaged devices at High Power Levels.

Designers of MMICs tend to more heavily rely on model and CAD driven design flows, due to the availability of commercial Process Design Kits PDK's, which contain models and layouts of all circuit elements and structures available in the given semi conductor manufacturing process along with the rules governing their layout through "Design Rule Checking" or (DRC).

The quality of commercial PDK's has become more important with the growth in foundry-less MMIC design business model via foundries selling space on wafer runs. In this case the designers work more independently of the foundry, which may not be located on the same site or within the same company.

Although MMIC designers rely heavily on CAD tools during the design process designs may still be conducted over multiple wafer fabrication iterations with space

allocated on wafers for development of designs not just raw production. This is often in addition to the foundries own Process Control Monitoring PCM sites PCMs sites give useful information about variability of process and opportunity for measurements to bench-mark or create models, or develop new techniques and analyses.

Design of High-Power Amplifiers however has a lower level of integration with CAD, the CAD tools being mainly used to layout physical structure and design matching networks that are based on impedance gained from load-pull measurements and reference designs provided by the device manufactures it is less common to use a commercially available Non-Linear model.

1.4 Transistor modeling Strategies

Transistor modeling strategies can be divided into categories. The first being physics based models, where the transistor is considered from its physical structure and the physical equations that describe its operation. These are mostly used by semi-conductor foundries during technology development and best describe unit cells. They tend to be too complex for use in CAD circuit design where structures containing multiples of unit cells are involved.

The second being analytical behavioral models of which there are many different varieties; common techniques rely on Direct Current (DC) measurements or DC-IV measurements of transistors which are fitted to generic functions capable of

describing the behavior of the measurements and or the device type and structure, then various s-parameter measurements are conducted to extract frequency dependent parasitic elements of the device being modeled. Figure 1 shows the construction of a very simple and approximate transistor model in ADS that has been scaled to the DC characteristics of a 4x75µm Gallium Arsenide (GaAs) High Electron Mobility Transistor (HEMT), which has been used in the simulations throughout the rest of the thesis.

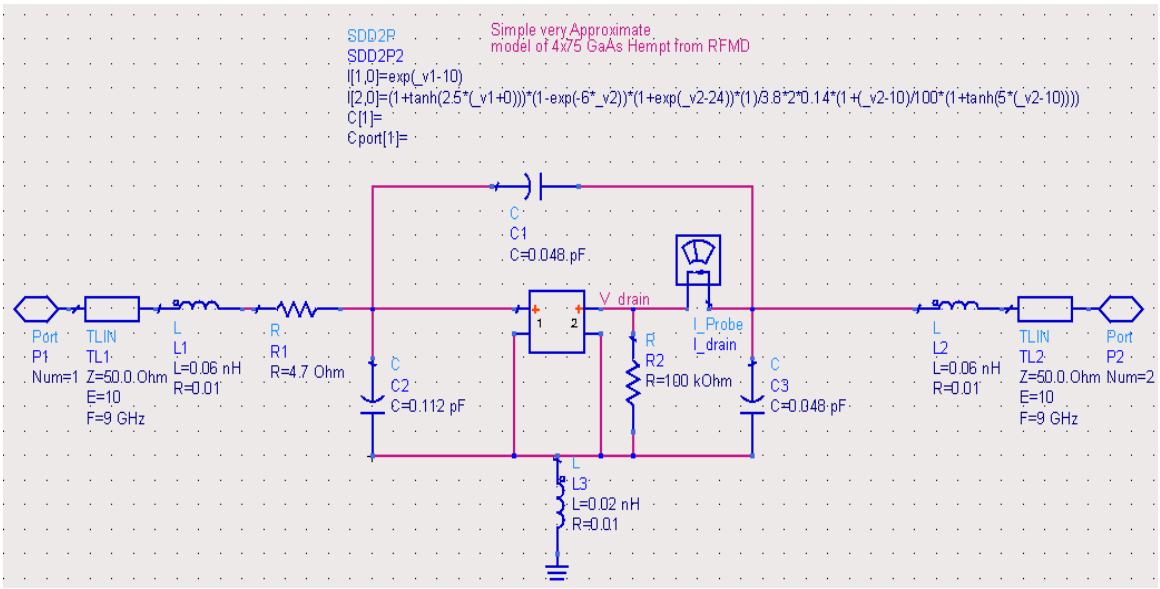

Figure (1)
Approximate Transistor model in ADS

All though the models discussed can be used and do provide good results, this thesis will focus on behavioural models that can be produced directly from measured data provided by NVNAs augmented with Active-Load-Pull systems. These being methods for Direct-Data Utilization [9] which require minimal processing or more involved techniques like the State Function Model [10] and Volterra techniques [11], and the Poly-Harmonic-Distortion Model [8].

The State-Function-Model or Current-State-Function-Model was developed from the Root Model, [12] a table based model which uses integration of Small Signal bias dependant s-parameters to approximate the Large-Signal state functions of the DUT. The State-Function-Model gives a reverse or inverse method to achieve the same result as the Root Model allowing the mapping between Large Signal RF Waveform Measurements and the Dynamic-IV's and DC-IV's of the DUT. Figure (2) shows the basic configuration of the state function or root model. The approaches to this type of model are outlined in [10] and can be implemented using time domain or frequency domain techniques [13].

The State-Function or Root Model concept has recently been used to generate Large Signal FET models [14] from multiple data sources including NVNA measurements, in conjunction with a Neural-Network extraction algorithm, to produce a model that is an advancement of the original state function model as it included extended structured Dynamic effects.

State Function Models have the advantage over all the other NVNA and load-pull based models. Because once extracted, they can be utilized in many simulation domains, they are not just limited to simulation of conditions similar to their extraction. For example a state function model could be used in a transient simulation, even when none of the original measurements were performed under transient conditions. This makes them very powerful, but these types of model require extensive data sets of widely varying conditions to be accurate and do not generally give a fast route for utilizing Large Signal Data in CAD software packages.

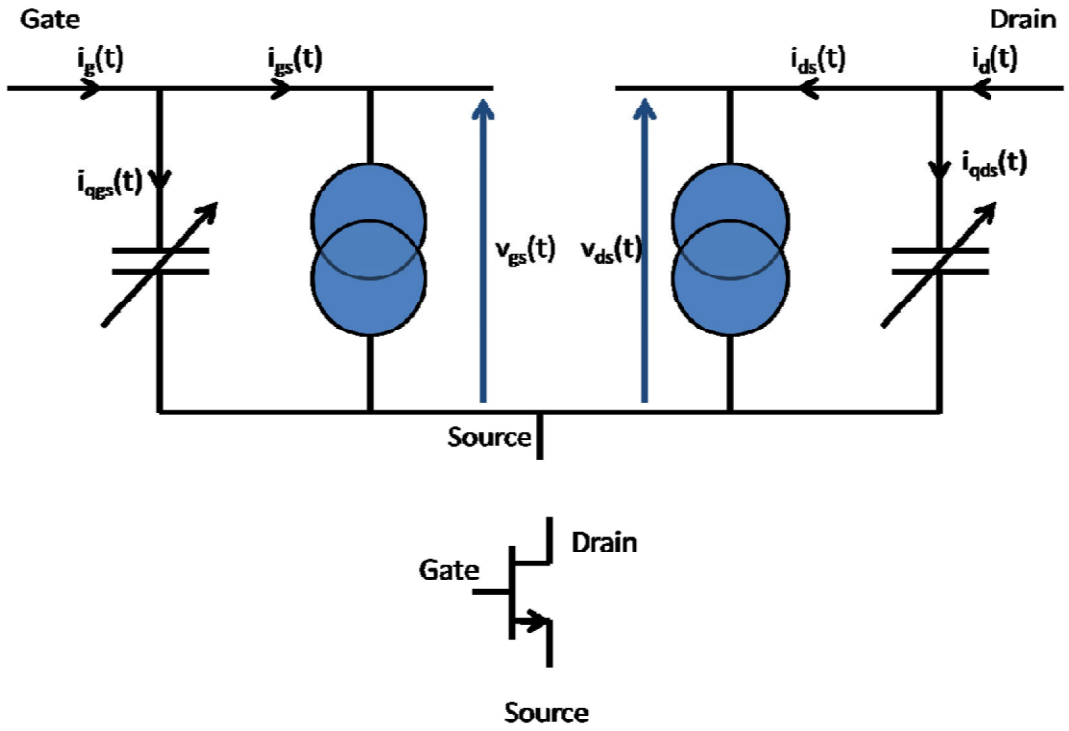

Current and charge functions used within the state function model

Gate current:

$$i_g(t) = i_{gs}(t) + i_{qgs}(t)$$
$$i_{gs}(t) = I_{gs}\left(v_{gs}(t), v_{ds}(t)\right)$$
$$i_{qgs}(t) = \frac{dQ_{gs}\left(v_{gs}(t), v_{ds}(t)\right)}{dt}$$

Drain current:

$$i_d(t) = i_{ds}(t) + i_{qds}(t)$$
$$i_{ds}(t) = I_{ds}\left(v_{gs}(t), v_{ds}(t)\right)$$
$$i_{qds}(t) = \frac{dQ_{ds}\left(v_{gs}(t), v_{ds}(t)\right)}{dt}$$

Figure (2) Current State Function Device Model

Another approach that uses NVNA data involves the construction of data Look-Up-Tables. One structure proposed at Cardiff University by Hao Qi et.al. in [9,15,16] which is being marketed as 'The Cardiff model' uses the frequency domain representations of the measured device plane RF-Waveforms for a selection of loading conditions, and a minimal amount of processing to generate a table that can

be imported into CAD software and used in as a model. This modeling structure is described in figure (3). The ideas demonstrated with the Cardiff model were built on soon after the release of the PNA-X when The Maury Microwave Corporation and Agilent Technologies released Arbitrary Load Dependant X-Parameters [17, 18]

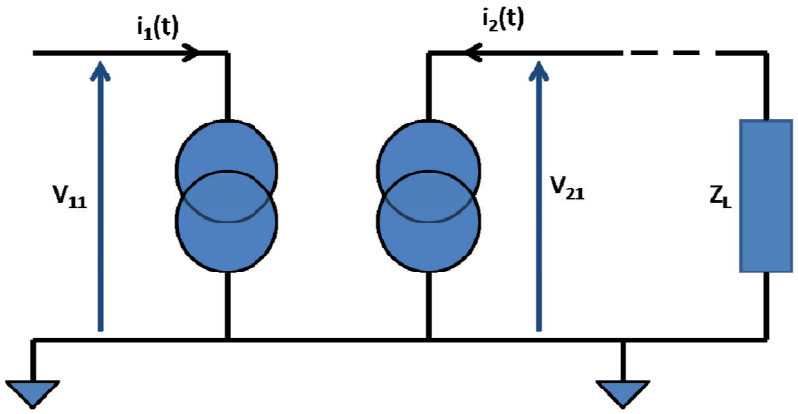

Relationships that define transfer between data file and simulation tool
Calculation of reflection coefficient at port 2 of the device under test

$$\Gamma_L = \frac{Z_L - Z_0}{Z_L + Z_0} = \frac{V_{21} + I_{21}Z_0}{V_{21} + I_{21}Z_0}$$

$$Z_0 = 50\Omega$$

The Value of I_{21} in this equation is the value at the previous iteration of the simulation and can be difficult to obtain and conditional statements have to be used along with this calculation to insure the simulator is able to Converge
Calculation of the current at the ports of the device under test

$$i_p(t) = \sum_{h=0}^{h=H} \Re\left\{V_{11}^h Y_{ph}(V_{11}, \Gamma_L, V_{10}, V_{20}) e^{jh\omega_0 t}\right\}$$

The instantaneous values of the functions Y_{ph} are looked up in a data file containing many conditions of the state variables V_{11}, G_L, V_{10}, V_{20} and are calculated as shown below

$$Y_{ph}(V_{11}, \Gamma_L, V_{10}, V_{20}) = \frac{I_{ph}(V_{11}, \Gamma_L, V_{10}, V_{20})}{V_{11}^h}$$

Figure (3) Cardiff Look-up Table [9, 15, 16]

1.5 Thesis Objectives

This Thesis presents a selection of methods for representing fundamental and harmonic load-pull data as collected using Non-Linear Network analysers within simulation packages as functional data sets “behavioural models”.

Different strategies were employed to analyse the non-linear behaviour of different high frequency devices. These included phase polynomial methods for fundamental only and for fundamental and harmonic stimuli. Also non-linear mixing based polynomial models of transistor loading effects were considered. These are discussed with comparison to the recent developments surrounding the Poly-Harmonic Distortion (PHD) model and its derivatives.

The methods discussed in this thesis have been demonstrated on a range of different devices and device technologies these include Gallium Arsenide “GaAs” Hetro-junction Bipolar Transistors, Gallium Arsenide and Gallium Nitride High Electron Mobility transistors GaAs, GaN HEMTs.

The main objectives of this thesis are, to establish the best standard set of CW Non-Linear measurements to perform on an unknown device to gain a functional data set, which can comprise a basic model having enough functionality and accuracy to aid the design of Power Amplifiers. Specifically those which rely on harmonic terminations for example the classes “B” and “J”.

To establish similarities and differences between the Poly-Harmonic Distortion model and mixing based models identifying whether it is necessary to perturb simultaneously every harmonic in the system.

Also to what level of non-linearity of harmonics needs to be considered when measuring high frequency transistors. Can harmonic terminations as different as short or open circuits, be considered as linear perturbations?
Does the perturbation of harmonics change the observed polynomial order of the device under tests behavior?

1.6 Synopsis of Main Chapters

Chapter 2: Large-Signal S-Parameters to the Poly-Harmonic-Distortion model

The Literature Review discusses the origin and development of the Poly-Harmonic-Distortion model framework through developments in large signal S-parameter measurement techniques and other measurement driven design and modeling techniques based on NVNA and Load-Pull Measurements.

The chapter is divided into two sections; the first section of this chapter discusses the attempts at applying s-parameters to the design of Large Signal Transistor Amplifiers. Then the second section discusses the origins and formulation of the Poly-Harmonic Distortion model. In this chapter the model displayed in section 1.4 is used to demonstrate the techniques described in the literature

Chapter 3: Modeling Device behavior at a Fundamental frequency

This Chapter contains a detailed discussion of the application of the Poly-Harmonic-Distortion Model, Hot-S-Parameters and the author's investigations into mixing based descriptions to model Constant Wave (CW) fundamental only load-pull data of unpackaged transistors and the level of approximation each model makes to this end. Thus providing information about the ability of each model to encapsulate design relevant information.

Chapter 4: Multi-Harmonic Device models in the frequency domain

This chapter develops the modeling approaches discussed and demonstrated in the previous chapter adding functionality to account for changes to harmonic terminations. Simulations are also provided to give insight into the ability of the Poly-Harmonic Distortion model to account for the behavior of harmonics in load-pull situations.

Chapter 5: Design of a Class-J X-Band Monolithic Power Amplifier

This chapter demonstrates the application of the developed models to the design of an X-band MMIC amplifier. The design work was conducted as collaborative research project with QinetiQ Ltd in Malvern, UK to design a high efficiency X-band MMIC amplifier. The author providing the model and measurements that assisted in

the design, the collaboration was successfully completed; showing the value of precise measurement based non-linear models within the design cycle.

1.7 References

1. A chat with the man behind mobiles, *Maggie Shiels, BBC-News , downloaded 28/10/2010 http://newsvote.bbc.co.uk/mpapps/pagetools/print/news.bbc.co.uk/1/hi/uk/2963619.stm*

2. The other transistor: early history of the metal-oxide semi-conductor field-effect transistor, *Robert G. Arns, Engineering Science and Education Journal October 1998. pp 233-240*

3. Method and Apparatus for Controlling Electric Currents, J.E. Lilienfeild *US-patent 1,745,175, filed 8th October 1926*

4. Method of Making Miniaturized Electronic Circuits, J.S. Kilby, US Patent 3,261,081, Filed Feb. 6th 1959

5. SPICE (Simulation Program with Integrated Circuit Emphasis), *Nagel, L. W, and Pederson, D. O., Memorandum No. ERL-M382, University of California, Berkeley, Apr. 1973 Download from http://www.eecs.berkeley.edu/Pubs/TechRpts/1973/ERL-382.pdf*

6. RF Power Amplifiers for Wireless Communications *Steve C. Cripps Second Edition Artech House, 2006 ISBN-10: 1-59693-018-7*, *Chapter 12 Load-Pull Techniques*

7. X-Parameters: The new paradigm for measurement, modeling and design of nonlinear RF and microwave components
David E. Root, Jason Horn, Loren Betts, Chad Gillease, Jan Verspect Microwave Engineering Europe, Dec 2008, www.mwee.com

8. Broad-Band Poly-Harmonic Distortion (PHD) Behavioural Models From Fast Automated Simulations and Large Signal Vectorial Network Measurements
David E. Root, Jan Verspecht, David Sharrit, John Wood, Alex Cognata IEEE Transactions on Microwave Theory and Techniques Vol 53, No.11, 2005

9. Nonlinear Data Utilization: Direct Data Look-up to Behavioural Modelling
Hao Qi, PHD Thesis Cardiff University, Feb 2008

10. Accurate extraction of nonlinear intrinsic transistor current state functions from Large Signal Waveform measurements
M.C. Currás-Francos, P.J. Tasker, M.Fernández-Barciela, Y. Campos-Roca, E. Sánchez,29th European Microwave Conference, Munich 1999, pp262-265

11. The Volterra input-output map of a high frequency amplifier as a practical alternative to load-pull measurements
Verbeyst, F.; Bossche, M.V.;
Instrumentation and Measurement Technology Conference, 1994. IMTC/94. Conference Proceedings. 10th Anniversary. Advanced Technologies in I & M., 1994 IEEE
Digital Object Identifier: 10.1109/IMTC.1994.352068
Publication Year: 1994 , Page(s): 283 - 286 vol.1

12. Technology Independent Large Signal Non Quasi-Static FET Models by Direct Construction from Automatically Characterized Device Data,
Root, David E.; Fan, Siqi; Meyer, Jeff; , Microwave Conference, 1991. 21st European , vol.2, no., pp.927-932, 9-12 Sept. 1991
doi: 10.1109/EUMA.1991.336465
http://ieeexplore.ieee.org/stamp/stamp.jsp?tp=&arnumber=4136405&isnumber=4136399

13. Frequency domain-based approach for nonlinear quasi-static FET model extraction from large-signal waveform measurements
T.M. Martín-Guerrero, J.D. Baños-Polglase, C. Camacho-Peñalosa, M. Fernández-Barciela,D.G. Morgan, P.J. Tasker, 1st European Microwave Integrated Circuits Conference, 2006 EuMA,pp441-444

14. Large-signal FET Model with Multiple Time Scale Dynamics from Nonlinear Vector Network Analyser Data

Jianjun Xu, Jason Horn, Masaya Iwamoto, David E. Root, MTT IMS2010 pp417-420

15. A Novel Nonlinear "Truth Model on Demand" for Rapid Large Signal Power Amplifier Design
Hao Qi, Johannes Benedikt, Paul Tasker, INMMIC 2006, pp 68-71

16. A Novel Approach for Effective Import of Nonlinear Device Charicteristics into CAD for Large Signal Power Amplifier Design
Hao Qi, Johannes Benedikt, Paul Tasker, MTT IMS 2006, pp 477-480

17. Load Pull +NVNA =Enhanced X-Parameters for High Mismatch and Technology-Independent Large-Signal Device Models
Gary Simpson, Jason Horn, Dan Gunyan, David E Root,
Application Note 5A.041,www.maurymw.com

18. Load-pull + NVNA = enhanced X-parameters for PA designs with high mismatch and technology-independent large-signal device models
Simpson, G.; Horn, J.; Gunyan, D.; Root, D.E.; ARFTG Microwave Measurement Symposium, 2008 72nd , vol., no., pp.88-91, 9-12 Dec. 2008
doi: 10.1109/ARFTG.2008.4804301
URL:http://ieeexplore.ieee.org/stamp/stamp.jsp?tp=&arnumber=4804301&isnumber=4804274

Chapter 2 – Large-Signal S-Parameters to the Poly-Harmonic-Distortion model

2.1. Introduction

This chapter aims to review the origin and development of the Poly-Harmonic-Distortion model framework and its links to the measurement systems that have driven its development. The first section of this chapter discusses the attempts at applying s-parameters to the design of transistor amplifiers operating under large signal conditions. It is then shown how these investigations lead to the formulation of the Poly-Harmonic-Distortion (PHD) model. A discussion of present work on the PHD model is provided and how it is currently being applied to model load-pull data. The examples discussed are explained with the aid of simulations to demonstrate extraction processes used at each stage.

2.2. Extension of Scattering-parameter measurement techniques for use with devices operating in Large-Signal regimes

Scattering-Parameters or “s-parameters” have become the most generally used network representation in the microwave engineering community. This is due to their ability to directly encapsulate measurements made by Vector Network Analyzers whilst being a simple tool for visualizing the effective response of measured components within systems. Scattering-Parameters were popularised in the 1960’s with papers by Youla. D.C. [1], and Kurokawa. K.[2]. Kurokawa’s paper was the first publication to present the scattering matrix in a form that is recognisable today by microwave engineers.

Both papers presented the scattering matrix in general form with the ability for the ports of the scattering matrix to be normalized to any real or complex-impedance and where each port could take on, different normalized impedance. This feature has subsequently been dropped by the majority of practicing engineers who typically consider only the standard system impedances of 50 and 75 Ohms. However, the general definitions are still in use within CAD tools. Figure (1) shows the s-parameter definition of a two port network.

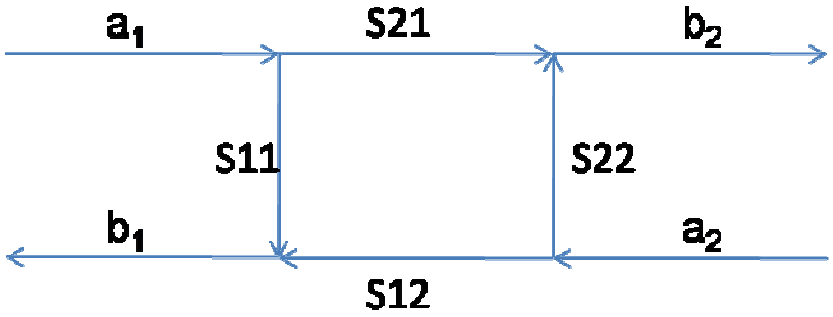

S-Parameter Definitions

$$S11 = \left.\frac{b_1}{a_1}\right|_{a_2=0}, S21 = \left.\frac{b_2}{a_1}\right|_{a_2=0}$$

$$S12 = \left.\frac{b_1}{a_2}\right|_{a_1=0}, S22 = \left.\frac{b_2}{a_2}\right|_{a_1=0}$$

$$\begin{bmatrix} b_1 \\ b_2 \end{bmatrix} = \begin{bmatrix} S11 & S12 \\ S21 & S22 \end{bmatrix} \begin{bmatrix} a_1 \\ a_2 \end{bmatrix}$$

$$[B] = [S][A]$$

Travelling wave definitions for power waves

$$a_n = \frac{V_n^+}{\sqrt{\Re(Z_n)}} = \frac{V_n + I_n Z_n}{2\sqrt{\Re(Z_n)}}$$

$$b_n = \frac{V_n^-}{\sqrt{\Re(Z_n)}} = \frac{V_n - I_n Z_n^*}{2\sqrt{\Re(Z_n)}}$$

Figure (1)
S-Parameter Definitions for a two port network

2.2.1 Advantages of s-parameters as a high frequency measurement technique

S-parameters fully describe the behavior of a multi-port linear networks operating at a single frequency. By superposition the description of their behavior simultaneously at multiple frequencies can be calculated, however this assumption does not hold true for even weakly non-linear systems. Nevertheless, for transistors operating in a small signal regime where the error caused is small, s-parameters give useful insight into stability, gain and matching conditions that are valuable in the design of transistor based amplifiers.

S-parameters also have the convenience of describing the behavior observed when a linear network is measured by a Vector-Network-Analyzer (VNA). This undoubtedly aided the industry wide adoption of s-parameters in the 1960's with the commercial release of the VNA by Hewlet Packard and their popular Application notes.[2] [3]

Vector Network Analyzers are usually configured to measure 2-port networks but recently multiport network analyzers have become available. Measurement of the s-parameters of microwave networks is accomplished by a VNA by injecting a reference signal from a 50 Ohm source at one port and observing the responses at all other ports while they are terminated into 50 Ohm impedances. The measurement is then repeated at all other ports in the system allowing the scattering matrix of the system to be populated [3]. This measurement technique as stated

[2] Hewlett Packard spun out their non computer related divisions to become Agilent Technologies in 1999

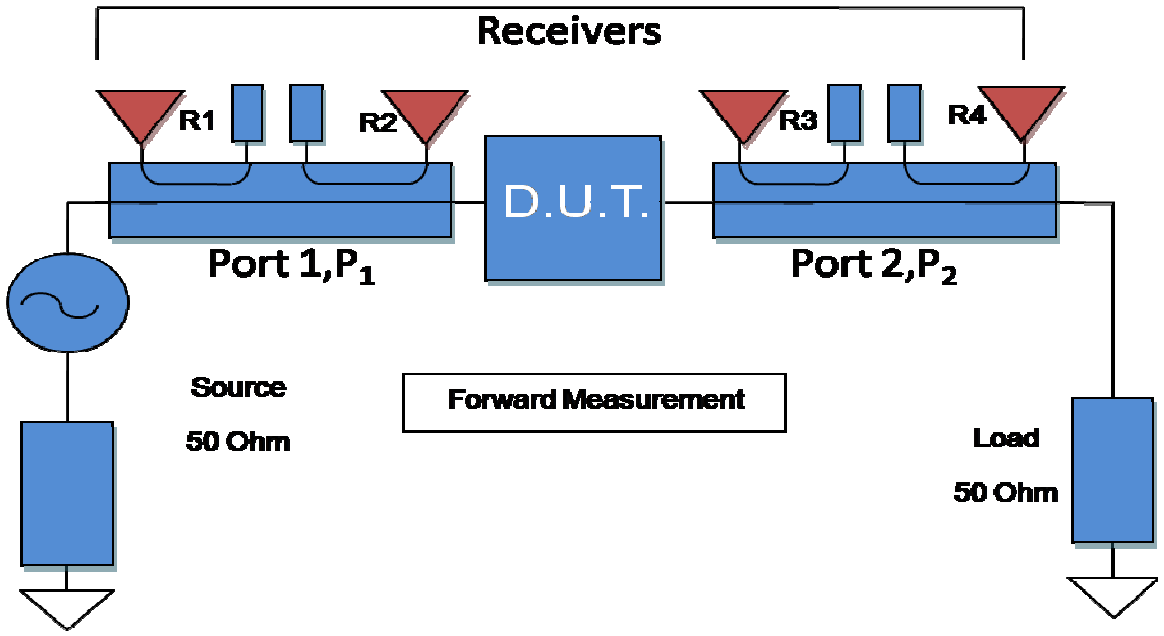

$$S11_{raw} = \frac{R2}{R1}, S21_{raw} = \frac{R3}{R1}, P_{2Match,raw} = \frac{R4}{R3}$$

In ideal case $S11_{raw}$=S11, $S21_{raw}$=S21 *and* $P_{2,Match}$= *0*

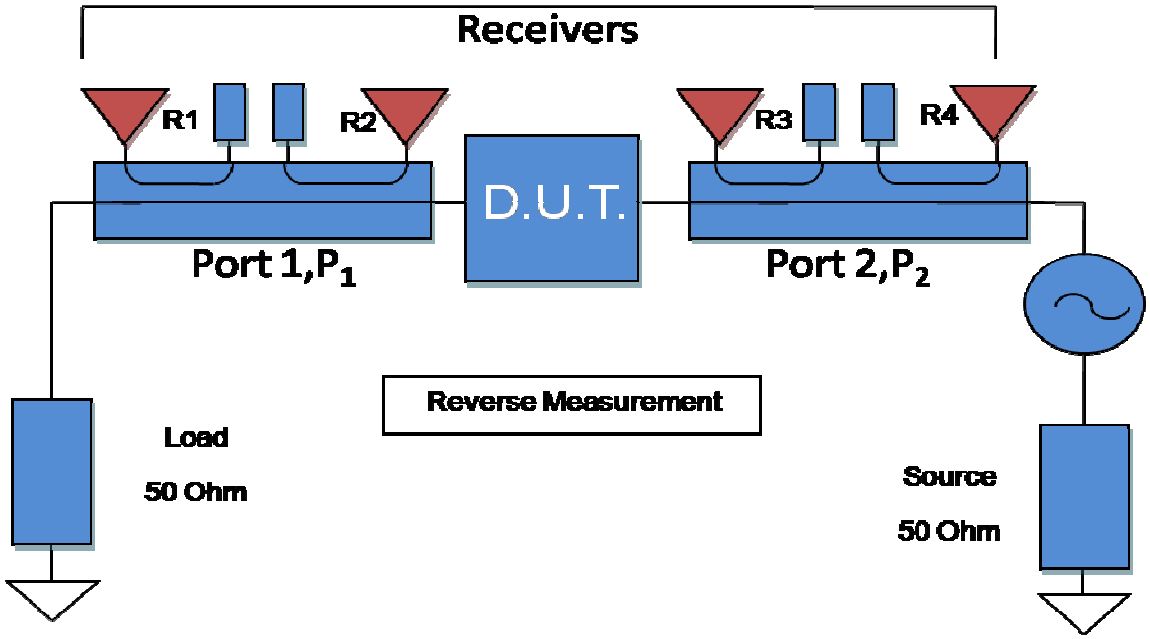

$$S22_{raw} = \frac{R3}{R4}, S12_{raw} = \frac{R2}{R4}, P_{1Match,raw} = \frac{R1}{R2}$$

In ideal case $S11_{raw}$=S11, $S21_{raw}$=S21 *and* $P_{2,Match}$= *0*

Figure (2)
Standard Network Analyser S-Parameter Measurements

allows the use of a microwave source and a load termination with finite impedance (standard value 50 ohms), which allows the measurement setup to be practical at microwave frequencies. Figure (2) gives an overview of standard s-parameter measurements with a network analyzer.

2.2.2 The problem with s-parameters for measuring Large Signal device operation

The advantages of using s-parameters to describe linear systems being known, attempts were made at UHF frequencies and up to 1.5GHz to apply s-parameters to the measurement of large signal devices. W.H. Leighton and R.J Chaffin presented papers on the design of RF amplifiers with "Large Signal S-Parameters" in 1973[3] [4, 5]. The papers concluded that s-parameters gave insight into the operation of devices under large signal conditions. However, they observed that the measured s-parameters were bias and drive dependent. This made the s-parameters difficult to use to directly represent the device behavior. The s-parameters were most relevant when harmonics were either not strongly influencing device behavior, or the device under test's (DUT) parasitic capacitances isolated the DUT's harmonic output from external circuitry. They also stated that to maximize the relevance of the s-parameters, the DUT should be operated as close to the final operating conditions as possible.

To demonstrate the experiment that was conducted by Leighton and Chaffin, a simulation has been conducted using the harmonic balance simulator within ADS.

[3] There was an earlier reference given in the text O. Müller, "Large-Signal S-Parameters measurement of Class-C operated Transistors." Nachrichtentech. Z., Oct 1968, Text for this reference could not be found.

Here the s-parameters of a model of a 4x75µm Gallium Arsenide (GaAs) High-Electron-Mobility-Transistor (HEMT) have been extracted over a power sweep. Figure (3) shows the extracted s-parameters.

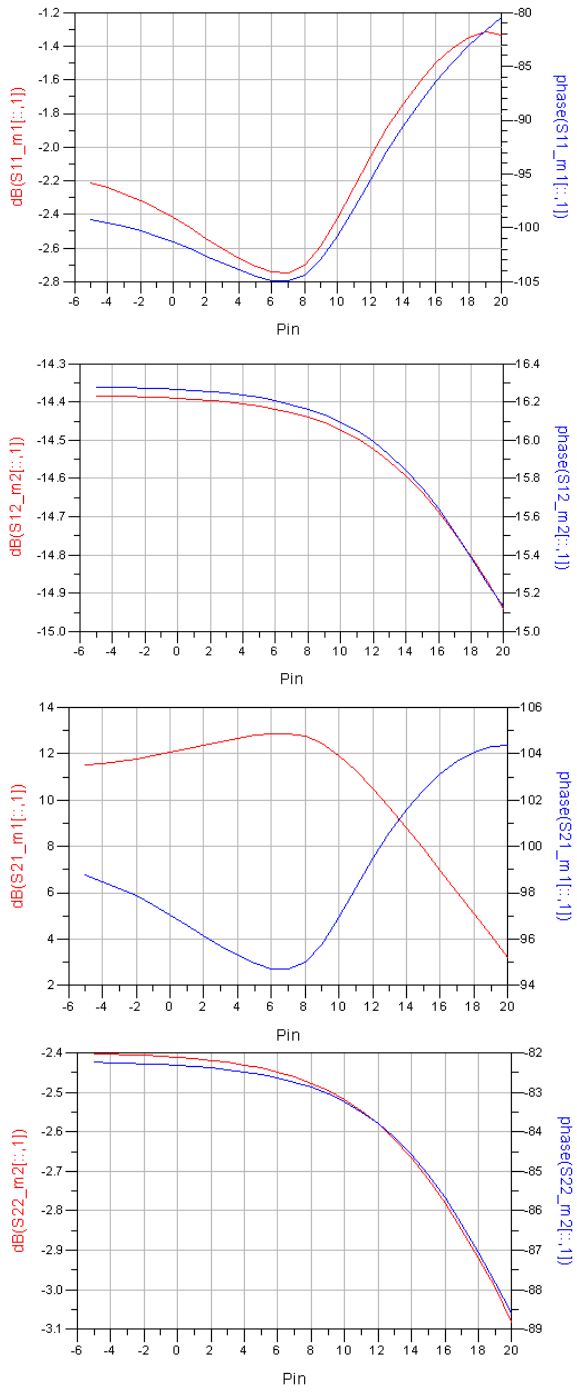

(top-left) S11; (top-right) S12; (bottom-left) S21; (bottom-right) S22

Figure (3)
S-Parameters Extracted From Simulation vs drive power [dBm]

The extracted s-parameters clearly show power dependence. S_{21} shows a classic gain compression curve and S_{11} moves with drive as would be expected. It is also observed that S_{22} and S_{12} change with drive.

Apart from the drive dependence it is not immediately obvious that there is anything else wrong with the s-parameters. Since the simulation was conducted using harmonic balance, it is possible to examine the operation of the device more closely. Figure (4) shows the intrinsic and extrinsic output current and voltage during the simulation.

It can be seen that under large-signal conditions the device output for the forward measurement moves through the device IV-space and interacts with the device boundary conditions in a completely different way to the reverse measurement. This means that under large-signal conditions, as the drive increases, the s-parameter set reflects less the actual forward “desired” operation of the device. In effect the forward and reverse s-parameters no longer represent the device behaviour under the same conditions. Therefore, it would become impossible to use these s-parameters to accurately match the device or predict output power of the device into different loading conditions at high drive.

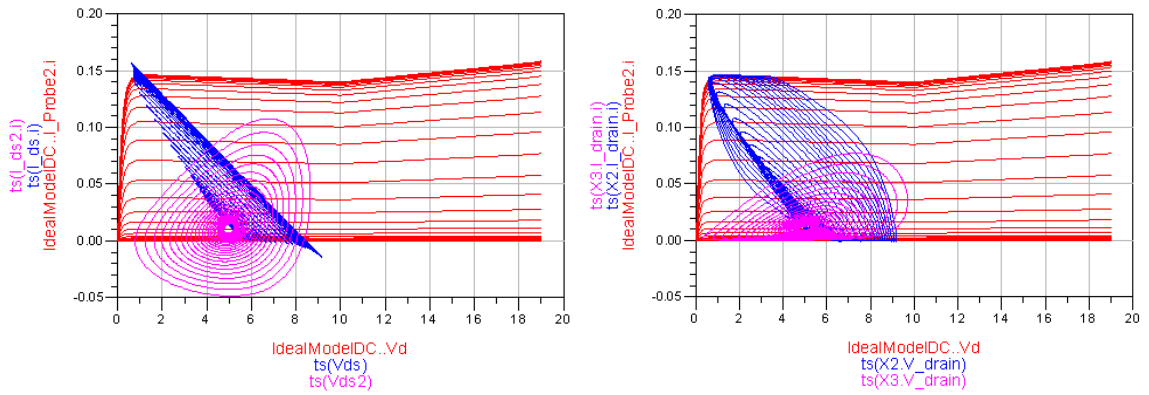

Figure (4)
(Red) DC-IV's
(pink) reverse measurement; (blue) forward measurement
(left) extrinsic (right) intrinsic

(below) layers within a simplfied transistor model

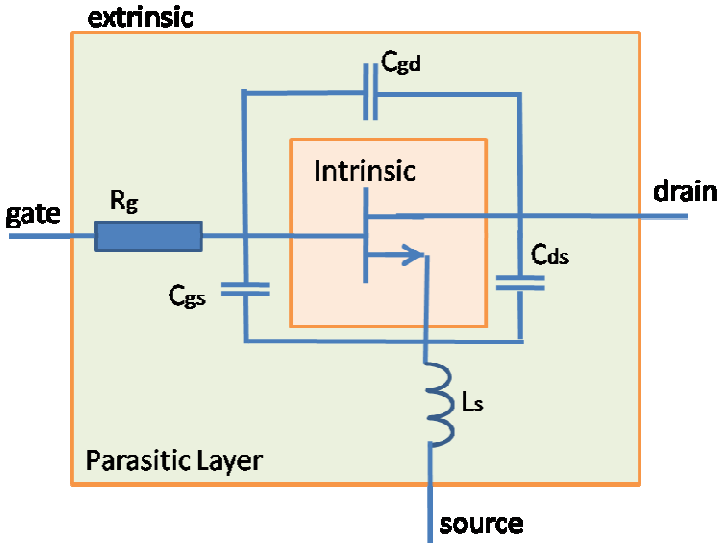

2.2.3 Improving the relevance of the measurement of "S_{22}"

W.H. Leighton and R.J Chaffin [4, 5] highlighted the problems with linear s-parameters when applied to large signal transistor operation. Their measurement system was configured in the same way as a standard VNA, and part of their conclusion was that the measurement of S_{12} and S_{22} did not give reasonable results. In 1977 S. R. Mazmder and P. D. van der Puije presented a novel solution to the

measurement of "S_{22}" whilst keeping the D.U.T. closer to a forward large signal operating point [6, 7]. In their paper titled "*"Two Signal" Method of Measuring the Large-Signal S-Parameters of Transistors"* a system is explained where by a constant signal is applied to one port of an active device - for example the gate or base for transistors. This constant input signal causes the development of another larger signal at the output of the DUT which allows the measurement of S_{11} and S_{21}. The new approach then required another signal to be injected at the output simultaneously to the constant input signal, which is used to allow calculation of S_{22} and S_{12}.

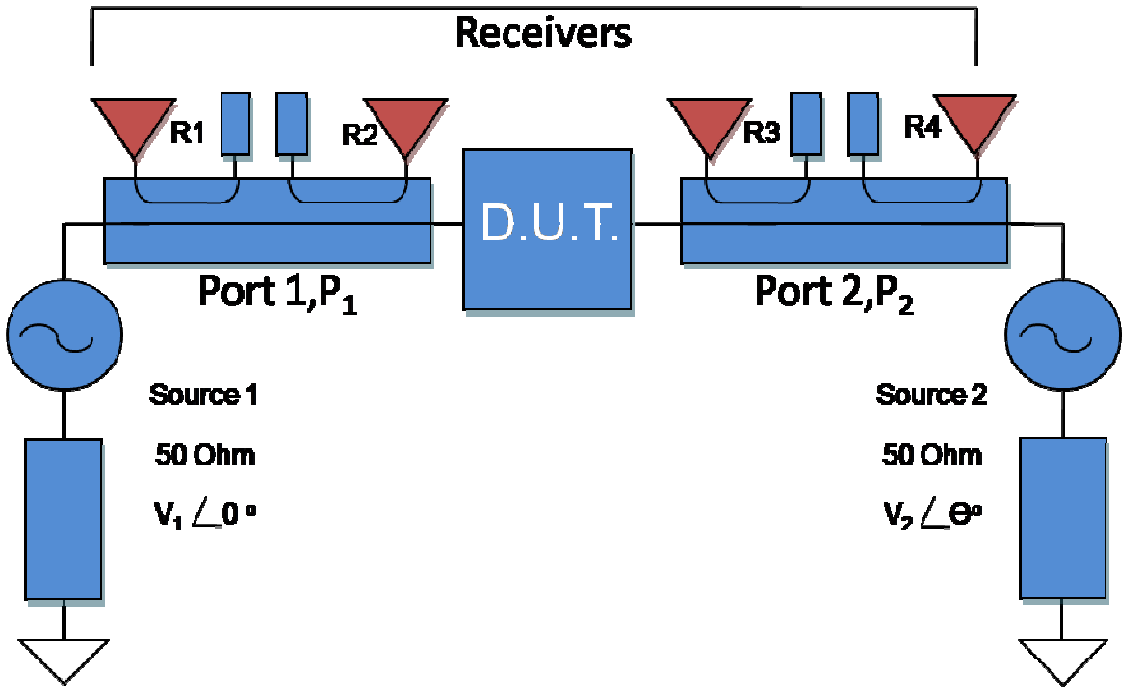

Assuming Ideal Network Analyser

$$S11=\frac{R2}{R1}=\frac{b_1}{a_1}\bigg|_{a_2=0},S21=\frac{R3}{R1}=\frac{b_2}{a_1}\bigg|_{a_2=0},P_{2Match}=\frac{R4}{R3}=\frac{a_2}{b_2}=0$$

Forward parameters measured with source 2 switched off

When Source 2 is switched on

$$a_1=\frac{V_1}{\sqrt{50}},a_2=\frac{V_2}{\sqrt{50}}\angle\theta$$

Erroneous S-parameters are measured as

$$S11'=\frac{R2}{R1}=\frac{b_1}{a_1},S21'=\frac{R3}{R1}=\frac{b_2}{a_1},S22'=\frac{R3}{R4}=\frac{b_2}{a_2},S12'=\frac{R2}{R4}=\frac{b_1}{a_2},L=\frac{R1}{R4}=\frac{a_1}{a_2}$$

Using the parameters from above and the original forward S-parameters

$$S12=(S11'-S11)L$$
$$S22=(S21'-S21)L$$

Or

$$S22=S22'-S21L$$
$$S12=S12'-S11L$$

This process can be repeated for multiple phases of V_2
If DUT is Passive all results should give the same S12 and S22

Figure (5)
Two-signal method for the measurement of S-Parameters.

Figures (5-6) give a more detailed description of the two-signal method. This is the first reference to a technique that has later been called Hot s-parameters or Hot-S_{22}. The paper noted that via this method more realistic estimates of S_{12}, S_{22} could be achieved. It also showed that although the method gave expected results when the reverse injected signal was small, at higher amplitudes the same distortion effects observed by Leighton and Chaffin would appear. The simulation of the previous section has been expanded to demonstrate the two signal method for extracting Hot s-parameters. Figure (7) shows the raw parameters that would be seen on a VNA.

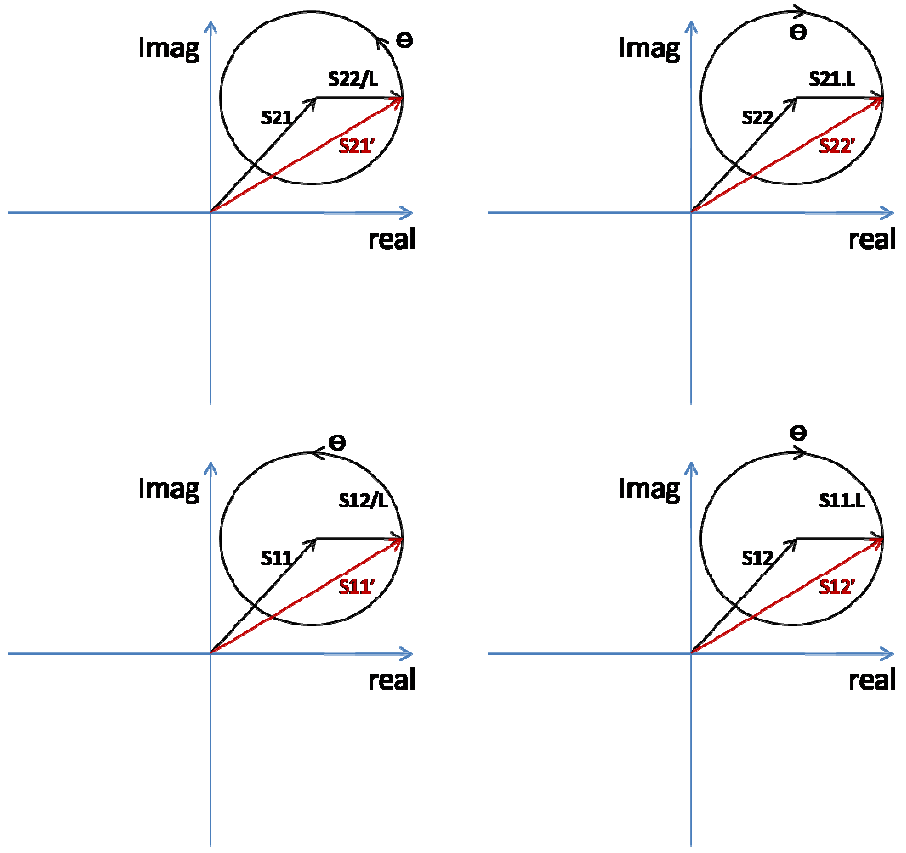

Figure (6)
Geometric representation of the Two-Signal method for Measuring S-Parameters

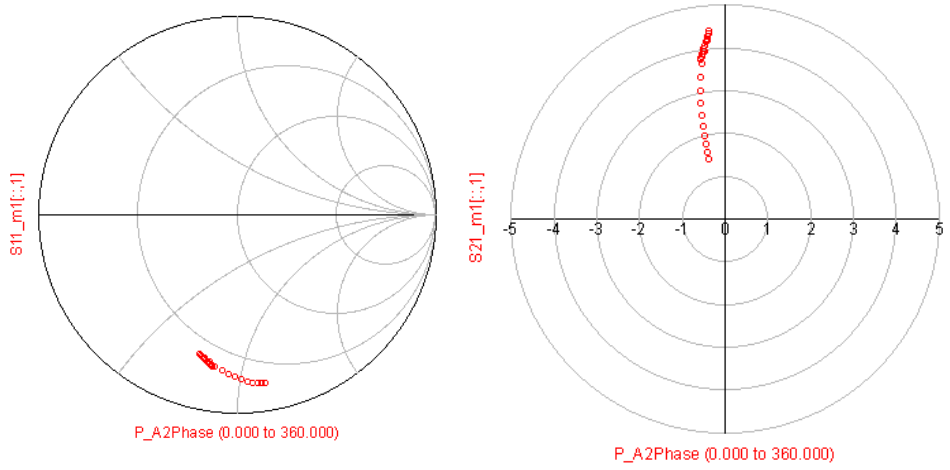

Using only single source at port 1
(top-left) S11; (top-right) S21;

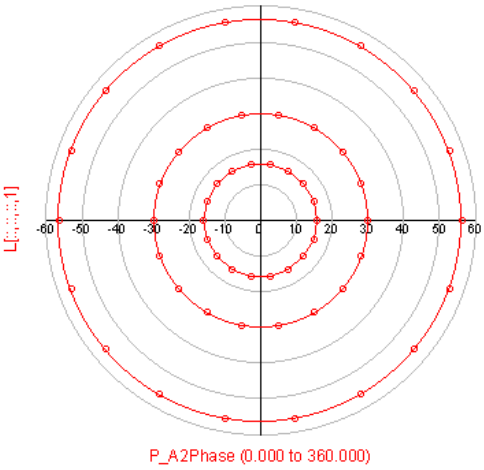

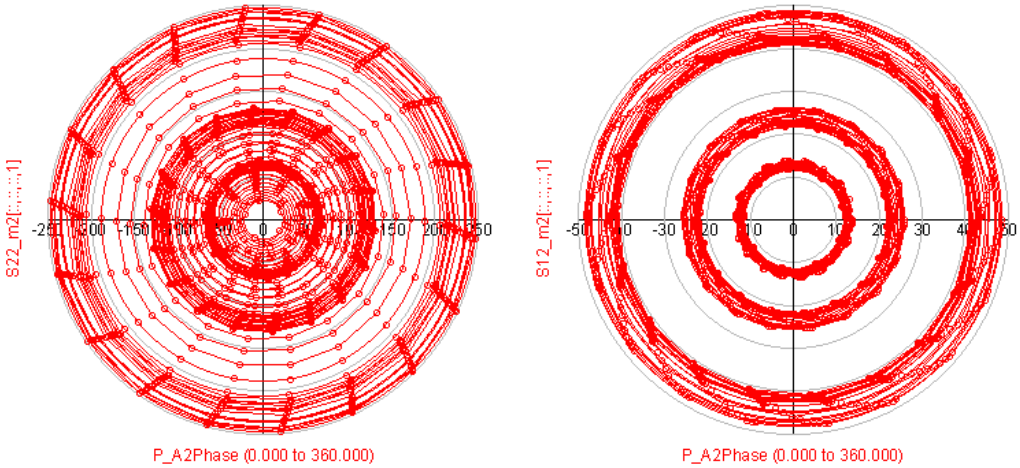

With Two sources port 1 and port 2
(middle) L; (bottom-left) S22; (bottom-right) S12

Figure (7)
Observed S-Parameters during Hot-S-Parameter Simulation

The results in figure (7) show the same forward s-parameters as the previous example, but the reverse s-parameters are now calculated from the perturbations of the large signal State. These measurements are dominated by the forward large signal state and are not immediately usable until they are processed according to equations 1 and 2. Values for the actual S_{22} and S_{12} calculated are shown in Figure (8).

$$S22 = S22' - S21L \quad \textit{eqn (1)}$$

$$S12 = S12' - S11L \quad \text{eqn (2)}$$

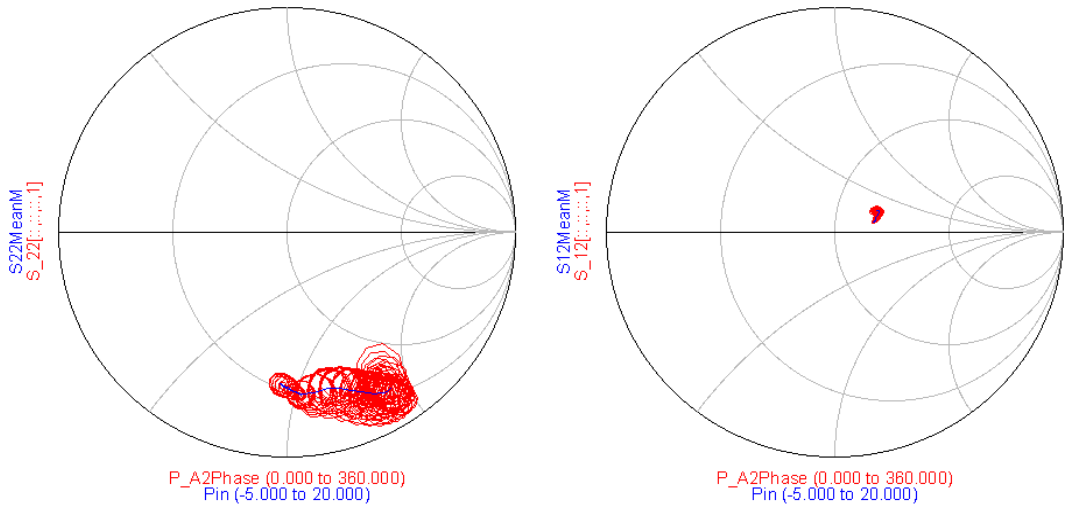

(Blue) mean of extracted S22 (left), S12 (right)

Figure (8)

Output S-parameters extracted by two signal method

It can be seen in figure 8 that although the method provides values for S_{22} and S_{12} the values are dependent on the magnitude and phase of the pertibation at port 2. This was observed by Mazmder and van der Puije and the paper suggested that the best values that could be obtained from this extraction were then the mean of the residual perturbations. The full set of s-parameters are shown in figure 9.

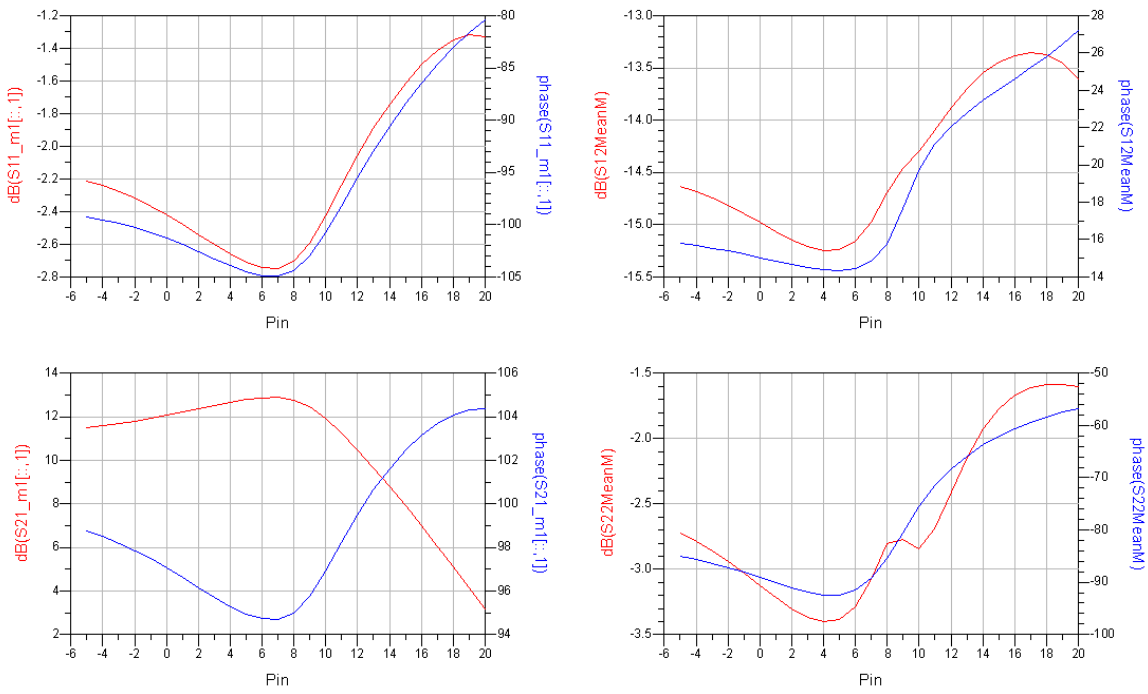

(top-left) S11; (top-right) S12; (Bottom-left) S21; bottom-right) S22;

Figure (9)
Extracted S-Parameters

Comparison of the s-parameters in figure (9) with the previously extracted s-parameters in Figure (3) shows that both methods agree at low drive levels and deviation occurs at higher drive levels as the value obtained for S_{22} with the two signal method has a much larger range of movement over drive. As in the previous example, the intrinsic and extrinsic device operation in terms of voltage and current can be viewed in figure (10). By comparing the forward and the two source states it can be seen that the operational state of the device is closely maintained throughout the whole simulated measurement. This leads to the improved estimate of S_{22}. The problems seen in these measurements were not explored further by Mazmder and van der Puije but were picked up later by other groups.

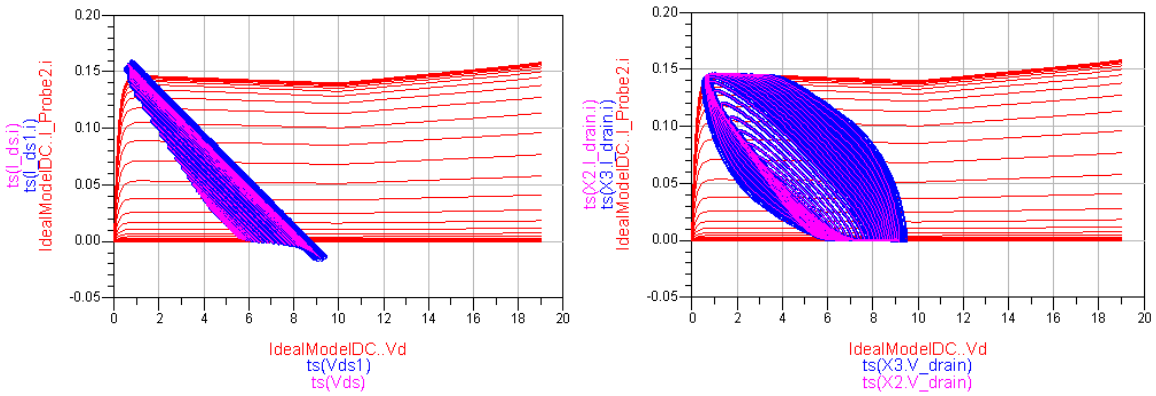

(pink) forward measurement; (blue) pertibated measurement
(left) extrinsic (right) intrinsic

Figure (10)
Device voltage and current durring measurement

2.2.4 Development of Hot S-Parameters

S. R. Mazmder and P. D. van der Puije started the interest in Hot s-parameter measurements; however, the topic was not really investigated again until new instruments became available in the 1990's. The release of the Microwave Transition Analyzer (MTA) and the Large Signal Network Analyzer (LSNA) by Agilent were particularly significant. These instruments provided measurement of the travelling waves at a calibrated reference plane which allows for the Hot-S_{22} measurement problem to be solved differently to the method used by Mazmder and van der Puije. Figure (11) explains how the Hot-S_{22} problem can be solved by using measurements of the traveling waves at the device ports combined with a Least-Squares-method of data extraction.

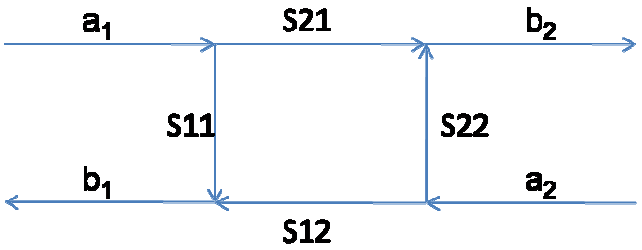

$$b_1 = S_{11}a_1 + S_{12}a_2$$

$$b_2 = S_{21}a_1 + S_{22}a_2$$

If multiple samples are taken then:

$$\begin{bmatrix} b_{1,0} & b_{2,0} \\ b_{1,1} & b_{2,1} \\ \vdots & \vdots \\ b_{1,n} & b_{2,n} \end{bmatrix} = \begin{bmatrix} a_{1,0} & a_{2,0} \\ a_{1,1} & a_{2,1} \\ \vdots & \vdots \\ a_{1,n} & a_{2,n} \end{bmatrix} \begin{bmatrix} S_{11} & S_{21} \\ S_{12} & S_{22} \end{bmatrix}$$

$$[B] = [A][S]$$

Solving for the S-Parameters:

$$[A]^H [B] = [A]^H [A][S]$$

$$[S] = \left([A]^H [A]\right)^{-1} [A]^H [B]$$

$$\begin{bmatrix} S_{11} & S_{21} \\ S_{12} & S_{22} \end{bmatrix} = \begin{bmatrix} \dfrac{\sum b_1 a_1 * \sum |a_2|^2 - \sum b_1 a_1 * \sum a_1 * a_2}{\sum |a_1|^2 \sum |a_2|^2 - \sum a_1 a_2 * \sum a_1 * a_2} & \dfrac{\sum b_2 a_2 * \sum |a_1|^2 - \sum b_2 a_1 * \sum a_1 a_2 *}{\sum |a_1|^2 \sum |a_2|^2 - \sum a_1 a_2 * \sum a_1 * a_2} \\ \dfrac{\sum b_1 a_2 * \sum |a_1|^2 - \sum b_1 a_1 * \sum a_1 a_2 *}{\sum |a_1|^2 \sum |a_2|^2 - \sum a_1 a_2 * \sum a_1 * a_2} & \dfrac{\sum b_2 a_2 * \sum |a_1|^2 - \sum b_2 a_1 * \sum a_1 a_2 *}{\sum |a_1|^2 \sum |a_2|^2 - \sum a_1 a_2 * \sum a_1 * a_2} \end{bmatrix}$$

Subscript 'n' dropped for connivance: $a_1 = a_{1,n}, b_1 = b_{1,n}, a_2 = a_{2,n}, b_2 = b_{2,n}$

Least-Squares Algorithm for Hot-S22 Extraction figure (11)

During this period work by J. Vershpect [8, 9, 10] introduced the theory of describing functions, Quadratic Hot S-parameters and then extended Hot S-parameters. These extended Hot S-parameters have strong similarities to the later Poly-Harmonic-Distortion model. Work by F. Verbeyst and M. Vanden Bosche, where a method of constructing fully non-linear s-parameters from expansions of the Volterra series [11, 12, 13] which they named Volterra Input Output Map (VIOMAP) was also important.

Verspecht's describing functions are a way of collecting all the parameters that are affecting the ports of a transistor. Equation 3 shows the describing function proposed in [9] this equation is important because the s-parameters themselves are not present. In the papers of Verspect, the focus is shifted from describing the s-parameters to describing the travelling waves at the device ports. This move was aided by the use of the new instruments which gave access to phase coherent measurements of harmonics and fully calibrated measurements of the travelling waves and not just the measurement of ratios, unlike previous work which focused on just the s-parameters at a fundamental or Carrier frequency. Figure (12) shows the other way of looking at Hot-S_{22} measurement data. Shown in the figure are the actual values of the travelling waves recorded during the Hot-S_{22} simulation in the previous section.

$$B_{ij} = F_{ij}(A_{11}, A_{12},..., A_{1N}, A_{21},.., A_{MN}, R_1, R_2,..., R_N) \quad \text{eqn 3 [9]}$$

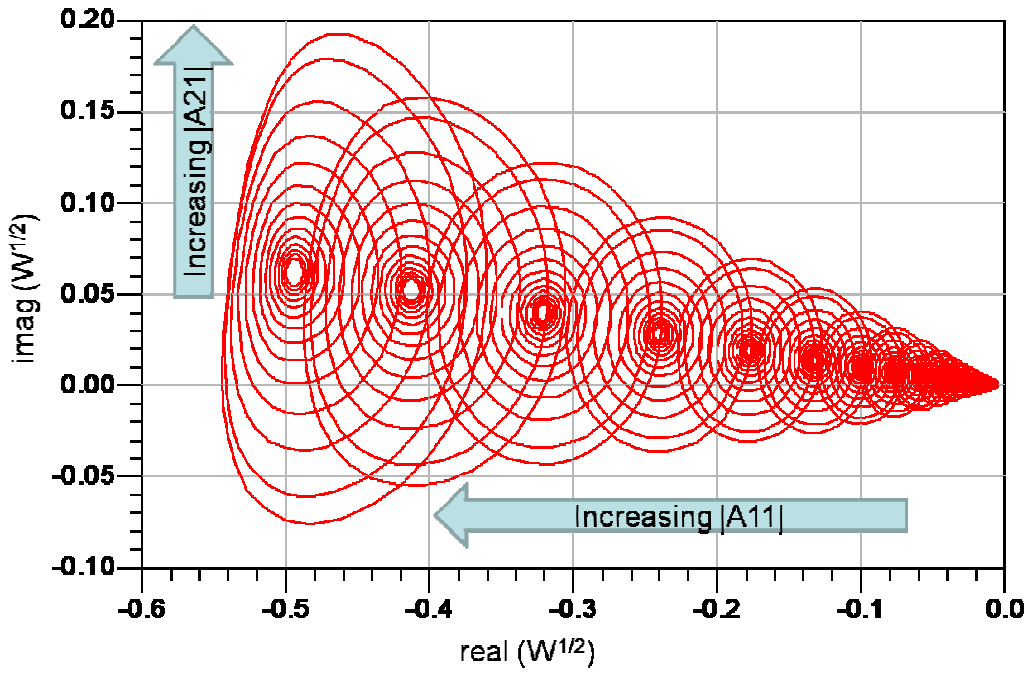

Figure (12) Hot-S22 measurement example – shown are travelling waves rather than ratio S-parameters.

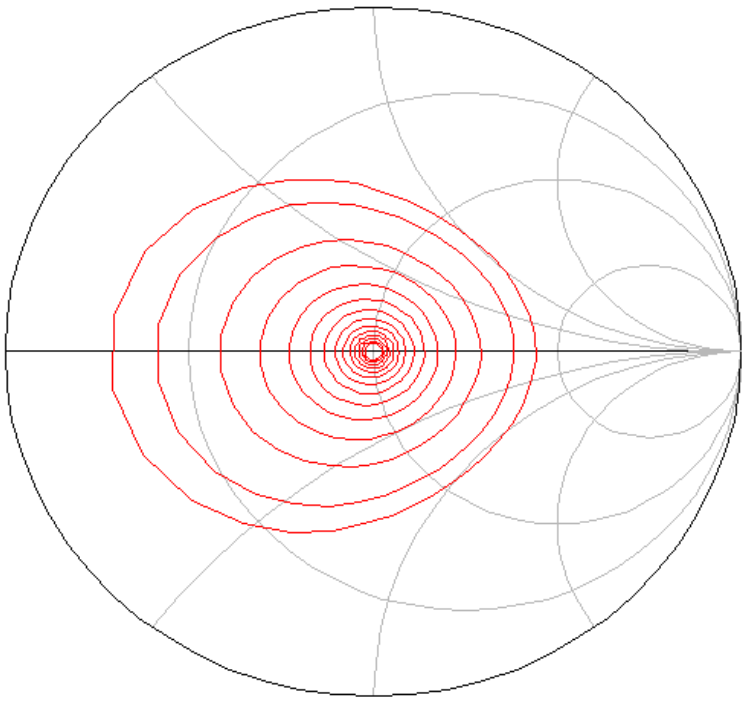

Figure (13)
Load perturbation due to second source
Ploted on 50 Ohm Smith Chart

The other important aspect of this work is the move away from fixed impedance environments. The link between the extraction measurements and load-pull contours can be seen in Figure (13), where the amount by which the load was perturbed during a Hot-S_{22} measurement is shown. It is clear that this link is very important if Hot-S_{22} measurements are to be used to extract relevant device performance parameters under Large-Signal conditions that cannot be achieved using small signal s-parameter design relationships.

2.3. Development of the Poly-Harmonic-Distortion-Model

This Section describes the development of the Poly-Harmonic Distortion (PHD) model from its early roots in the search for large signal scattering parameters, into its current forms in X-Parameters and S-functions.

2.3.1 Conversion Matrices and mixer theory

This section gives a brief overview of the construction of conversion matrices and how they have been formulated for use with s-parameters. Conversion Matrix Theory was first associated with the design of microwave mixers. The early theories were developed by Torrey. H. C. and C. A. Whitmer in their work on crystal rectifiers [14]. This was later explained and expanded upon by S.A. Maas in his book on Microwave Mixers [15].

Conversion matrices are used to give a mathematical framework to the frequency translations observed and engineered in a mixer. Figure (14) gives an example of the use of a microwave mixer for down conversion and describes the major observed frequencies.

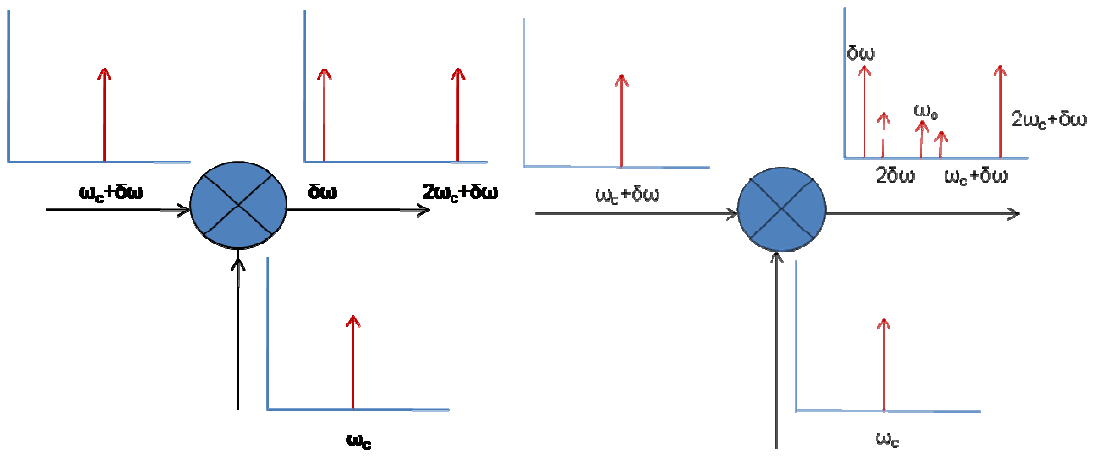

Figure (14)
(left) Use of a Mixer for down conversion (Ideal)
(right) Use of a Mixer for down conversion (practical)

Figure (15) shows the impedance conversion matrix which describes the time domain multiplication of an impedance waveform with a current waveform to form a new voltage waveform that is represented in the frequency domain by the use of a matrix convolution.

$$v(t) = z(t)i(t)$$
$$F\{v(t)\} = F\{z(t)i(t)\}$$
$$F\{v(t)\} = F\{z(t)\} * F\{i(t)\}$$

The process of convolution can be written in matrix form in the frequency domain using a Toplitz Matrix
As shown below forming the Impedance Conversion matrix

$$\begin{bmatrix} V_{-N}* \\ V_{-N+1}* \\ \vdots \\ V_{-1}* \\ V_0 \\ V_1 \\ \vdots \\ V_{N-1} \\ V_N \end{bmatrix} = \begin{bmatrix} Z_0 & Z_{-1} & Z_{-2} & \cdots & \cdots & Z_{-N} & \cdots & Z_{-2N} \\ Z_1 & Z_0 & Z_{-1} & \cdots & \cdots & Z_{-N+1} & \cdots & Z_{-2N+1} \\ \vdots & \vdots & \vdots & \ddots & \iddots & \vdots & \iddots & \vdots \\ Z_{N-1} & Z_{N-2} & Z_{N-3} & \cdots & \cdots & Z_{-1} & \cdots & Z_{-N-1} \\ Z_N & Z_{N-1} & Z_{N-2} & \cdots & \cdots & Z_0 & \cdots & Z_{-N} \\ Z_{N+1} & Z_N & Z_{N-1} & \cdots & \cdots & Z_1 & \cdots & Z_{-N+1} \\ \vdots & \vdots & \vdots & \iddots & \ddots & \vdots & \ddots & \vdots \\ Z_{2N-1} & Z_{2N-2} & Z_{2N-3} & \cdots & \cdots & Z_{N-1} & \cdots & Z_{-1} \\ Z_{2N} & Z_{2N-1} & Z_{2N-2} & \cdots & \cdots & Z_N & \cdots & Z_0 \end{bmatrix} \begin{bmatrix} I_{-N}* \\ I_{-N+1}* \\ \vdots \\ I_{-1}* \\ I_0 \\ I_1 \\ \vdots \\ I_{N-1} \\ I_N \end{bmatrix}$$

$$[V] = [Z][I]$$

Figure (15)
Impedance conversion matrix [15]

Using the impedance and admittance conversion matrices Maas then described the process of converting these matrices to their scattering parameter equivalents using the standard relationships given in eqn. 1.

$$[S] = (1 + [Y])^{-1}(1 - [Y]) = (1 + [Z])^{-1}([Z] - 1) \quad \text{eqn. 1[15]}$$

The work on mixer theory was used by T. Gasseling et.al. [16], where a two-port conversion matrix was used to investigate parametric oscillations of a Hetrojunction Bipolar Transistor (HBT). Their matrix representation is given in eqn. 2 [16]. Parametric Oscillations occur at different frequencies to the main stimuli and can be

related to a fractional-N relationship within the device. It is common to observe these relationships but as explained in [16] they are very complicated to predict.

$$\begin{bmatrix} b_1*(KF_0-f) \\ \vdots \\ b_1(f) \\ \vdots \\ b_1(KF_0+f) \\ b_2*(KF_0-f) \\ \vdots \\ b_2(f) \\ \vdots \\ b_2(KF_0-f) \end{bmatrix} = [S] \begin{bmatrix} a_1*(KF_0-f) \\ \vdots \\ a_1(f) \\ \vdots \\ a_1(KF_0+f) \\ a_2*(KF_0-f) \\ \vdots \\ a_2(f) \\ \vdots \\ a_2(KF_0+f) \end{bmatrix} \qquad \text{eqn.2. [16]}$$

The [S] Matrix in equation 2 [16] was populated by measuring Hot Small Signal S-Parameters at relevant frequencies whilst the DUT is run at a Large-Signal operating point. The Hot S-parameters can then be used to predict the stability factor at each frequency. The conclusion of this work was that an observed parametric oscillation was predicted by the Hot S-parameter measurements.

Significantly, this paper was the first to present a full s-parameter matrix that, whilst filled with linear terms, was capable of predicting cross frequency behavior under large signal operation and containing representations for all relevant frequencies within the formulation.

2.3.2 Investigations into linearized models of large signal data as extensions to s-parameters

In 2005 the topic of producing linearized s-parameters from large signal data was revisited. In the paper by Verspect et.al. [17] a matrix factorization was presented, which forms a base for the Poly-Harmonic-Distortion model. The result of this factorization is given in eqn.3. This equation is important as it added a set of vectors describing the system state and partitions the conjugate of the stimuli into a separate matrix product:

$$\left[\vec{B}\right] = \left[\vec{B}_0\right] + [S]\left[\vec{A}\right] + [S']\left[\vec{A}*\right] \quad \text{eqn.3. [17]}$$

This paper also introduced time normalisation that is used in the PHD model. The paper presented an extraction method for the parameters of eqn.3. This method is shown in figure (16) after restricting the time reference i.e. $\angle a_1 = 0$

$$B_j = B_{0i} + S_i a_j + S_j' a_j^*$$

$$\begin{bmatrix} B_1 \\ B_2 \\ \vdots \\ B_j \end{bmatrix} = B_{0i} \begin{bmatrix} 1 \\ 1 \\ \vdots \\ 1 \end{bmatrix} + S_i \begin{bmatrix} a_0 \\ a_1 \\ \vdots \\ a_j \end{bmatrix} + S_i' \begin{bmatrix} a_0 \\ a_1 \\ \vdots \\ a_j \end{bmatrix}$$

$$\begin{bmatrix} B_1 \\ B_2 \\ \vdots \\ B_j \end{bmatrix} = \begin{bmatrix} 1 & a_0 & a_0^* \\ 1 & a_1 & a_1^* \\ \vdots & \vdots & \vdots \\ 1 & a_j & a_j^* \end{bmatrix} \begin{bmatrix} B_{0i} \\ S_i, \\ S_i \end{bmatrix}$$

$$[B] = [\beta][s]$$

$$[s] = \left([\beta]^H [\beta] \right)^{-1} [\beta]^H [B]$$

Where the Super-Script “H” refers to the Hermitian Conjugate operation
(Complex conjugate of all elements in the transposed matrix)

Figure (16) [17]
Extraction of Linearized S-Parameters

The paper concluded that a linearization of the scattering functions had been found which encompassed conversion matrix theory previously in use for electrical mixers which could now be used to describe weakly non-linear states in amplifiers. However, more study was required to validate the method.

2.3.3 Phase-Normalization and time reference adjustment

The phase normalization in use for all the methods discussed in this section [18, 19, 20] sets the phase of the injected fundamental signal at port 1 to zero. This is so that the injection at the fundamental at port 1 happens at time t=0. When this is conducted for multiple measurements it allows all the measurements to be compared. This process can be found in most Mathematics texts [21] and makes use of the time shifting property of the Fourier transform.

Figure (17) demonstrates the time re-referencing principle. In the figure, two waveforms have been constructed, the original waveform (red triangles) and a time shifted version of the waveform (blue circles). The original waveform was constructed using eqn. 4.

$$S(t) = \cos\left(\frac{2\pi t}{T}\right) + \cos\left(2\frac{2\pi t}{T}\right) + \cos\left(3\frac{2\pi t}{T}\right) \quad \text{eqn. 4.}$$

Time shifting of the waveform in this figure is accomplished using eqn. 5.

$$\begin{aligned} S(t-\tau) &= \cos\left(\frac{2\pi(t-\tau)}{T}\right) + \cos\left(2\frac{2\pi(t-\tau)}{T}\right) + \cos\left(3\frac{2\pi(t-\tau)}{T}\right) \\ &= \cos\left(\frac{2\pi t}{T} - \frac{2\pi\tau}{T}\right) + \cos\left(2\frac{2\pi t}{T} - 2\frac{2\pi\tau}{T}\right) + \cos\left(3\frac{2\pi t}{T} - 3\frac{2\pi\tau}{T}\right) \end{aligned} \quad \text{eqn. 5.}$$

This process preserves the harmonic relationships within the waveforms and therefore the waveform shape, but importantly allows multiple measurements to be viewed simultaneously from the same reference point in time. This is important as most nonlinear network analyzer hardware does not preserve a time reference between measurements, and a common time reference must be preserved for derived models to be successfully used in simulation packages.

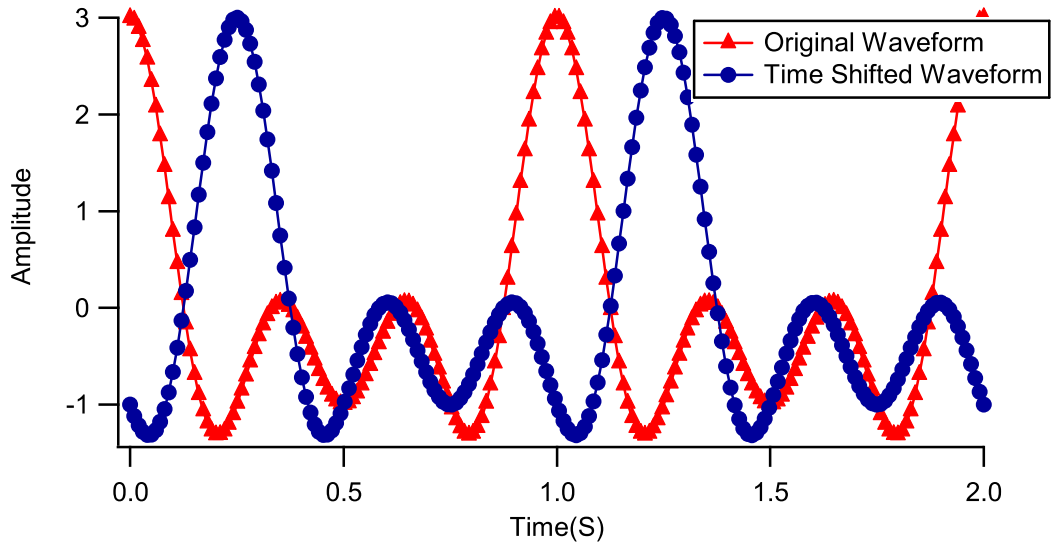

Figure (17)
Time Referencing and phase Normalization of the Poly-harmonic-Distortion Model

In the Poly-Harmonic-Distortion-model this process is represented in the frequency domain as follows in eqn. 6:

$$P^h = e^{jh\vartheta} = e^{jh(\angle a1)} = e^{jh\left(\frac{2\pi\tau}{T}\right)} = e^{jh\omega\tau} \qquad \text{eqn. 6.}$$

Each component of the signals incident and scattered from the DUT is multiplied by 'P' to the power of its harmonic number, as in eqn. 7.

$$G(\omega h) = f(\omega h)P^h \qquad \text{eqn.7.}$$

2.3.4 The Poly-Harmonic-Distortion Model

The main papers on the Poly-Harmonic-Distortion model were published in 2005, by J. Verschpect and D.E. Root [18, 19] these papers presented work based around eqn. 8, which describes the Poly-Harmonic-Distortion model.

$$B_{pm} = \sum_{qn} S_{pq,mn}\left(|A_{11}|\right)P^{m-n}A_{qn} + \sum_{qn} T_{pq,mn}\left(|A_{11}|\right)P^{m-n}A_{qn}^{*} \quad \text{eqn.8. [18]}$$

The Poly-Harmonic-Distortion model was proposed as a simple way of capturing the transmission behavior of non-linear system components for use in simulation of cascaded systems. To this end, it stated that it was necessary to not only capture behavior at the frequency or frequencies of interest but to also capture the behavior of all other spurious products in the system. It was also intended that these models should allow full intellectual property (IP) protection. In effect, none of the information contained within the model would allow the user to reverse engineer the model or the component the model was created for. This is a problem with models that contain physical circuit information or equivalent circuit models. The papers also intended that the model should be developed without any prior knowledge of the DUT and should be extracted using a simple set of measurements.

As discussed, the PHD model is heavily based on previous work involving extraction of large signal or Hot s-parameters. In these measurements it became common practice to use perturbations by another source at the same and different frequencies to extract parameters from the DUT. The same techniques were refined for the extraction of the Poly-Harmonic-Distortion model. One of the main assumptions of the Poly-Harmonic-Distortion Model and the reason for its name, is the assumption that small perturbations of any harmonic or carrier can be treated as linear perturbations of every other spectral line in the system at every port and that these interactions can then just be added. This was called "*The Harmonic Super Position Principle*" in [18, 19] and is shown graphically in Figure (18).

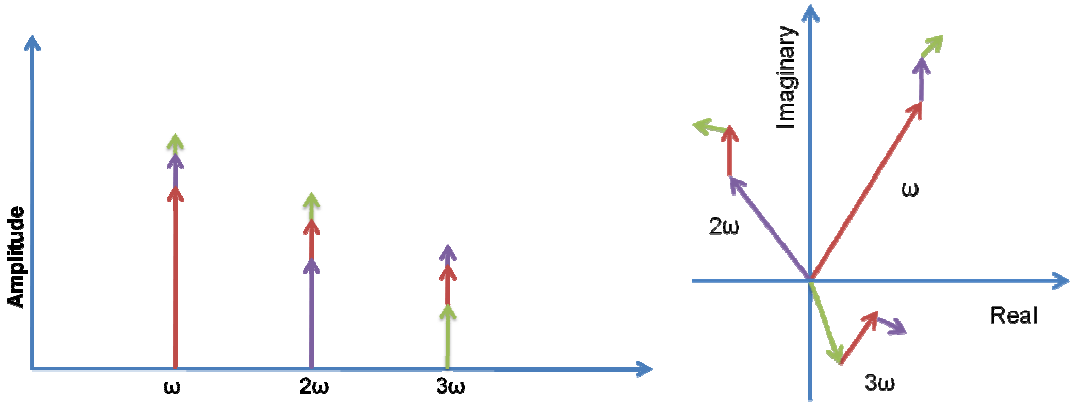

Figure (18)
Harmonic Super-Position-Principle [18, 19]

The Harmonic Super Position concept leads to the linear equation of the PHD model (eqn. 8.) which has 'N' dimensions representing all the ports at each of the harmonics but is linear at all ports and harmonics.

As stated, the PHD Model is represented by a linear equation which allows for a very limited set of measurements to be used to extract the model coefficients. Namely a reference measurement, a small perturbation of the reference state and the quadrature of the perturbation can be used to directly compute the parameter set. This calculation is shown in Figure (19). It is noted that figure (19) presents the minimum extraction measurement set and it would probably not give the best or most accurate extraction due to the measurement uncertainty. As in previous sections the extraction process from figure (19) has been simulated on the model of a 4x75µm GaAs HEMT. The results of this process are shown in figures (20, 22). The results show the same trends for S_{11} and S_{21} as in the previously presented s-parameter and the Hot-S_{22} measurements. However, the X-Parameter extraction seems to have solved the ambiguity in the Hot-S_{22} where the method was corrupted

by phase dependence that was not accounted for within the s-parameters. This is due to the assumption of the presence of the phase conjugated terms "$X^{(T)}$". The phase conjugate term appears when the forward S_{21} term is ether expanding or compressing and goes through a minimum when the gradient of S_{21} is near zero between the expansive and compressive regions of the power sweep. The gain expansion in S_{21} is due to the bias point of the modeled transistor. Shown in figure (10) are the intrinsic and extrinsic voltage and current waveforms from the extraction process which are very similar to the Hot S_{22} case.

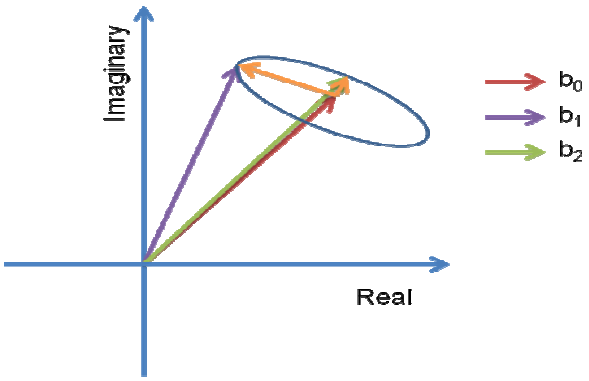

Assuming that three measurements of the scattered b-wave at a port have been made for three distinct values of the incident a-wave at the same port then:

$$a_0 = 0 \quad ; b_0 = b_0'$$
$$a_1 = a \quad ; b_1 = b_1'$$
$$a_2 = a^* ; b_1 = b_2'$$
$$P = 1$$

From these results:

$$S_{21} a_1 = X_F = b_0 = b_0'$$
$$S_{22} = X_S$$
$$T_{22} = X_T$$

and

$$(1) \quad \begin{aligned} b_1 &= X_F + X_S a_1 + X_T a_1^* \\ b_1' &= X_F + X_S a + X_T a^* \end{aligned}$$

and

$$(2) \quad \begin{aligned} b_2 &= X_F + X_S a_2 + X_T a_2^* \\ b_2' &= X_F + X_S a^* + X_T a \end{aligned}$$

Solving (1) and (2) simultaneously gives:

$$X_T = \frac{(b_1 - X_F)a_2 + (b_2 - X_F)a_1}{a_1^* a_2 - a_2^* a_1}$$
$$X_T = \frac{(b_1' - b_0')a^* + (b_2' - b_0')a}{(a^*)^2 - a^2}$$

and

$$X_S = \frac{(b_1 - X_F)a_2^* + (b_2 - X_F)a_1}{a_1 a_2^* - a_2 a_1^*}$$
$$X_S = \frac{(b_1' - b_0')a + (b_2' - b_0')a}{a^2 - (a^*)^2}$$

Figure (19)
Extraction of the Poly-Harmonic-Distortion-Model [18]

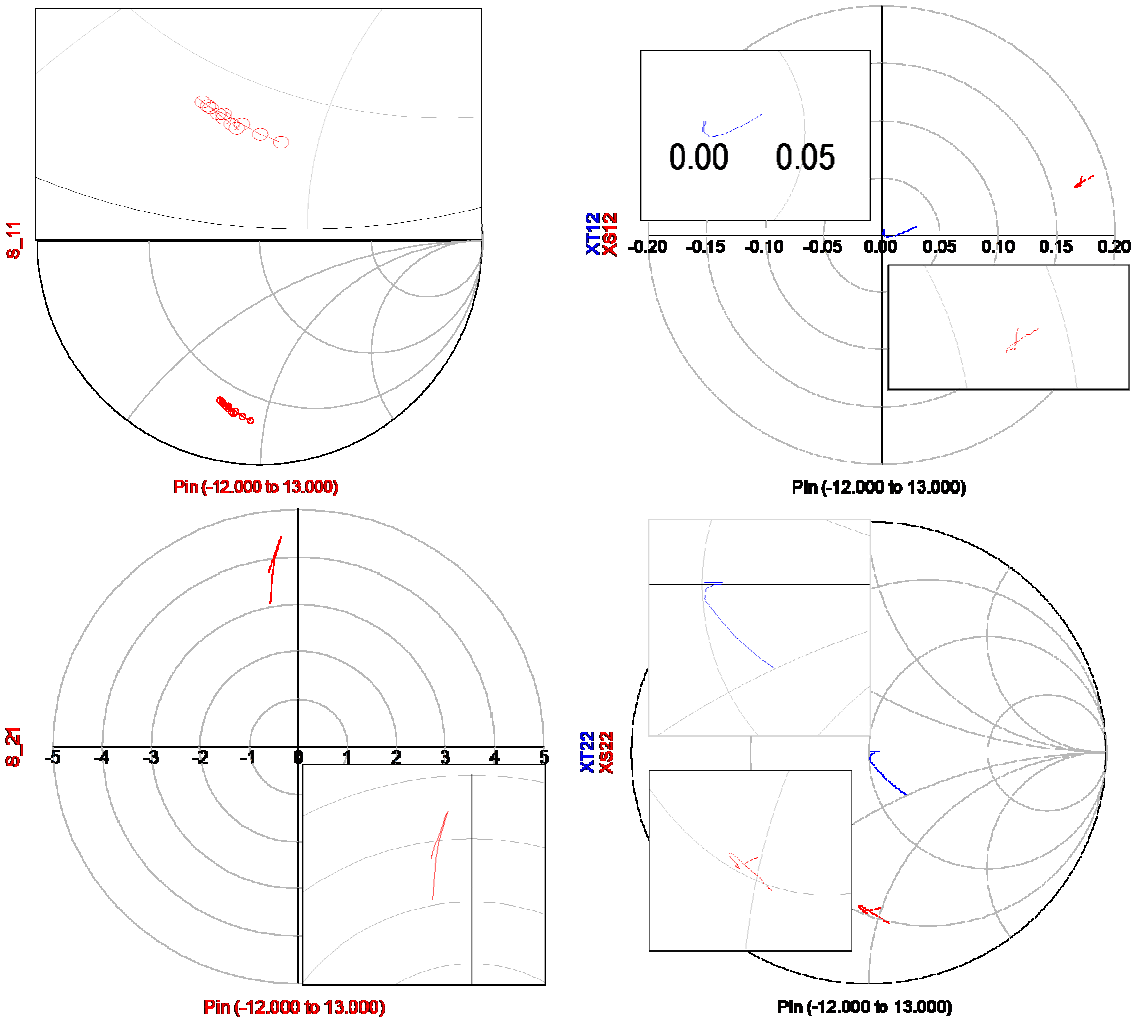

Figure (20)
Results of the simulated extraction of the PHD model on a 4x75um GaAs HEMT

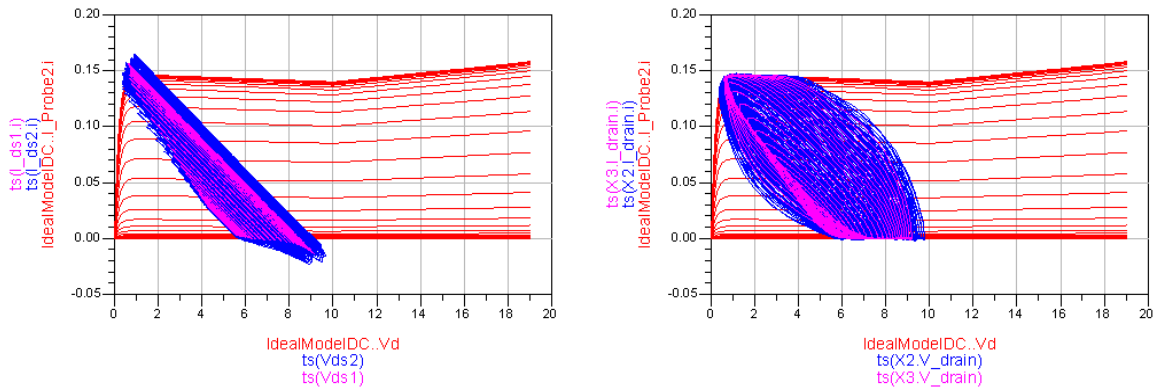

Figure (21)
Device Voltage and Current during the simulated extraction of the PHD model on a 4x75um GaAs HEMT

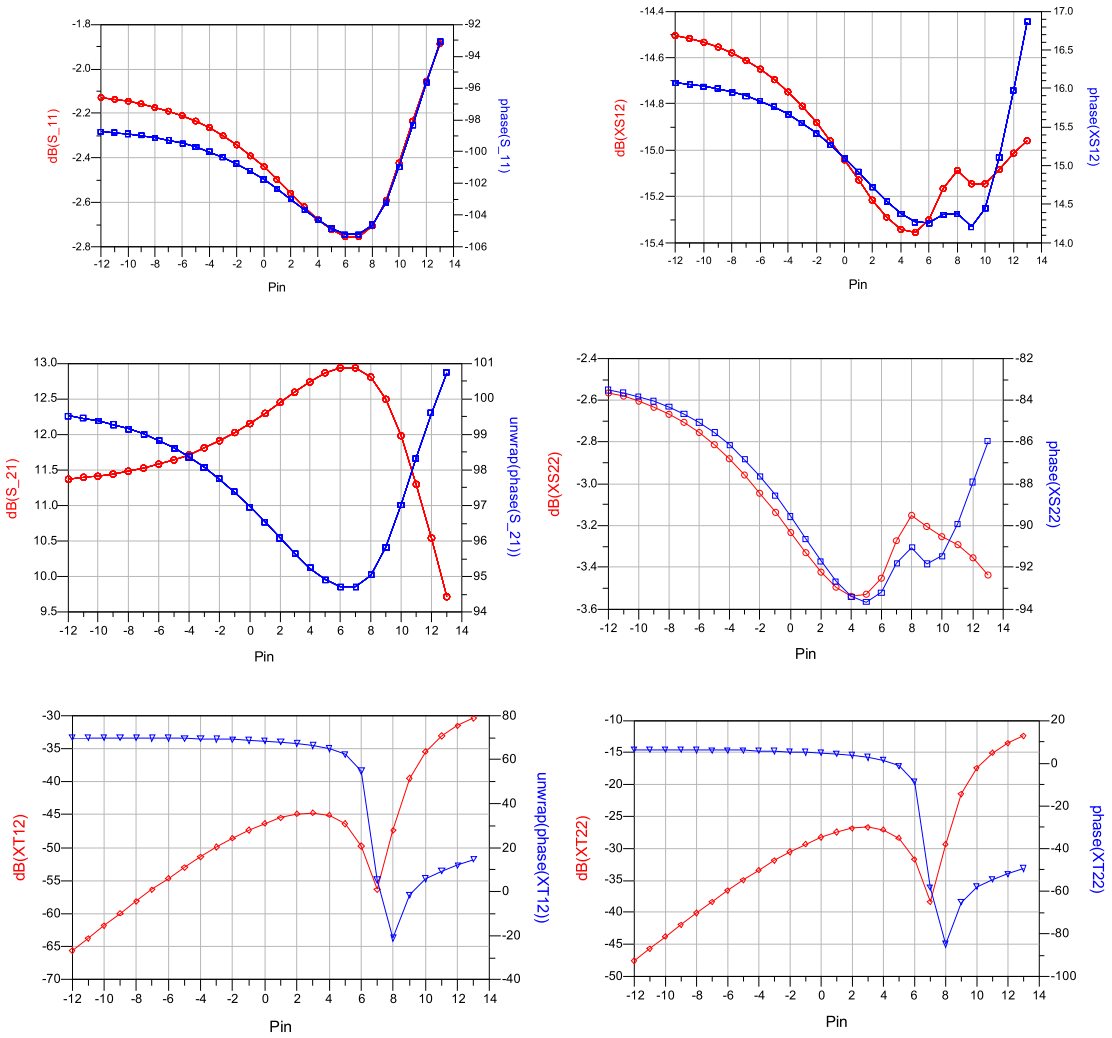

Figure (22)
Results of the simulated extraction of the PHD model on a 4x75um GaAs HEMT

2.3.5 Current trends In Poly-Harmonic Distortion-modeling

The release of the PNA-X in 2008 included an optional NVNA feature which provided the measurement of X-parameters. X-parameters are a restructuring of the Poly-Harmonic-Distortion model which simplifies the terminology used providing a more commercial framework. The updated form is shown in eqn.9. [20], the method of measurement of the X-parameters is explained in the literature but is based on those

presented in the original papers [18, 19]. Although these explain the hardware setup they do not give the exact software setup, for instance the number of measurement points and the extraction algorithm used.

The author believes that the X-parameter extraction process involves more measurements than those presented in figure (19) and probably the structuring of the equation into a Least Squares Problem. This information has not been directly published by Agilent Technologies, but a possible solution is shown in figure (23). This approach is more in line with the method presented in [17]. In a further development, the X-parameters have been measured in conjunction with passive load-pull tuners to create a load look-up table based X-parameter model [22] which is discussed further in the next section and figure (24) shows a description of how the author assumes this model works.

$$\frac{b_{p,h}}{P^h} = X^{(F)}_{p,h}(DC,|A_{11}|) + \sum_{p_S,h_S}\left\{X^{(S)}_{ph}(DC,|A_{11}|)A_{p_S,h_S}P^{-h_S}\right\} + \sum_{p_S,h_S}\left\{X^{(T)}_{ph}(DC,|A_{11}|)\left(A_{p_S,h_S}\right)^* P^{h_S}\right\} \quad \text{eqn.9.[20]}$$

Agilent's reformulation of the Poly-Harmonic-Distortion model is not the only commercially available formulation. Belgian company NMDG and Rhode-Swarchz have released a competing formulation called S-functions, as shown in eqn. 10. [23]

$$B = H(a_1(f_0), a_2(f_0), v_{dc}) + S_k(a_1(f_0), a_2(f_0), v_{dc})A(kf_0) + S_{kc}S_k(a_1(f_0), a_2(f_0), v_{dc})A(kf_0)^*$$

eqn. 10, [23]

The approach taken for the measurement of this model differs from the solution provided by Agilent in so much as the perturbing signals are injected at a different but close frequency to those created by the signal that sets the initial Large Signal state. This frequency offset allows the parameters that are extracted to be directly related to independent spectral lines. This can be viewed as a continuous time extraction of the PHD model if the injected signals are considered as phase modulation. Additionally, tools are available through NMDG for the analysis of S-functions.

Presented here is a method for formulating the extraction of the poly-harmonic distortion-model as a Least Squares Problem in matrix form. Assuming that the phase of "A_1" has already been set to zero and all components adjusted accordingly. The X-Parameter equation can be written for the fundamental and second harmonic as:

$$b_{p,h} = X^{F}_{p,h} + X^{S}_{p,h,2,1}a_{2,1} + X^{T}_{p,h,2,1}a_{2,1}{}^{*} + X^{S}_{p,h,2,2}a_{2,2} + X^{T}_{p,h,2,2}a_{2,2}{}^{*}$$

If multiple samples of points on this equation are taken where more than the minimal set of measurements are made then:

$$\begin{bmatrix} b_{p,h,0} \\ b_{p,h,1} \\ \vdots \\ b_{p,h,n} \end{bmatrix} = \begin{bmatrix} X^{F}_{p,h} + X^{S}_{p,h,2,1}a_{2,1,0} + X^{T}_{p,h,2,1}a_{2,1,0}{}^{*} + X^{S}_{p,h,2,2}a_{2,2,0} + X^{T}_{p,h,2,2}a_{2,2,0}{}^{*} \\ X^{F}_{p,h} + X^{S}_{p,h,2,1}a_{2,1,1} + X^{T}_{p,h,2,1}a_{2,1,1}{}^{*} + X^{S}_{p,h,2,2}a_{2,2,1} + X^{T}_{p,h,2,2}a_{2,2,1}{}^{*} \\ \vdots \\ X^{F}_{p,h} + X^{S}_{p,h,2,1}a_{2,1,n} + X^{T}_{p,h,2,1}a_{2,1,n}{}^{*} + X^{S}_{p,h,2,2}a_{2,2,n} + X^{T}_{p,h,2,2}a_{2,2,n}{}^{*} \end{bmatrix}$$

This is factorized as:

$$\begin{bmatrix} b_{p,h,0} \\ b_{p,h,1} \\ \vdots \\ b_{p,h,n} \end{bmatrix} = \begin{bmatrix} 1 & a_{2,1,0} & a_{2,1,0}{}^{*} & a_{2,2,0} & a_{2,2,0}{}^{*} \\ 1 & a_{2,1,1} & a_{2,1,1}{}^{*} & a_{2,2,1} & a_{2,2,1}{}^{*} \\ \vdots & \vdots & \vdots & \vdots & \vdots \\ 1 & a_{2,1,n} & a_{2,1,n}{}^{*} & a_{2,2,n} & a_{2,2,n}{}^{*} \end{bmatrix} \begin{bmatrix} X^{F}_{p,h} \\ X^{S}_{p,h,2,1} \\ X^{T}_{p,h,2,1} \\ X^{S}_{p,h,2,2} \\ X^{T}_{p,h,2,2} \end{bmatrix}$$

This can be represented symbolically with the equation:

$$[B] = [A][X]$$

Noting that [A] is complex and is not always square:

$$[A]^{H}[B] = [A]^{H}[A][X]$$

$$[X] = \left([A]^{H}[A]\right)^{-1}[A]^{H}[B]$$

Where the Super-Script "H" refers to the Hermitian Conjugate operation or the conjugate transpose of a matrix

The method presented can be expanded to fit the amount of measurements that can be made by any particular setup but it is noted that X^S and X^T Parameters cannot be extracted at for stimuli that is not perturbed.

Figure (23)
Least Squares Extraction of the Poly-Harmonic-Distortion-Model [17, 20]

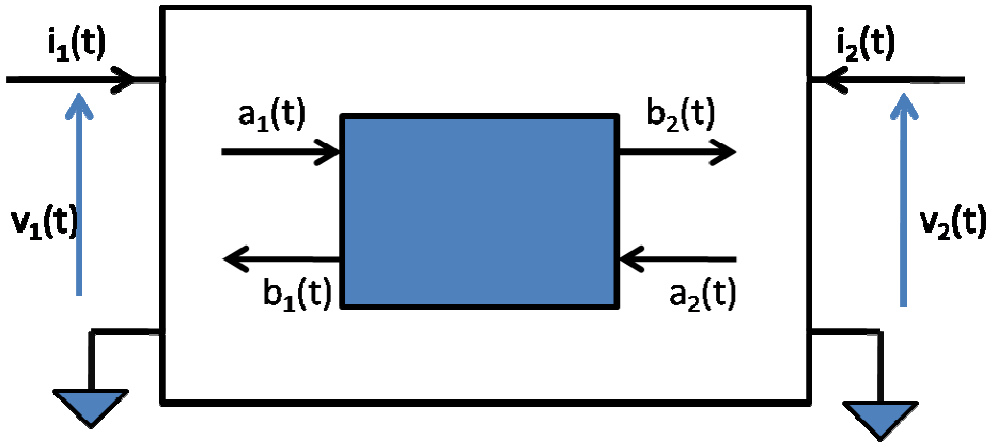

Relationships that are used to transfer between data file and simulation tool

Calculated Before Look-up:

$$\Gamma_L = \frac{Z_L - Z_0}{Z_L + Z_0} = \frac{V_{21} + I_{21}Z_0}{V_{21} + I_{21}Z_0}$$

$$Z_0 = 50\Omega$$

$$a_p(t) = \frac{v_p(t) + Z_0 i_p(t)}{2\sqrt{\Re(Z_0)}}$$

Calculated After Look-up:

$$b_p(t,\Gamma_L,V_{10},V_{2,0},p,\omega_0,|A_{11}|) = \sum_{h=1}^{H} \Re\left\{X^{(F)}(\Gamma_L,V_{10},V_{2,0},p,h,\omega_0,|A_{11}|)P^h e^{jh\omega_0 t}\right\} +$$

$$\sum_{h=2}^{h=H}\sum_{p_S=1}^{2}\sum_{h_S=2}^{H_S} \Re\left\{X^{(S)}(\Gamma_L,V_{10},V_{2,0},p,h,p_S,h_S,\omega_0,|A_{11}|)P^{h-h_S} A_{p_S,h_S} e^{jh\omega_0 t}\right\} +$$

$$\sum_{h=2}^{h=H}\sum_{p_S=1}^{2}\sum_{h_S=2}^{H_S} \Re\left\{X^{(T)}(\Gamma_L,V_{10},V_{2,0},p,h,p_S,h_S,\omega_0,|A_{11}|)P^{h+h_S} A_{p_S,h_S} e^{jh\omega_0 t}\right\}$$

Note $X^{(S)}$ or $X^{(T)}$ are not used from the fundamental frequency "A" waves only from harmonics

$A_{ps,hs}$ are retrieved from the Spectral components of $a_p(t)$

New node voltages returned to simulation as:

$$v_p(t) = \left(a_p(t) + b_p(t,\Gamma_L,V_{10},V_{2,0},h,\omega_0,|A_{11}|)\right)\sqrt{\Re(Z_0)}$$

Figure (24) Load Dependant X-Parameters [20, 22, 24]

2.4. Discussion

To summarize this section the different methods and techniques that have lead to the development of the Poly-Harmonic Distortion model have been discussed and

described. In turn the methods that are relevant to this thesis have been demonstrated these being normal s-parameter measurements Hot S_{22} and the Poly-Harmonic distortion model. These have been demonstrated with the use of simulations performed on a model of a 4x75µm GaAs HEMT. Figures (25-26) show the results of these simulations, it can be seen in figure (25) that the forward s-parameters "S_{21}" and "S_{11}" for all the methods give the same results but the reverse parameters figure (26) give different results under Large Signal conditions but tend toward the same small signal point at low drive levels. So far however no conclusions have been drawn about the accuracy of any of the methods that have been discussed and how useful or misleading the parameterizations could be regarding to design data.

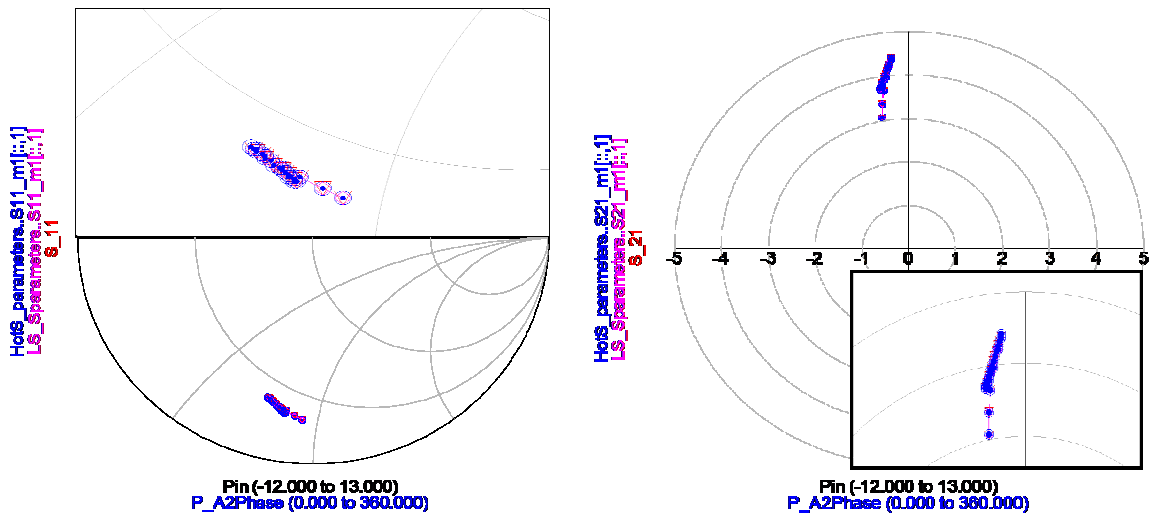

Figure (25)
Extracted forward S-Parameters by 3 methods
Normal Network Analyser Extraction (pink)
Hot S-Parameters (blue)
PHD model (red)

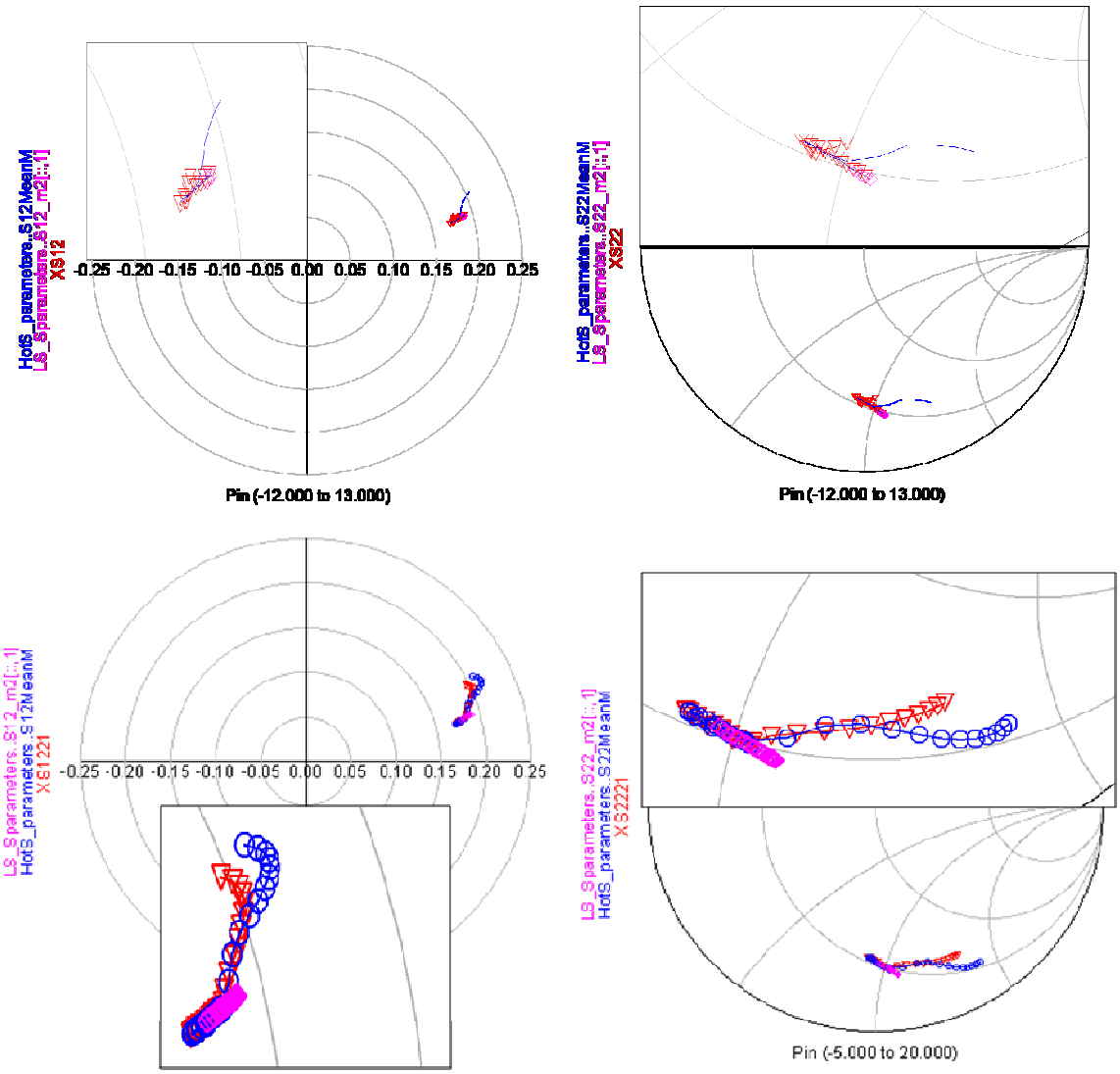

Figure (26)
Extracted Reverse S-Parameters by 3 methods
Normal Network Analyser Extraction (pink)
Hot S-Parameters (blue)
PHD model (red)

At this point it would be prudent to consider how relevant this direction of research is; as it was indicated in the introduction, industry has adopted Load-Pull as its standard technique for collecting design data about non-linear devices. Industry had lost most of its interest in “Large Signal” or “Hot” S-Parameters, however, the release of the X-parameters, sold under the premise that they would replace the use of s-parameters for Non-Linear devices and fix the ambiguities of “Large Signal” and “Hot” S-

Parameters, has revived the interest in these techniques. This has lead directly to their publicized application to Load-Pull where the author assumes they made a change to the stated X-parameter formulation this was shown in figure (24). In this figure a method was displayed that used a Look-Up-Table (LUT) instead of X-parameters at the fundamental frequency. The author considers this as a fundamental admission, where previously the X-parameters were a replacement to s-parameters, this change would detract from this claim and brings up the question "Will there ever be a Non-Linear equivalent to s-parameters?" and how useful are the X-parameters for encapsulating design relevant data.

The following chapters discuss these points in more detail, and propose other related techniques for looking at the problem of encapsulating design relevant data for use in CAD packages. This will be based around waveform measurements and simulations of active load pull and measurements with active perturbations of transistors for the purpose of designing transistor amplifiers.

2.5. References

1. On Scattering Matrices Normalised to Complex Port Impedances
   Youla. D.C, Proc IRE. vol 49, July 1961, p 1221

2. Power waves and the Scattering Matrix
   K. Kurokawa, IEEE Transactions on Microwave Theory and Techniques, 1965, pages194-202

3. AN 154 S-Parameter Design

Agilent Technologies, Inc. 1990, 2000, 2006, Printed in USA, June 20, 2006, 5952-1087

4. RF Amplifier Design with Large Signal S-Parameters

   William. H. Leighton, Roger J. Chaffin, John G. Webb

   IEEE Transactions on Microwave Theory and Techniques Vol MTT-21, No.12, December 1973.

5. Large-Signal S-Parameter Characterization of UHF Power Transistors

   R. J. Chaffin and W.H. Leighton, MTT 1973.

6. An Experimental Method of Characterizing Nonlinear 2-Ports and its Application to Microwave Class-C Transistor Power Amplifier Design

   S. R. Mazmder P. D. van der Puije

   IEEE Journal of Solid-State Circuits, Vol SC-12, No. 5, October 1977

7. “Two-Signal” Method of Measuring the Large-Signal S-Parameters of Transistors

   Shamsur. R. Mazmder P. D. van der Puije

   IEEE Transactions on Microwave Theory and Techniques Vol MTT-26, No.6, June 1978.

8. Hot S-Parameter Techniques: 6 = 4+2

   Jan Verspecht, Denis Barataud, Jean-Pierre Teyssier, Jean-Michel Nébus

   66th ARFTG Conference, December 2005

9. Characterizing Components under Large Signal Excitation: Defining Sensible 'Large Signal S-Parameters'?!
Jan Vershpect, Marc Vanden Bossche, Frans Verbeyst
49th ARFTG Conference, 1997

10. Everything you've always wanted to know about Hot S22
(but were afraid to ask),*Jan Verspect, Presented at the Workshop Introducing New Concepts in Non-linear Network Design, MTT-IMS 2002,Fall Power Amplifier Symposium 2009*

11. The Volterra input-output map of a high frequency amplifier as a practical alternative to load-pull measurements
Verbeyst, F.; Bossche, M.V.;
Instrumentation and Measurement Technology Conference, 1994. IMTC/94. Conference Proceedings. 10th Anniversary. Advanced Technologies in I & M., 1994 IEEE
Digital Object Identifier: 10.1109/IMTC.1994.352068
Publication Year: 1994 , Page(s): 283 - 286 vol.1

12. Verbeyst, Frans; Bossche, Marc Vanden; , "VIOMAP, 16QAM and Spectral Regrowth: Enhanced Prediction and Predistortion based on Two-Tone Black-Box Model Extraction," *ARFTG Conference Digest-Spring, 45th* , vol.27, no., pp.19-28, May 1995

doi: 10.1109/ARFTG.1995.327101

13. Verbeyst, Frans; , "Using Orthogonal Polynomials as Alternative for VIOMAP to Model Hardly Nonlinear Devices," *ARFTG Conference Digest-Spring, 47th* , vol.29, no., pp.112-120, June 1996
doi: 10.1109/ARFTG.1996.327171

14. Crystal Rectifiers, *Torrey. H. C., C. A. Whitmer, New York: McGraw-Hill 1948*

15. Microwave *Mixers Stephen A. Maas Second Edition Artech House, 1993 ISBN 0-8900605-1*, *Chapter 4 Diode Mixer Theory, section 4.3.2*

16. Hot Small-Signal S-Parameter Measurements of Power Transistors Operating Under Large-Signal Conditions in a Load-Pull Enviroment for the Study of Nonlinear Parametric Interactions
Tony Gassling, Denis Barataud, Sébastien Mons, Jean-Michel Nebus, Jean Pierre Villotte, Juan J. Obregon, Raymond Quere
IEEE Transactions on Microwave Theory and Techniques Vol 52, No.3,pp 805-812, March 2004.

17. Linearization of Large Signal Scattering Functions
Jan Verspecht, Dylan F. Williams, Dominique Schreurs, Kate A. Remley, Michael D. McKinley
IEEE Transactions on Microwave Theory and Techniques Vol 53,No.4,pp 1369-1376, 2005

18. Poly Harmonic Distortion Modelling

David E. Root, Jan Verspecht,

IEEE Microwave Magazine, Vol. 7, Issue 3, June 2006, pp. 44-57

19. Broad-Band Poly-Harmonic Distortion (PHD) Behavioural Models from Fast Automated Simulations and Large Signal Vectorial Network Measurements.

David E. Root, Jan Verspecht, David Sharrit, John Wood, Alex Cognata

IEEE Transactions on Microwave Theory and Techniques Vol 53,No.11,2005

20. X-Parameters: The new paradigm for measurement, modeling and design of nonlinear RF and microwave components

David E. Root, Jason Horn, Loren Betts, Chad Gillease, Jan Verspect

Microwave Engineering Europe,Dec 2008,www.mwee.com

21. Advanced Engineering Mathematics,

Glin James, Third Edition, Pearson Educational LTD, 1993, 1994, ISBN0 13045425-7, section 5.33, pp359-360

22. Load Pull + NVNA = Enhanced X-Parameters for PA Designs with High Mismatch and Technology-Independent Large-Signal Device Moels

Gary Simpson, Jason Horn, Dan Gunyan, David E Root,

Application Note 5A.041,www.maurymw.com

23. SFunctions.pdf, downloaded from http://www.nmdg.be/start.html on 12th August 2010, page 6

24. A Novel Approach for Effective Import of Nonlinear Device Characteristics into CAD for Large Signal Power Amplifier Design,
Hao Qi, Johannes Benedikt, Paul Tasker, MTT IMS 2006, pp477,480

Chapter 3 – modeling device behavior at a fundamental frequency

3.1 Introduction

This chapter contains a detailed discussion of the application of the Poly-Harmonic-Distortion Model and Hot-S-Parameters. Also the author's investigations into mixing based descriptions to model continuous wave (CW) load-pull data of transistors and the level of approximation each model makes to this end, providing information about the ability of each model to encapsulate design information. The author notes that the Poly-Harmonic-Distortion model was originally designed to look at cascaded systems constructed from designed and matched components and the work in the following sections should not detract from the results of those investigations.

3.2 Detailed study of Hot-S-Parameters and PHD models when used to model fundamental load-pull

In this section the simulations that were presented in chapter 2 have been revisited and further developed to explain in more detail the extraction of Hot-S-Parameters

and PHD Model. Figure (1)(top) shows a data set produced by the simulation where a sweep of the magnitude and phase difference between the fundamental travelling waves at the ports of the simulated device has been made. This is shown in figure (2); figure (1) (bottom) shows the gain and power curves for the center of the sweep. The labeled points ‘A’,’B’ and ‘C’ are points at which the extraction of Hot-S-Parameters and PHD model will been made.

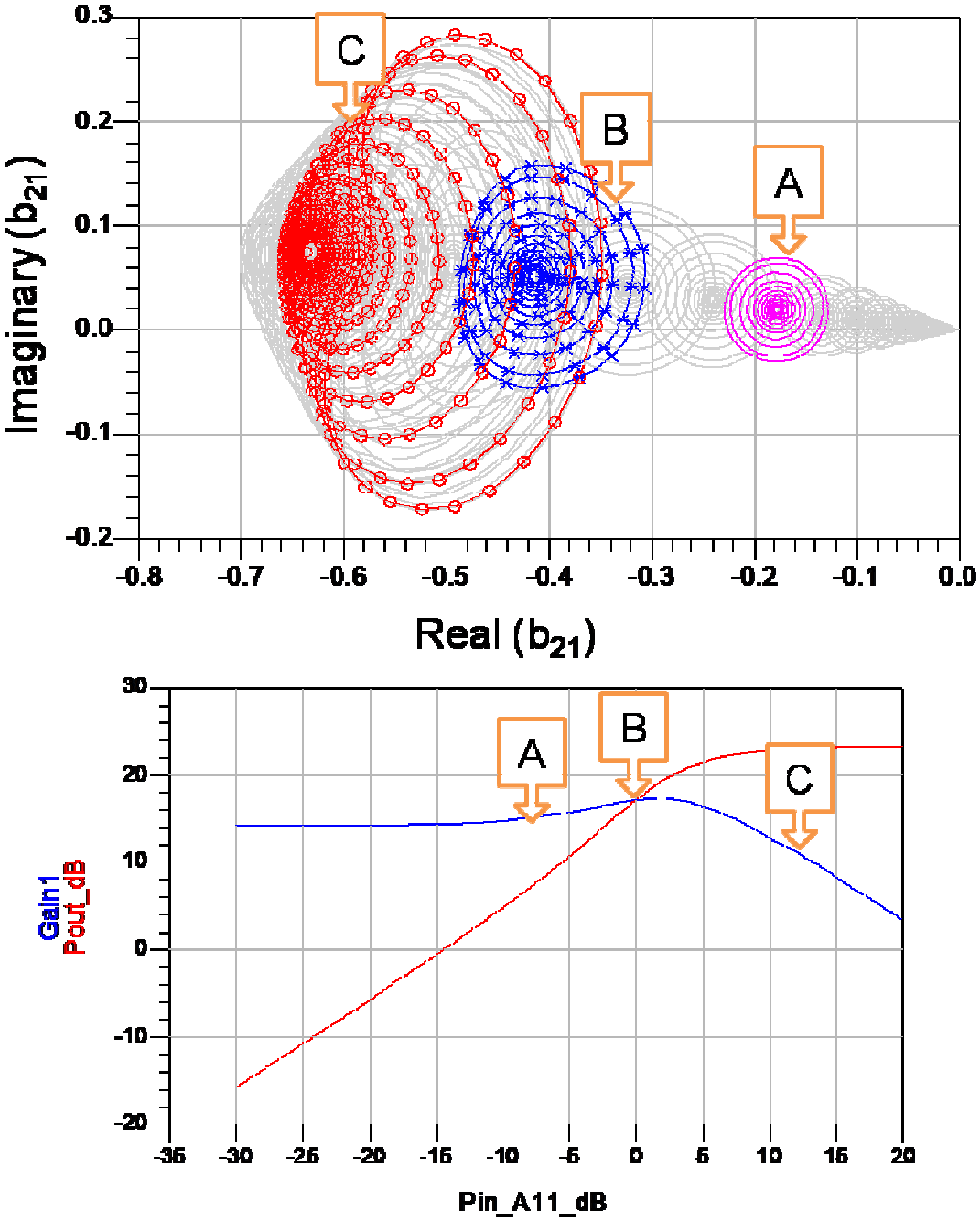

Figure (1)
Simulated Hot-S-Parameter Measurements

Figure (2)
Hot-S-Parameter sweeps of a two-port-network

Figure (3a) shows the extraction of PHD Model and Hot-S-Parameters at Location 'A' in figure 1. At Location 'A' the device under test is operating in an approximately linear manor. In this region the loci drawn by sweeping the magnitude and phase of 'A_{21}' is nearly circular, also indicating that the device can be approximated to a linear system under these conditions. Figure (3b) shows the load perturbations due to the sweep of 'A_{21}' and figure (3c) shows the difference in the predictions of power around the sweep of phase for the largest magnitude of 'A_{21}'; between the PHD Model, Hot-S-Parameters and the harmonic balance simulation. At this level of $|A_{11}|$ and within this region of the sweep the both the X-parameter and the s-parameter extractions agree with each other and both model the devices' performance accurately.

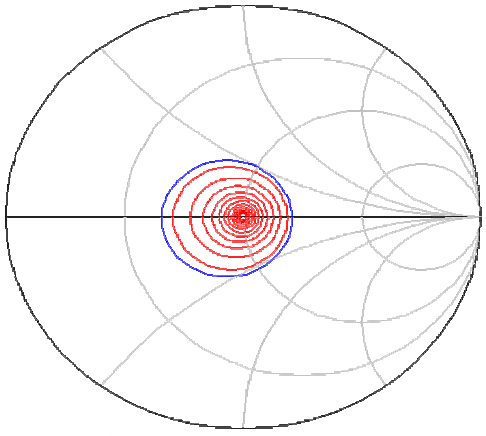

Figure (3A)
Extraction of Hot S-Parameters and PHD Model at point (A) in figure (1)
Output Load Area Swept

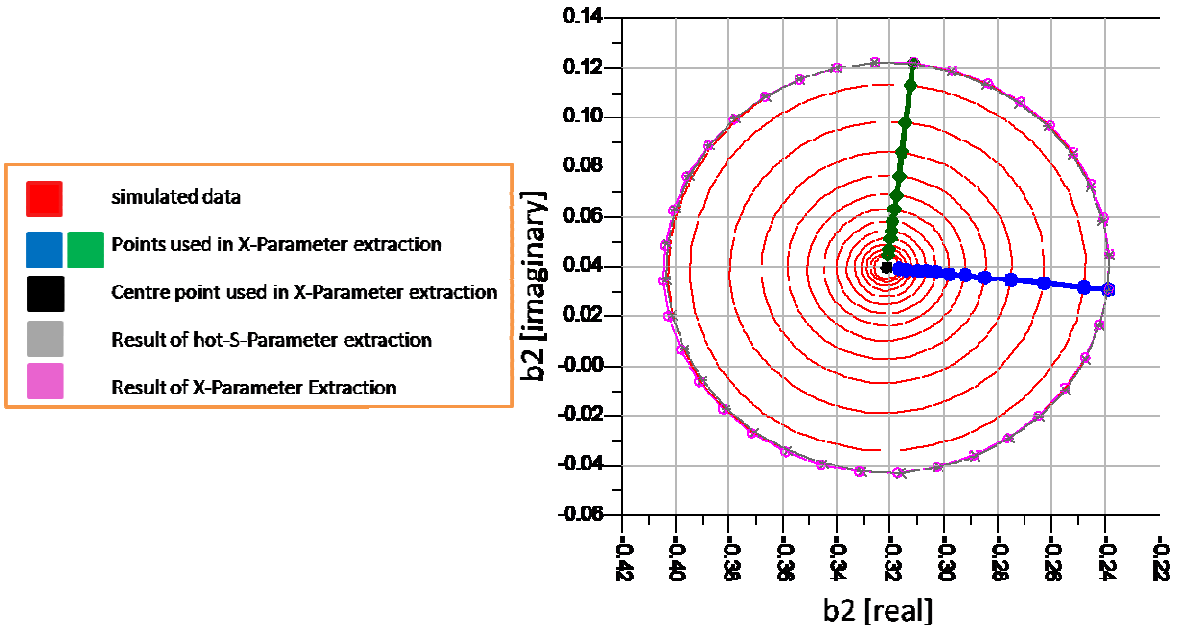

Figure (3B)
Extraction of Hot S-Parameters and PHD Model at point (A) in figure (1)
Simulated and extracted Loci of b_{21}

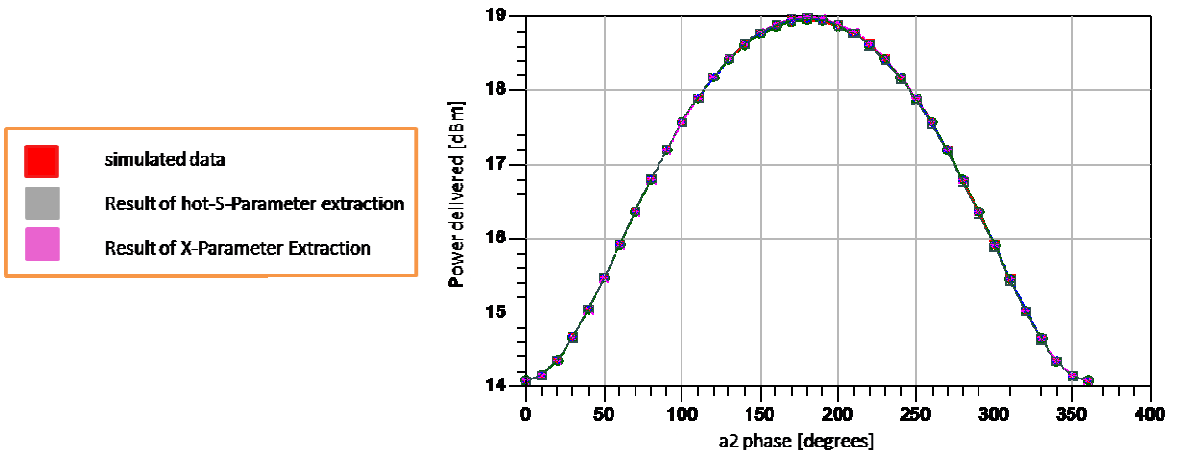

Figure (3C)
Extraction of Hot S-Parameters and PHD Model at point (A) in figure (1)
Simulated and extracted power delivered by 'b_{21}'

Moving further up the sweep of '$|A_{11}|$' to location 'B' figure (4), the loci of 'B_{21}' have become distorted, due to a compression at locations within the sweep. The extraction of both the Hot S-Parameters and the PHD Model has begun to fail. Figure (4c) shows the prediction of the power that each extraction would give it can be seen that both the PHD Model and the Hot S-Parameters failed to predict the

compressive region within the sweep and that the PHD Model give a less accurate prediction of the output power from the simulated device than the Hot S-Parameter solution. The PHD Model solution is less accurate due to the fact that it was locked onto three extraction points, one at the origin of the 'A_{21}'loci, and the two quadrature points on the loci. This gives good agreement on the non compressed sides of the loci and poor agreement on the compressed side where the over prediction of power occurs. The Hot S-Parameter extraction is better but still fails, because it finds the best mean solution to fit the observed data set. It should also be noted that different extraction algorithms for the PHD Model can give improved results, but are still unable to capture the actual device behaviour.

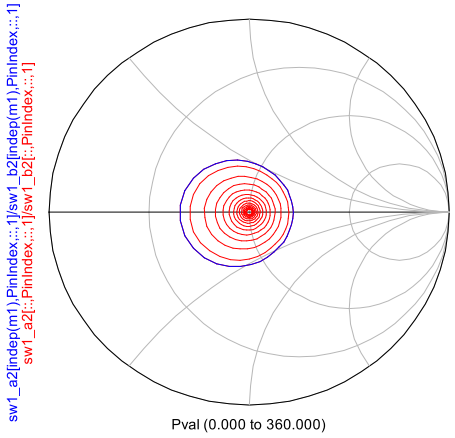

Figure (4A)
Extraction of Hot S-Parameters and PHD Model at point (B) in figure (1)
Output Load Area Swept

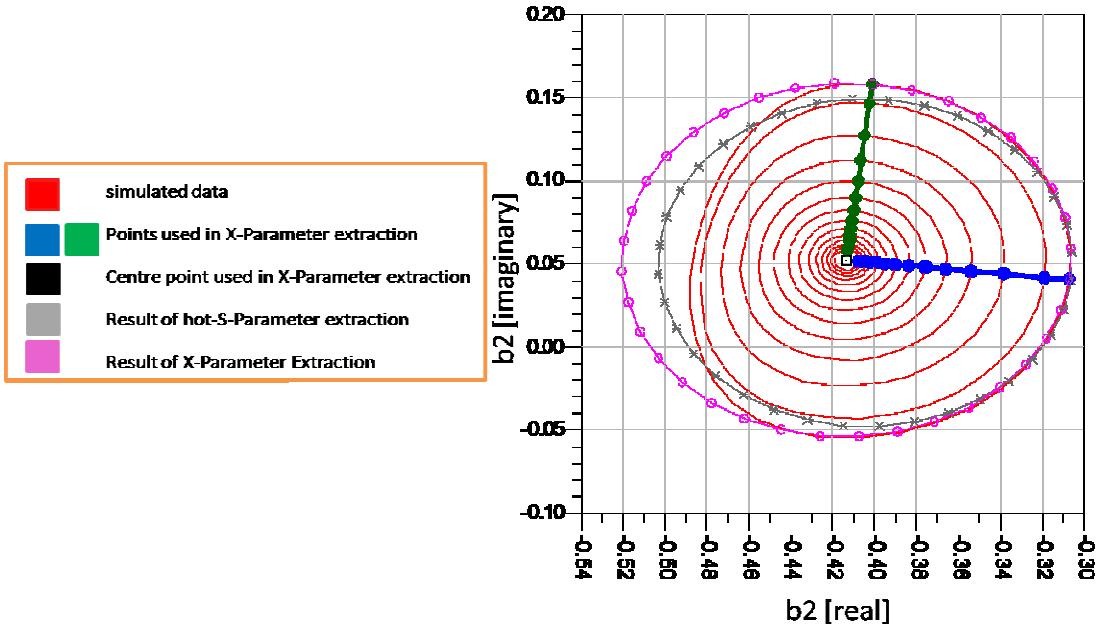

Figure (4B)
Extraction of Hot S-Parameters and PHD Model at point (B) in figure (1)
Simulated and extracted Loci of b_{21}

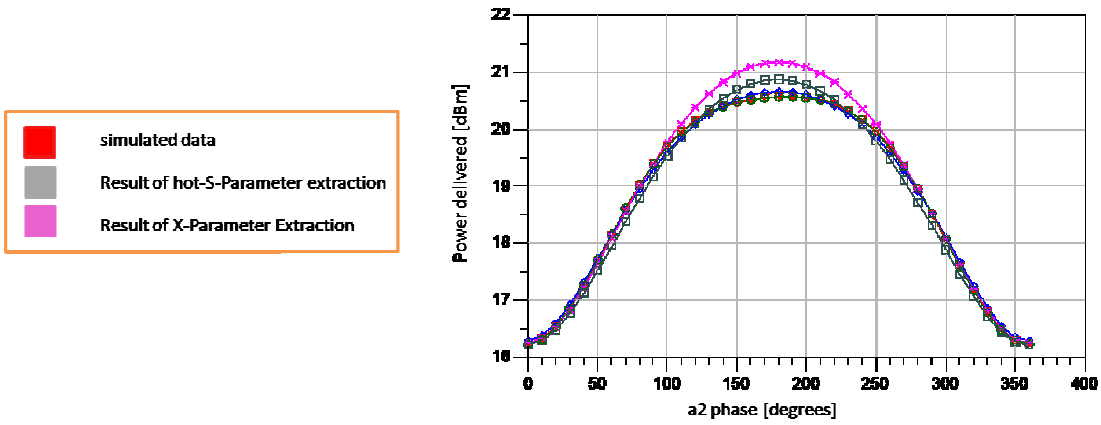

Figure (4C)
Extraction of Hot S-Parameters and PHD Model at point (B) in figure (1)
Simulated and extracted power delivered by 'b_{21}'

Figures (5) and (6) show the same extraction when applied at the highest level of $|A_{11}|$, approximately the 3dB compression point for the largest $|A_{21}|$, figure (5) and a smaller $|A_{21}|$ figure (6). Figure (5) shows the same but more accentuated problems as in figure (4), but in figure (6) as the magnitude of $|a_{21}|$ is reduced, the Hot S-

Parameters and the PHD Model give better results and more accurately represent the simulated data sets.

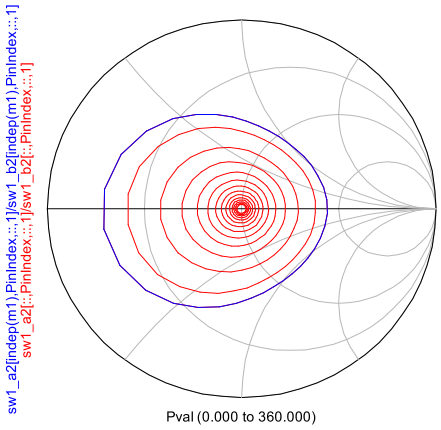

Figure (5A)
Extraction of Hot S-Parameters and PHD Model at point (C) in figure (1)
Output Load Area Swept

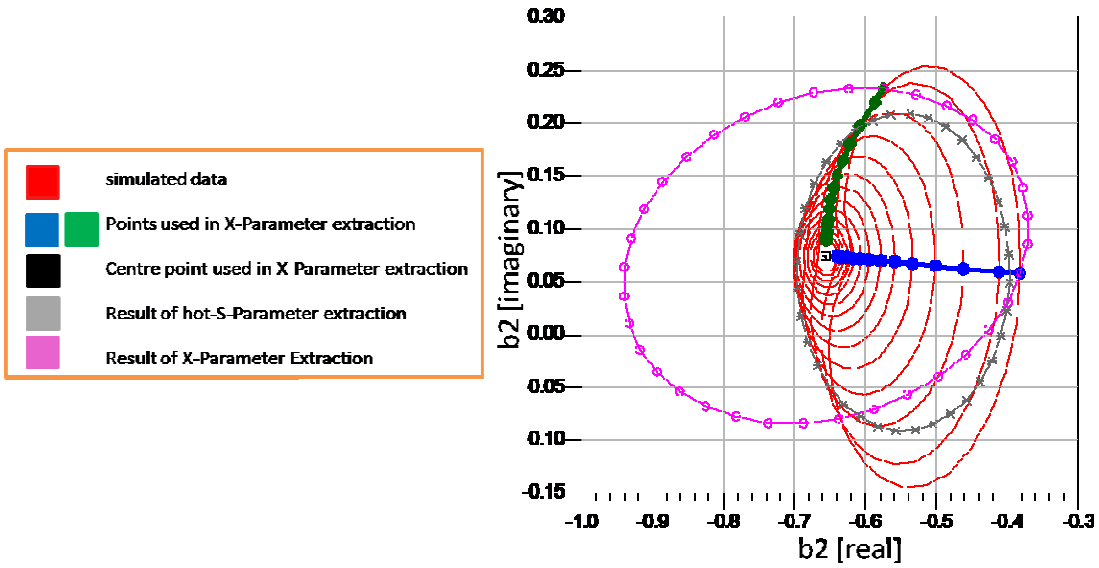

Figure (5B)
Extraction of Hot S-Parameters and PHD Model at point (C) in figure (1)
Simulated and extracted Loci of b_{21}

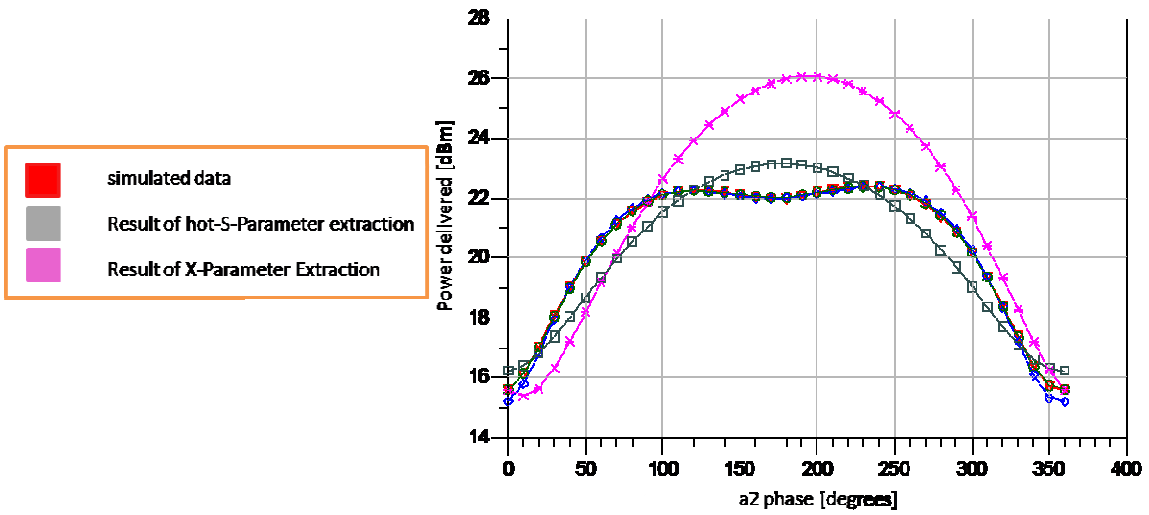

Figure (5C)
Extraction of Hot S-Parameters and PHD Model at point (C) in figure (1)
Simulated and extracted power delivered by 'b_{21}'

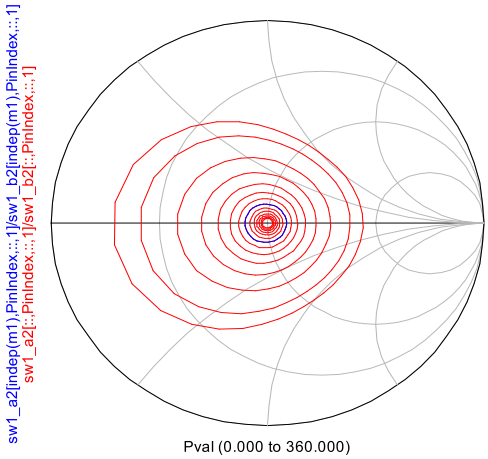

Figure (6A)
Extraction of Hot S-Parameters and PHD Model at point (C) in figure (1)
Output Load Area Swept

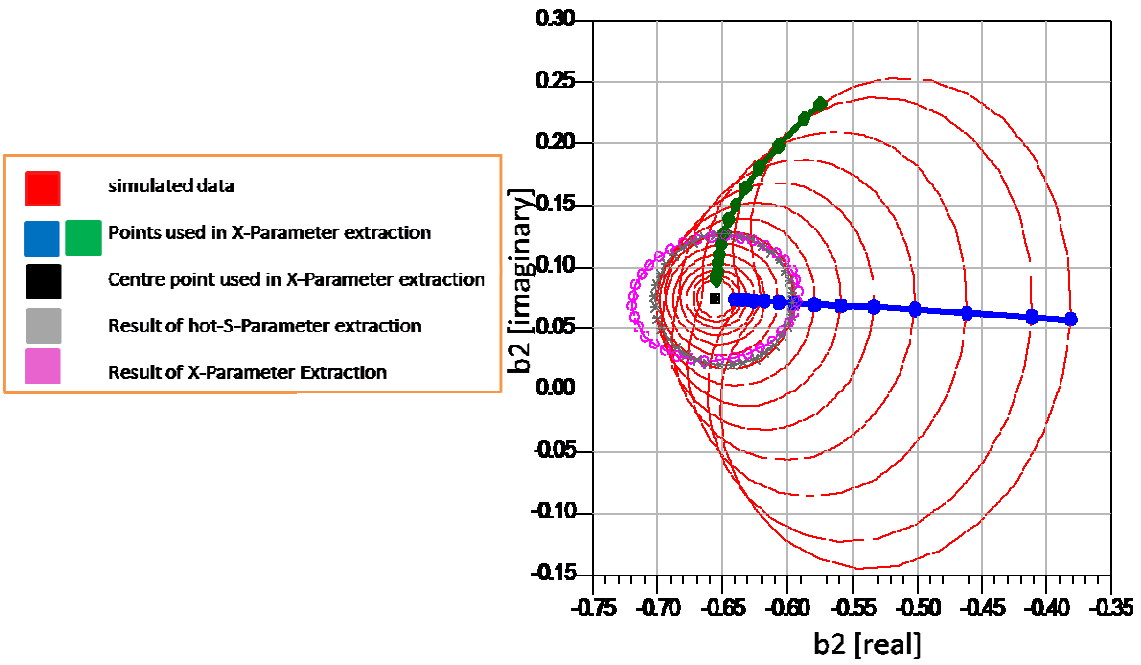

Figure (6B)
Extraction of Hot S-Parameters and PHD Model at point (C) in figure (1)
Simulated and extracted Loci of b_{21}

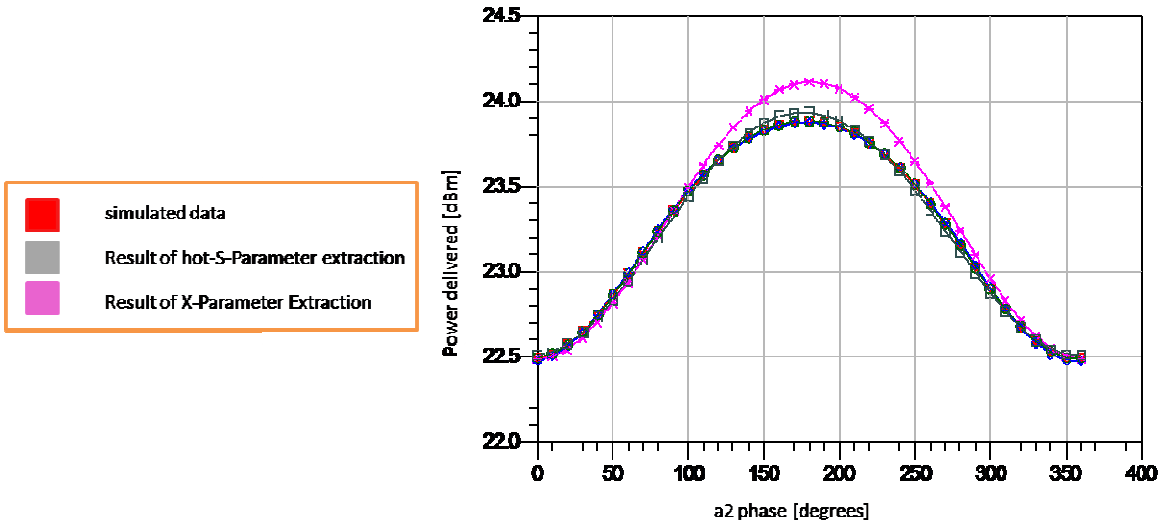

Figure (6C)
Extraction of Hot S-Parameters and PHD Model at point (C) in figure (1)
Simulated and extracted power delivered by 'b_{21}'

Figures (3), (4), (5) and (6) show how the extracted Hot S-Parameters and PHD model predict the devices output power, and the values of 'B_{21}' that were used within the extraction process it has not been discussed how these parameters behave

when used to extrapolate or interpolate. Figures (7) and (8) show extrapolation and interpolation of hot S-Parameters and the PHD model at the highest level of $|A_{11}|$. As in figures (5) and (6), figure (7a) shows how the use of Hot S-Parameters give erroneous extrapolation results. In this figure a nearly circular loci of 'B_{21}' is scaled up to predict a 'B_{21}' loci that is neither circular nor located around the same origin as the original extraction. Figure 7b shows the same problem the other way round. Here the largest 'B_{21}' locus was fitted, and the extracted parameters were used to predict smaller 'B_{21}' loci. This fails at the centre because of the failure of the extraction process to predict the locations of the smaller 'B_{21}' loci, as the origin of the loci cannot be included within the extraction. The extrapolation using the PHD Model shows the same problems as with the Hot-S-Parameters, when a small drive loci is used to predict large drive loci of 'B_{21}' in figure (8a). But unlike the Hot-S-Parameters as the origin of the loci was used in the extraction process the PHD Model is able to interpolate back to the origin of the loci and the parameters work best closer to the origin.

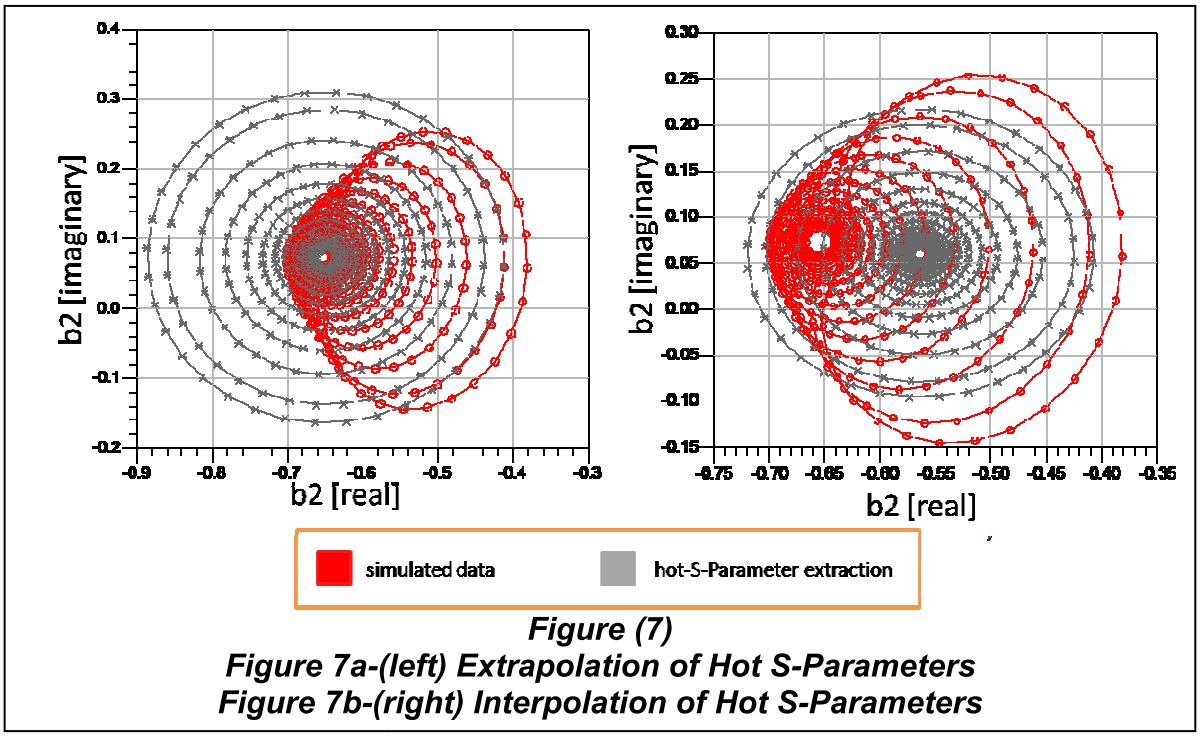

Figure (7)
Figure 7a-(left) Extrapolation of Hot S-Parameters
Figure 7b-(right) Interpolation of Hot S-Parameters

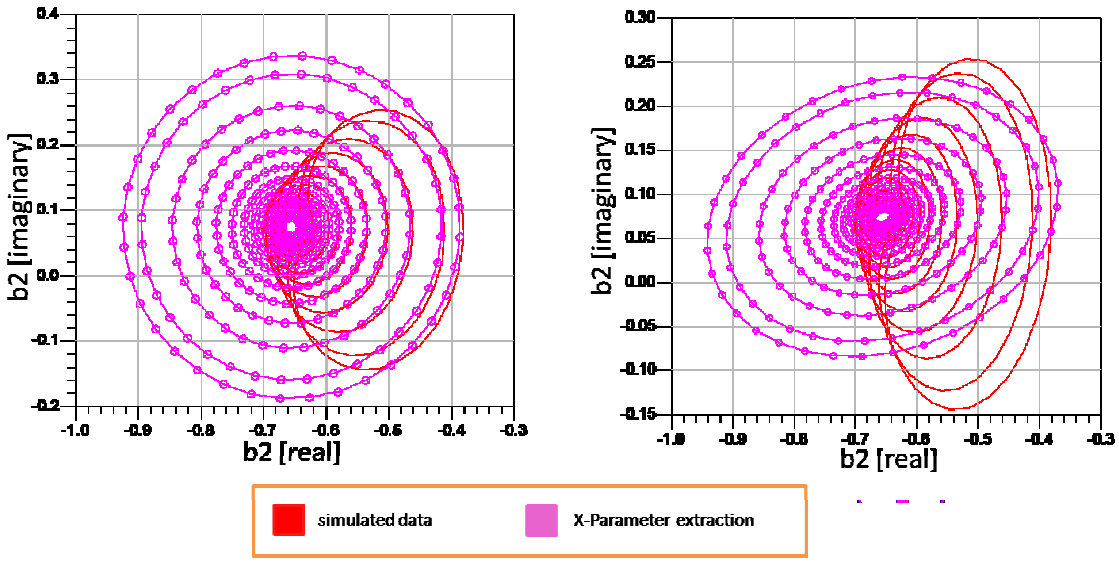

Figure (8)
Figure 8a-(left) Extrapolation of PHD Model
Figure 8b- (right) Interpolation of PHD Model

These simulations give some insight into the expected accuracy of any extraction of Hot S-Parameters and the PHD Model. Both methods generate linear-parameterizations which cannot be guaranteed to predict outside the linear region of the DUT output characteristic. In the compressive region of the DUT characteristic, the area over which the assumption holds reduces as a function of how compressed the DUT is. This observation was made also in [1] where the author suggested that Polynomials of higher order were needed to model significant areas of load-pull data that are required to model a design relevant data, this conclusion can also be inferred in work by Vershpect [2]. These observations explain why Agilent adopted a lookup table approach when looking at fundamental load-pull using X-parameters.

3.3 Development of generic models of the effects of fundamental load-Pull

The previous section explained the problems with using Hot S-Parameters and the PHD Model to represent fundamental load-pull data. To develop the ideas further it

was decided to investigate other related frameworks to see if better descriptors of load pull could be found. One such route was exploited by H. Qi in [3][4] and will be developed further in this section.

In [3-4] H. Qi used a polynomial method which can be related to the voltera series as shown in (1) or (2) to derive 3rd order equivalents of the Poly-Harmonic-Distortion Model. The result that was derived in Qi's work is shown in (3)

$$\begin{aligned} b_p(t) = &\left(g_0 + g_1 a_1(t) + g_2\left(a_1(t)\right)^2 + \ldots + g_n\left(a_1(t)\right)^n\right)\times \\ &\left(k_0 + k_1 a_2(t) + k_2\left(a_2(t)\right)^2 + \ldots + k_m\left(a_2(t)\right)^n\right) \end{aligned} \quad (1)$$

$$b_p(t) = \left(g_0 + g_1\left(a_1(t) + a_2(t)\right) + g_2\left(a_1(t) + a_2(t)\right)^2 + \ldots + g_n\left(a_1(t) + a_2(t)\right)^n\right) \quad (2)$$

$$\begin{aligned} b_1 &= S_{11}a_1 + T_{11}a_1 * Q^2 + S_{12}a_2 + T_{12}a_2 * P^2 \\ b_2 &= S_{21}a_1 + T_{21}a_1 * Q^2 + S_{22}a_2 + T_{22}a_2 * P^2 \end{aligned} \quad (3)$$

$$a_1(t) = |a_{11}|\cos(\omega t + \angle a_{11}) = |a_{11}|\cos(\theta + \angle a_{11}) = \Re\left\{|a_{11}|e^{j\theta}e^{j\angle a_{11}}\right\} \quad (4)$$

$$a_2(t) = |a_{21}|\cos(\omega t + \angle a_{21}) = |a_{21}|\cos(\theta + \angle a_{11}) = \Re\left\{|a_{21}|e^{j\theta}e^{j\angle a_{21}}\right\} \quad (5)$$

By substituting (4) and (5) into (2), then assuming that only the fundamental frequency is injected into the system, then expanding the equations and collecting terms that return to the fundamental frequency the equations figure 9 can be derived[4].

[4] An extended derivation is provided in appendix 1

$$\theta = \omega t$$
$$P = e^{j\angle a_{11}}$$
$$Q = e^{j\angle a_{21}}$$
$$\Phi = e^{j(\angle a_{21} - \angle a_{11})} = Q/P$$

$$b_{21} = \Re\left\{ e^{j\theta} P \left(\begin{array}{l} \frac{g_3 k_2 |a_{21}|^2 |a_{11}|^3}{16} \Phi^{-2} + \\ \left(\frac{g_2 k_1 |a_{21}\| a_{11}|^2}{4} + \frac{3 g_2 k_3 |a_{21}|^3 |a_{11}|^2}{16} \right) \Phi^{-1} + \\ \left(g_1 k_0 |a_{11}| + \frac{3 g_3 k_0 |a_{11}|^3}{4} + \frac{g_1 k_2 |a_{11}\| a_{21}|^2}{2} + \frac{3 g_3 k_2 |a_{21}|^2 |a_{11}|^3}{8} \right) + \\ \left(g_0 k_1 |a_{21}| + \frac{3 g_0 k_3 |a_{21}|^3}{4} + \frac{g_2 k_1 |a_{21}\| a_{11}|^2}{2} + \frac{3 g_2 k_3 |a_{21}|^3 |a_{11}|^2}{8} \right) \Phi + \\ \left(\frac{g_1 k_2 |a_{11}\| a_{21}|^2}{4} + \frac{3 g_3 k_2 |a_{21}|^2 |a_{11}|^3}{16} \right) \Phi^2 + \\ \frac{g_2 k_3 |a_{21}|^3 |a_{11}|^2}{16} \Phi^3 \end{array} \right) \right\}$$

(6)

Figure (9)
Result of 3rd order expansion of eqn 1

Equation (6) in figure (9) can be summarized with a describing function as in (7) which has the same phase reference adjustment as the Poly Harmonic Distortion model [3]. Equation (8) provides one expansion of the describing function in (7) where the magnitude dependence has been absorbed into the $R_n(\ldots)$ functions.

$$b_{21}(\theta) = \Re\left\{ e^{j\theta} P . B_{21}\left(|a_{21}|, |a_{11}|, \Phi \right) \right\} \quad (7)$$

$$\begin{aligned} B_{21}\left(|a_{21}|, |a_{11}|, \Phi \right) = {} & R_{-2}\left(|a_{21}|, |a_{11}| \right) \Phi^{-2} + R_{-1}\left(|a_{21}|, |a_{11}| \right) \Phi^{-1} + R_0\left(|a_{21}|, |a_{11}| \right) + \\ & R_1\left(|a_{21}|, |a_{11}| \right) \Phi + R_2\left(|a_{21}|, |a_{11}| \right) \Phi^2 + R_3\left(|a_{21}|, |a_{11}| \right) \Phi^3 \end{aligned} \quad (8)$$

The Poly-Harmonic-Distortion model can be calculated from the functions $R_{-1}(\ldots)$, $R_0(\ldots)$ and $R_1(\ldots)$ to calculate X^T, X^F and X^S as in equation (9) which can also be used to test the validity of the Poly-Harmonic-Distortion model in any particular situation.

relate to S_{21} and S_{22}. The original equations presented by H. Qi can be written in a similar manner and is shown in (9) and (10)

$$b_1 = S_{11}|a_1|P + T_{11}|a_1|\frac{Q^2}{P} + S_{12}|a_2|Q + T_{12}|a_2|\frac{P^2}{Q} =$$
$$P\left(S_{11}|a_1| + T_{11}|a_1|\left(\frac{Q}{P}\right)^2 + S_{12}|a_2|\frac{Q}{P} + T_{12}|a_2|\left(\frac{Q}{P}\right)^{-1}\right) = \qquad (9)$$
$$P\left(T_{12}|a_2|\Phi^{-1} + S_{11}|a_1| + S_{12}|a_2|\Phi + T_{11}|a_1|\Phi^2\right)$$

$$b_2 = S_{21}|a_1|P + T_{21}|a_1| * \frac{Q^2}{P} + S_{22}|a_2|Q + T_{22}|a_2|\frac{P^2}{Q}$$
$$P\left(S_{21}|a_1| + T_{21}|a_1|\left(\frac{Q}{P}\right)^2 + S_{22}|a_2|\frac{Q}{P} + T_{22}|a_2|\left(\frac{Q}{P}\right)^{-1}\right) = \qquad (10)$$
$$P\left(T_{22}|a_2|\Phi^{-1} + S_{21}|a_1| + S_{22}|a_2|\Phi + T_{21}|a_1|\Phi^2\right)$$

	Φ^{-6}	Φ^{-5}	Φ^{-4}	Φ^{-3}	Φ^{-2}	Φ^{-1}	Φ^{0}	Φ^{1}	Φ^{2}	Φ^{3}	Φ^{4}	Φ^{5}	Φ^{6}	Φ^{7}
$\lvert a_{21}\rvert^0$							1st							
$\lvert a_{21}\rvert^1$						3rd		1st						
$\lvert a_{21}\rvert^2$					3rd		3rd		3rd					
$\lvert a_{21}\rvert^3$				5th		3rd		3rd		3rd				
$\lvert a_{21}\rvert^4$			5th		5th		5th		5th		5th			
$\lvert a_{21}\rvert^5$		7th		5th		5th		5th		5th		5th		
$\lvert a_{21}\rvert^6$	7th		7th		7th		7th		7th		7th		7th	
$\lvert a_{21}\rvert^7$		7th		7th		7th		7th		7th		7th		7th

	Φ^{-3}	Φ^{-2}	Φ^{-1}	Φ^{0}	Φ^{1}	Φ^{2}	Φ^{3}	Φ^{4}	Φ^{5}
$\lvert a_{21}\rvert^0$				1st					
$\lvert a_{21}\rvert^1$			3rd		1st				
$\lvert a_{21}\rvert^2$		5th		3rd		3rd			
$\lvert a_{21}\rvert^3$	7th		5th		3rd		5th		
$\lvert a_{21}\rvert^4$		7th		5th		5th		7th	
$\lvert a_{21}\rvert^5$			7th		5th		7th		
$\lvert a_{21}\rvert^6$				7th		7th			
$\lvert a_{21}\rvert^7$					7th				

$$\Phi = e^{j(\angle a_{21} - \angle a_{11})} = Q/P$$

Figure (10)
Terms generated up to 7th order by:
Figure (10a) (top) eqn 1
Figure (10b) (bottom) eqn 2

Figures (10a) and (10b) show the results of successive expansions of (1) and (2) after collection terms that arrive back at the fundamental frequency. In Figures (10a) and (10b), looking across the top of the figures the phase difference between the input and output fundamental signals a_{11} and a_{21} is raised from negative powers through to positive powers and down the vertical axis powers of the magnitude of a_{21} are represented each element that is filled is colour coded and labelled to represent the order of the term that generated it, in equations (1) and (2). It is interesting to note that for both initial equations (1) or (2) that the same space and locations would

be filled at infinite order and by populating the grids in (10) it would not be possible to determine the original source polynomial. The results shown in figure (10) probably have similarities to the VIOMAP formulations suggested by Verbyst in [5]. If in figure (10a) the magnitude terms are implied by functional variables as in (6) and (7) equations (8) and (9) can be written and for figure 7b.

$$b_p\left(|a_{11}|,|a_{21}|,bias,frequency,\theta\right)=\Re\left\{e^{j\theta}P\sum_{n=N-1}^{N}R\left(|a_{11}|,|a_{21}|,bias,frequency\right)\Phi^n\right\} \quad (8)$$

$$B_p\left(|a_{11}|,|a_{21}|,bias,frequency,\Phi\right)=\sum_{n=N-1}^{N}R\left(|a_{11}|,|a_{21}|,bias,frequency\right)\Phi^n \quad (9)$$

$$b_p\left(|a_{11}|,|a_{21}|,bias,frequency,\theta\right)=\Re\left\{e^{j\theta}P\sum_{n=-\frac{1}{2}(N-1)}^{\frac{1}{2}(N+1)}R\left(|a_{11}|,|a_{21}|,bias,frequency\right)\Phi^n\right\} \quad (10)$$

$$B_p\left(|a_{11}|,|a_{21}|,bias,frequency,\Phi\right)=\sum_{n=-\frac{1}{2}(N-1)}^{\frac{1}{2}(N+1)}R\left(|a_{11}|,|a_{21}|,bias,frequency\right)\Phi^n \quad (11)$$

It should be noted however that equations (8) - (10) do not provide a linearization or a simplification of the complexity of the original equations. Instead they allow the phase behaviour of the DUT to the incident travelling waves to be partitioned from the response to the magnitude of them. To extract a set of values for the coefficients to these functions requires only a sweep of the phase difference between the incident travelling wave's a_{11} and a_{21} while there magnitudes are held constant. After collecting these data sets, it is possible to extract the coefficients using a method of means or averages similar to that of the complex Discrete Fourier Transform DFT, or the complex Fast Fourier Transform FFT; this is an extension of the method used in [1]. If 'X' samples are taken of $B_p(\ldots)$ at equidistant phase locations then the coefficients of (9) can be extracted using (10) or a equivalent.

$$R_n\left(|a_{11}|,|a_{21}|,bias,frequency\right)=\sum_{x=0}^{X}B_p\left(|a_{11}|,|a_{21}|,bias,frequency,x\right)e^{-j2\pi n\frac{x}{X}}$$
$$n\in Z,\ -\frac{X}{2}\le n\le\frac{X}{2} \qquad (10)$$

This technique has been demonstrated on the simulated Hot S-Parameter data of the previous section and the Zero Order, 3rd order and 5th order extractions in phase in terms of (11) are shown in figure 11.

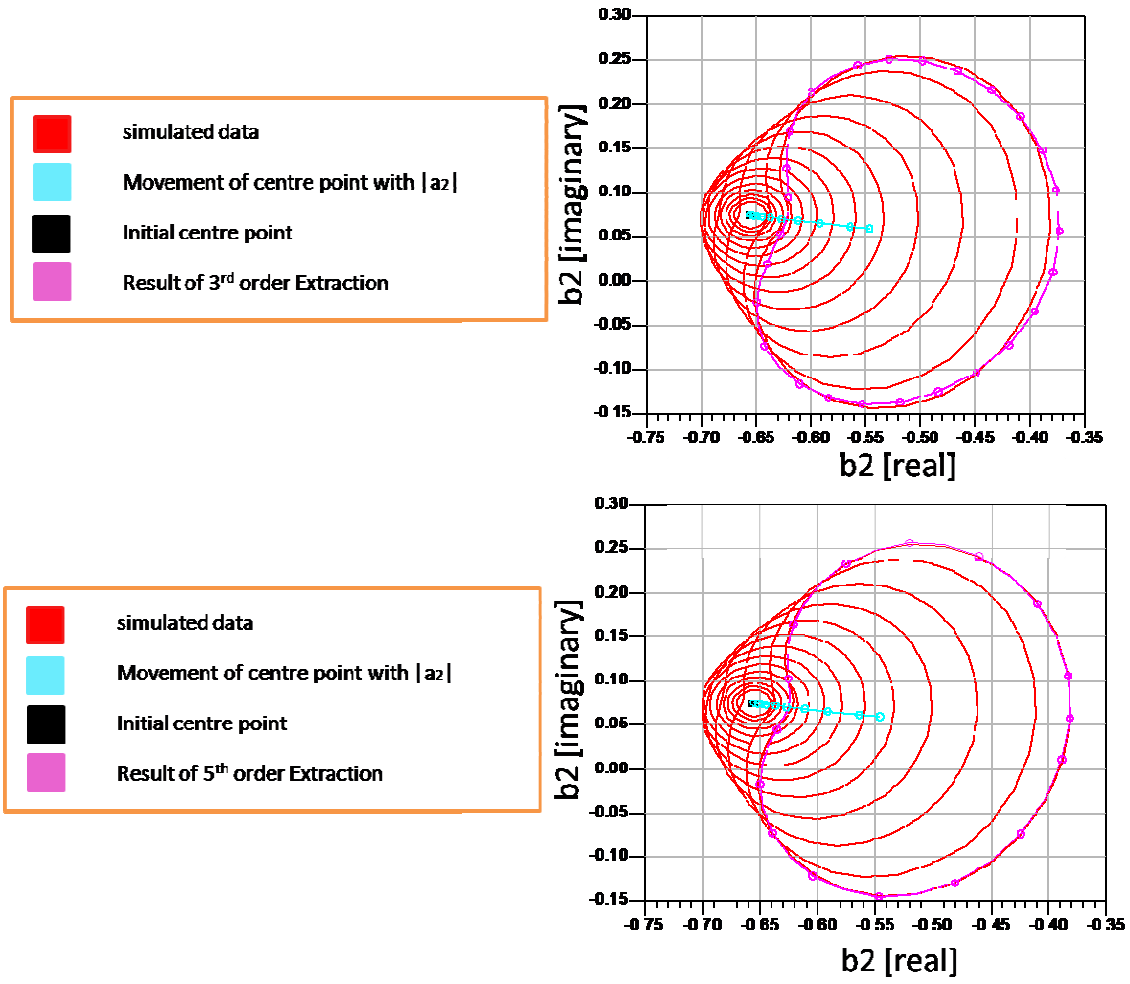

Figure 11
Figure 11a (top) 3rd order extraction in phase
Figure 11b (bottom) 5th order extraction in phase

Figure 11 showed a 0, 3rd and 5th order extractions in phase. The extraction at zero order which is the mean location of each b21 loci has been performed for each magnitude of 'a_{21}' this shows that the centre term in the extraction process moves as

a function of the amplitude of 'a_{21}' as expected from figure (10), this movement limits the range of the PHD model, as the PHD model would assume that the large signal point X^F is Invariant to the magnitude of 'a_{21}'. The 3rd and 5th order extractions show successively better fits to the simulated data for the largest value of $|a_{21}|$, the order to which the extraction of phase terms can be extracted depends on the number of phase locations measured.

Performing the extraction process for the full set of coefficients, in the case this is limited to the 36 data points so that coefficients -17 through to18 can be extracted. Plotting the magnitudes of the coefficients relative to coefficient Zero, figure (12) can be generated. Figure 13 shows the same extraction process where the phase sweep has been conducted in 1^o steps and 360 coefficients have been extracted. The two figures show that care must be taken to ensure that aliased coefficients do not raise the noise floor of the extraction above that of the measurement system.

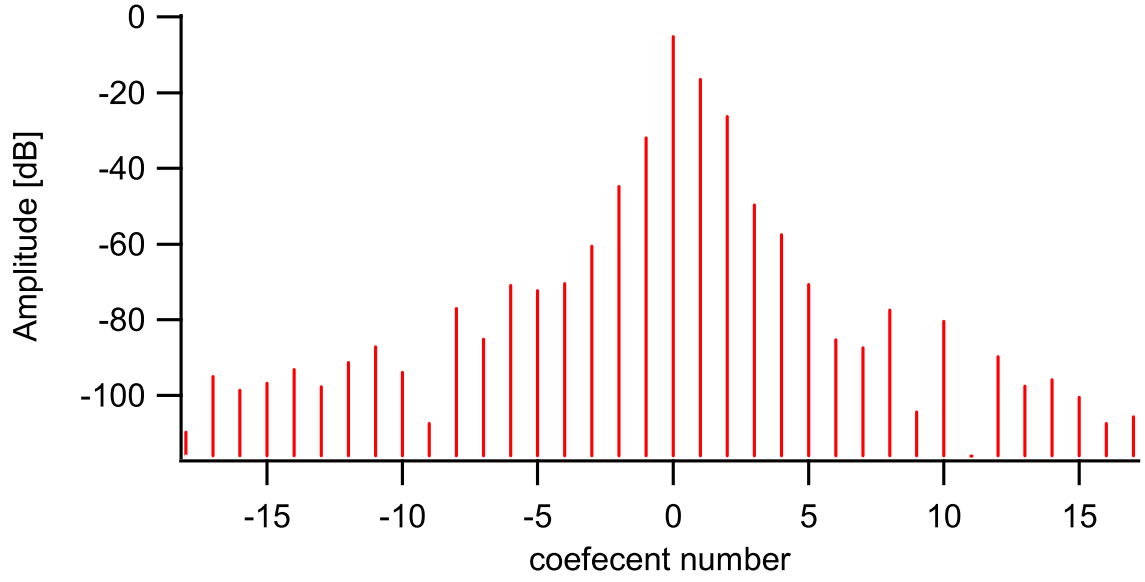

Figure (12)
Results of full extraction process on simulation with 36 phase steps

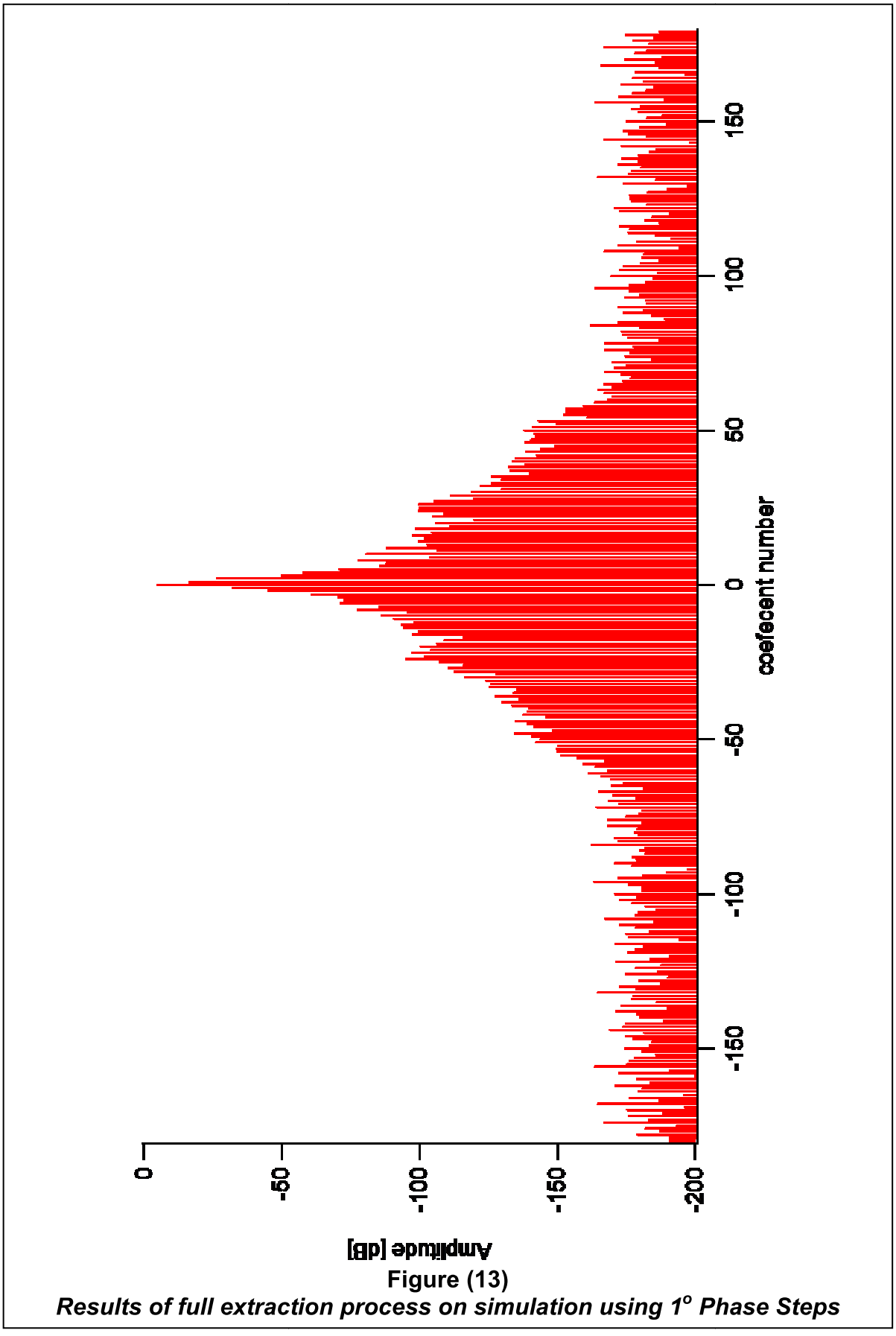

Figure (13)

Results of full extraction process on simulation using 1° Phase Steps

Inclusion of harmonics can be accomplished by extending the formulation as in equation 12, which was used to propose the Direct Waveform Look Up Table, DWLUT in [1].

$$b_{p,h}\left(|a_{11}|,|a_{21}|,bias,frequency,\theta\right)=\Re\left\{e^{j\theta}P^{h}\sum_{n=-\frac{1}{2}(N-1)}^{\frac{1}{2}(N+1)}R_{p,h}\left(|a_{11}|,|a_{21}|,bias,frequency\right)\Phi^{n}\right\} \quad (12)$$

3.4 Measurement and extraction of Model

The previous section discussed the formulation of a general mixing based behavioural model of fundamental load-pull and extracted parts of the model on data sets generated from simulations. In this section the practical considerations and adjustments to the framework will be discussed, as an attempt to directly measure the functions in (9) and (11) is made. This is different from previous work that extracted them from grids load-pull measurements. The results of the extraction of a model of a HBT device supplied by Mimix Europe (now MACOM) will be demonstrated.

3.4.1 Measurement system

The measurement system in use for this extraction is a nonlinear network analyzer system that has been developed at Cardiff University Centre for High Frequency Engineering by Tasker, Benedikt, Williams and others [6]. The systems available are modified network analyzer architectures with receivers capable of measuring “GHz” time domain waveforms. In this thesis, the instruments used were the Microwave Transition Analyzer and a Tektronix Sampling Oscilloscope DSA8200. The system

can be calibrated to measure the voltage and current waveforms present immediate to DUT's RF ports. A diagram of one of these systems is provided in figure (13). The system augmented by an open loop Active-Load-Pull ALP system capable of emulating any passive impedance but can also be used for active injection measurements as in Hot S-Parameters.

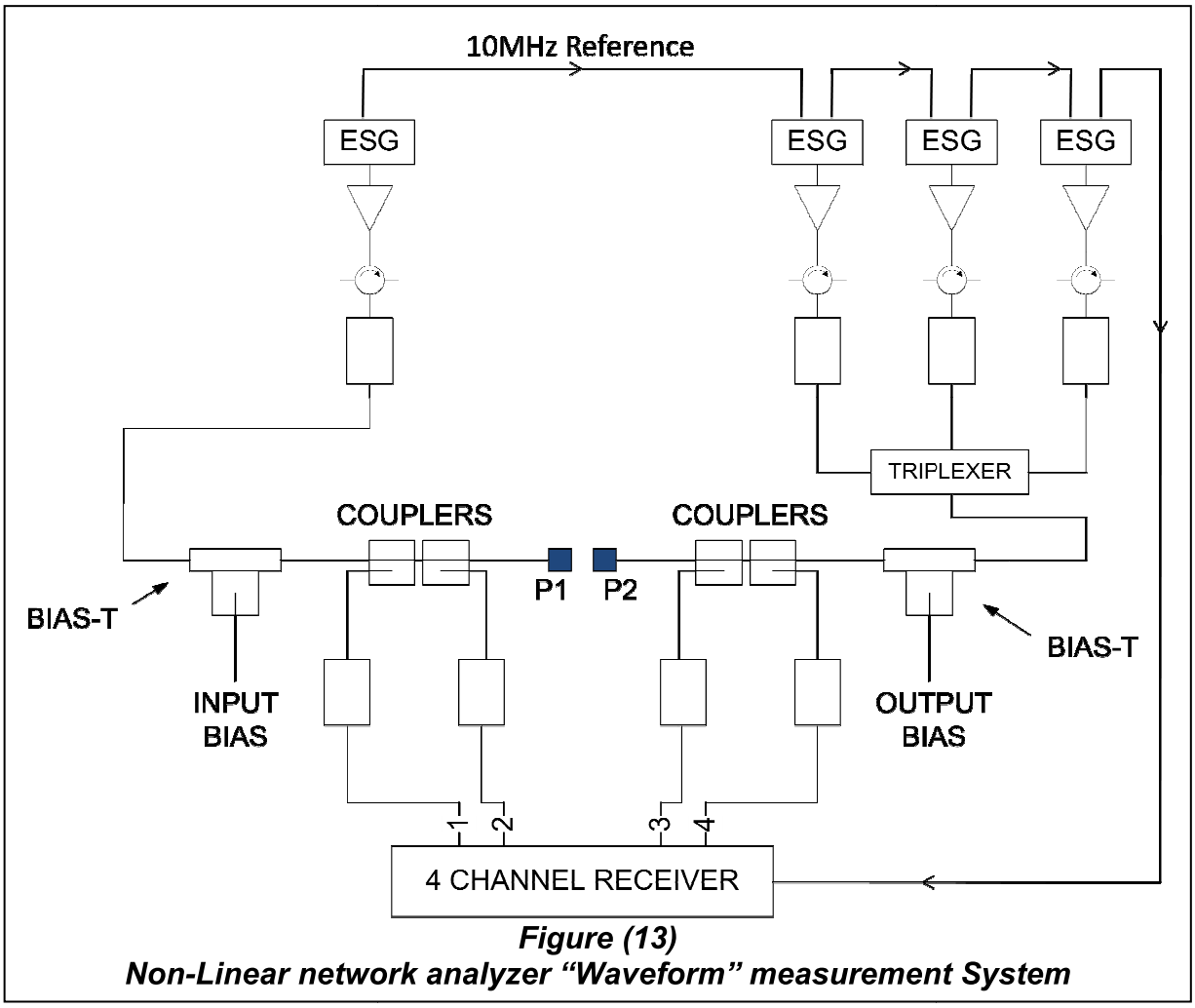

Figure (13)
Non-Linear network analyzer "Waveform" measurement System

3.4.2 Practical Considerations

The required load-pull locus can be achieved by terminating the device into a matched signal source as in the ALP system, injecting power and rotating the phase. However the signal source optimally has a 50 Ohm output impedance, but not

exactly, and the optimum impedance of the DUT may not be anywhere near 50 Ohms. Also any connection between the signal source and the DUT degrades the match to the DUT. This means, that although during the Hot S-Parameter sweep, it was intended to inject a set of waves for 'a_{21}' that map out a circle on the complex plane. In practice the finite reflection coefficient terminating the DUT will distort the sweep as shown in figure (10).

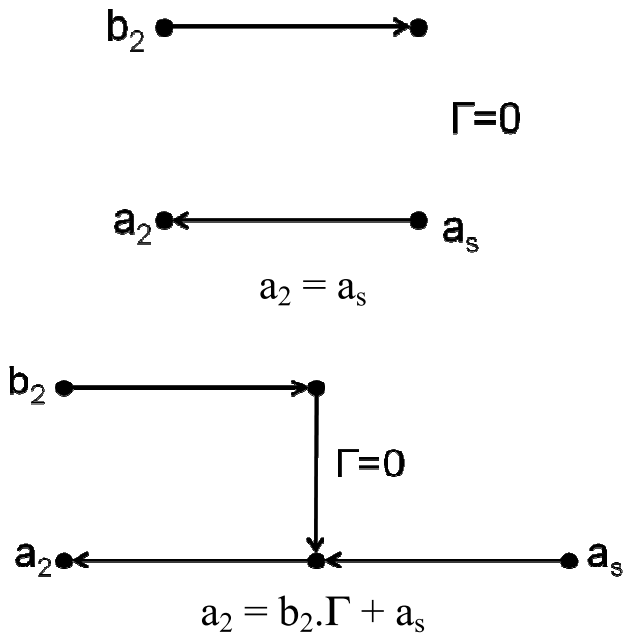

Figure (14)
(Top)Flow diagram of Ideal System load
(Bottom)Flow diagram of Actual System load
in 50 Ohm Referenced System

These problems can be corrected by renormalizing the travelling waves to the impedances presented at the DUT reference planes using eqn's (13) and (14). These are similar to the renormalizations that were demonstrated in [1] which come from the original definitions of travelling waves and s-parameters [7], and were used in [1] to improve the model accuracy.

$$a_2 = \frac{\left(a_1\left(2\Re(Z_2) + Z_1^* - Z_2^*\right) + b_1\left(Z_1 + Z_2^* - 2\Re(Z_2)\right)\right)}{2\sqrt{\Re(Z_1)\Re(Z_2)}} \qquad (13)$$

$$b_2 = \frac{a_1(Z_1^* - Z_2^*) + b_1(Z_1 + Z_2^*)}{2\sqrt{\Re(Z_1)\Re(Z_2)}} \quad (14)$$

To allow the measurement to be conducted near the devices optimum impedance for power, the a_{21} signal is injected on top of a reflective termination through a directional coupler which modifies the system shown in figure (13). The new configuration is shown in figure (15) and in [1] which allows adjustment of the impedance to which the measurements are normalised.

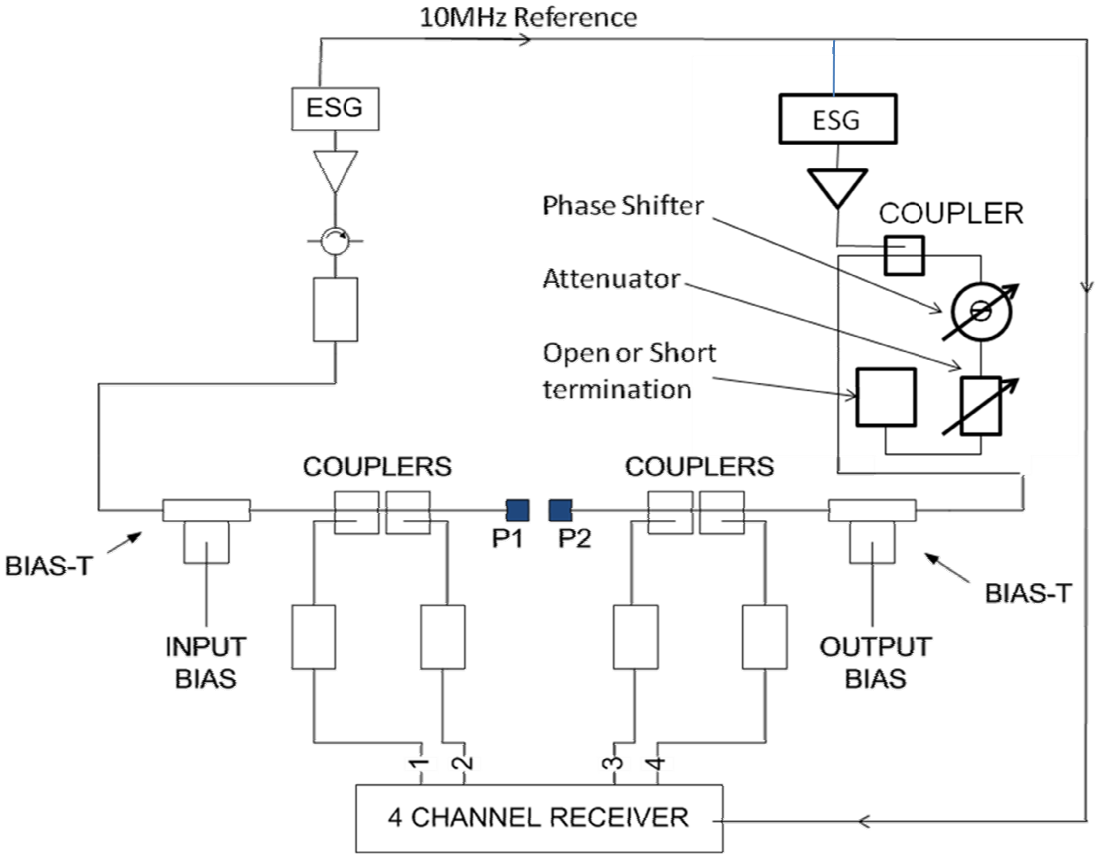

Figure (15)
Architecture for generating the required load-pull loci by integrating an active source with a passive load-pull system

3.4.3 Measurement Results

The techniques and system outlined were applied to a GaAs 8x2x30μm 0.5W HBT operating at 0.9 GHz, Device supplied by Mimix broadband. During the RF

waveform measurements at each input drive level (fixed $|A_{11}|$), a measurement of a Hot S-Parameter/ Load-pull loci consisting of a sequence of n=64 uniformly stepped source phase points, for a sequence of 11 constant $|A_{21}|$ values were measured. The resulting load-pull data is shown in Figure 16. The output power load-pull contours from these measurements show that the load-pull surface covered a 3dB output power range.

The corresponding stimulus A_{11} and A_{21} and response B_{11} and B_{21} travelling waves, as measured, referenced to 50 Ohms are shown in figure 17. The observed behaviour of B_{21} clearly indicating that the device is exhibiting non-linear behaviour. These transform to the required data, for model extraction, of simple fixed A_{11}, circular A_{21} contours, as shown in Figure 18, after renormalization to the system impedance, which was set to be close to the device's optimum impedance of Zopt=37.13 + j 20.02 Ω.

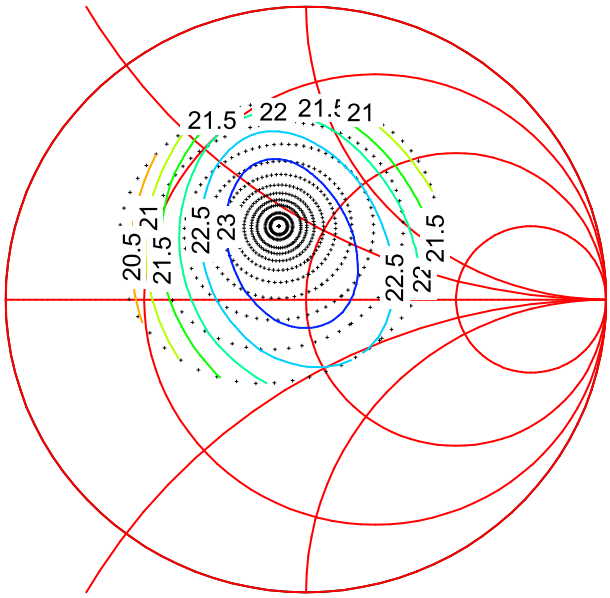

Figure (16)
Measured load-pull loci and the associated output power contours.

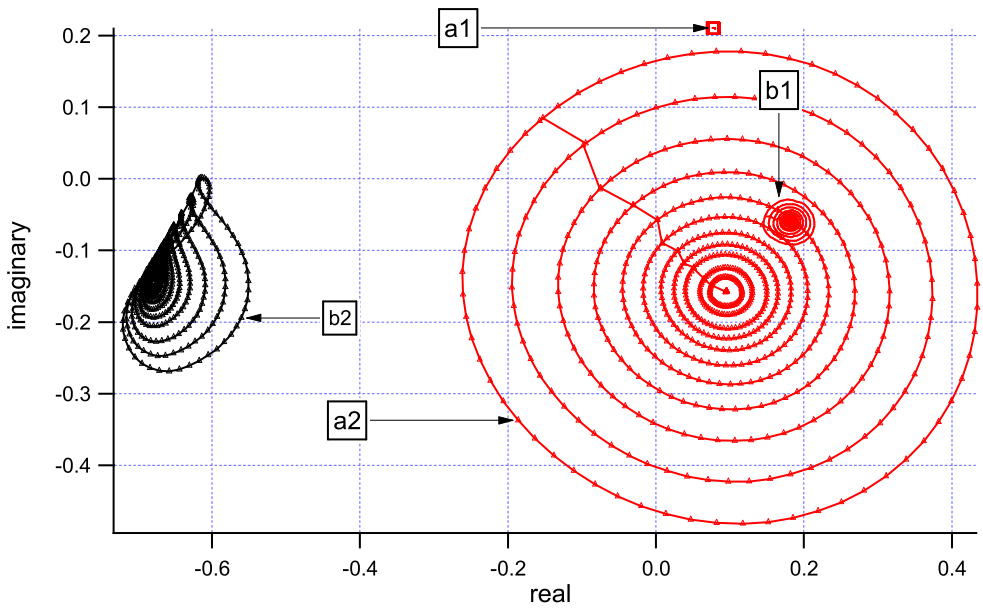

Figure (17)
Measured 'a' and 'b' travelling waves from the sequence of load-pull loci, referenced to the system impedance

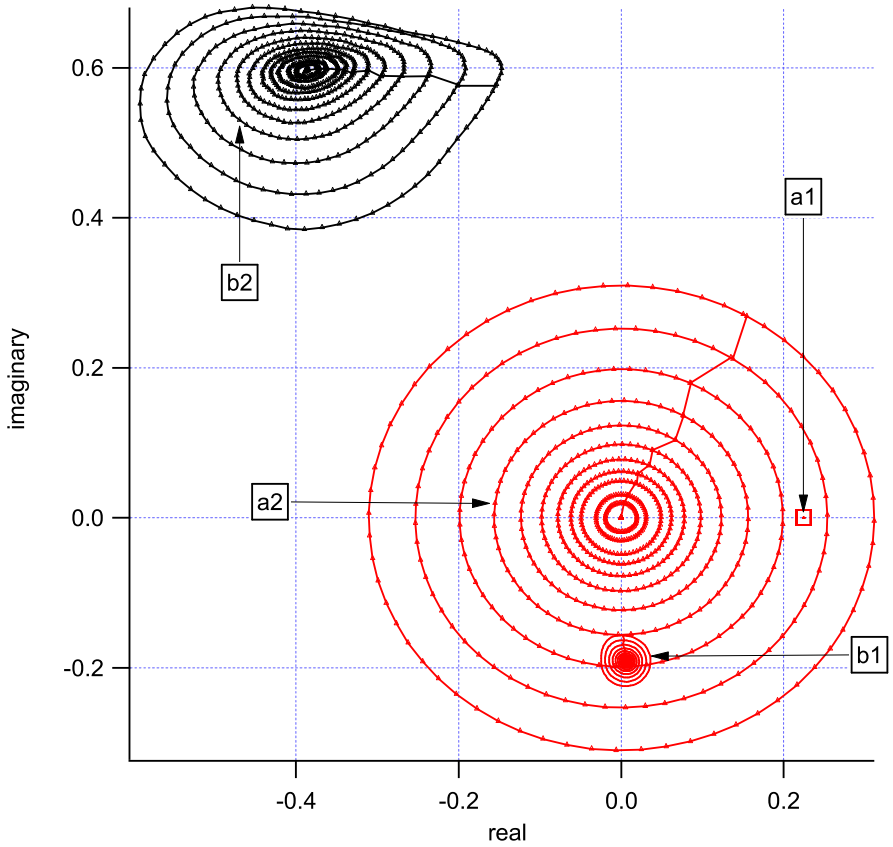

Figure (18)
Measured a and b travelling wave on the sequence of load-pull loci, once renormalized.

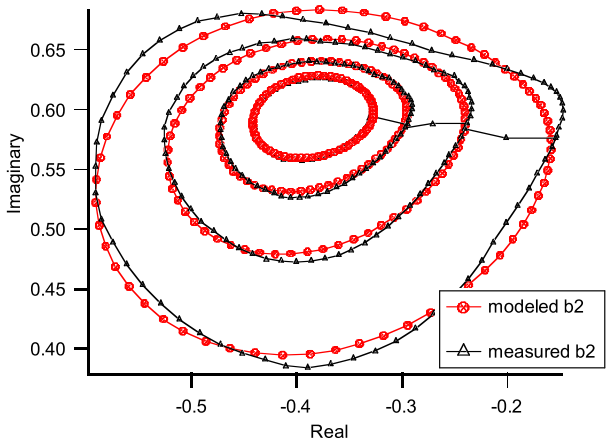

Figure (19)
Comparison the measured and modelled b_2' travelling wave using the 3rd order S and T parameter DWLU behavioural model. As proposed by H. Qi

Figure (19) shows the results of the 3rd order extraction that was proposed by Qi, using the extraction process outlined in this thesis. As can be seen in the figure the extraction fails to map exactly the B_{21} data which is consistent with the formulation being only 3rd order, where as, the data maps a higher order function. At low magnitudes of 'A_{21}', however the model tracks the actual response more closely. Thus 3rd order is clearly adequate for small values of A_{21}, but as A_{21} increases higher orders mixing terms must be considered.

Increasing the order of the extraction, as shown in Figure 20, up to 5th order provides a behavioural model that can now more accurately predict 'B_{21}', and hence the load pull-contours. Figure 21 compares the output power load-pull contours computed from both the measured B_{21} response and the modelled B_{21} performance. Transforming to power contours shown power prediction is within 0.1dB

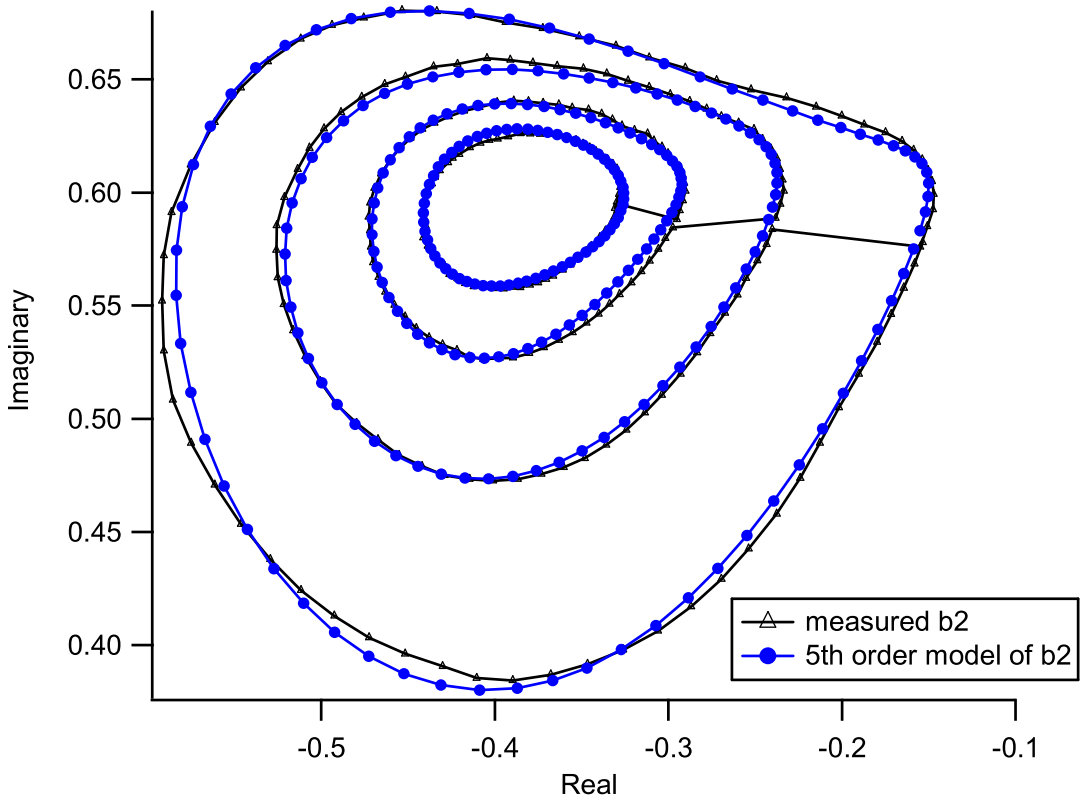

figure (20)
Comparison the measured and modelled b_2' travelling wave using the higher order DWLU behavioural model.

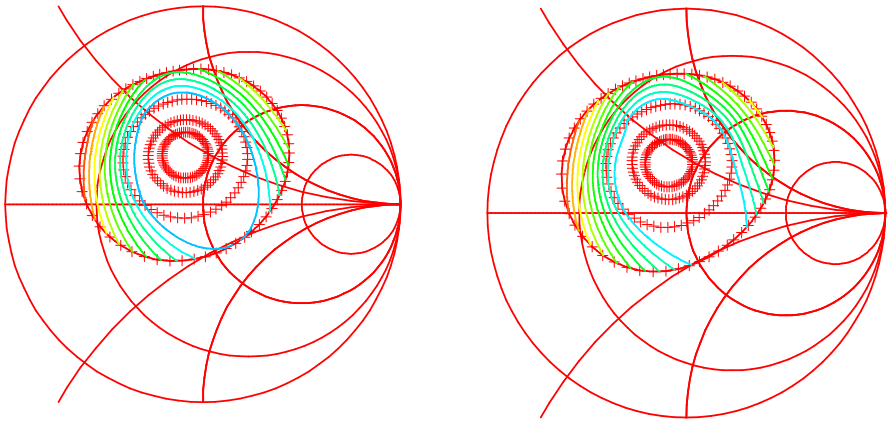

figure (21)
Comparison of modelled (right) and measured (left) output load-pull contours.

This extraction process would seem to have been successful, but when the extraction was extended in an attempt to extract the equivalent of figure 12, the extraction process broke down, after some investigation it was found to be due to

drift and locking errors. The signal sources in the measurement system figures 10 and 11 where the phase of the sources is locked by a 10MHz reference. It was found that the errors due to this could be corrected using a “time-base” interpolation algorithm, on the phase to correct the phase locations, or by a Least-Mean-Squares approach with the actual phase locations as described in figure 22. The results of these extractions are shown in figures 23-24, and the plot of the coefficient spectrum is shown in figure 25 and using an interpolation algorithm.

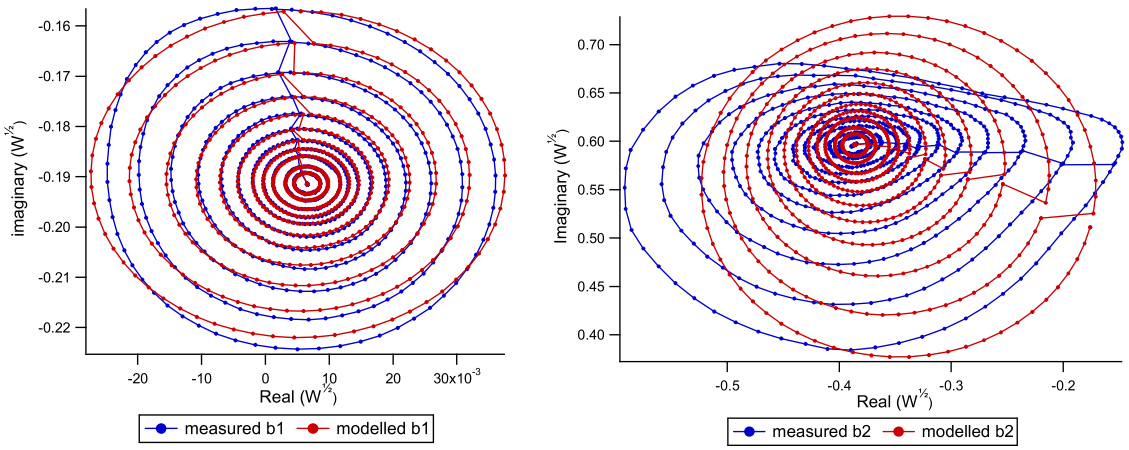

Hot S-Parameters-Linear

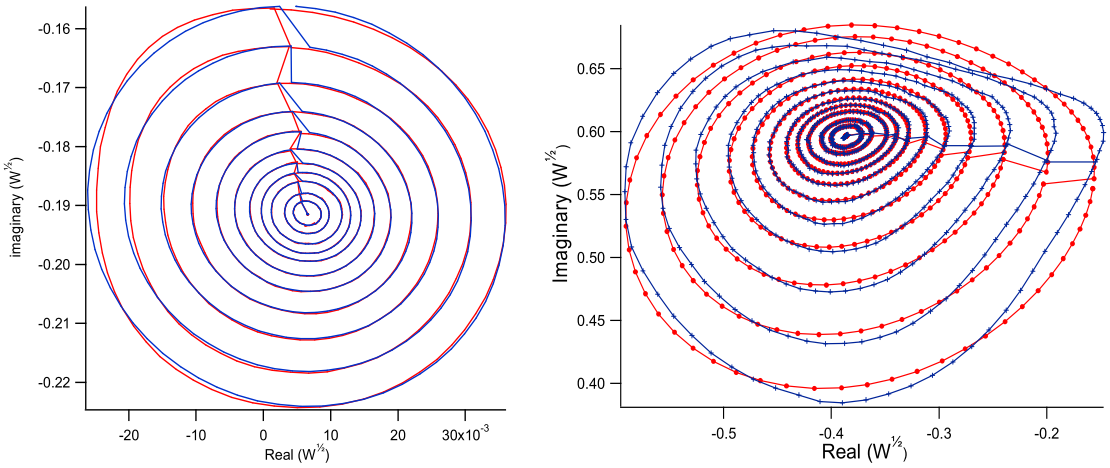

3rd Order

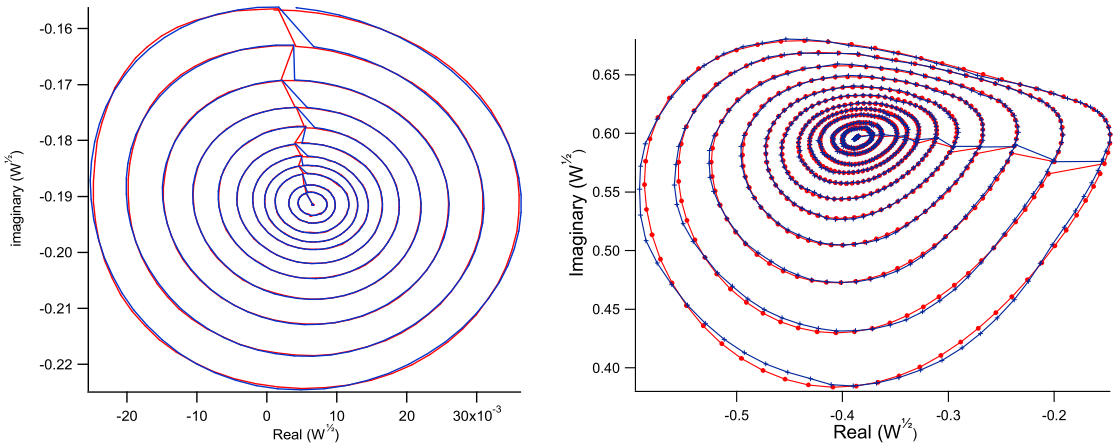

5th Order

Figure (23)

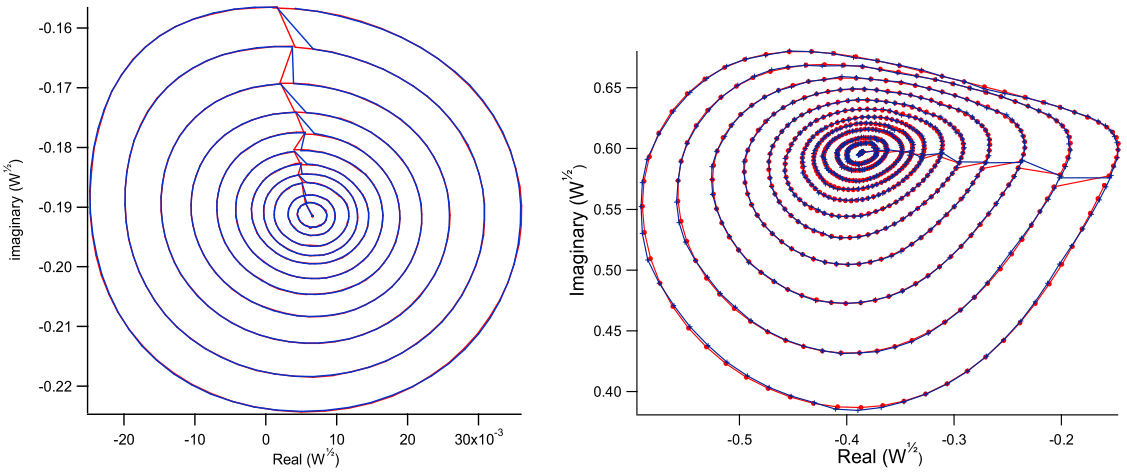

7th Order

Figure (24)

It can be seen that the extraction process improves the fit of the data as the order of the extraction was increased up until the 7th to 9th orders. Above which little improvement in the fit to the data was observed, this can be seen in figure (25) where a clear noise floor to the extraction is observed. This is considered by the author to be very useful artefact of the extraction which, when limited to phase, can be considered as a orthogonal set as in the case of the Fourier transform, allowing all possible coefficients to be evaluated independently of the others and limited to number of points measured. This allows the quality of fit and the measurement to be assessed by looking at the 'phase coefficient spectrum'. Figure (26) shows again the measured and modelled Load-pull contours.

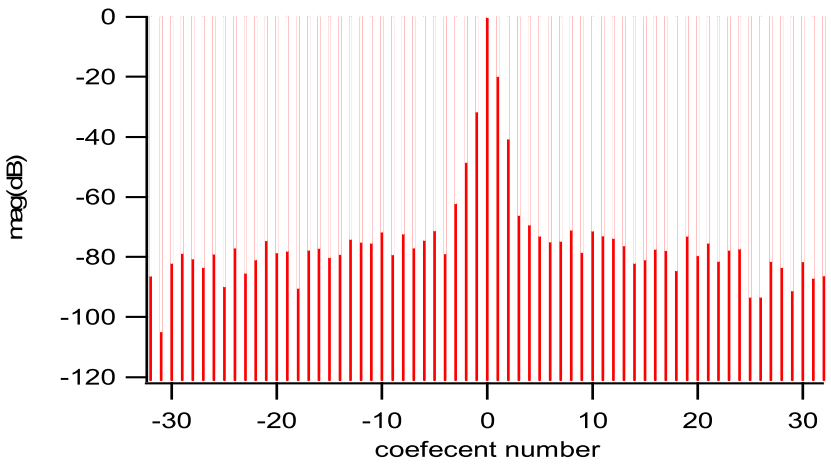

Figure (25)
Coefficient spectrum for $R_{2,1,n}$ for a 10x75μm GaAs HEMT for Largest $\|a_{21}\|$

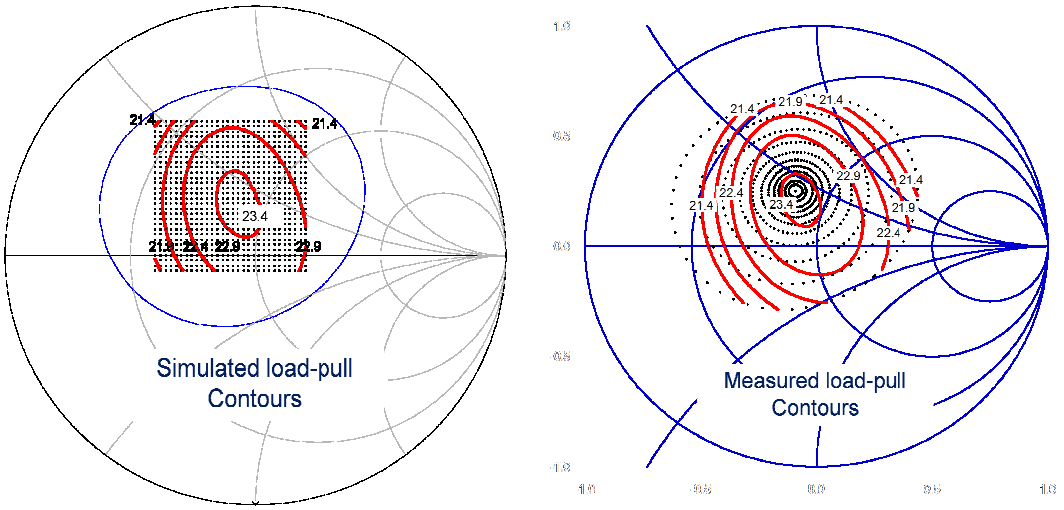

Figure (26)
Comparison of modelled (left) and measured (right) output load-pull contours.

3.4.4 Amplitude Dependence of coefficients within model

The previous sections looked at extracting phase polynomials from Hot S-Parameter-Load-Pull data sets, from the formulations presented in section 3.3 and figure (10). The phase polynomials are expected to be dependent on the amplitude of the stimuli. Figure (27) shows the amplitude dependence determined from the HBT

measurements and Figure (28) shows the equivalent coefficients extracted simulation results.

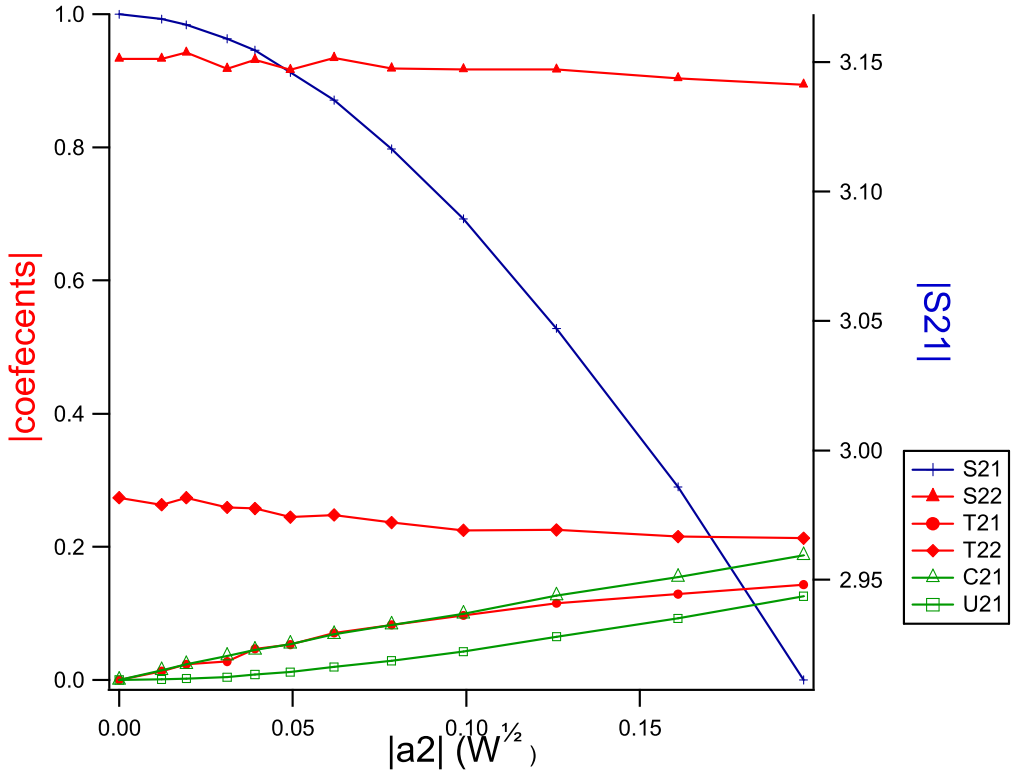

Figure (27)
Coefficient Amplitude dependence from GaAs HBT Measurements

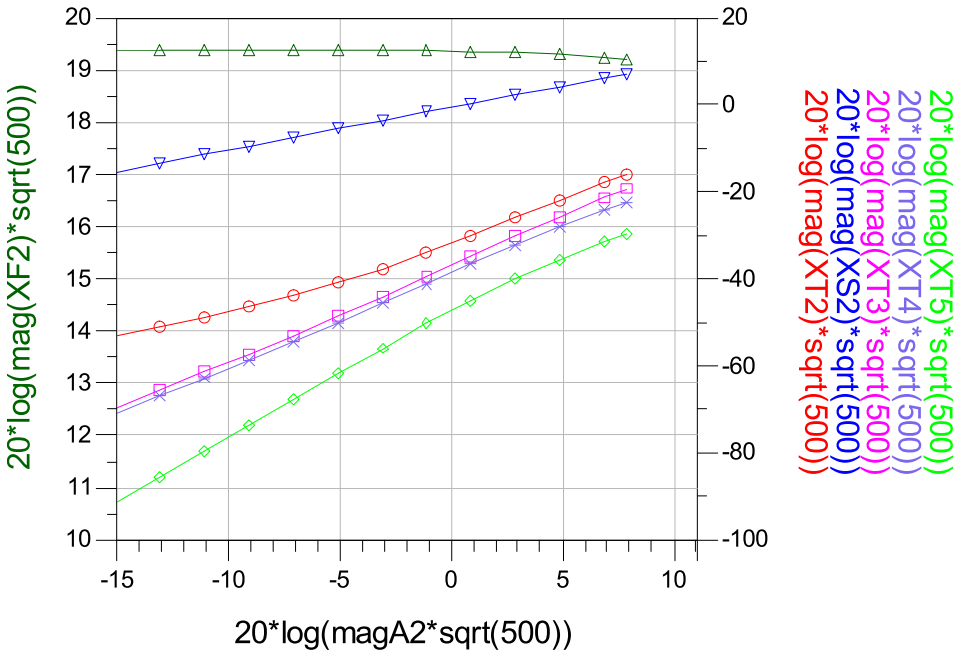

Figure 28
Coefficient Amplitude dependence from Simulation at location B figure 1

Figures (27) and (28) show a strong quadratic dependence, hence can be modelled as a polynomial of even powers of the magnitude of $|a_{21}|$; this is summarised in equation 15.

$$R_{2,0}/a_{11} = S21 = \sum_{n=0}^{N} \alpha_n |a_{21}|^{2n} \quad (15)$$

It can be seen in this equation, and figures, that as the magnitude of 'A_{21}' increases S_{21} moves away from its initial value. This process can be fitted to (15) this behaviour is a major limiting factor in approximations made by Hot S-Parameters, X-parameters and the PHD model, as it means, that the invariance of the initial large signal state cannot be assumed at values of $|A_{21}|$ that are considered to be large. The limit of this approximation can only be determined through measurement where higher orders are considered as presented in this chapter. These figures also show the two different ways of looking at the coefficient data in figure (27). This is as

power dependent s-parameters, and figure (28) shows the relative contributions made by specific coefficients.

3.5 Discussion

A measurement configuration has been presented that enables the extraction of a non-linear Direct Waveform Look-Up tables (DWLU) formulated behavioural model, based on the extraction of polynomials of phase. The measurement technique exploits combined active and passive load-pull architecture.

The techniques from this chapter allow the investigation of the approximate methods like Hot S-Parameters, and the PHD model. A method is suggested for testing the validity of the PHD model. Investigations into hot-S-Parameters and the PHD model have been made which show and explain the issues with these methods when applied to the response of the injected signals at fundamental frequency, and discusses' one way in which these methods could be bench marked against amplitude dependent coefficients from the phase extraction process. The poly-harmonic distortion framework includes models of the effects of harmonics in the system. In this chapter only the effect of the fundamental stimuli on harmonics has been considered, but the effect of harmonics on the fundamental has not been mentioned. The next chapter will look in more detail, at the how harmonic terminations can be modelled, and how the Poly-Harmonic distortion model approximates these processes.

3.6 References

1. S. Woodington, T. Williams, H. Qi, D. Williams, L. Pattison, A. Patterson, J. Lees, J. Benedikt, P. J. Tasker, A Novel Measurement Based Method Enabling Rapid Extraction of a RF Waveform Look-up Table Based Behavioural Model,IMS 2008

2. Jan Verspect;
   Everything you've always wanted to know about Hot S22
   (but were afraid to ask), Presented at the Workshop Introducing New Concepts in Non-linear Network Design, MTT-IMS 2002 and Fall Power Amplifier Symposium 2009

3. Hao Qi ,Nonlinear Data Utilization: Direct Data Look-up to Behavioural Modelling, PHD Thesis Cardiff University, Feb 2008

4. Hao Qi; Benedikt, J.; Tasker, P.J.; , Nonlinear Data Utilization: From Direct Data Lookup to Behavioral Modeling, Microwave Theory and Techniques, IEEE Transactions on , vol.57, no.6, pp.1425-1432, June 2009
   doi: 10.1109/TMTT.2009.2019996

5. Verbeyst, F.; Bossche, M.V.;
   The Volterra input-output map of a high frequency amplifier as a practical alternative to load-pull measurements

Instrumentation and Measurement Technology Conference, 1994. IMTC/94. Conference Proceedings. 10th Anniversary. Advanced Technologies in I & M., 1994 IEEE

Digital Object Identifier: 10.1109/IMTC.1994.352068

Publication Year: 1994, Page(s): 283 - 286 vol.1

6. Williams, D.J.; Tasker, P.J.; An automated active source and load pull measurement system, High Frequency Postgraduate Student Colloquium, 2001. 6th IEEE , vol., no., pp.7-12, 2001

doi: 10.1109/HFPSC.2001.962150

7. On Scattering Matrices Normalised to Complex Port Impedances

Youla. D.C, Proc IRE. vol 49, July 1961, p 1221

Chapter 4 – Multi-Harmonic Device models in the frequency domain

4.1 Introduction

In chapter 3 and [1], models of fundamental only load-pull data were formulated and a model of a GaAs HBT operating at 0.9 GHz was produced. In this process, the model was extracted by populating a look up table of “polynomials of phase” that described the load-pull contours of the device. The selected measurement and extraction approach introduced could also be used to examine the order of mixing required to be modeled to achieve a specified degree of accuracy. The process is completed by analysing the magnitude variation of the coefficients. These models looked at harmonics as outputs and not as inputs. This chapter will investigate further the effect of load-pull harmonic terminations.

4.2 Models of individual harmonic terminations

Models of harmonic terminations can be produced in a similar manner to those of the fundamental load as in the chapter 3, by considering the incident travelling waves at the harmonic frequency and the port that has been chosen. As in the previous chapter, these will be explored through simulation. For consistency the same operating conditions as in chapter 3 will been considered. Figure (1) shows the locations along a simulated fundamental power sweep at which the extraction will be conducted, and figure (2) shows the setup of the simulation for this sweep. Within this section, only injection at the second harmonic will be considered.

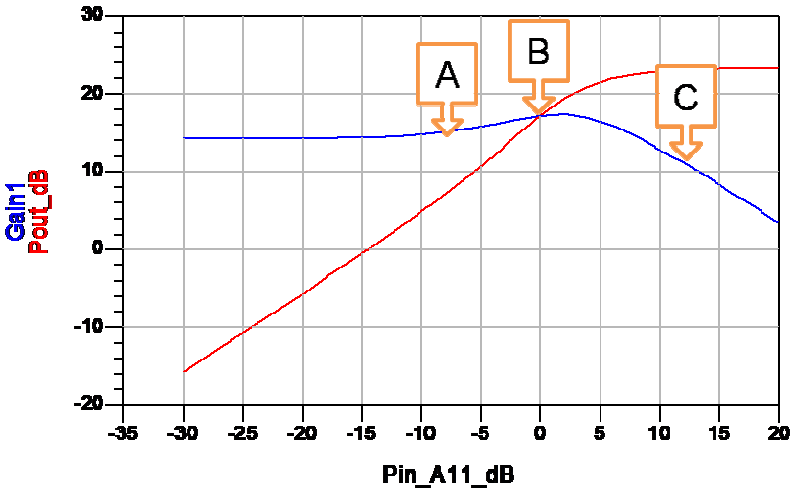

Figure (1)
Power sweep at fundamental frequency

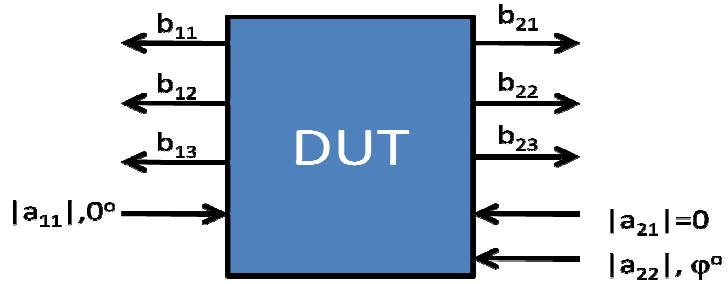

Figure (2)
Active injection sweeps of a two-port-network
With second harmonic injection considering harmonic as well as
Fundamental outputs from the network

Extraction in linear region location (A) figure (1):

Figures 3A to 3F show the results of the extraction process as performed at location (A) in figure (1). The extraction has been performed in the same manner as discussed in the previous chapter (3) and can be performed using equations (1-3). It should be noted that the phase operator is modified for the new conditions equation (2). As in chapter 3 a conversion of (1-3) to the PHD model can be considered as shown in equation (4). Figure (3A) shows the pattern of loads that were covered by the sweep (red) and the (blue -circles) represent the unit circle within which the load is absorbing energy and outside the load network is generating energy. It is of interest to note that to complete the loci drawn by the sweep of A_{22} the load will move from inside to outside the unit circle.

Also the loci are always centred on the reference impedance of the system in this case 50 ohms.

$$b_{p,h}\left(|a_{11}|,|a_{22}|,bias,frequency,\theta\right)=\Re\left\{e^{j\theta}P^{h}\sum_{n=-\frac{1}{2}(N-1)}^{\frac{1}{2}(N+1)}R_{p,h}\left(|a_{11}|,|a_{22}|,bias,frequency\right)\varphi^{n}\right\} \quad (1)$$

$$\varphi=e^{j(\angle a_{22}-2\angle a_{11})} \quad (2)$$

$$R_n\left(|a_{11}|,|a_{22}|,bias,frequency\right)=\sum_{x=0}^{X}B_p\left(|a_{11}|,|a_{22}|,bias,frequency,x\right)e^{-j2\pi n\frac{x}{X}}$$
$$n\in Z,\ -\frac{X}{2}\le n\le\frac{X}{2} \quad (3)$$

$$X_{p,h}^{F}\left(|a_{11}|\right)=R_{p,h,0}\left(|a_{22}|,|a_{11}|\right)$$

$$\frac{\partial X_{p,h}^{F}\left(|a_{11}|\right)}{\partial|a_{22}|}=\frac{\partial R_{p,h,0}\left(|a_{22}|,|a_{11}|\right)}{\partial|a_{22}|}=0$$

$$X_{p,h}^{S}\left(|a_{11}|\right)=\frac{\partial R_{p,h,1}\left(|a_{22}|,|a_{11}|\right)}{\partial|a_{22}|},\ X_{p,h}^{T}\left(|a_{11}|\right)=\frac{\partial R_{p,h,-1}\left(|a_{22}|,|a_{11}|\right)}{\partial|a_{22}|}$$

These relationships are valid only when for one magnitude of $|a_{11}|$ X^F, X^S and X^T can be considered constant while $|a_{22}|$ changes and also while no other R_n coefficient is significant otherwise no conversion exists.

Eqn (4)

Figures 3B and 3C show the resulting effects on the power-waves scattered at the output. It can be seen that the second harmonic has very little effect on the travelling waves at the fundamental and third harmonic. The loci produced within the simulation at these frequencies are small and this means that at this drive level re-mixing of the second harmonic has very little effect on the output of the DUT. The locus of second harmonic is much larger in size but has circular form, which indicates a near linear response to the injected signal. All of these observations are consistent with the location of point (A) within the fundamental power sweep.

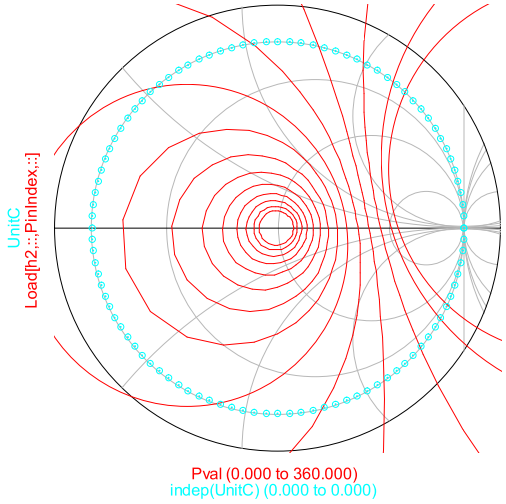

Figure (3A)
load coverage at second harmonic from Location (A) in figure (1)

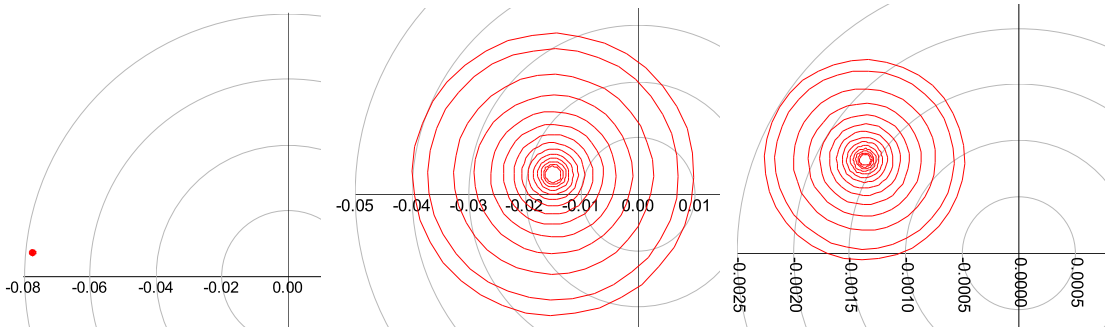

Figure (3B)
Fundamental loci of b_{21} (left)
Second harmonic loci of b_{22} (middle)
Third harmonic loci of b_{23} (bottom)
from Location (A) in figure (1)

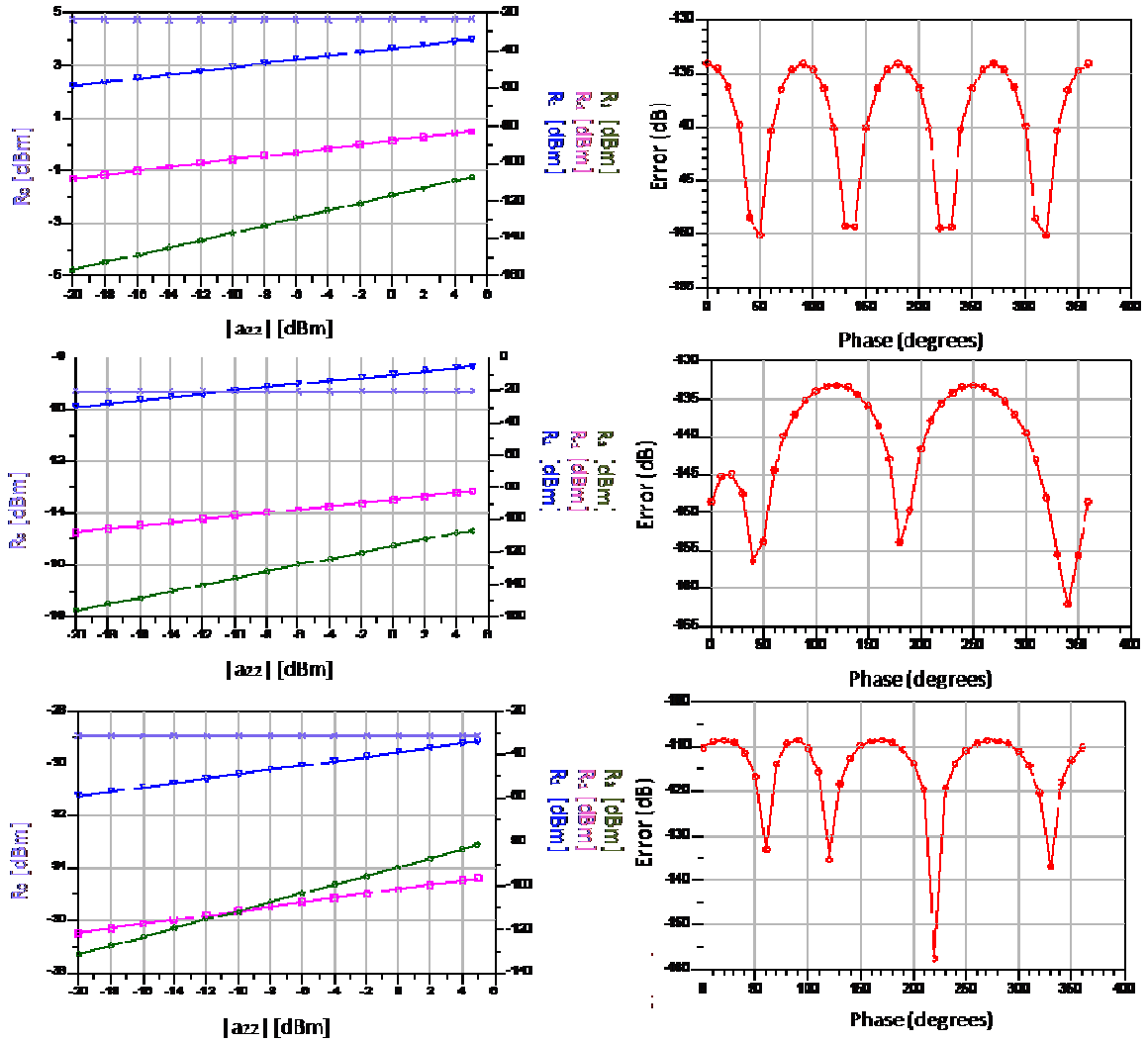

(left) Extracted coefficients vs. magnitude of $|a_{22}|$
(right) Error in coefficients vs. phase of a_{22} for largest value of $|a_{22}|$
from location (A) in figure (1)
(Top) fundamental
(Middle) second harmonic
(Bottom) third harmonic
Figure (3C)

Figure (3D) shows the extracted coefficients and the error in the extractions at the largest magnitude of A_{22}. These confirm the observations from figures 3B and 3C showing that, in the linear rejoin of the DUT, the only significant coefficients are R_0 and R_1. At this level R_{-1} and R_2 are insignificant, they are visible in the simulation, but would be below the measurement range, noise floor, of the measurement system described in chapter (3). These figures show that at high drive levels the 3rd

harmonic R_2 can overtake R_{-1}. This is interesting as it breaks the rules from equation (4). Figure (3E) shows the effect of the simulated measurement on the fundamental load-line current waveforms and voltage waveforms for four phases of A_{22}. At the largest simulated value of $|A_{22}|$ it can be seen that the perturbations affect all of these characteristics but do not push them into the device boundary conditions. This being consistent with “linear operation”.

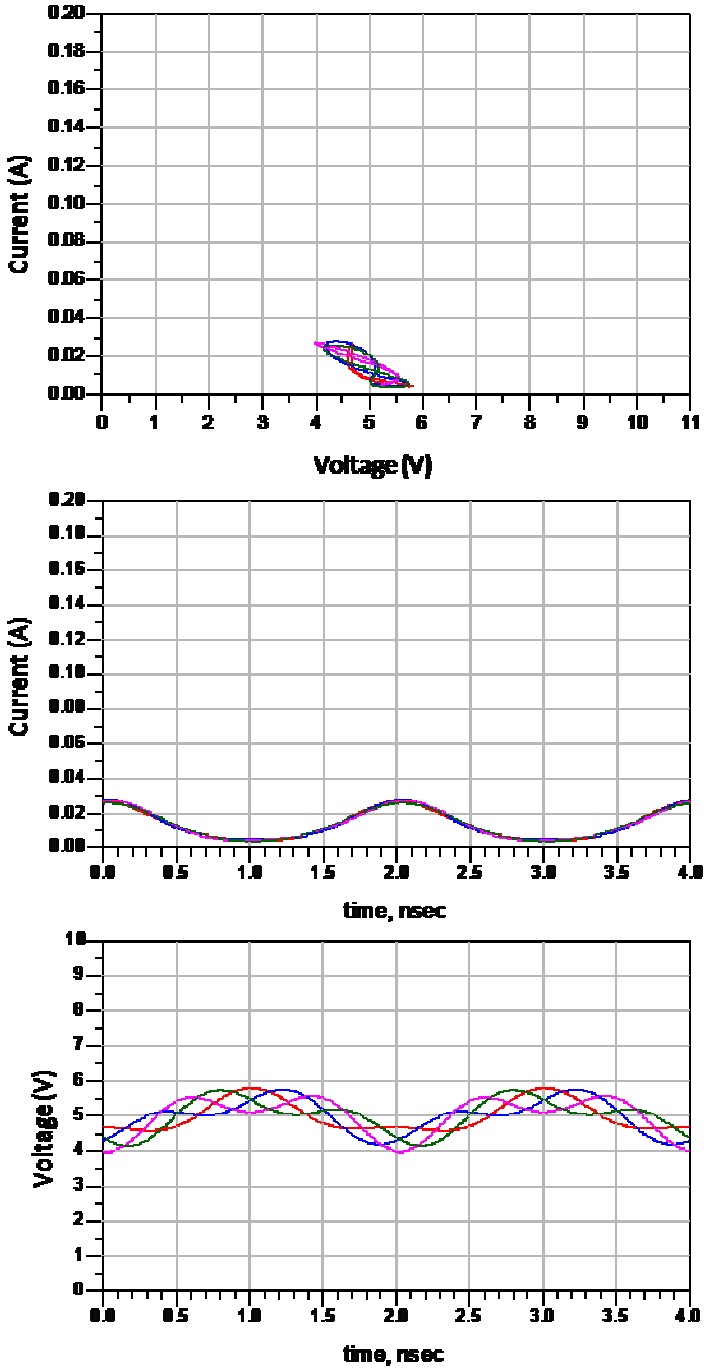

Device waveforms for 4 phases (0°, 90°, 180°, 360°)
of the largest Magnitude of $|a_{22}|$ from location (A) in figure (1)
(Top) Load Line
(Middle) current waveform
(Bottom) voltage waveform
Figure (3D)

Extraction at peak gain location (B) figure (1):

Figure 4A shows the pattern of loads that were covered by the sweep in the same manner as figure 3A figures 4B and 4C show the loci of B_{21}, B_{22} and B_{23} as drawn out by the sweep. At this location in the power sweep, the gain is at its highest value and the device is about to go into compression. This can be seen at the fundamental and third harmonic, where the loci of the fundamental and third harmonic have started to become coupled to the phase and magnitude of the second harmonic. This has the interesting consequence that it is possible to use the second harmonic to null or cancel the third harmonic.

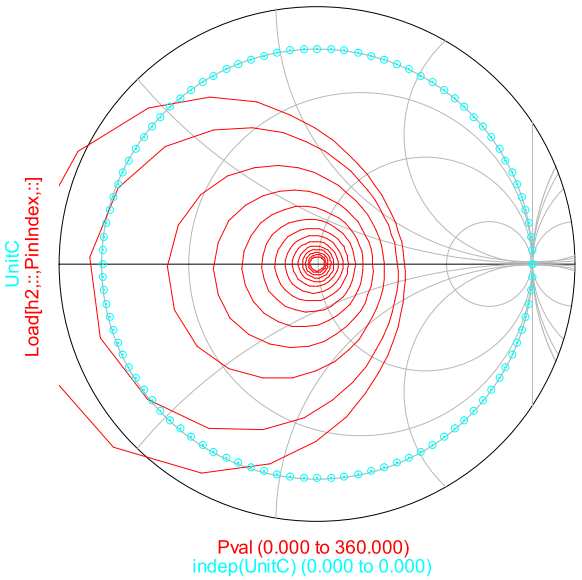

Figure (4A)
Load coverage at second harmonic from Location (B) in figure (1)

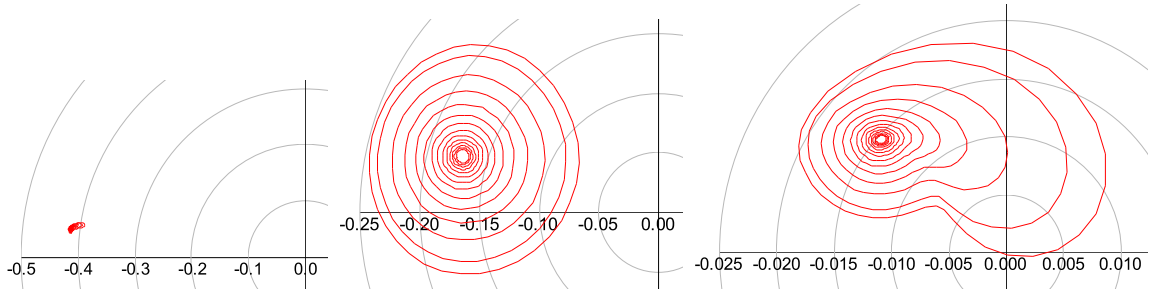

Figure (4B)
Fundamental loci of b_{21} (left)
Second harmonic loci of b_{22} (middle)
Third harmonic loci of b_{23} (right)
from Location (B) in figure (1)

Figure (4C) shows the extracted coefficients and the error that occurs when the coefficients that fill the PHD model are used. At this level the coefficients R_1, R_{-1}, R_2 have become more significant, the difference in magnitude with respect to R_0 and R_1 has decreased by 10dB at the highest level of $|a_{22}|$ and the coefficients are deviating from the linear assumptions in equation (4), these changes are due to the onset of compression.

As the magnitude of the coefficients has increased, the significance of the higher order terms has become greater. This has caused the error when using the PHD model coefficients to predict the loci due to the highest level of $|a_{22}|$ to also increase, to approximately -47dB.

Figure (4E) shows the load-lines, current waveforms and voltage waveforms for four phases of a_{22} 0 °, 90 °,180 °,270° at the largest magnitude of $|a_{22}|$ it can clearly be seen that at one of the points the current waveform has its top cut off by the knee region of the device as the voltage reaches a minimum value this results in the part of the loci where the third harmonic and fundamental have higher rates of change, and also why PHD model begins to struggle.

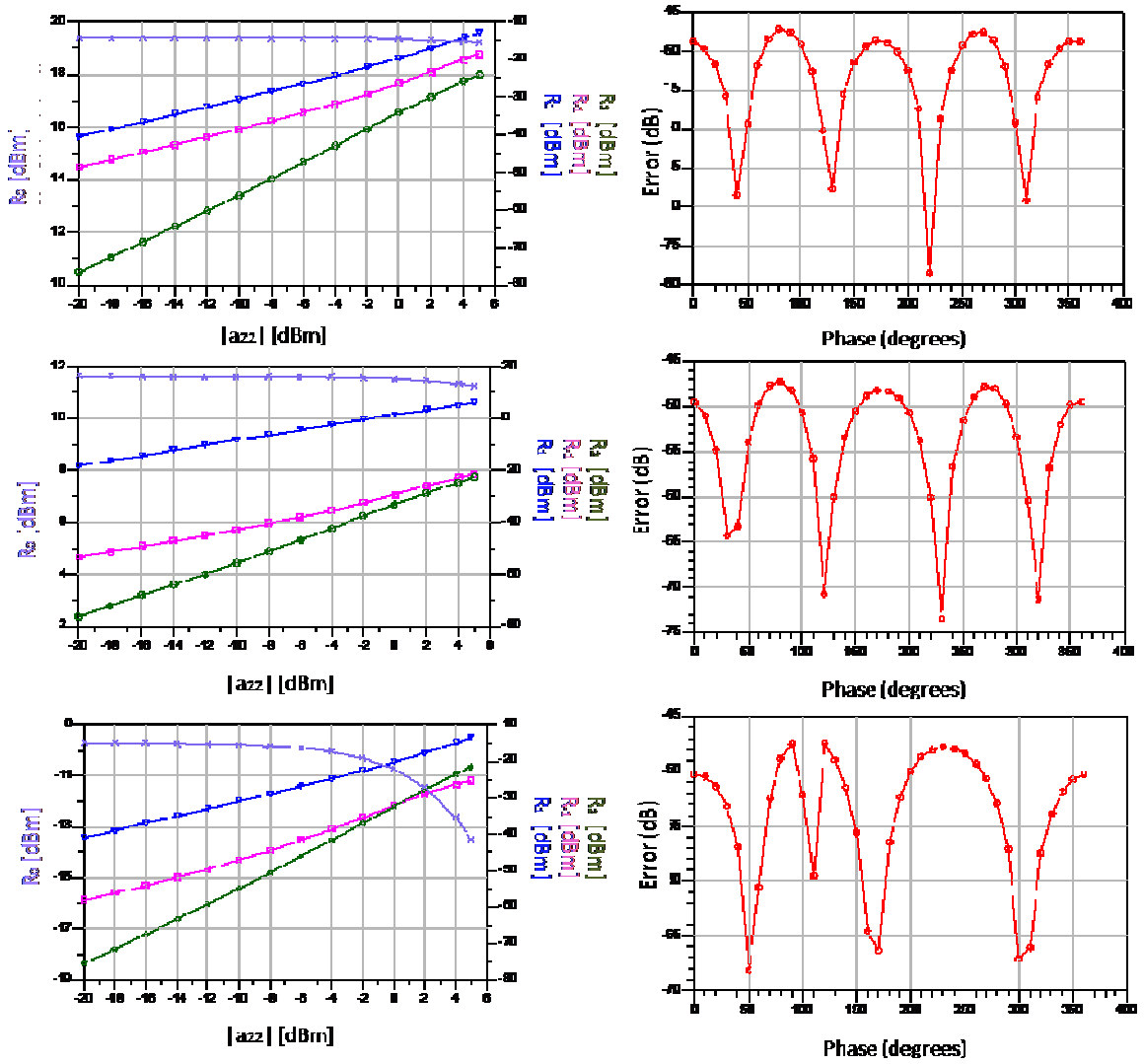

(left) Extracted coefficients vs. magnitude of $|a_{22}|$
(right) Error in coefficients vs. phase of a_{22} at largest value of $|a_{22}|$
from location (B) in figure (1)
(Top) fundamental
(Middle) second harmonic
(Bottom) third harmonic
Figure (4C)

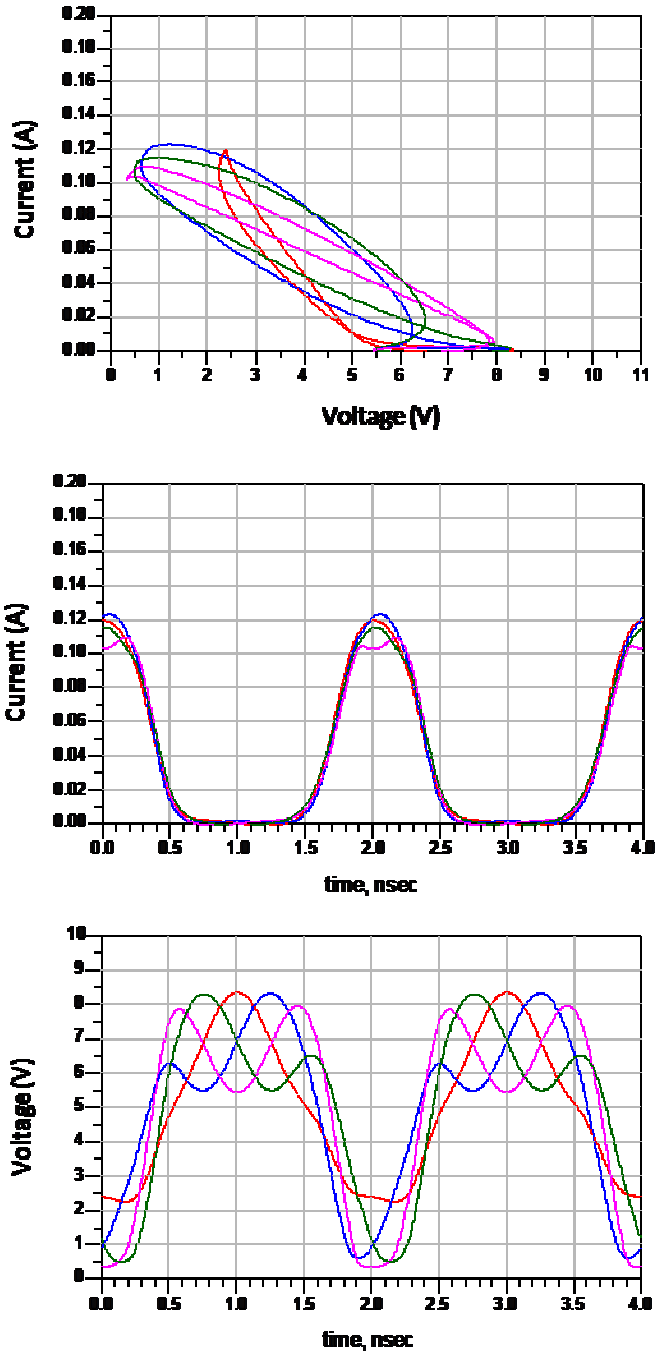

Device waveforms for 4 phases (0°, 90°, 180°, 360o)
of the largest Magnitude of $|a_{22}|$ from location (B) in figure (1)
(Top) Load Line
(Middle) current waveform
(Bottom) voltage waveform
Figure (4D)

Extraction at 3dB gain compression location (C) figure (1):

Figure 5A shows the pattern of loads that were covered by the sweep in the same manner as figure 3A figures 5B and 5C show the loci of b_{21},b_{22} and b_{23} as drawn out by the sweep.

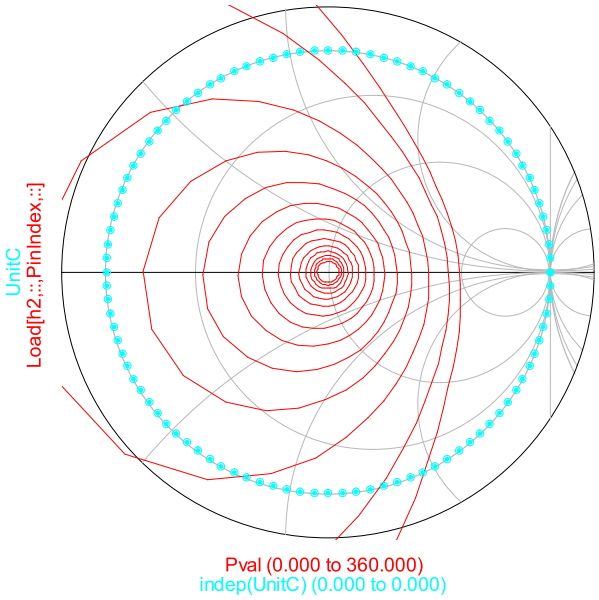

Figure (5A)
Load coverage at second harmonic from Location (C) in figure (1)

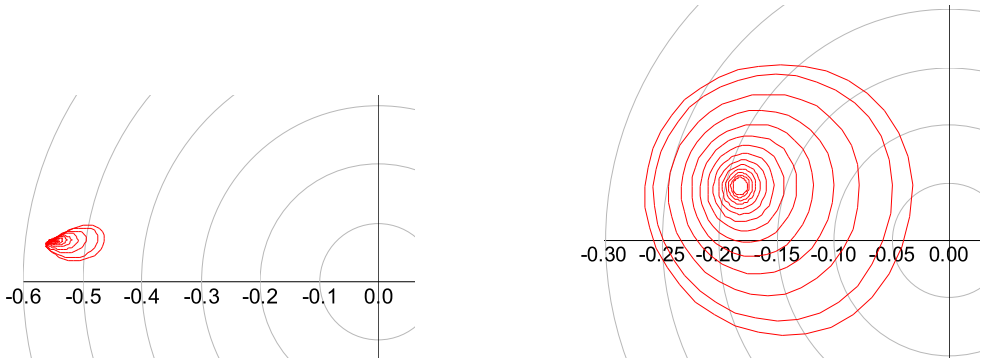

Figure (5B)
Fundamental loci of b_{21} (left)
Fundamental loci of b_{22} (right)
from Location (C) in figure (1)

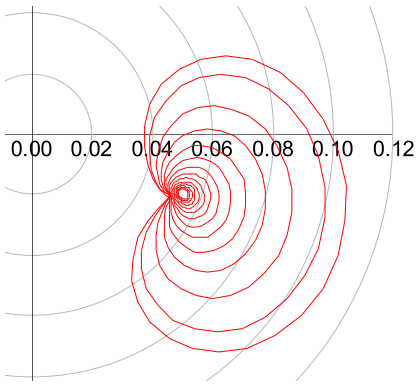

Figure (5C)
loci of b_{23}
from Location (C) in figure (1)

Figures (5B) and (5C) show that the loci at the fundamental and third harmonic are more coupled to the second harmonic at the 3dB point than at locations (A) and (B). It becomes stronger than the R_{-1} term and along with the magnitude dependence of this coefficient, results in a further increase in the error between the simulated data and that produced by the PHD model.

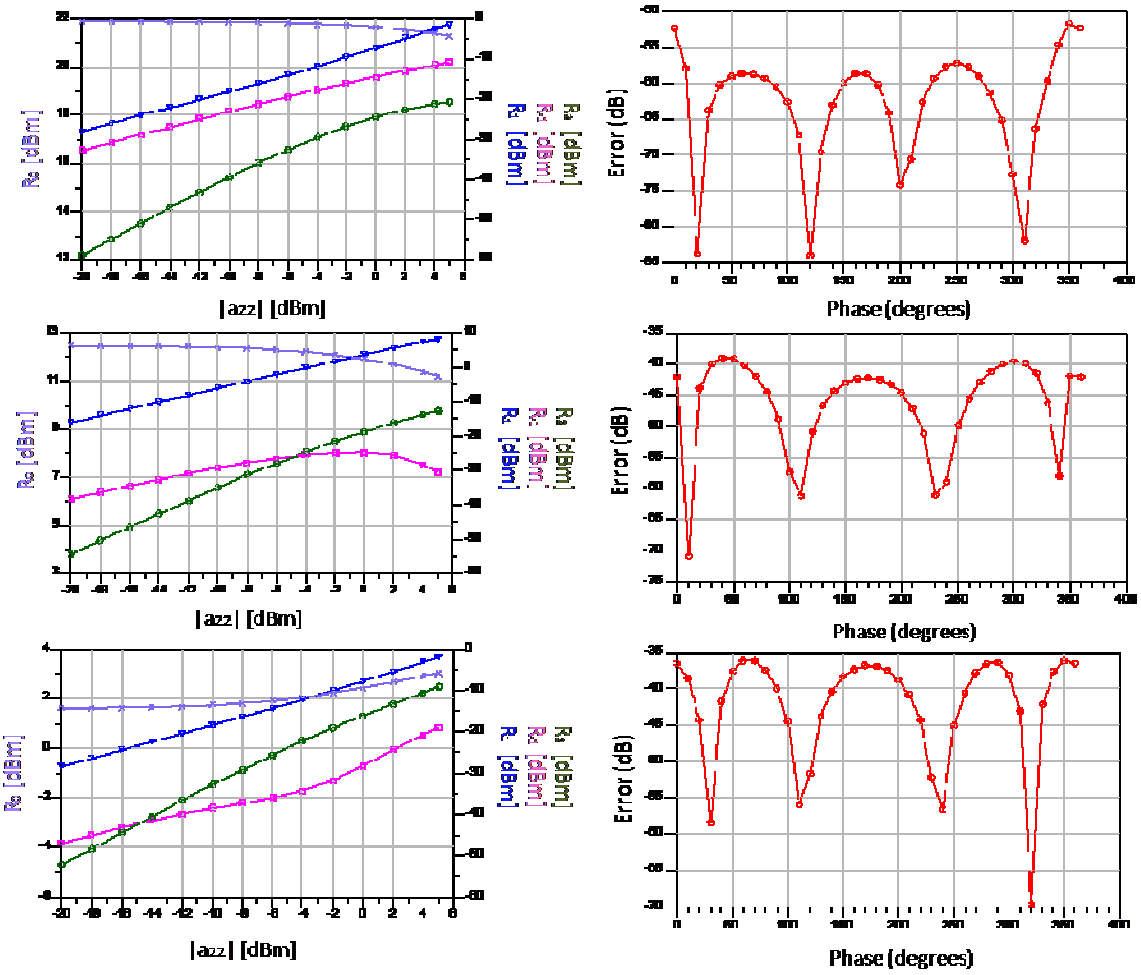

(left) Extracted coefficients vs. magnitude of $|a_{22}|$
(right) Error in coefficients vs. phase of a_{22} for largest magnitude of $|a_{22}|$
from location (C) in figure (1)
(Top) fundamental
(Middle) second harmonic
(Bottom) third harmonic
Figure (5D)

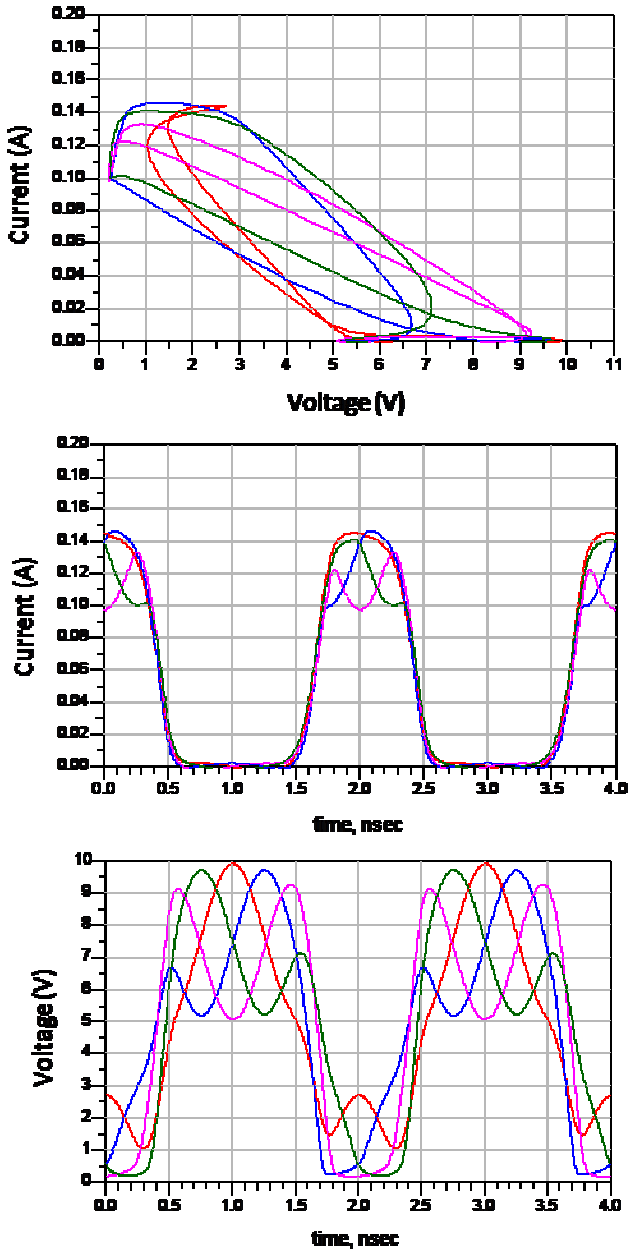

Device waveforms for 4 phases (0°, 90°, 180°, 360°)
of the largest Magnitude of $|a_{22}|$ from location (C) in figure (1)
(Top) Load Line
(Middle) current waveform
(Bottom) voltage waveform
Figure (5E)

Figure 5E shows the load-lines, current waveforms and voltage waveforms for four phases of a_{22} (0 °, 90 °, 180 °, 270°) for the maximum value of $|a_{22}|$ these show the compression in the waveforms but it can also be seen that there are still a group of second harmonic phases that are able to hold off the compression of the simulated

device. These phases represent the class-B mode of operation at the point of compression.

For the 3dB compression level a higher order extraction has been performed for the three harmonics. This is shown in figure (6) this extraction gave the maximum error of -65 dB

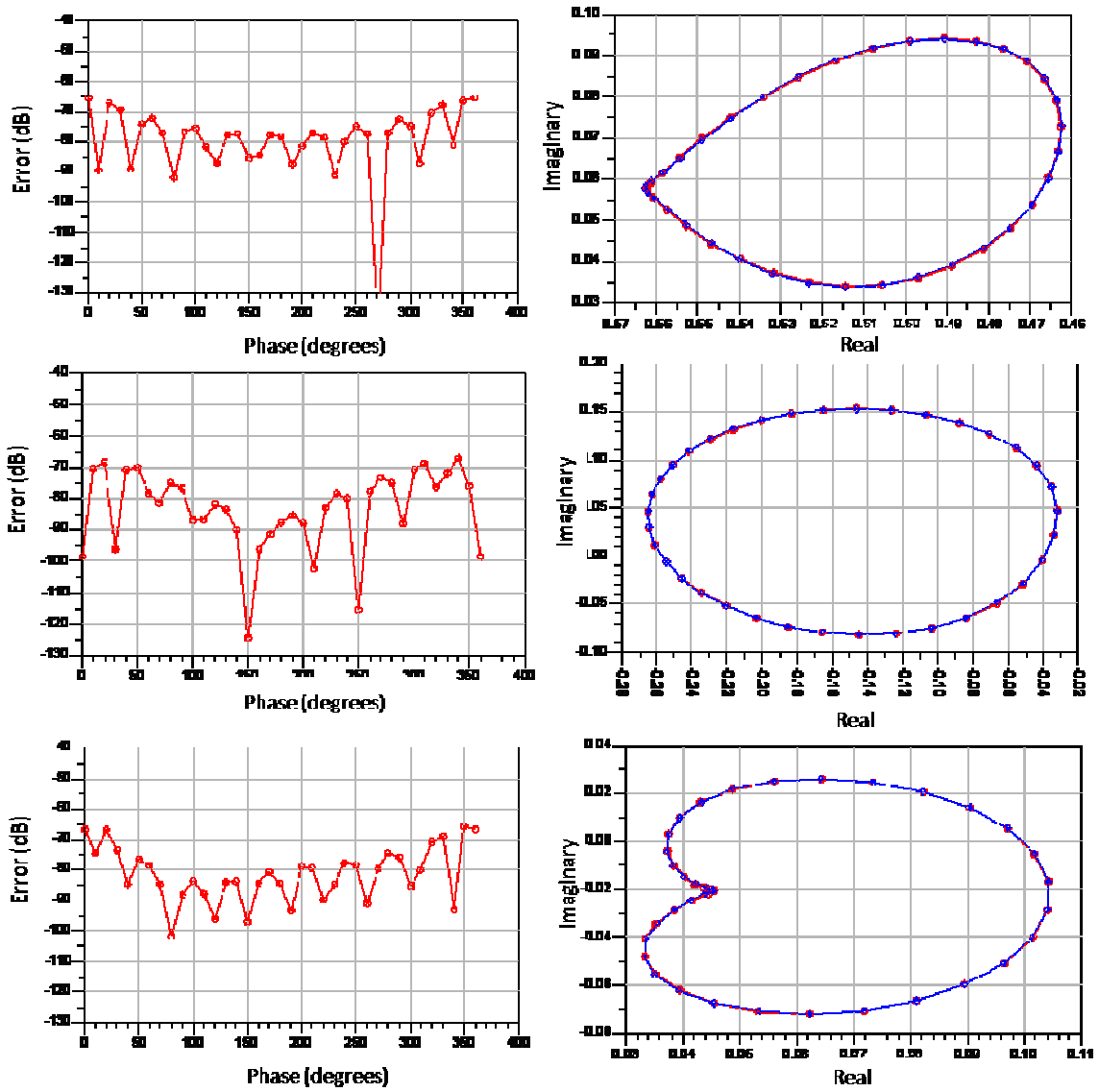

Results of 7th order extraction at 3dB compression point
(Left) error between simulated and modelled loci of b_{2h}
(right) Simulated and modeled loci of b_{2h}
(Top) fundamental
(Middle) second harmonic
(Bottom) third harmonic
Figure (6)

The simulations in this section have provided insight into the use of the PHD model, for the description of second harmonic load-pull. They have shown that it is not always possible to assume that the second harmonic causes interactions that can be assumed to be linear, with the other harmonics and signals present at the ports of the DUT. It should however be noted that at lower injected signal levels the PHD

model relationships were found to hold and that these would provide large ranges of load-pull prediction. If these models are to be used in design, then a measurement system that integrates fundamental and harmonic load-pull is necessary. In the next section, the methods described in the previous sections are adapted to analyze simultaneous fundamental and harmonic interactions during load-pull.

4.3 Multiple Harmonic Interactions

The models discussed in the previously section 4.2 and chapter 3 describe how changes such as load impedance at the fundamental frequency affects harmonically related frequencies or how changes to the load at any harmonic affect every other output of the nonlinear system. Any simultaneous changes to terminations at frequencies other than the one under consideration are unaccounted for leading to degradation in the accuracy of the model. It is common in the design of transistor amplifiers to exploit optimized load terminations at the fundamental and harmonic frequencies e.g. class AB, B, J, F and E.

Hence it is useful to consider multiple terminations simultaneously for example the fundamental and second harmonic loads at port 2 as shown in figure (7). This is useful in the design of transistor amplifiers that rely on simultaneous terminations at the fundamental and harmonic frequencies e.g. class AB, B, J, F and E. Chapter 3 and the previous section 4.2 presented these models in the form of polynomials of phase which are shown in equations (5) and (6).

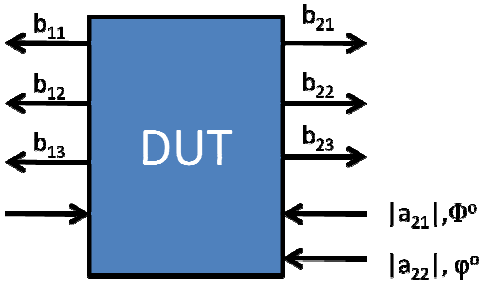

Figure (7)

$$b_p\left(|a_{11}|,|a_{21}|,bias,frequency,\theta\right)=\Re\left\{e^{j\theta}P\sum_{n=-\frac{1}{2}(N-1)}^{\frac{1}{2}(N+1)}R\left(|a_{11}|,|a_{21}|,bias,frequency\right)\Phi^n\right\} \quad (5)$$

$$b_{p,h}\left(|a_{11}|,|a_{22}|,bias,frequency,\theta\right)=\Re\left\{e^{j\theta}P^h\sum_{n=-\frac{1}{2}(N-1)}^{\frac{1}{2}(N+1)}R_{p,h}\left(|a_{11}|,|a_{22}|,bias,frequency\right)\varphi^n\right\} \quad (6)$$

Extending these formulations as in [2] requires the consideration of cross mixing between the signals. The phase vector from (6) can become part of the coefficient set generated from (5) as shown in (7)

$$R_{p,h,n}=G_{p,h,n}\left(|a_{1,1}|,|a_{2,1}|,|a_{2,2}|,\varphi\right) \quad (7)$$

In a measurement, to extract these additional coefficients, the phase vector φ should be rotated around 360°. The resulting coefficients would then be expected to produce periodic changes in the coefficients with respect to the phase vector Φ. These effects can be captured by (8)

$$R_{p,h,n}=\sum_r\left\{G_{p,h,n,r}\left(|a_{1,1}|,|a_{2,1}|,|a_{2,2}|\right)\varphi^r\right\} \quad (8)$$

$$b_{p,h}=P_1^h\sum_n\sum_r\left\{G_{p,h,n,r}\left(|a_{1,1}|,|a_{2,1}|,|a_{2,2}|\right)\Phi^n\varphi^r\right\} \quad (9)$$

Substituting the coefficients from (8) into (5) forms (9). The coefficients in this equation are only functions of the stimuli magnitudes and are independent of their phases. It can also be noted that the phase difference between the two signals at

the output are accounted for by the cross product terms in this equation, i.e. the terms that are related to $\angle a_{21} + \angle a_{22}$ and $\angle a_{21} - \angle a_{22}$.

In order to extract these coefficients two conditions must be met. Firstly, datasets containing sweeps of the phase component of the fundamental phase vector are required with the second harmonic phase vector held constant. Secondly, datasets containing sweeps of the phase component of the second harmonic phase vector are required whilst the fundamental phase vector is held constant.

4.4 Measurements and observations

To demonstrate the necessary measurement approach, results were taken for a 10x75µm GaAs HEMT device, operating at 9GHz using the waveform measurement system developed at Cardiff University [3]. The measurement strategy followed included spinning the second harmonic phase vector around 360 degrees in 18-degree steps whilst holding the fundamental phase vector constant. This was repeated as the fundamental phase vector was spun around 360 degrees, with points distributed every 18 degrees. Finally, the entire process was carried out with varying magnitudes of the fundamental and second harmonic stimuli at port 2 ($|a_{21}|$ and $|a_{22}|$).

This dataset was renormalized to the measured system impedances and the fundamental phase at port 1 was removed. The complex values of a_{21}, a_{22}, b_{21} and b_{22} for a subset of these measurements have been plotted in Figure 4. Examining

this data importantly shows that the perturbations of the fundamental b_{21} at the output of the device due to the phase of a_{21} and a_{22} produce closed forms in b_{22} and b_{21}. This allows the separation of fundamental and harmonic functions when coefficients are extracted.

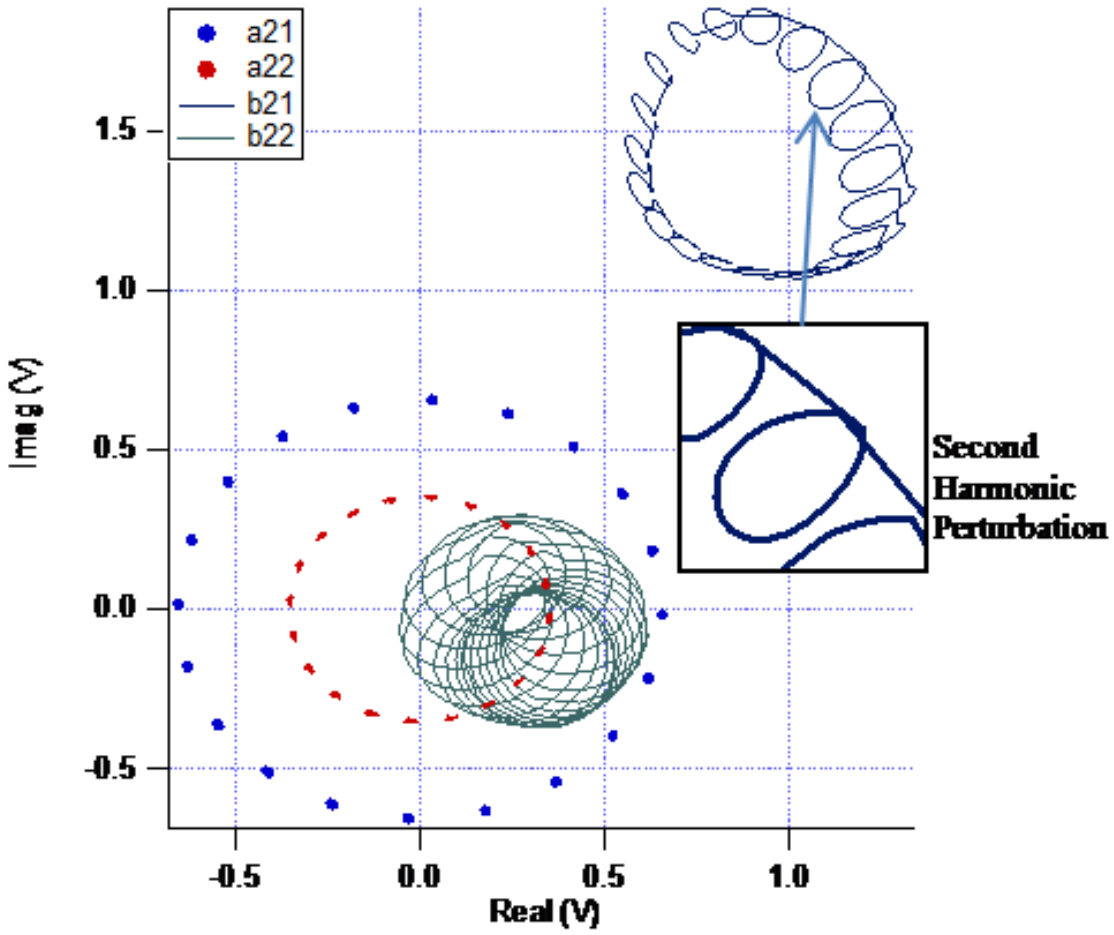

Figure 8
Sample of the recorded travelling waves during the measurement Sequence

4.4.1 Comparison with the Poly-Harmonic-Distortion model

The extraction process can be demonstrated with a dataset whereby one magnitude point in each of the sets of a_{21} and a_{22} are used to extract the model coefficients. Based on the formulation of (9), there are two approaches to this process. Firstly, if the magnitude functions are not included, Eqn. 9 can be regarded as a 2-Dimensional Fourier transform. Alternatively, the coefficients in Eqn. 9 can be extracted using the Polynomial Least Mean Squares Method (LMS). It has to be noted that the Fourier transform provides the best method due to the fact that all the model coefficients can be extracted in one process, without over-fitting the data. However, this technique suffers when it is presented with data that does not include ideal sample points, thereby causing leakage into other sample bins. This effect can be overcome by interpolation onto the nearest ideal sample point. The LMS algorithm avoids the leakage problem by allowing measured points to be used as independent data.

In order to illustrate the complexity of the coefficient space required, the dataset presented in Fig. 4 was overlaid with a dataset produced by a 5^{th} order model and analysed using two different cases.

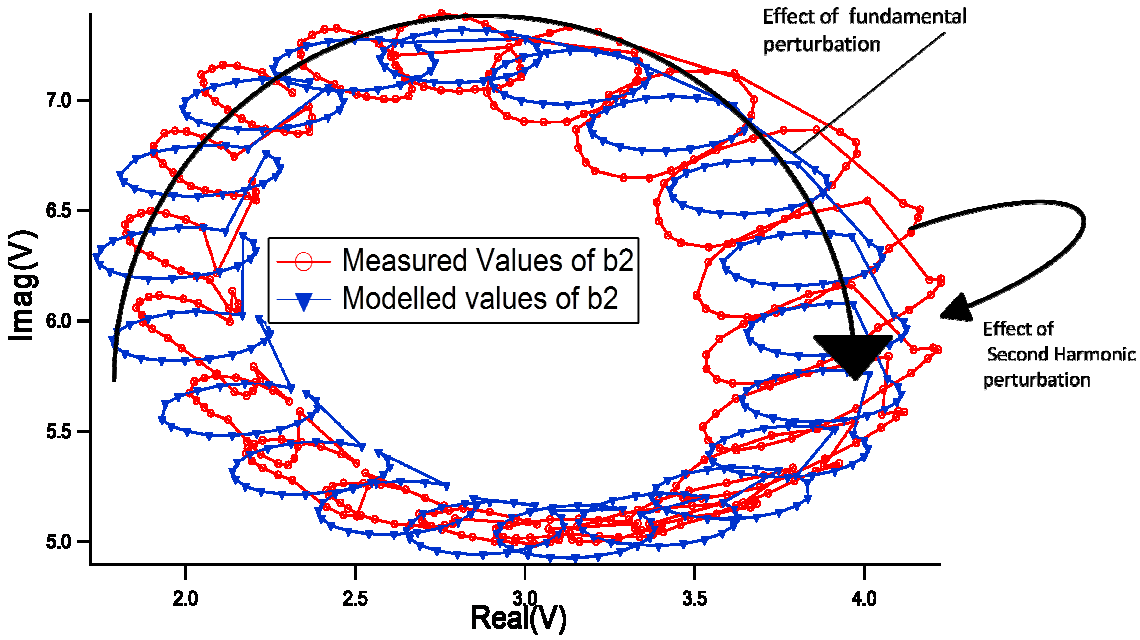

Figure 9
Measured and modelled values of b_{21}

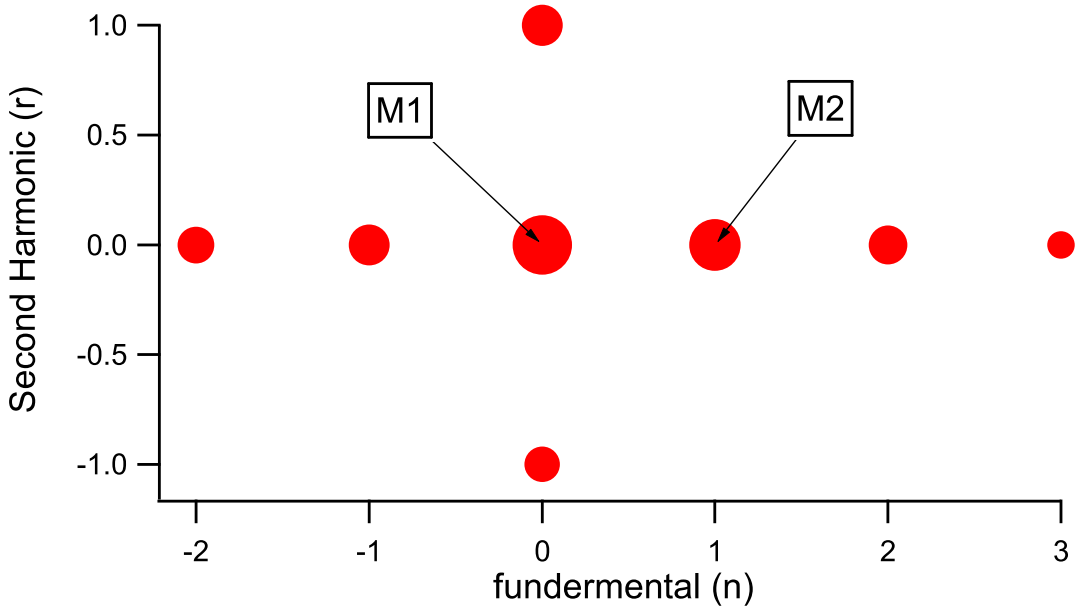

Figure 10
Extracted coefficients plotted where the size of the point represents the magnitude of the coefficient

In the first case (Fig. 5 and Fig. 6), the 5th order model is represented by the coefficient space as shown in Fig 6. In this figure, the magnitude of each coefficient

is represented by the size of its data point. The largest point, indicated by "m1" is the most dominant term in the extraction process and is equivalent to $S_{21}|a_{11}|$. "m2" is equivalent to $S_{22}|a_{21}|$ and this term is the second most dominant in the coefficient set. Figures 5 and 6 indicate that this model is able to reproduce most of the form of the perturbation due to the mixing of the fundamental phase with the input stimuli (a_{11}); however it is unable to model the interactions of the second harmonic signal (a_{22}) with the input fundamental signal (a_{11}). This is due to the mixing between the injected second harmonic signal at the output (a_{22}) and the injected fundamental signal at the output (a_{21}). The average error produced in this extraction was 1.8%.

In the second case (Fig. 7 and Fig. 8) the optimum number of coefficients which includes cross product terms has been added to enable capturing of the output mixing behaviour. This allows the model to properly track changes in the second harmonic's perturbation around all phases of the fundamental value of b_{21}. The average error resulting from this extraction was 0.25%.

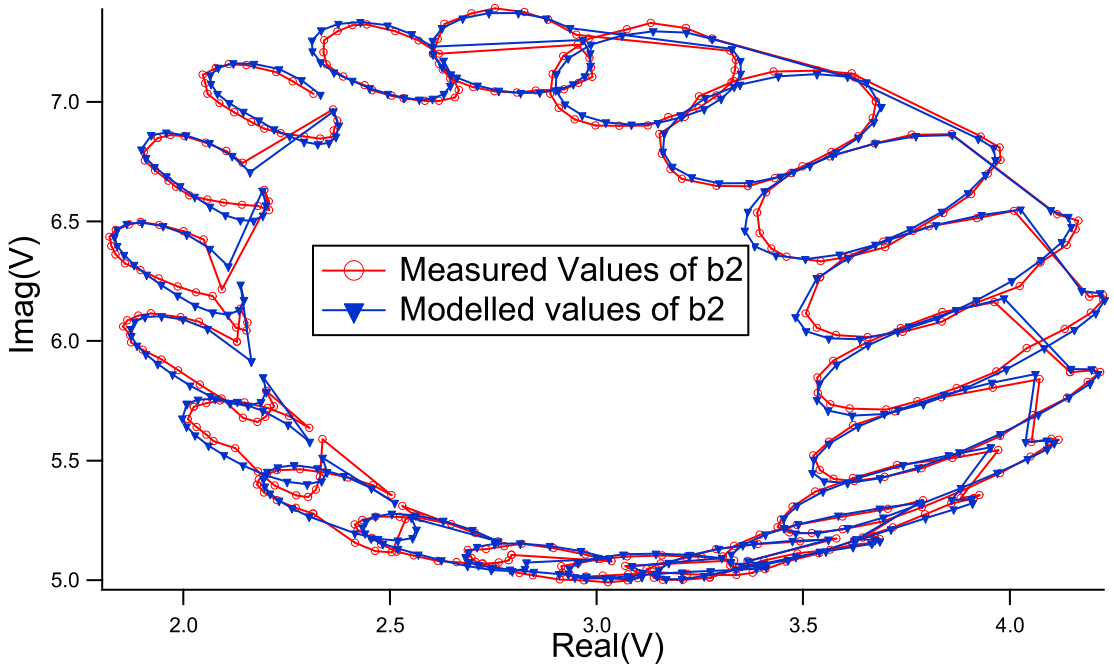

Figure 11
Measured and modelled values of $b_{2,1}$

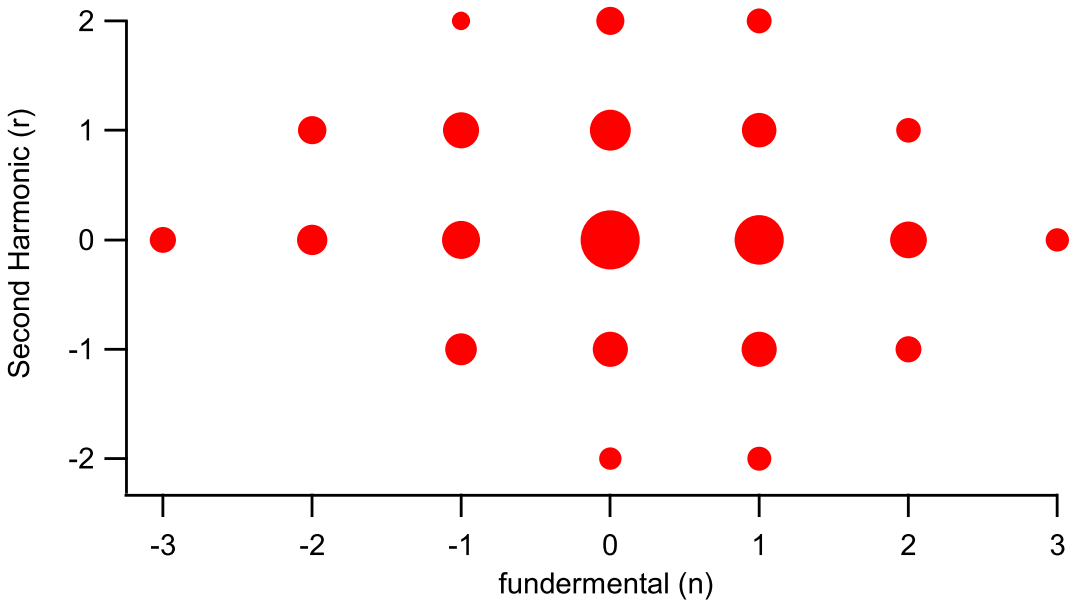

Figure 12

Extracted coefficients plotted where the size of the Point represents the Magnitude of the coefficient

4.4.2 Verification and Validation of modelling techniques

The discussed model can be structured within Computer Aided design software utilizing a Frequency domain Defined Device (FDD) [4]. The FDD enables computation of the incident travelling waves at the device ports, which are then used to compute new spectral voltages at these ports. The process discussed in this paper is repeated on all valid harmonics within the system at each device port to enable this functionality. An illustration of this has been conducted on an example data point, with measured and modelled voltage and current waveforms shown in Fig 9, 10.

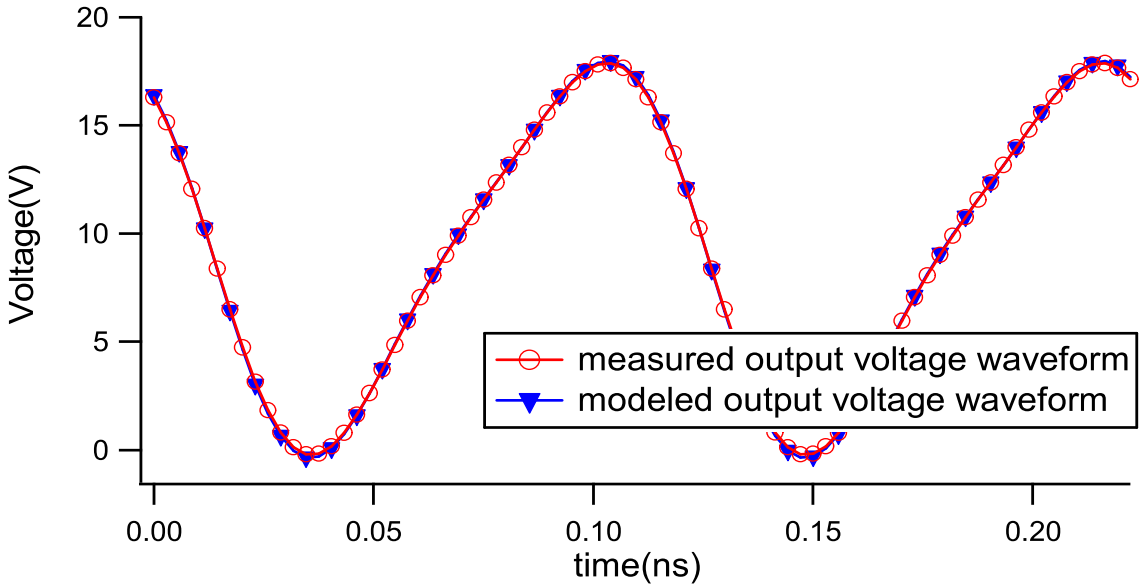

Figure 13

Measured and modelled output voltage waveforms

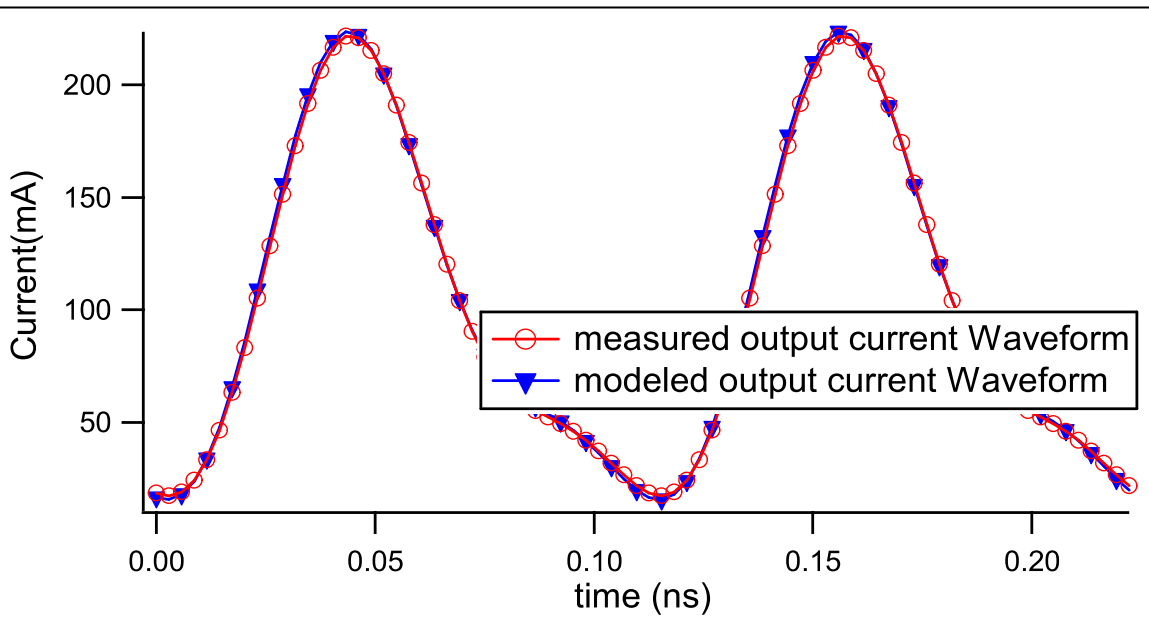

Figure 14

Measured and modelled output current waveforms

4.5. Discussion

A behavioural modelling framework based on mixing theory has been demonstrated, capable of taking into account the changes of load impedance at the fundamental and second harmonic frequencies. The optimum number of coefficients which includes cross product terms was deduced from the analysis of successive different extractions of the model. The model was able to track changes in the second harmonic's perturbation around all phases of the output fundamental signal. The model is also capable of encapsulating the device-plane waveforms within its structure.

4.5. References

1. S. Woodington, T. Williams, H. Qi, D.Williams, L. Pattison, A. Patterson, J. Lees, J. Benedikt, P. J. Tasker, "A Novel measurement based method enabling rapid extraction of a RF waveform look-up table based behavioral model" Microwave Symposium Digest IEEE MTT-S International, Page(s) 1453-1456, 15-20 June 2008

2. Woodington, S.; Saini, R.; Williams, D.; Lees, J.; Benedikt, J.; Tasker, P.J.; , "Behavioural model analysis of active harmonic load-pull measurements," Microwave Symposium Digest (MTT), 2010 IEEE MTT-S International , vol.,

no., pp.1688-1691, 23-28 May 2010

doi: 10.1109/MWSYM.2010.5517261

3. P.J. Tasker et al. “A vector corrected high power on wafer measurement system with a frequency range for higher harmonics up to 40GHz”, Proc. 24th European Microwave Conference 1994, pp 1367-1372

4. Tasker. P.J “Practical Waveform Engineering”, Microwave Magazine, IEEE Volume 10, Issue 7, pp 65-67, December 2009

Chapter 5 –Design of a Class-J X-Band Monolithic Power Amplifier

5.1 Introduction

The previous chapters (3) and (4) introduced new model frameworks that the author has developed for encapsulating relevant data for the design of high frequency transistor amplifiers. This chapter demonstrates the application of these new models in an X-band MMIC amplifier design. The design work was conducted as a collaborative research project with QinetiQ Ltd in Malvern, UK to design a high efficiency X-band MMIC amplifier [1]. The collaboration was successfully completed; showing the value of precise measurement based non-linear models within the design cycle.

This chapter also discusses attempts to use the PHD model frame work to perform various equation based analyses. For instance, the transformation of parameters to

different network representations and the location of optimum power, and the use of the Coarse Non-Linear models to drive an open loop active load pull system.
Finally, this chapter will provide an in-depth discussion of the roles of measurement based, partially formulated models in the design cycle of high frequency amplifiers.

5.2 Integration of modelling frameworks into CAD environments

The release of the X-Parameter [2] framework demonstrated simulator configurations which allow the implementation of the models discussed within this thesis within the Agilent Advanced Design System circuit simulator. An example configuration adapted for the models generated in chapter (4) is shown in figure (1). Figure (2) shows one Element of the 'mdf' file used as the core of the model, and figure (3) shows the integration of the model into a simple harmonic balance simulation.

The functional block in ADS comprises of a Frequency Defined Device (FDD) which is configured as two voltage sources the aim of the equations wrapped around the FDD are to calculate the two node voltages that would be present at the terminals of the device given a set of inputs i.e. 'a-waves'. These are calculated from probes of the voltages at the FDD terminals and the currents flowing into the nodes, each iteration of the harmonic balance simulation, controlling the model.

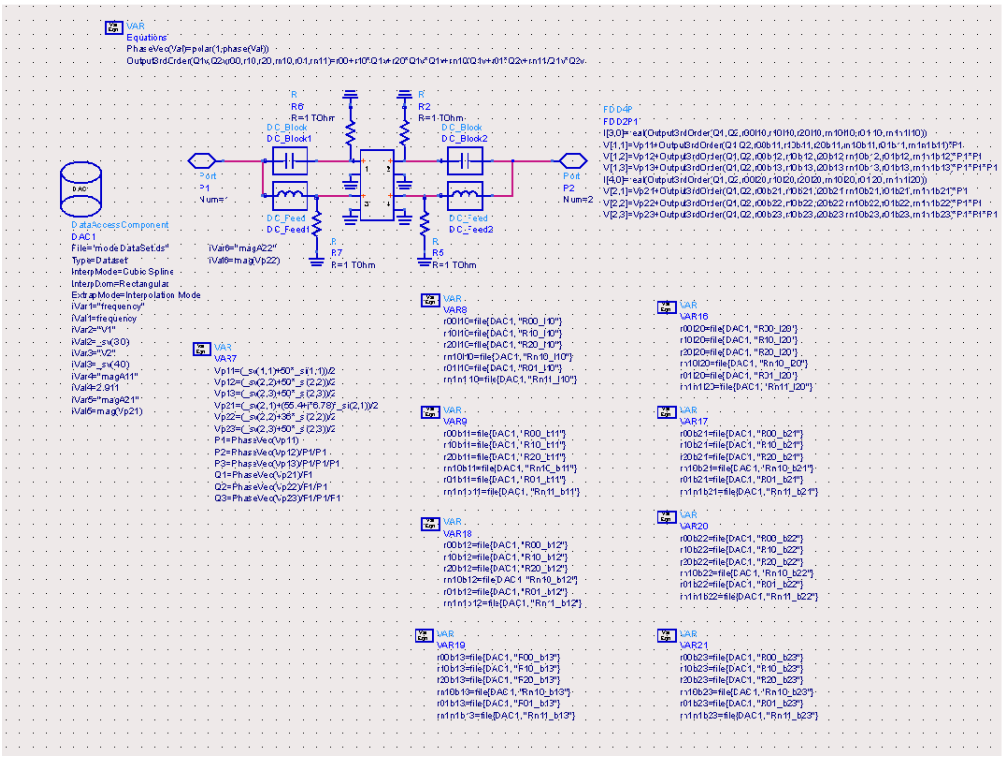

Example Implementation of fundamental and Second harmonic model in the ADS CAD environment
Figure 1

```
VAR frequency(real) =9.0000e+09
VAR V1(real) =-0.799585
VAR V2(real) =9.00
VAR magA11(real) =2.911180
VAR magA21(real) =2.590096
VAR magA22(real) =1.266839
BEGIN
%      row(real)    R00_I10(complex)  R10_I10(complex)  R20_I10(complex)  Rn10_I10(complex)
%      R01_I10(complex)  Rn11_I10(complex)
%      R00_b11(complex)  R10_b11(complex)  R20_b11(complex)  Rn10_b11(complex)
%      R01_b11(complex)  Rn11_b11(complex)
%      R00_b12(complex)  R10_b12(complex)  R20_b12(complex)  Rn10_b12(complex)
%      R01_b12(complex)  Rn11_b12(complex)
%      R00_b13(complex)  R10_b13(complex)  R20_b13(complex)  Rn10_b13(complex)
%      R01_b13(complex)  Rn11_b13(complex)
%      R00_I20(complex)  R10_I20(complex)  R20_I20(complex)  Rn10_I20(complex)
%      R01_I20(complex)  Rn11_I20(complex)
%      R00_b21(complex)  R10_b21(complex)  R20_b21(complex)  Rn10_b21(complex)
%      R01_b21(complex)  Rn11_b21(complex)
%      R00_b22(complex)  R10_b22(complex)  R20_b22(complex)  Rn10_b22(complex)
%      R01_b22(complex)  Rn11_b22(complex)
%      R00_b23(complex)  R10_b23(complex)  R20_b23(complex)  Rn10_b23(complex)
%      R01_b23(complex)  Rn11_b23(complex)
0      0.000022    -0.000000   -0.000008    -0.000000    0.000001    0.000001    -0.000008    0.000000
-0.000002    -0.000003    -0.000003    0.000000
-2.121465    -0.772818    0.241804     0.049392     0.003466    -0.005493    -0.018308    0.006989
-0.052656    -0.063050    -0.014886    -0.004136
0.190893     0.157504     -0.011903    0.100664     -0.012214    0.008524     -0.036501    0.008390
0.153518     -0.010059    0.003352     0.000609
-0.001868    -0.002269    0.000577     -0.001392    0.000070     -0.000063    0.000431     0.000045
-0.001477    0.000151     -0.000065    -0.000167
0.110944     0.000005     0.008465     0.012106     0.000618     -0.000911    0.008468     -0.012103
0.002004     -0.001903    0.000551     -0.001311
2.930536     5.862481     -0.149203    -1.400553    0.032551     0.106044     0.159273     -0.077227
-0.233819    -0.119267    0.125953     0.009277
0.747348     -0.157231    0.287173     0.136599     0.047224     -0.090413    -0.031731    -0.033592
-0.099192    -0.706554    -0.022499    -0.070520
-0.000967    0.001622     0.001639     0.000283     0.000436     -0.001169    0.000283     -0.000614
-0.002316    0.002945     -0.000152    -0.000927
END
```

Mdf file used to wrap the model parameters for the use in the simulation tool
Figure 2

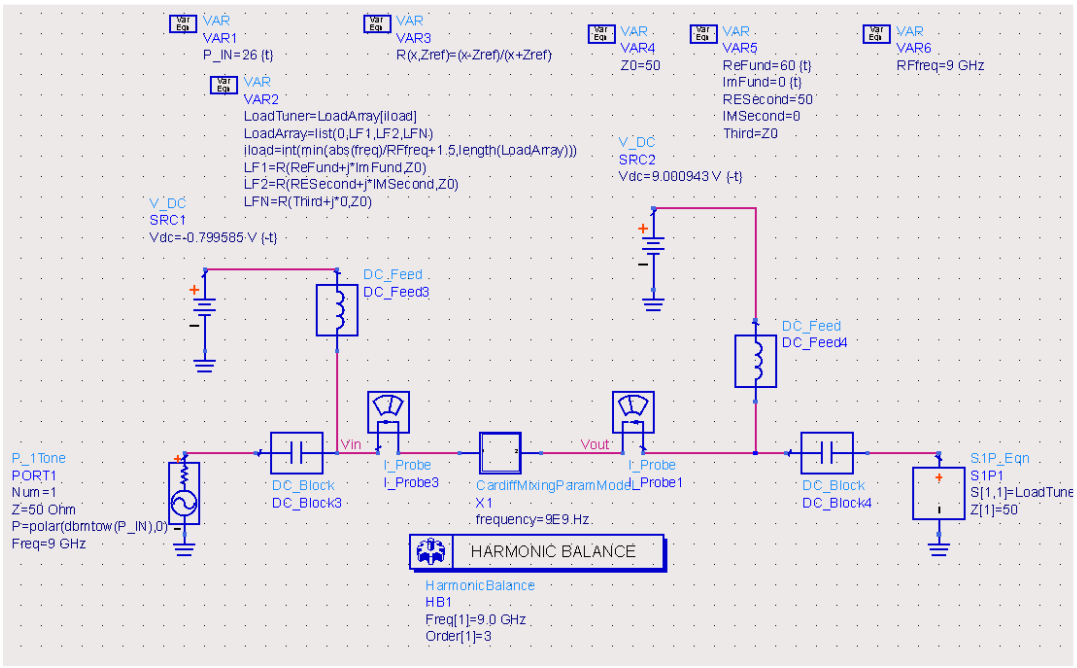

Integration of model within a harmonic balance simulation
Figure 3

.

5.3 Design and Fabrication of a Class-J MMIC amplifier

The class-J amplifier was first proposed by S.C Cripps in [3] as a way of developing power from a reactively mismatched class-B Biased transistor by reactively offsetting the second harmonic and successive terminations to recover the output power and Efficiency. These ideas were further developed and demonstrated with the construction of a 1.5-2 GHz 10W amplifier by Wright [4] and the identification of a extended 'Class-B' design space in [5,6] by Wright, Cripps, Benedikt and Tasker.

In this section of work an attempt was made to exploit the ideas presented by Cripps and Wright et.al, for the design of an X-band MMIC amplifier operating between 7.5 and 11.5 GHz, having 60% efficiency over this bandwidth.

5.3.1 Measurement and Modelling of a GaAs HEMT for use in the design process

The class-J continuous design space identifies a rejoin of fundamental and second harmonic impedances within which the same drain or output efficiency can be obtained from a transistor biased in class-B. This region comprises of a set of reactance's at a fixed resistance for the fundamental and a related loss-less set of reactive second harmonic terminations $|\Gamma|=1$.

To measure and confirm the existence of the Class-J design space, it is required that a chosen fundamental Impedance, and the second harmonic impedance is swept all around the perimeter of the smith chart to identify the location and value of the maximum efficiency. Repeating this process at successive fundamental terminations, results in the identification of the continuous class J design space.
These measurements are time consuming and rely, on the operator of the waveform measurement system to have the ability, knowledge and time to perform these measurements correctly. In response to this it was proposed to use the techniques demonstrated in chapter-4 to identify the design space for the continuous class-J design. The extraction demonstrated in chapter 4 provides equivalent data to that needed for the design of a class-J amplifier whilst requiring less operator setup time and more automation of the measurements. The Class-J space can then be found by post processing measurement data. For this section of work and for Chapter-4 the data collected was the same. Figure 4 shows the results of directly post processing the measurement results to identify the Class-J design space. Figures 5 and 6 show the class-J design space extracted after converting the data set into the

model described in Chapter 4 and re-identifying the class-J design space. The data set and model were found to be in good agreement.

The model was provided to QinetiQ Malvern where the design of a class-J amplifier was conducted the results of which are discussed in the following section.

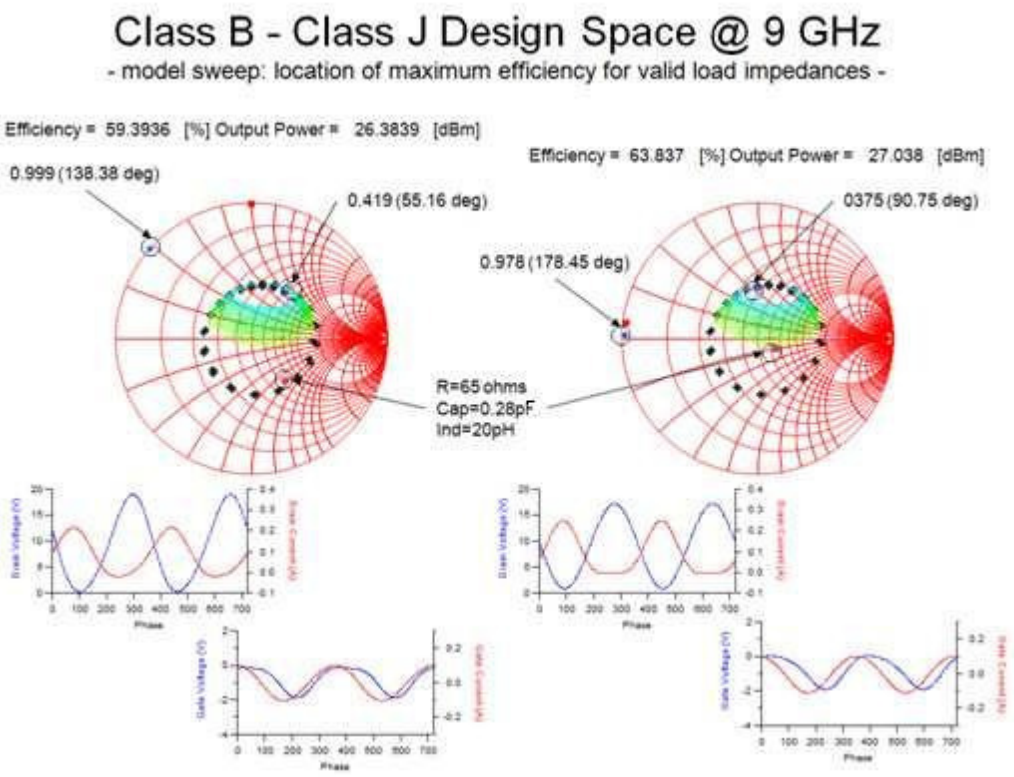

Identification of Class J Design Space at 9GHz
Figure 4

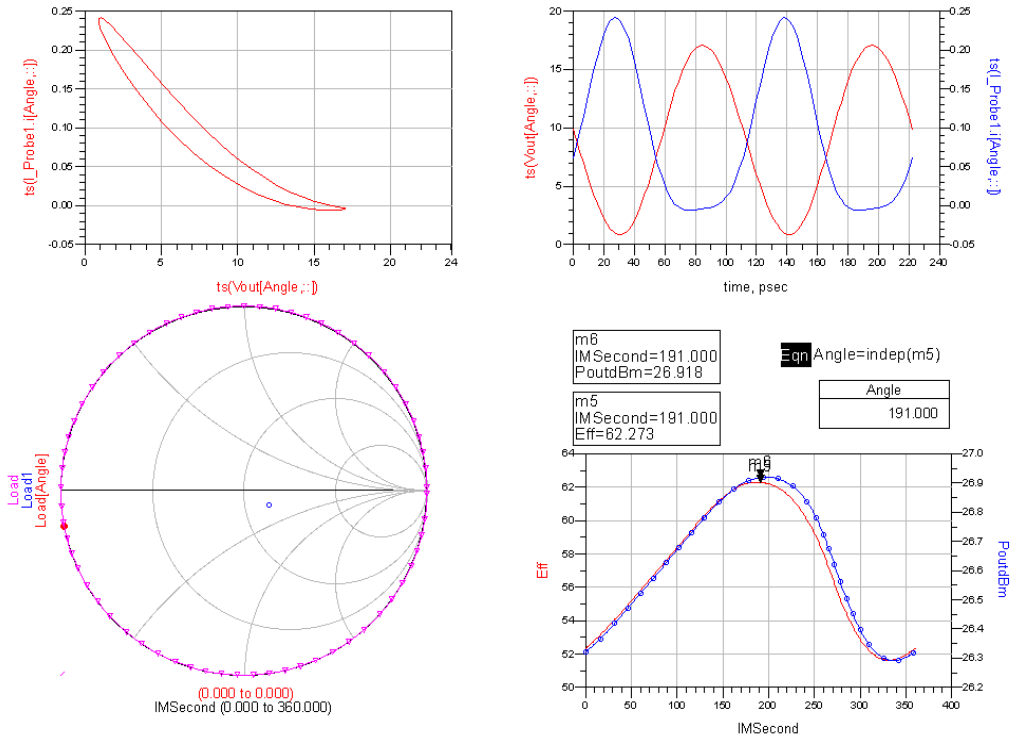

Class-J design space extracted from Model
Figure 5

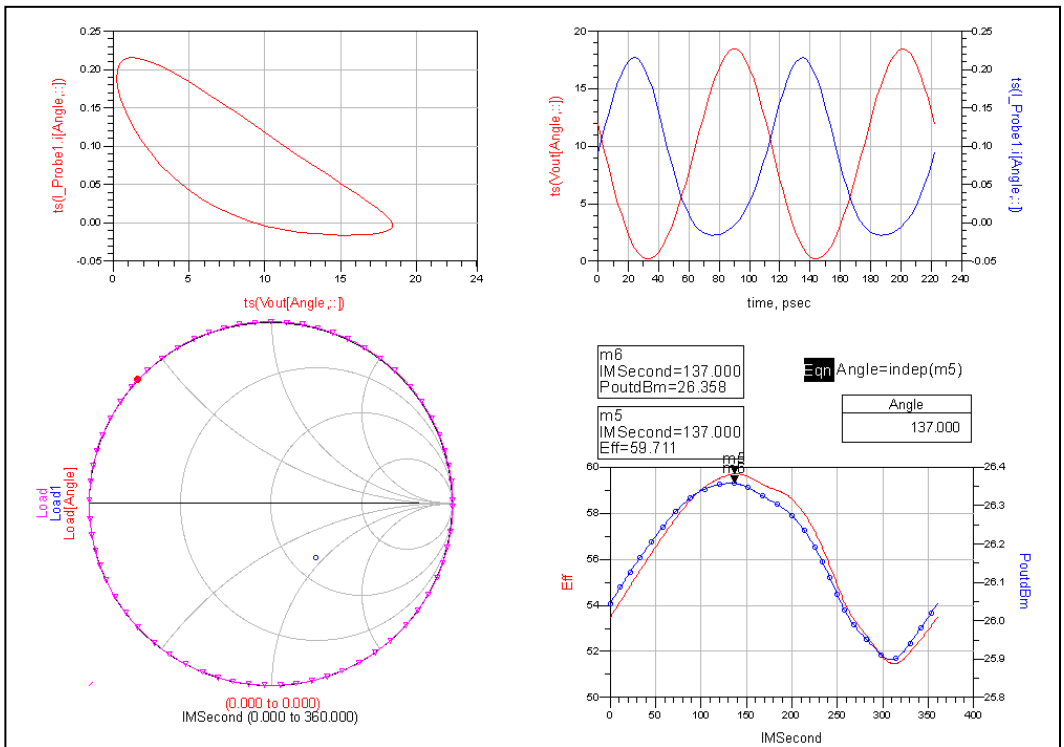

class-J design space extracted from model
Figure 6

5.3.2 Results from Measurement of Fabricated Amplifier

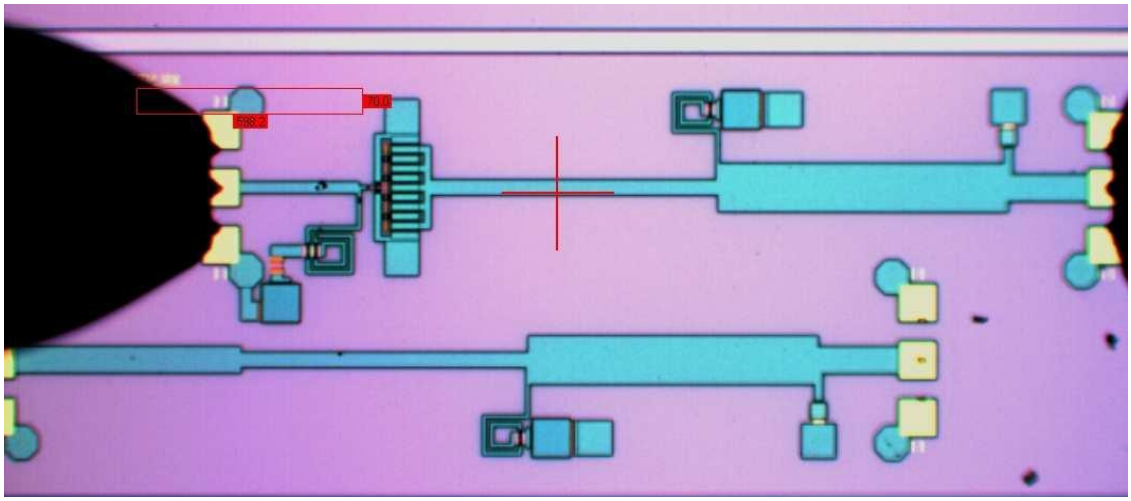

Figure 7
Fabricated Mimic Amplifier test Cell

Figure 7 shows an image of the prototyped MMIC amplifier cell, the amplifier has an output matching network that exploits the Class-J to Class-B continuum of modes. The achieved performance of the amplifier at 1dB of compression is shown in figure 8 figure 9 shows the drain efficiency vs. input power and output power vs. input power curves for the test cell.

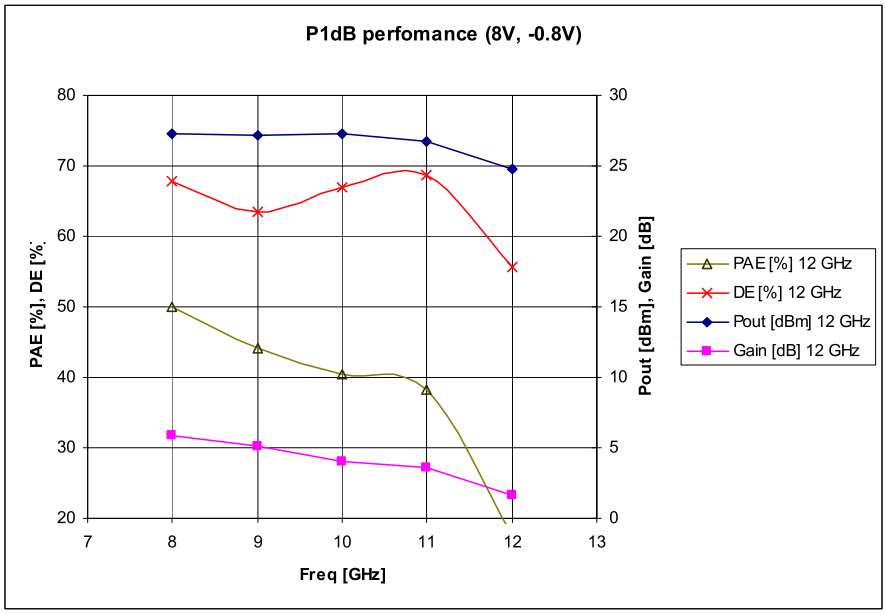

Figure 8
Measured device performance at 1dB of compression

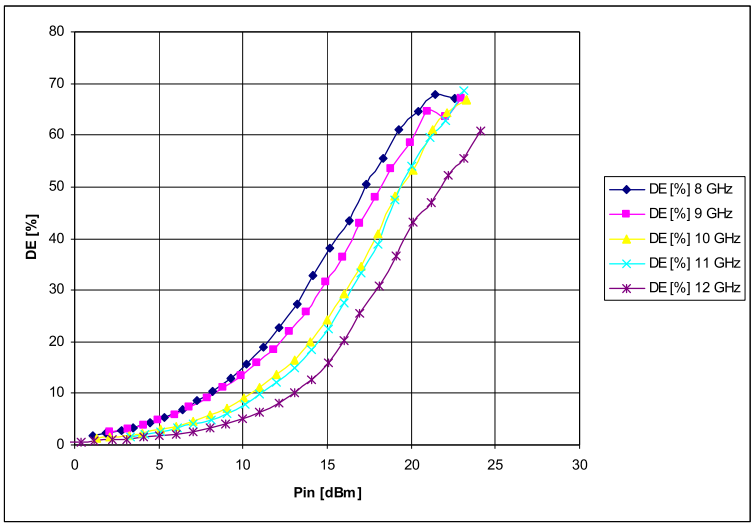

Figure 9a
Drain efficiency vs. input power

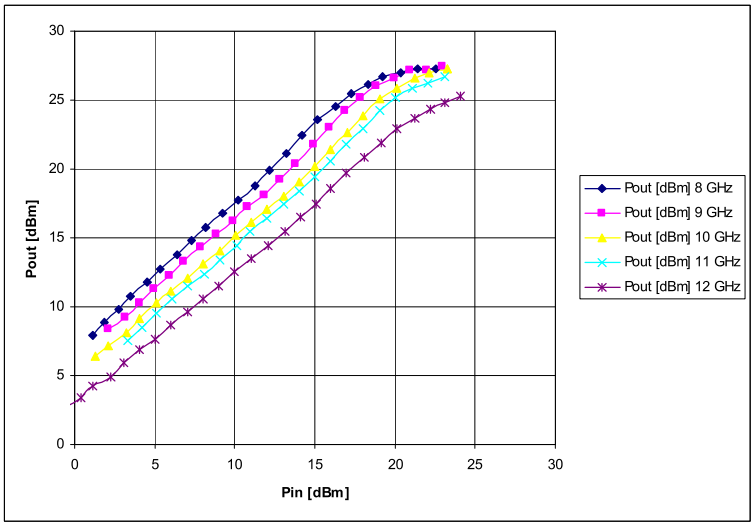

Figure 9a
Output power vs. input power

The measurements show that the amplifier has a drain efficiency that is greater than 60% at 1dB compression over a 30% bandwidth the power added efficiency is limited by the gain of the amplifier, the output power of approximately 0.5W is maintained over the 30% bandwidth.

5.4 Discussion

The collaborative work carried out, has demonstrated how the modelling work described in chapters 3 and 4 of this thesis can be successfully applied to the design of high frequency amplifiers. This work also demonstrated that it was possible to construct an amplifier biased on the class-J and B continuum of modes at X-Band frequencies.

5.5 References

1. J.Powell, M. Uren, T. Martin, S. Cripps, P. Tasker, J. Benedikt, S.Woodington, A. Mclachlan

   "Investigation of high efficiency amplifiers at X-band using GaAs p-HEMT and GaN HFET technologies"

   QinetiQ Ltd, Malvern, Cardiff University, Selex Galileo, Edinburgh,

   Electro-Magnetic Remote Sensing (EMRS) Defence Technology Centre (DTC), 7th Annual Technical Conference,13th -14th July 2010,Conference Proceedings

2. X-Parameters: The new paradigm for measurement, modeling and design of nonlinear RF and microwave components

   David E. Root, Jason Horn, Loren Betts, Chad Gillease, Jan Verspect

   Microwave Engineering Europe,Dec 2008,www.mwee.com

3. Cripps, S.C., RF Power Amplifiers For Wireless Communications. 2nd ed. 2006: Artech House. 4.2, pp68

4. P. Wright, J. Lees, P. J. Tasker, J. Benedikt, S. C. Cripps, “An Efficient, linear, broadband class-J-mode PA realised using waveform engineering,” IEEE MTT-S 2009 International Microwave Symposium Digest, pp. 653-656, Boston, MA, USA, 7-12 June 2009.

5. P. Wright, J. Lees, P. J. Tasker, J. Benedikt, S. C. Cripps, “A Methodology for Realizing High Efficiency Class-J in a Linear and Broadband PA,” IEEE Transactions on Microwave Theory and Techniques, Volume 57, Issue 12, pp. 3196-3204, December-2009.

6. S.C. Cripps, P.J. Tasker, A.L Clarke, J Lees, J. Benedikt, “On the Continuity of High Efficiency Modes in Linear RF Power Amplifiers ”, IEEE Microwave and Wireless Components Letters 19(10) 2009 pp665

Chapter 6 – Conclusions

6.1 Discussion

In this thesis the author has investigated the Poly-Harmonic-Distortion model and related Techniques. The development of the PHD model has been discussed in detail; it was shown how the model was developed from attempts to extend the available S-Parameter formulations and measurement solutions to allow the capture of relevant performance and network information about high frequency transistors operating under large signal regimes.

The thesis, through simulated case studies and an in-depth literature review, shows how the poly-harmonic distortion model improved on earlier attempts based on Large-Signal-S-Parameters. Also an attempt was made at quantifying the range of applicability of the PHD model technique when applied to predicting non-linear devices operation when both fundamental and harmonic load are varied, ideally over the complete Smith Chart. It was shown that the PHD model has a limited range of applicability when applied to directly model the effect of fundamental load-pull. It is not possible to directly infer the extrapolation range, the PHD model will have without

performing the necessary measurements. These measurements allow the magnitude dependence of the coefficients to be investigated using Eqn (9).

$$X^F\left(|a_{11}|\right) = R_0\left(|a_{21}|,|a_{11}|\right)$$

$$\frac{\partial X^F\left(|a_{11}|\right)}{\partial|a_{21}|} = \frac{\partial R_0\left(|a_{21}|,|a_{11}|\right)}{\partial|a_{21}|} = 0$$

$$X^S\left(|a_{11}|\right) = \frac{\partial R_1\left(|a_{21}|,|a_{11}|\right)}{\partial|a_{21}|},\ X^T\left(|a_{11}|\right) = \frac{\partial R_{-1}\left(|a_{21}|,|a_{11}|\right)}{\partial|a_{21}|}$$

These relationships are valid only when for one magnitude of $|a_{11}|$ X^F, X^S and X^T can be considered constant while $|a_{21}|$ changes and also while no other R_n coefficient is significant if not no conversion exists.

Eqn (9)

As it was concluded that the PHD model failed to capture all the information measured with respect to fundamental load variation. Hence, an extended fundamental load-pull model was developed and investigated. To do this it was decided to keep the measurement as close to those specified in the original PHD model framework as possible. It was then shown that by increasing the size of the perturbation applied to the device under incrementally the higher order effects could be observed whilst covering reasonable areas of fundamental load variation. A mathematical framework was developed that allowed these higher order variations to be modelled; captured as polynomials of phase between the injected signals at the device ports using Fourier methods.

The PHD model as well as capturing device behavior at the fundamental frequency also has terms that allow the modeling of harmonic behavior. These terms are shown to have a greater range of applicability when applied to second harmonic

load-pull at a fixed fundamental load. However, they were unable to simultaneously track fundamental and harmonic behaviour. To account for this the model framework was expanded to include harmonic terms this took the form of a phase polynomial with multiple dimensions where each dimension accounted for a new stimulus. These models were tested firstly by producing a fundamental stimuli only model of a 0.5W GaAs HBT at 0.9GHz, and then a fundamental and second harmonic model of a 0.5W GaAs pHEMT at 9GHz. The later model was used to assist a third party in design of a Class-J MMIC amplifier the results of which were briefly shown in chapter-5. This demonstrated that the model contained enough information to be useful in the design process. It also showed that the class J-B design space could be located at X-Band in devices that were produced by a commercially available process.

6.2 Future work

The model frame work as developed and discussed in this thesis as stated in chapter 4 is extendable to allow investigations into multi- harmonic interactions in this thesis. This was demonstrated with the fundamental and second harmonic load impedances. This work could be developed further, by investigating the inclusion of other terminating impedances on the device ports, and also with further trials of the model within design environment. This would provide more detail on the limitations and applicability of the discussed techniques. Also development of these modeling techniques could lead to useful tools for analysis of yield and conformity of multiple devices.

As part of the investigations conducted into the PHD model within this thesis various equation based techniques were identified. A detailed investigation of one such technique lead to improvements in the algorithm driving load convergence of the open loop active load-pull system developed by Tasker et.al [1], further details of this can be found in [2]. As well as improving active load-pull algorithms, other techniques were found which may allow algebraic transformation of the PHD model framework and stability analysis and location of optimum power. Development of these could lead to useful circuit analysis and synthesis tools.

6.3 Conclusion

This thesis conducted a detailed impartial investigation into the Poly-Harmonic-Distortion Model. As a result of this investigation a non-linear mixing based frame work was demonstrated, that can be used to capture fundamental and second harmonic load-pull effects. The modelling framework was demonstrated as applied to the design of a Class J amplifier.

The author believes that the developed model provides a framework that simplifies the measurements required for modelling multi-harmonic load-pull interactions without loss of information. The construction of the model allows decisions about the required order of the model to be made in a structured manner.

6.4 References

1. P.J. Tasker et al. “A vector corrected high power on wafer measurement system with a frequency range for higher harmonics up to 40GHz”, Proc. 24th European Microwave Conference 1994, pp 1367-1372

2. Saini, R.S.; Woodington, S.; Lees, J.; Benedikt, J.; Tasker, P.J.; , "An intelligence driven active loadpull system," Microwave Measurements Conference (ARFTG), 2010 75th ARFTG , vol., no., pp.1-4, 28-28 May 2010 doi: 10.1109/ARFTG.2010.5496327
URL: http://ieeexplore.ieee.org/stamp/stamp.jsp?tp=&arnumber=5496327&isnumber=5496310

Appendices

A1. Formulae Reference

A1.0.0 Matirix definitions

Definition of "H" Hemation Conjugate or Conjugate Transpose

The element-wise conjugate followed by the Transpose operation or

Transpose operation followed by the element-wise conjugate

$$\begin{bmatrix} a & b \\ c & d \end{bmatrix}^H = conj\left(\begin{bmatrix} a & b \\ c & d \end{bmatrix}^T\right) = \begin{bmatrix} a* & c* \\ b* & d* \end{bmatrix}$$

A1.0.1 Trigonometric identities

$$\cos(\theta) = \frac{1}{2}\left(e^{j\theta} + e^{-j\theta}\right) = \frac{1}{2}\left(a + a^{-1}\right)$$

$$\cos^2(\theta) = \frac{1}{4}\left(a^{+1} + a^{-1}\right)^2 = \frac{1}{4}\left(a^{+2} + 2a^{+1}a^{-1} + a^{-2}\right)$$
$$= \frac{1}{4}\left(a^{+2} + a^{-2} + 2\right) = \frac{1}{2}\cos(2\theta) + \frac{1}{2}$$

$$\cos^3(\theta) = \frac{1}{8}\left(a^{+1} + a^{-1}\right)^3 = \frac{1}{8}\left(a^{+3} + 3a^{+2}a^{-1} + 3a^{+1}a^{-2} + a^{-3}\right)$$
$$= \frac{1}{8}\left(a^{+3} + a^{-3} + 3\left(a^{+1} + a^{-1}\right)\right) = \frac{1}{4}\cos(3\theta) + \frac{3}{4}\cos(\theta)$$

$$\cos^4(\theta) = \frac{1}{16}\left(a^{+1} + a^{-1}\right)^4 = \frac{1}{16}\left(a^{+4} + 4a^{+3}a^{-1} + 6a^{+2}a^{-2} + 4a^{-3}a^{1} + a^{-4}\right)$$
$$= \frac{1}{16}\left(a^{+4} + a^{-4} + 4\left(a^{+2} + a^{-2}\right) + 6\right) = \frac{1}{16}\cos(4\theta) + \frac{1}{4}\cos(2\theta) + \frac{3}{8}$$

$$\cos^5(\theta) = \frac{1}{32}\left(a^{+1} + a^{-1}\right)^5 = \frac{1}{32}\left(a^{+5} + 5a^{+4}a^{-1} + 10a^{+3}a^{-2} + 10a^{2}a^{-3} + 5a^{1}a^{-4} + a^{-5}\right)$$

$$= \frac{1}{32}\left(a^{+5} + a^{-5} + 5\left(a^{+3} + a^{-3}\right) + 10\left(a^{+1} + a^{-1}\right)\right) = \frac{1}{32}\cos(5\theta) + \frac{5}{32}\cos(3\theta) + \frac{5}{16}\cos(\theta)$$

$$\cos(\theta)\cos(\alpha) = \frac{1}{4}\left(e^{+j\theta} + e^{-j\theta}\right)\left(e^{+j\alpha} + e^{-j\alpha}\right) = \frac{1}{4}\left(e^{+j\theta}e^{+j\alpha} + e^{+j\theta}e^{-j\alpha} + e^{-j\theta}e^{+j\alpha} + e^{-j\theta}e^{-j\alpha}\right)$$

$$= \frac{1}{2}\cos(\theta + \alpha) + \frac{1}{2}\cos(\theta - \alpha)$$

A1.1. Polynomial Expansions: chapter 3

$$\left(g_0 + g_1 + g_2 + \ldots + g_n\right)\left(k_0 + k_1 + k_2 + \ldots + k_n\right)$$

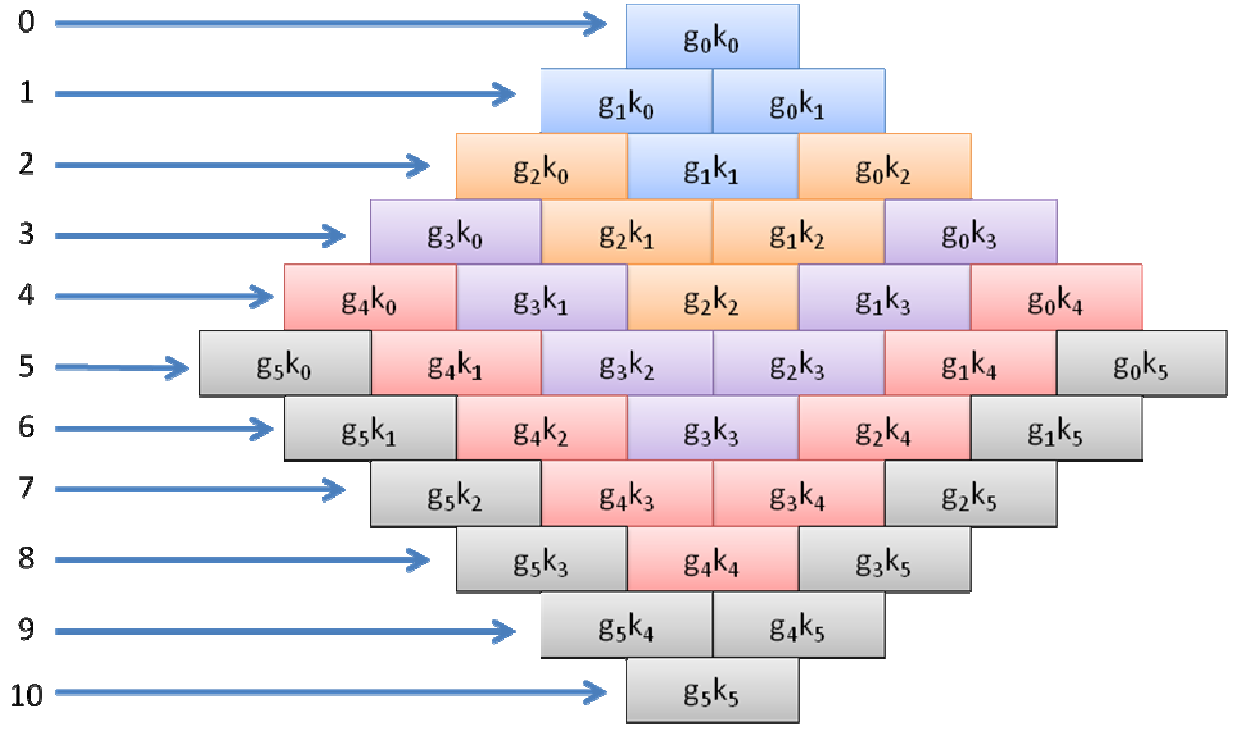

$$\left(g_0x^0 + g_1x^1 + g_2x^2 + \ldots + g_nx^n\right)\left(k_0y^0 + k_1y^1 + k_2y^2 + \ldots + k_ny^n\right)$$

$$x = A\cos(\theta + \varphi_A)$$

$$y = B\cos(\theta + \varphi_B)$$

$$\theta = \omega t$$

Terms at fundamental frequency due to 3rd order expansion

1	$g_1 k_0 A\cos(\theta+\varphi_A)$	$g_0 k_1 B\cos(\theta+\varphi_B)$
3	$\frac{3g_3 k_0 A^3}{4}\cos(\theta+\varphi_A)$	$\frac{3g_0 k_3 B^3}{4}\cos(\theta+\varphi_B)$
5	$\frac{g_1 k_2 AB^2}{4}\cos(\theta+2\varphi_B-\varphi_A)$ $\frac{g_1 k_2 AB^2}{2}\cos(\theta+\varphi_A)$	$\frac{g_2 k_1 BA^2}{4}\cos(\theta+2\varphi_A-\varphi_B)$ $\frac{g_2 k_1 BA^2}{2}\cos(\theta+\varphi_B)$
7	$\frac{g_3 k_2 B^2 A^3}{16}\cos(\theta+3\varphi_A-2\varphi_B)$ $\frac{3g_3 k_2 B^2 A^3}{16}\cos(\theta+2\varphi_B-\varphi_A)$ $\frac{3g_3 k_2 B^2 A^3}{8}\cos(\theta+\varphi_A)$	$\frac{g_2 k_3 B^3 A^2}{16}\cos(\theta+3\varphi_B-2\varphi_A)$ $\frac{3g_2 k_3 B^3 A^2}{16}\cos(\theta+2\varphi_A-\varphi_B)$ $\frac{3g_2 k_3 B^3 A^2}{8}\cos(\theta+\varphi_B)$

Terms at fundamental frequency due to 3rd order expansion in complex form

1	$\Re\left\{g_1 k_0 A e^{j\theta}e^{j\varphi_A}\right\}$	$\Re\left\{g_0 k_1 B e^{j\theta}e^{j\varphi_B}\right\}$
3	$\Re\left\{\frac{3g_3 k_0 A^3}{4}e^{j\theta}e^{j\varphi_A}\right\}$	$\Re\left\{\frac{3g_0 k_3 B^3}{4}e^{j\theta}e^{j\varphi_B}\right\}$
5	$\Re\left\{\frac{g_1 k_2 AB^2}{4}e^{j\theta}e^{2j\varphi_B}e^{-j\varphi_A}\right\}$ $\Re\left\{\frac{g_1 k_2 AB^2}{2}e^{j\theta}e^{j\varphi_A}\right\}$	$\Re\left\{\frac{g_2 k_1 BA^2}{4}e^{j\theta}e^{2j\varphi_A}e^{-j\varphi_B}\right\}$ $\Re\left\{\frac{g_2 k_1 BA^2}{2}e^{j\theta}e^{j\varphi_B}\right\}$
7	$\Re\left\{\frac{g_2 k_3 B^3 A^2}{16}e^{j\theta}e^{3j\varphi_B}e^{-2j\varphi_A}\right\}$ $\Re\left\{\frac{3g_2 k_3 B^3 A^2}{16}e^{j\theta}e^{2j\varphi_A}e^{-j\varphi_B}\right\}$ $\Re\left\{\frac{3g_2 k_3 B^3 A^2}{8}e^{j\theta}e^{j\varphi_B}\right\}$	$\Re\left\{\frac{g_3 k_2 B^2 A^3}{16}e^{j\theta}e^{3j\varphi_A}e^{-2j\varphi_B}\right\}$ $\Re\left\{\frac{3g_3 k_2 B^2 A^3}{16}e^{j\theta}e^{2j\varphi_B}e^{-j\varphi_A}\right\}$ $\Re\left\{\frac{3g_3 k_2 B^2 A^3}{8}e^{j\theta}e^{j\varphi_A}\right\}$

$$\Re\left\{e^{j\theta}e^{j\varphi_A}\left(\begin{array}{l}\left(g_1k_0A+\frac{3g_3k_0A^3}{4}+\frac{g_1k_2AB^2}{2}+\frac{3g_3k_2B^2A^3}{8}\right)+\\\left(\frac{g_1k_2AB^2}{4}+\frac{3g_3k_2B^2A^3}{16}\right)e^{2j\varphi_B}e^{-j2\varphi_A}+\\\frac{g_3k_2B^2A^3}{16}e^{2j\varphi_A}e^{-2j\varphi_B}\end{array}\right)\right\}$$

$$\Re\left\{e^{j\theta}e^{j\varphi_A}\left(\begin{array}{l}\left(g_0k_1B+\frac{3g_0k_3B^3}{4}+\frac{g_2k_1BA^2}{2}+\frac{3g_2k_3B^3A^2}{8}\right)e^{j\varphi_B}e^{-j\varphi_A}+\\\left(\frac{g_2k_1BA^2}{4}+\frac{3g_2k_3B^3A^2}{16}\right)e^{j\varphi_A}e^{-j\varphi_B}+\\\frac{g_2k_3B^3A^2}{16}e^{3j\varphi_B}e^{-3j\varphi_A}\end{array}\right)\right\}$$

$$\Phi = e^{j\varphi_B}e^{-j\varphi_A}$$

$$\Re\left\{e^{j\theta}e^{j\varphi_A}\left(\begin{array}{l}\left(g_1k_0A+\frac{3g_3k_0A^3}{4}+\frac{g_1k_2AB^2}{2}+\frac{3g_3k_2B^2A^3}{8}\right)+\\\left(\frac{g_1k_2AB^2}{4}+\frac{3g_3k_2B^2A^3}{16}\right)\Phi^2+\\\frac{g_3k_2B^2A^3}{16}\Phi^{-2}\end{array}\right)\right\}+$$

$$\Re\left\{e^{j\theta}e^{j\varphi_A}\left(\begin{array}{l}\left(g_0k_1B+\frac{3g_0k_3B^3}{4}+\frac{g_2k_1BA^2}{2}+\frac{3g_2k_3B^3A^2}{8}\right)\Phi+\\\left(\frac{g_2k_1BA^2}{4}+\frac{3g_2k_3B^3A^2}{16}\right)\Phi^{-1}+\\\frac{g_2k_3B^3A^2}{16}\Phi^3\end{array}\right)\right\}$$

$$P = e^{j\varphi_A}$$

$$\Re\left\{e^{j\theta}P\left(\begin{array}{l}\frac{g_3k_2B^2A^3}{16}\Phi^{-2}+\\ \left(\frac{g_2k_1BA^2}{4}+\frac{3g_2k_3B^3A^2}{16}\right)\Phi^{-1}+\\ \left(g_1k_0A+\frac{3g_3k_0A^3}{4}+\frac{g_1k_2AB^2}{2}+\frac{3g_3k_2B^2A^3}{8}\right)+\\ \left(g_0k_1B+\frac{3g_0k_3B^3}{4}+\frac{g_2k_1BA^2}{2}+\frac{3g_2k_3B^3A^2}{8}\right)\Phi+\\ \left(\frac{g_1k_2AB^2}{4}+\frac{3g_3k_2B^2A^3}{16}\right)\Phi^2+\\ \frac{g_2k_3B^3A^2}{16}\Phi^3\end{array}\right)\right\}$$

	Φ^{-6}	Φ^{-5}	Φ^{-4}	Φ^{-3}	Φ^{-2}	Φ^{-1}	Φ^{0}	Φ^{1}	Φ^{2}	Φ^{3}	Φ^{4}	Φ^{5}	Φ^{6}	Φ^{7}
$\lvert a_{21}\rvert^0$							1st							
$\lvert a_{21}\rvert^1$						3rd		1st						
$\lvert a_{21}\rvert^2$					3rd		3rd		3rd					
$\lvert a_{21}\rvert^3$				5th		3rd		3rd		3rd				
$\lvert a_{21}\rvert^4$			5th		5th		5th		5th		5th			
$\lvert a_{21}\rvert^5$		7th		5th		5th		5th		5th		5th		
$\lvert a_{21}\rvert^6$	7th		7th		7th		7th		7th		7th		7th	
$\lvert a_{21}\rvert^7$		7th		7th		7th		7th		7th		7th		7th

$$b_{p,h}=P^h\sum_{n=N-1}^{N}R\left(\left|a_{11}\right|,\left|a_{21}\right|\right)\Phi^n$$

$$g_0+g_1\left(A_1+A_2\right)+g_2\left(A_1+A_2\right)^2+\ldots+g_n\left(A_1+A_2\right)^n$$

$$g_0 + g_1 A_1 + g_1 A_2 + g_2 A_1^2 + 2g_2 A_1 A_2 + g_2 A_2^2 + g_3 A_1^3 + 3g_3 A_1^2 A_2 + 3g_3 A_1 A_2^2 + g_3 A_2^3$$

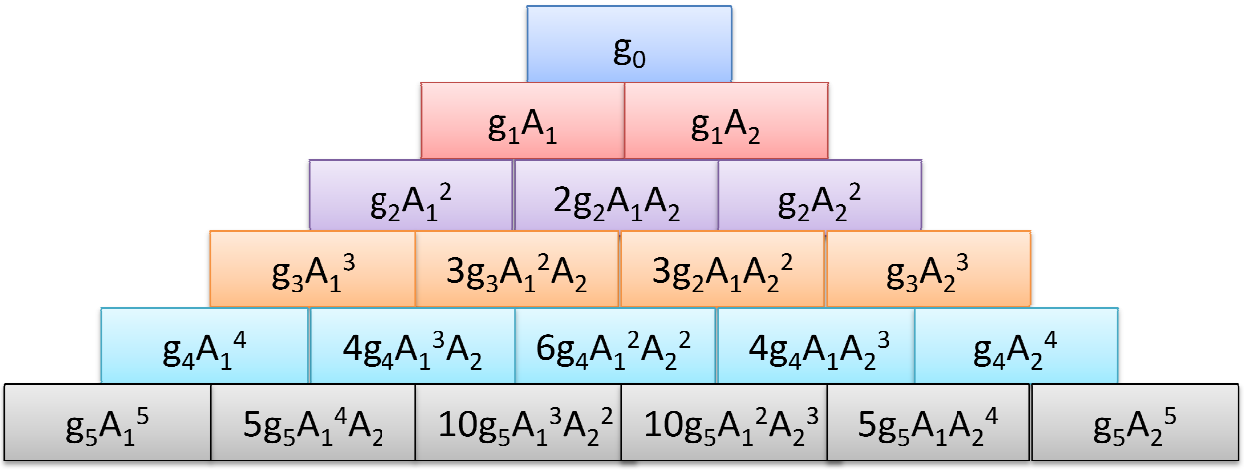

$$A_1 = A\cos(\theta + \varphi_A)$$

$$A_2 = B\cos(\theta + \varphi_B)$$

$$\theta = \omega t$$

$$g_1 A\cos(\theta + \varphi_A) + g_1 B\cos(\theta + \varphi_B) +$$
$$g_3 A^3 \cos^3(\theta + \varphi_A) + g_3 B^3 \cos^3(\theta + \varphi_B) +$$
$$g_3 A^2 B\cos^2(\theta + \varphi_A)\cos(\theta + \varphi_B) + g_3 B^2 A\cos(\theta + \varphi_A)\cos^2(\theta + \varphi_B)$$

$$g_1 A\cos(\theta + \varphi_A) + g_1 B\cos(\theta + \varphi_B) +$$
$$\frac{g_3 A^3}{4}\cos(3\theta + 3\varphi_A) + \frac{3g_3 A^3}{4}\cos(\theta + \varphi_A) +$$
$$\frac{g_3 B^3}{4}\cos(3\theta + 3\varphi_B) + \frac{3g_3 B^3}{4}\cos(\theta + \varphi_B) +$$
$$\frac{g_3 A^2 B}{4}\cos(3\theta + 2\varphi_A + \varphi_B) + \frac{g_3 A^2 B}{4}\cos(\theta + 2\varphi_A - \varphi_B) + \frac{g_3 A^2 B}{2}\cos(\theta + \varphi_B) +$$
$$\frac{g_3 B^2 A}{4}\cos(3\theta + 2\varphi_B + \varphi_A) + \frac{g_3 B^2 A}{4}\cos(\theta + 2\varphi_B - \varphi_A) + \frac{g_3 B^2 A}{2}\cos(\theta + \varphi_A)$$

$$g_1 A\cos(\theta + \varphi_A) + g_1 B\cos(\theta + \varphi_B) +$$
$$\frac{3g_3 A^3}{4}\cos(\theta + \varphi_A) + \frac{3g_3 B^3}{4}\cos(\theta + \varphi_B) +$$
$$\frac{g_3 A^2 B}{4}\cos(\theta + 2\varphi_A - \varphi_B) + \frac{g_3 A^2 B}{2}\cos(\theta + \varphi_B) +$$
$$\frac{g_3 B^2 A}{4}\cos(\theta + 2\varphi_B - \varphi_A) + \frac{g_3 B^2 A}{2}\cos(\theta + \varphi_A)$$

$$\Re\left\{e^{j\theta}e^{j\varphi_A}\left(\begin{array}{l} g_1A+g_1Be^{j\varphi_B}e^{-j\varphi_A}+\frac{3g_3A^3}{4}+\frac{3g_3B^3}{4}e^{j\varphi_B}e^{-j\varphi_A} \\ +\frac{g_3A^2B}{4}e^{j\varphi_A}e^{-j\varphi_B}+\frac{g_3A^2B}{2}e^{j\varphi_B}e^{-j\varphi_A}+\frac{g_3B^2A}{4}e^{2j\varphi_B}e^{-j2\varphi_A}+\frac{g_3B^2A}{2} \end{array}\right)\right\}$$

$$\Re\left\{e^{j\theta}e^{j\varphi_A}\left(\begin{array}{l} \left(g_1A+\frac{3g_3A^3}{4}+\frac{g_3B^2A}{2}\right)+\left(g_1B+\frac{3g_3B^3}{4}+\frac{g_3A^2B}{2}\right)e^{j\varphi_B}e^{-j\varphi_A} \\ +\frac{g_3A^2B}{4}e^{j\varphi_A}e^{-j\varphi_B}+\frac{g_3B^2A}{4}e^{2j\varphi_B}e^{-j2\varphi_A} \end{array}\right)\right\}$$

$$\Phi=e^{j\varphi_B}e^{-j\varphi_A},P=e^{j\varphi_A}$$

$$\Re\left\{e^{j\theta}e^{j\varphi_A}\left(\left(g_1A+\frac{3g_3A^3}{4}+\frac{g_3B^2A}{2}\right)+\left(g_1B+\frac{3g_3B^3}{4}+\frac{g_3A^2B}{2}\right)\Phi+\frac{g_3A^2B}{4}\Phi^{-1}+\frac{g_3B^2A}{4}\Phi^2\right)\right\}$$

$$\Re\left\{e^{j\theta}P\left(\left(g_1A+\frac{3g_3A^3}{4}+\frac{g_3B^2A}{2}\right)+\left(g_1B+\frac{3g_3B^3}{4}+\frac{g_3A^2B}{2}\right)\Phi+\frac{g_3A^2B}{4}\Phi^{-1}+\frac{g_3B^2A}{4}\Phi^2\right)\right\}$$

	Φ^{-3}	Φ^{-2}	Φ^{-1}	Φ^{0}	Φ^{1}	Φ^{2}	Φ^{3}	Φ^{4}	Φ^{5}
$\lvert a_{21}\rvert^0$				1st					
$\lvert a_{21}\rvert^1$			3rd		1st				
$\lvert a_{21}\rvert^2$		5th		3rd		3rd			
$\lvert a_{21}\rvert^3$	7th		5th		3rd		5th		
$\lvert a_{21}\rvert^4$		7th		5th		5th		7th	
$\lvert a_{21}\rvert^5$			7th		5th		7th		
$\lvert a_{21}\rvert^6$				7th		7th			
$\lvert a_{21}\rvert^7$					7th				

$$b_{p,h}=P^h\sum_{n=-\frac{1}{2}(N-1)}^{\frac{1}{2}(N+1)}R\left(|a_{11}|,|a_{21}|\right)\Phi^n$$

A1.2 Least Squares Hot-S-Parameter Extraction

A1.2.1 Full version

$$b_1 = S_{11}a_1 + S_{12}a_2$$

$$b_2 = S_{21}a_1 + S_{22}a_2$$

If multiple samples are taken then:

$$\begin{bmatrix} b_{1,0} & b_{2,0} \\ b_{1,1} & b_{2,1} \\ \vdots & \vdots \\ b_{1,n} & b_{2,n} \end{bmatrix} = \begin{bmatrix} a_{1,0} & a_{2,0} \\ a_{1,1} & a_{2,1} \\ \vdots & \vdots \\ a_{1,n} & a_{2,n} \end{bmatrix} \begin{bmatrix} S_{11} & S_{21} \\ S_{12} & S_{22} \end{bmatrix}$$

$$[B] = [A][S]$$

$$[A]^H [B] = [A]^H [A][S]$$

$$\begin{bmatrix} a_{1,0}* & a_{1,1}* & \cdots & a_{1,n}* \\ a_{2,0}* & a_{2,1}* & \cdots & a_{2,n}* \end{bmatrix} \begin{bmatrix} b_{1,0} & b_{2,0} \\ b_{1,1} & b_{2,1} \\ \vdots & \vdots \\ b_{1,n} & b_{2,n} \end{bmatrix} = \begin{bmatrix} a_{1,0}* & a_{1,1}* & \cdots & a_{1,n}* \\ a_{2,0}* & a_{2,1}* & \cdots & a_{2,n}* \end{bmatrix} \begin{bmatrix} a_{1,0} & a_{2,0} \\ a_{1,1} & a_{2,1} \\ \vdots & \vdots \\ a_{1,n} & a_{2,n} \end{bmatrix} \begin{bmatrix} S_{11} & S_{21} \\ S_{12} & S_{22} \end{bmatrix}$$

$$\begin{bmatrix} \sum b_1 a_1* & \sum b_2 a_1* \\ \sum b_1 a_2* & \sum b_2 a_2* \end{bmatrix} = \begin{bmatrix} \sum |a_1|^2 & \sum a_1 * a_2 \\ \sum a_1 a_2* & \sum |a_2|^2 \end{bmatrix} \begin{bmatrix} S_{11} & S_{21} \\ S_{12} & S_{22} \end{bmatrix}$$

$$[S] = \left([A]^H [A] \right)^{-1} [A]^H [B]$$

$$\begin{bmatrix} S_{11} & S_{21} \\ S_{12} & S_{22} \end{bmatrix} = \begin{bmatrix} \sum |a_1|^2 & \sum a_1 * a_2 \\ \sum a_1 a_2* & \sum |a_2|^2 \end{bmatrix}^{-1} \begin{bmatrix} \sum b_1 a_1* & \sum b_2 a_1* \\ \sum b_1 a_2* & \sum b_2 a_2* \end{bmatrix}$$

$$\begin{bmatrix} S_{11} & S_{21} \\ S_{12} & S_{22} \end{bmatrix} = \frac{1}{\Delta} \begin{bmatrix} \sum |a_2|^2 & -\sum a_1 * a_2 \\ -\sum a_1 a_2* & \sum |a_1|^2 \end{bmatrix} \begin{bmatrix} \sum b_1 a_1* & \sum b_2 a_1* \\ \sum b_1 a_2* & \sum b_2 a_2* \end{bmatrix}$$

$$\Delta = \sum |a_1|^2 \sum |a_2|^2 - \sum a_1 a_2 * \sum a_1 * a_2$$

$$\begin{bmatrix} S_{11} & S_{21} \\ S_{12} & S_{22} \end{bmatrix} = \begin{bmatrix} \dfrac{\sum b_1 a_1 * \sum |a_2|^2 - \sum b_1 a_1 * \sum a_1 * a_2}{\sum |a_1|^2 \sum |a_2|^2 - \sum a_1 a_2 * \sum a_1 * a_2} & \dfrac{\sum b_2 a_2 * \sum |a_1|^2 - \sum b_2 a_1 * \sum a_1 a_2 *}{\sum |a_1|^2 \sum |a_2|^2 - \sum a_1 a_2 * \sum a_1 * a_2} \\ \dfrac{\sum b_1 a_2 * \sum |a_1|^2 - \sum b_1 a_1 * \sum a_1 a_2 *}{\sum |a_1|^2 \sum |a_2|^2 - \sum a_1 a_2 * \sum a_1 * a_2} & \dfrac{\sum b_2 a_2 * \sum |a_1|^2 - \sum b_2 a_1 * \sum a_1 a_2 *}{\sum |a_1|^2 \sum |a_2|^2 - \sum a_1 a_2 * \sum a_1 * a_2} \end{bmatrix}$$

A1.2.2 Half version

$$b_1 = S_{11} a_1 + S_{12} a_2$$

$$b_2 = S_{21} a_1 + S_{22} a_2$$

Assuming impedances are normalized out of the equation

$$b_1 = X_1 + S_{12} a_2$$

$$b_2 = X_2 + S_{22} a_2$$

$$\begin{bmatrix} b_{1,0} & b_{2,0} \\ b_{1,1} & b_{2,1} \\ \vdots & \vdots \\ b_{1,n} & b_{2,n} \end{bmatrix} = \begin{bmatrix} 1 & a_{2,0} \\ 1 & a_{2,1} \\ \vdots & \vdots \\ 1 & a_{2,n} \end{bmatrix} \begin{bmatrix} X_1 & X_2 \\ S_{12} & S_{22} \end{bmatrix}$$

$$[B] = [A][S]$$

$$[A]^H [B] = [A]^H [A][S]$$

$$\begin{bmatrix} 1 & 1 & \cdots & 1 \\ a_{2,0} * & a_{2,1} * & \cdots & a_{2,n} * \end{bmatrix} \begin{bmatrix} b_{1,0} & b_{2,0} \\ b_{1,1} & b_{2,1} \\ \vdots & \vdots \\ b_{1,n} & b_{2,n} \end{bmatrix} = \begin{bmatrix} 1 & 1 & \cdots & 1 \\ a_{2,0} * & a_{2,1} * & \cdots & a_{2,n} * \end{bmatrix} \begin{bmatrix} 1 & a_{2,0} \\ 1 & a_{2,1} \\ \vdots & \vdots \\ 1 & a_{2,n} \end{bmatrix} \begin{bmatrix} X_1 & X_2 \\ S_{12} & S_{22} \end{bmatrix}$$

$$\begin{bmatrix} \sum b_1 & \sum b_2 \\ \sum b_1 a_2 * & \sum b_2 a_2 * \end{bmatrix} = \begin{bmatrix} N & \sum a_2 \\ \sum a_2 * & \sum |a_2|^2 \end{bmatrix} \begin{bmatrix} X_1 & X_2 \\ S_{12} & S_{22} \end{bmatrix}$$

$$[S] = \left([A]^H [A] \right)^{-1} [A]^H [B]$$

$$\begin{bmatrix} X_1 & X_2 \\ S_{12} & S_{22} \end{bmatrix} = \begin{bmatrix} N & \sum a_2 \\ \sum a_2 * & \sum |a_2|^2 \end{bmatrix}^{-1} \begin{bmatrix} \sum b_1 & \sum b_2 \\ \sum b_1 a_2 * & \sum b_2 a_2 * \end{bmatrix}$$

$$\begin{bmatrix} X_1 & X_2 \\ S_{12} & S_{22} \end{bmatrix} = \frac{1}{\Delta}\begin{bmatrix} \sum|a_2|^2 & -\sum a_2 \\ -\sum a_2 * & N \end{bmatrix}\begin{bmatrix} \sum b_1 & \sum b_2 \\ \sum b_1 a_2 * & \sum b_2 a_2 * \end{bmatrix}$$

$$\Delta = N\sum|a_2|^2 - \sum a_2 * \sum a_2$$

$$\begin{bmatrix} X_1 & X_2 \\ S_{12} & S_{22} \end{bmatrix} = \begin{bmatrix} \frac{\sum b_1 \sum|a_2|^2 - \sum b_1 a_2 * \sum a_2}{N\sum|a_2|^2 - \sum a_2 * \sum a_2} & \frac{\sum b_2 \sum|a_2|^2 - \sum b_2 a_2 * \sum a_2}{N\sum|a_2|^2 - \sum a_2 * \sum a_2} \\ \frac{N\sum b_1 a_2 * - \sum b_1 \sum a_2 *}{N\sum|a_2|^2 - \sum a_2 * \sum a_2} & \frac{N\sum b_2 a_2 * - \sum b_2 \sum a_2 *}{N\sum|a_2|^2 - \sum a_2 * \sum a_2} \end{bmatrix}$$

A1.3 Least Squares Poly-Harmonic-Distortion Extraction

Presented here is a method for formulating the extraction of the poly-harmonic distortion-model as a Least Squares Problem in matrix form. Assuming that the phase of a1 has already been set to zero and all components adjusted accordingly.

The X-parameter equation can be written as:

$$b_{p,h} = X^F_{p,h} + X^S_{p,h,2,1}a_{2,1} + X^T_{p,h,2,1}a_{2,1}{}^* + X^S_{p,h,2,2}a_{2,2} + X^T_{p,h,2,2}a_{2,2}{}^*$$

If multiple samples of points on this equation are taken:

$$\begin{bmatrix} b_{p,h,0} \\ b_{p,h,1} \\ \vdots \\ b_{p,h,n} \end{bmatrix} = \begin{bmatrix} X^F_{p,h} + X^S_{p,h,2,1}a_{2,1,0} + X^T_{p,h,2,1}a_{2,1,0}{}^* + X^S_{p,h,2,2}a_{2,2,0} + X^T_{p,h,2,2}a_{2,2,0}{}^* \\ X^F_{p,h} + X^S_{p,h,2,1}a_{2,1,1} + X^T_{p,h,2,1}a_{2,1,1}{}^* + X^S_{p,h,2,2}a_{2,2,1} + X^T_{p,h,2,2}a_{2,2,1}{}^* \\ \vdots \\ X^F_{p,h} + X^S_{p,h,2,1}a_{2,1,n} + X^T_{p,h,2,1}a_{2,1,n}{}^* + X^S_{p,h,2,2}a_{2,2,n} + X^T_{p,h,2,2}a_{2,2,n}{}^* \end{bmatrix}$$

$$\begin{bmatrix} b_{p,h,0} \\ b_{p,h,1} \\ \vdots \\ b_{p,h,n} \end{bmatrix} = \begin{bmatrix} 1 & a_{2,1,0} & a_{2,1,0}{}^* & a_{2,2,0} & a_{2,2,0}{}^* \\ 1 & a_{2,1,1} & a_{2,1,1}{}^* & a_{2,2,1} & a_{2,2,1}{}^* \\ \vdots & \vdots & \vdots & \vdots & \vdots \\ 1 & a_{2,1,n} & a_{2,1,n}{}^* & a_{2,2,n} & a_{2,2,n}{}^* \end{bmatrix}\begin{bmatrix} X^F_{p,h} \\ X^S_{p,h,2,1} \\ X^T_{p,h,2,1} \\ X^S_{p,h,2,2} \\ X^T_{p,h,2,2} \end{bmatrix}$$

$$[B] = [A][X]$$

$$[A]^H[B] = [A]^H[A][X]$$

$$[X] = \left([A]^H [A]\right)^{-1} [A]^H [B]$$

For the case of only one Xf, Xs, Xt and where a is the perturbations

$$\begin{bmatrix} X^F \\ X^S \\ X^T \end{bmatrix} = \frac{1}{\Delta} \begin{bmatrix} \left(\sum |a|^2\right)^2 - \sum a^2 \sum \left(a^2\right)^* & \sum a^* \sum a^2 - \sum a \sum |a|^2 & \sum a \sum \left(a^2\right)^* - \sum a^* \sum |a|^2 \\ \sum \left(a^2\right)^* \sum a - \sum a^* \sum |a|^2 & N \sum |a|^2 - \sum a^* \sum a & \left(\sum a^*\right)' - N \sum \left(a^2\right)^* \\ \sum a^* \sum a^2 - \sum a \sum |a|^2 & \left(\sum a\right)^2 - N \sum a^2 & N \sum |a|^2 - \sum a \sum a^* \end{bmatrix} \times \begin{bmatrix} \sum b \\ \sum ba^* \\ \sum ba \end{bmatrix}$$

$$\Delta = N\left(\left(\sum |a|^2\right)^2 - \sum \left(a^2\right)^* \sum a^2\right) + \sum a\left(\sum \left(a^2\right)^* \sum a - \sum a^* \sum |a|^2\right) + \sum a^*\left(\sum a^* \sum a^2 - \sum |a|^2 \sum a\right)$$

$$X^F = \frac{\sum b\left\{\left(\sum |a|^2\right)^2 - \sum a^2 \sum \left(a^2\right)^*\right\} + \sum ba^*\left\{\sum a^* \sum a^2 - \sum a \sum |a|^2\right\} + \sum ba\left\{\sum a \sum \left(a^2\right)^* - \sum a^* \sum |a|^2\right\}}{N\left(\left(\sum |a|^2\right)^2 - \sum \left(a^2\right)^* \sum a^2\right) + \sum a\left(\sum \left(a^2\right)^* \sum a - \sum a^* \sum |a|^2\right) + \sum a^*\left(\sum a^* \sum a^2 - \sum |a|^2 \sum a\right)}$$

$$X^S = \frac{\sum b\left\{\sum \left(a^2\right)^* \sum a - \sum a^* \sum |a|^2\right\} + \sum ba^*\left\{N \sum |a|^2 - \sum a^* \sum a\right\} + \sum ba\left\{\left(\sum a^*\right)' - N \sum \left(a^2\right)^*\right\}}{N\left(\left(\sum |a|^2\right)^2 - \sum \left(a^2\right)^* \sum a^2\right) + \sum a\left(\sum \left(a^2\right)^* \sum a - \sum a^* \sum |a|^2\right) + \sum a^*\left(\sum a^* \sum a^2 - \sum |a|^2 \sum a\right)}$$

$$X^T = \frac{\sum b\left\{\sum a^* \sum a^2 - \sum a \sum |a|^2\right\} + \sum ba^*\left\{\left(\sum a\right)^2 - N \sum a^2\right\} + \sum ba\left\{N \sum |a|^2 - \sum a \sum a^*\right\}}{N\left(\left(\sum |a|^2\right)^2 - \sum \left(a^2\right)^* \sum a^2\right) + \sum a\left(\sum \left(a^2\right)^* \sum a - \sum a^* \sum |a|^2\right) + \sum a^*\left(\sum a^* \sum a^2 - \sum |a|^2 \sum a\right)}$$

A1.4 Re-Normalization of travelling waves

$$a = \frac{V + IZ}{2\sqrt{\Re(Z)}} \quad b = \frac{V - IZ^*}{2\sqrt{\Re(Z)}}$$

$$a - b = \frac{V + IZ}{2\sqrt{\Re(Z)}} - \frac{V - IZ^*}{2\sqrt{\Re(Z)}}$$

$$a - b = \frac{IZ + IZ^*}{2\sqrt{\Re(Z)}}$$

$$a-b=\frac{I\left(Z+Z^{*}\right)}{2\sqrt{\Re(Z)}}=\frac{I2\Re(Z)}{2\sqrt{\Re(Z)}}=I\sqrt{\Re(Z)}$$

$$I=\frac{(a-b)}{\sqrt{\Re(Z)}}$$

$$aZ^{*}=\frac{VZ^{*}+IZZ^{*}}{2\sqrt{\Re(Z)}}\qquad bZ=\frac{VZ-IZZ^{*}}{2\sqrt{\Re(Z)}}$$

$$aZ^{*}+bZ=\frac{VZ^{*}+IZZ^{*}}{2\sqrt{\Re(Z)}}+\frac{VZ-IZZ^{*}}{2\sqrt{\Re(Z)}}$$

$$aZ^{*}+bZ=\frac{VZ^{*}+VZ}{2\sqrt{\Re(Z)}}=V\frac{Z^{*}+Z}{2\sqrt{\Re(Z)}}=V\frac{2\Re(Z)}{2\sqrt{\Re(Z)}}=V\sqrt{\Re(Z)}$$

$$V=\frac{aZ^{*}+bZ}{\sqrt{\Re(Z)}}$$

Voltage and current do not depend on normalization therefore

$$V=\frac{a_1Z_1^{*}+b_1Z_1}{\sqrt{\Re(Z_1)}}=\frac{a_2Z_2^{*}+b_2Z_2}{\sqrt{\Re(Z_2)}}$$

$$I=\frac{(a_1-b_1)}{\sqrt{\Re(Z_1)}}=\frac{(a_2-b_2)}{\sqrt{\Re(Z_2)}}$$

$$\frac{Z_2^{*}(a_1-b_1)}{\sqrt{\Re(Z_1)}}=\frac{(a_2Z_2^{*}-b_2Z_2^{*})}{\sqrt{\Re(Z_2)}}$$

$$\frac{a_1Z_1^{*}+b_1Z_1}{\sqrt{\Re(Z_1)}}-\frac{Z_2^{*}(a_1-b_1)}{\sqrt{\Re(Z_1)}}=\frac{a_2Z_2^{*}+b_2Z_2}{\sqrt{\Re(Z_2)}}-\frac{(a_2Z_2^{*}-b_2Z_2^{*})}{\sqrt{\Re(Z_2)}}$$

$$\frac{a_1Z_1^{*}+b_1Z_1}{\sqrt{\Re(Z_1)}}-\frac{Z_2^{*}(a_1-b_1)}{\sqrt{\Re(Z_1)}}=b_2\frac{Z_2+Z_2^{*}}{\sqrt{\Re(Z_2)}}=b_2\frac{2\Re(Z_2)}{\sqrt{\Re(Z_2)}}=2b_2\sqrt{\Re(Z_2)}$$

$$b_2=\frac{a_1(Z_1^{*}-Z_2^{*})+b_1(Z_1+Z_2^{*})}{2\sqrt{\Re(Z_1)\Re(Z_2)}}$$

$$\frac{(a_1-b_1)}{\sqrt{\Re(Z_1)}}=\frac{\left(a_2-\frac{a_1(Z_1*-Z_2*)+b_1(Z_1+Z_2*)}{2\sqrt{\Re(Z_1)\Re(Z_2)}}\right)}{\sqrt{\Re(Z_2)}}=\frac{a_2}{\sqrt{\Re(Z_2)}}-\frac{a_1(Z_1*-Z_2*)+b_1(Z_1+Z_2*)}{2\Re(Z_2)\sqrt{\Re(Z_1)}}$$

$$\frac{(a_1-b_1)}{\sqrt{\Re(Z_1)}}+\frac{a_1(Z_1*-Z_2*)+b_1(Z_1+Z_2*)}{2\Re(Z_2)\sqrt{\Re(Z_1)}}=\frac{a_2}{\sqrt{\Re(Z_2)}}$$

$$\frac{a_2}{\sqrt{\Re(Z_2)}}=\frac{\left(a_1\left(1+\frac{(Z_1*-Z_2*)}{2\Re(Z_2)}\right)+b_1\left(\frac{(Z_1+Z_2*)}{2\Re(Z_2)}-1\right)\right)}{\sqrt{\Re(Z_1)}}$$

$$a_2=\frac{(a_1(2\Re(Z_2)+Z_1*-Z_2*)+b_1(Z_1+Z_2*-2\Re(Z_2)))}{2\sqrt{\Re(Z_1)\Re(Z_2)}}$$

$$V^+=\frac{V+IZ}{2}\quad V^-=\frac{V-IZ^*}{2}$$

$$V^+-V^-=\frac{V+IZ}{2}-\frac{V-IZ^*}{2}$$

$$V^+-V^-=\frac{IZ+IZ*}{2}$$

$$V^+-V^-=\frac{I(Z+Z*)}{2}=\frac{I2\Re(Z)}{2}=I\Re(Z)$$

$$I=\frac{(V^+-V^-)}{\Re(Z)}$$

$$V^+Z*=\frac{VZ*+IZZ*}{2}\quad V^-Z=\frac{VZ-IZZ^*}{2}$$

$$V^+Z*+V^-Z=\frac{VZ*+IZZ*}{2}+\frac{VZ-IZZ^*}{2}$$

$$V^+Z*+V^-Z=\frac{VZ*+VZ}{2}=V\frac{Z*+Z}{2}=V\frac{2\Re(Z)}{2}=V\Re(Z)$$

$$V=\frac{V^+Z*+V^-Z}{\Re(Z)}$$

Voltage and current do not depend on normalization therefore

$$V = \frac{V_1^+ Z_1 * + V_1^- Z_1}{\Re(Z_1)} = \frac{V_2^+ Z_2 * + V_2^- Z_2}{\Re(Z_2)}$$

$$I = \frac{\left(V_1^+ - V_1^-\right)}{\Re(Z_1)} = \frac{\left(V_2^+ - V_2^-\right)}{\Re(Z_2)}$$

$$\frac{Z_2 * \left(V_1^+ - V_1^-\right)}{\Re\left(Z_1\right)} = \frac{\left(V_2^+ Z_2 * - V_2^- Z_2 *\right)}{\Re\left(Z_2\right)}$$

$$\frac{V_1^+ Z_1 * + V_1^- Z_1}{\Re(Z_1)} - \frac{Z_2 * \left(V_1^+ - V_1^-\right)}{\Re(Z_1)} = \frac{V_2^+ Z_2 * + V_2^- Z_2}{\Re(Z_2)} - \frac{\left(V_2^+ Z_2 * - V_2^- Z_2 *\right)}{\Re(Z_2)}$$

$$\frac{V_1^+ Z_1 * + V_1^- Z_1}{\Re\left(Z_1\right)} - \frac{Z_2 * \left(V_1^+ - V_1^-\right)}{\Re\left(Z_1\right)} = V_2^- \frac{Z_2 + Z_2 *}{\Re(Z_2)} = V_2^- \frac{2\Re(Z_2)}{\Re(Z_2)} = 2V_2^-$$

$$V_2^- = \frac{V_1^+ \left(Z_1 * - Z_2 *\right) + V_1^- \left(Z_1 + Z_2 *\right)}{2\Re(Z_1)}$$

$$\frac{\left(V_1^+ - V_1^-\right)}{\Re\left(Z_1\right)} = \frac{\left(V_2^+ - \frac{V_1^+ \left(Z_1 * - Z_2 *\right) + V_1^- \left(Z_1 + Z_2 *\right)}{2\Re(Z_1)}\right)}{\Re\left(Z_2\right)} = \frac{V_2^+}{\Re\left(Z_2\right)} - \frac{V_1^+ \left(Z_1 * - Z_2 *\right) + V_1^- \left(Z_1 + Z_2 *\right)}{2\Re(Z_2)\Re(Z_1)}$$

$$\frac{\left(V_1^+ - V_1^-\right)}{\Re\left(Z_1\right)} + \frac{V_1^+ \left(Z_1 * - Z_2 *\right) + V_1^- \left(Z_1 + Z_2 *\right)}{2\Re(Z_2)\Re(Z_1)} = \frac{V_2^+}{\Re\left(Z_2\right)}$$

$$\frac{V_2^+}{\Re\left(Z_2\right)} = \frac{\left(V_1^+ \left(1 + \frac{\left(Z_1 * - Z_2 *\right)}{2\Re(Z_2)}\right) + V_1^- \left(\frac{\left(Z_1 + Z_2 *\right)}{2\Re(Z_2)} - 1\right)\right)}{\Re\left(Z_1\right)}$$

$$V_2^+ = \frac{\left(V_1^+ \left(2\Re(Z_2) + Z_1 * - Z_2 *\right) + V_1^- \left(Z_1 + Z_2 * - 2\Re(Z_2)\right)\right)}{2\Re\left(Z_1\right)}$$

A1.5 further derivations

This section contains the full proofs and derivations used within this chapter

Inversion of the X-parameter Equation (A1.5.1)

Using the X-parameter formulation assuming only one input at port2

$$b_2 = X_f + X_s a_2 + X_T a_2^* \quad \textbf{(1)}$$

Finding the conjugate of (1)

$$b_2^* = X_f^* + X_s^* a_2^* + X_T^* a_2 \quad \textbf{(2)}$$

Divide both sides of (1) by X_T

$$\frac{b_2}{X_T} = \frac{X_f}{X_T} + \frac{X_s}{X_T} a_2 + a_2^* \quad \textbf{(3)}$$

Divide both sides of (2) by X_S^*

$$\frac{b_2^*}{X_s^*} = \frac{X_f^*}{X_s^*} + a_2^* + \frac{X_T^*}{X_s^*} a_2 \quad \textbf{(4)}$$

Subtract (4) from (3) to Eliminate a_2^* and then simplify

$$\frac{b_2}{X_T} - \frac{b_2^*}{X_s^*} = \frac{X_f}{X_T} + \frac{X_s}{X_T} a_2 + a_2^* + \left(-\frac{X_f^*}{X_s^*} - a_2^* - \frac{X_T^*}{X_s^*} a_2 \right)$$

$$\frac{b_2}{X_T} - \frac{b_2^*}{X_s^*} = \frac{X_f}{X_T} - \frac{X_f^*}{X_s^*} + \left(\frac{X_s}{X_T} - \frac{X_T^*}{X_s^*} \right) a_2$$

$$a_2 = \frac{\frac{b_2}{X_T} - \frac{b_2^*}{X_s^*} - \frac{X_f}{X_T} + \frac{X_f^*}{X_s^*}}{\left(\frac{X_s}{X_T} - \frac{X_T^*}{X_s^*} \right)}$$

$$a_2 = \frac{\frac{b_2}{X_T} - \frac{b_2*}{X_s*} - \frac{X_f}{X_T} + \frac{X_f*}{X_s*}}{\frac{X_s*X_T}{X_s*X_T}\left(\frac{X_s}{X_T} - \frac{X_T*}{X_s*}\right)}$$

$$a_2 = \frac{\left(\frac{X_s*X_Tb_2}{X_T} - \frac{X_s*X_Tb_2*}{X_s*} - \frac{X_s*X_TX_f}{X_T} + \frac{X_s*X_TX_f*}{X_s*}\right)}{\left(X_s*X_s - X_TX_T*\right)}$$

$$a_2 = \frac{\left(X_s*b_2 - X_Tb_2* - X_s*X_f + X_TX_f*\right)}{\left(X_s*X_s - X_TX_T*\right)} \quad \textbf{(5)}$$

$$a_2 = \frac{X_f*X_T - X_fX_s*}{\left(\left|X_s\right|^2 - \left|X_T\right|^2\right)} + \frac{X_s*}{\left(\left|X_s\right|^2 - \left|X_T\right|^2\right)}b_2 - \frac{X_T}{\left(\left|X_s\right|^2 - \left|X_T\right|^2\right)}b_2*$$

Summarised as:

$$a_2 = K_f + K_Sb_2 - K_Tb_2*$$

Verification

$$a_2 = \frac{\left(X_s*b_2 - X_Tb_2* - X_s*X_f + X_TX_f*\right)}{\left(X_s*X_s - X_TX_T*\right)} \quad \textbf{(5)}$$

$$b_2 = X_f + X_sa_2 + X_Ta_2* \quad \textbf{(6)}$$

Substituting (6) into (5) for b2 gives

$$= \frac{\left(X_s*\left(X_f + X_sa_2 + X_Ta_2*\right) - X_T\left(X_f + X_sa_2 + X_Ta_2*\right)* - X_s*X_f + X_TX_f*\right)}{\left(X_s*X_s - X_TX_T*\right)}$$

$$= \frac{X_s*X_f + X_s*X_sa_2 + X_s*X_Ta_2* - X_TX_f*}{\left(X_s*X_s - X_TX_T*\right)}$$

$$+ \frac{\left(-X_TX_s*a_2* - X_TX_T*a_2 - X_s*X_f + X_TX_f*\right)}{\left(X_s*X_s - X_TX_T*\right)}$$

$$= \frac{\left(X_s*X_sa_2 - X_TX_T*a_2\right)}{\left(X_s*X_s - X_TX_T*\right)} = \frac{\left(X_s*X_s - X_TX_T*\right)a_2}{\left(X_s*X_s - X_TX_T*\right)} = a_2$$

Proving that (5) is the inverse of (6) it should also be noted that this solution is not valid for values X_S and X_T Values where: $\left|X_s\right| = \left|X_T\right|$

Result in no valid inverse transform.

Matrix form of X-parameter Equations for fundamental and Second harmonic (A1.5.2)

$$b_{p,h} = X^F_{p,h} + \sum_{\alpha=1}^{N}\sum_{\beta=0}^{M}\left(X^S_{p,h,\alpha,\beta}a_{\alpha,\beta} + X^T_{p,h,\alpha,\beta}a_{\alpha,\beta}*\right), \mathrm{p} > 0$$

$$b_{2,1} = X^F_{2,1} + X^S_{2,1,2,1}a_{2,1} + X^T_{2,1,2,1}a_{2,1}* + X^S_{2,1,2,2}a_{2,2} + X^T_{2,1,2,2}a_{2,2}*$$

$$b_{2,1}* = X^F_{2,1}* + X^T_{2,1,2,1}*a_{2,1} + X^S_{2,1,2,1}*a_{2,1}* + X^T_{2,1,2,2}*a_{2,2} + X^S_{2,1,2,2}*a_{2,2}*$$

$$b_{2,2} = X^F_{2,2} + X^S_{2,2,2,1}a_{2,1} + X^T_{2,2,2,1}a_{2,1}* + X^S_{2,2,2,2}a_{2,2} + X^T_{2,2,2,2}a_{2,2}*$$

$$b_{2,2}* = X^F_{2,2}* + X^T_{2,2,2,1}*a_{2,1} + X^S_{2,2,2,1}*a_{2,1}* + X^T_{2,2,2,2}*a_{2,2} + X^S_{2,2,2,2}*a_{2,2}*$$

$$\begin{bmatrix} b_{2,1} \\ b_{2,1}* \\ b_{2,2} \\ b_{2,2}* \end{bmatrix} = \begin{bmatrix} X^F_{2,1} \\ X^F_{2,1}* \\ X^F_{2,2} \\ X^F_{2,2}* \end{bmatrix} + \begin{bmatrix} X^S_{2,1,2,1} & X^T_{2,1,2,1} & X^S_{2,1,2,2} & X^T_{2,1,2,2} \\ X^T_{2,1,2,1}* & X^S_{2,1,2,1}* & X^T_{2,1,2,2}* & X^S_{2,1,2,2}* \\ X^S_{2,2,2,1} & X^T_{2,1,2,1} & X^S_{2,2,2,2} & X^T_{2,2,2,2} \\ X^T_{2,1,2,1}* & X^S_{2,2,2,1}* & X^T_{2,2,2,2}* & X^S_{2,2,2,2}* \end{bmatrix} \begin{bmatrix} a_{2,1} \\ a_{2,1}* \\ a_{2,2} \\ a_{2,2}* \end{bmatrix}$$

$$[b] = [X^F] + [X^{ST}][a]$$

$$[X^{ST}]^{-1}([b] - [X^F]) = [a]$$

If $[X^{ST}]^{-1}$ exists the X-parameter relationship can be solved

Extracting impedance relationships from X-parameters

$$\begin{bmatrix} b_{2,1} \\ b_{2,1}* \\ b_{2,2} \\ b_{2,2}* \end{bmatrix} = \begin{bmatrix} X^F_{2,1} \\ X^F_{2,1}* \\ X^F_{2,2} \\ X^F_{2,2}* \end{bmatrix} + \begin{bmatrix} X^S_{2,1,2,1} & X^T_{2,1,2,1} & X^S_{2,1,2,2} & X^T_{2,1,2,2} \\ X^T_{2,1,2,1}* & X^S_{2,1,2,1}* & X^T_{2,1,2,2}* & X^S_{2,1,2,2}* \\ X^S_{2,2,2,1} & X^T_{2,1,2,1} & X^S_{2,2,2,2} & X^T_{2,2,2,2} \\ X^T_{2,1,2,1}* & X^S_{2,2,2,1}* & X^T_{2,2,2,2}* & X^S_{2,2,2,2}* \end{bmatrix} \begin{bmatrix} a_{2,1} \\ a_{2,1}* \\ a_{2,2} \\ a_{2,2}* \end{bmatrix}$$

$$a_{2,1} = \Gamma_{2,1} b_{2,1}$$
$$a_{2,2} = \Gamma_{2,2} b_{2,2}$$

$$\begin{bmatrix} b_{2,1} \\ b_{2,1}* \\ b_{2,2} \\ b_{2,2}* \end{bmatrix} = \begin{bmatrix} X^F_{2,1} \\ X^F_{2,1}* \\ X^F_{2,2} \\ X^F_{2,2}* \end{bmatrix} + \begin{bmatrix} X^S_{2,1,2,1} & X^T_{2,1,2,1} & X^S_{2,1,2,2} & X^T_{2,1,2,2} \\ X^T_{2,1,2,1}* & X^S_{2,1,2,1}* & X^T_{2,1,2,2}* & X^S_{2,1,2,2}* \\ X^S_{2,2,2,1} & X^T_{2,1,2,1} & X^S_{2,2,2,2} & X^T_{2,2,2,2} \\ X^T_{2,1,2,1}* & X^S_{2,2,2,1}* & X^T_{2,2,2,2}* & X^S_{2,2,2,2}* \end{bmatrix} \begin{bmatrix} \Gamma_{2,1} b_{2,1} \\ \Gamma_{2,1}* b_{2,1}* \\ \Gamma_{2,2} b_{2,2} \\ \Gamma_{2,2}* b_{2,2}* \end{bmatrix}$$

$$0 = \begin{bmatrix} X^F_{2,1} \\ X^F_{2,1}* \\ X^F_{2,2} \\ X^F_{2,2}* \end{bmatrix} + \begin{bmatrix} X^S_{2,1,2,1} & X^T_{2,1,2,1} & X^S_{2,1,2,2} & X^T_{2,1,2,2} \\ X^T_{2,1,2,1}* & X^S_{2,1,2,1}* & X^T_{2,1,2,2}* & X^S_{2,1,2,2}* \\ X^S_{2,2,2,1} & X^T_{2,1,2,1} & X^S_{2,2,2,2} & X^T_{2,2,2,2} \\ X^T_{2,1,2,1}* & X^S_{2,2,2,1}* & X^T_{2,2,2,2}* & X^S_{2,2,2,2}* \end{bmatrix} \begin{bmatrix} \Gamma_{2,1} b_{2,1} \\ \Gamma_{2,1}* b_{2,1}* \\ \Gamma_{2,2} b_{2,2} \\ \Gamma_{2,2}* b_{2,2}* \end{bmatrix} - \begin{bmatrix} b_{2,1} \\ b_{2,1}* \\ b_{2,2} \\ b_{2,2}* \end{bmatrix}$$

$$0 = \begin{bmatrix} X^F_{2,1} \\ X^F_{2,1}* \\ X^F_{2,2} \\ X^F_{2,2}* \end{bmatrix} + \begin{bmatrix} \Gamma_{2,1} X^S_{2,1,2,1} - 1 & \Gamma_{2,1}* X^T_{2,1,2,1} & \Gamma_{2,2} X^S_{2,1,2,2} & \Gamma_{2,2}* X^T_{2,1,2,2} \\ \Gamma_{2,1} X^T_{2,1,2,1}* & \Gamma_{2,1}* X^S_{2,1,2,1}* - 1 & \Gamma_{2,2} X^T_{2,1,2,2}* & \Gamma_{2,2}* X^S_{2,1,2,2}* \\ \Gamma_{2,1} X^S_{2,2,2,1} & \Gamma_{2,1}* X^T_{2,1,2,1} & \Gamma_{2,2} X^S_{2,2,2,2} - 1 & \Gamma_{2,2}* X^T_{2,2,2,2} \\ \Gamma_{2,1} X^T_{2,1,2,1}* & \Gamma_{2,1}* X^S_{2,2,2,1}* & \Gamma_{2,2} X^T_{2,2,2,2}* & \Gamma_{2,2}* X^S_{2,2,2,2}* - 1 \end{bmatrix} \begin{bmatrix} b_{2,1} \\ b_{2,1}* \\ b_{2,2} \\ b_{2,2}* \end{bmatrix}$$

$$\begin{bmatrix} b_{2,1} \\ b_{2,1}* \\ b_{2,2} \\ b_{2,2}* \end{bmatrix} = \begin{bmatrix} \Gamma_{2,1} X^S_{2,1,2,1} - 1 & \Gamma_{2,1}* X^T_{2,1,2,1} & \Gamma_{2,2} X^S_{2,1,2,2} & \Gamma_{2,2}* X^T_{2,1,2,2} \\ \Gamma_{2,1} X^T_{2,1,2,1}* & \Gamma_{2,1}* X^S_{2,1,2,1}* - 1 & \Gamma_{2,2} X^T_{2,1,2,2}* & \Gamma_{2,2}* X^S_{2,1,2,2}* \\ \Gamma_{2,1} X^S_{2,2,2,1} & \Gamma_{2,1}* X^T_{2,1,2,1} & \Gamma_{2,2} X^S_{2,2,2,2} - 1 & \Gamma_{2,2}* X^T_{2,2,2,2} \\ \Gamma_{2,1} X^T_{2,1,2,1}* & \Gamma_{2,1}* X^S_{2,2,2,1}* & \Gamma_{2,2} X^T_{2,2,2,2}* & \Gamma_{2,2}* X^S_{2,2,2,2}* - 1 \end{bmatrix}^{-1} \begin{bmatrix} -X^F_{2,1} \\ -X^F_{2,1}* \\ -X^F_{2,2} \\ -X^F_{2,2}* \end{bmatrix}$$

$$[B] = \left[\Gamma^{XST}\right]^{-1} \left(-\left[X^F\right]\right)$$

The solution or convergence now depends on the existence of $\left[\Gamma^{XST}\right]^{-1}$

Conversion of the X-parameter Equation into voltage and current relationships (A1.5.3)

$$v = \sqrt{Z}(a+b)$$

$$i = \frac{(a-b)}{\sqrt{Z}}$$

$$v = \sqrt{Z}\left(X_F + (X_S+1)a + X_T a^*\right)$$

$$v^* = \sqrt{Z}\left(X_F^* + (X_S^*+1)a^* + X_T^* a\right)$$

Developing a formulation for the "a" wave in terms of the voltage at the port

$$\frac{v}{\sqrt{ZX_T}} = \frac{X_F}{X_T} + \frac{(X_S+1)}{X_T}a + a^*$$

$$\frac{v^*}{\sqrt{Z}(X_S^*+1)} = \frac{X_F^*}{(X_S^*+1)} + a^* + \frac{X_T^*}{(X_S^*+1)}a$$

$$\frac{v}{X_T\sqrt{Z}} - \frac{v^*}{\sqrt{Z}(X_S^*+1)} = \frac{X_F}{X_T} - \frac{X_F^*}{(X_S^*+1)} + \left(\frac{(X_S+1)}{X_T} - \frac{X_T^*}{(X_S^*+1)}\right)a$$

$$\frac{v(X_S^*+1)}{\sqrt{Z}} - \frac{X_T v^*}{\sqrt{Z}} = X_F(X_S^*+1) - X_F^* X_T + \left(|X_S+1|^2 - |X_T|^2\right)a$$

$$a = \frac{v(X_S^*+1)}{\left(|X_S+1|^2 - |X_T|^2\right)\sqrt{Z}} - \frac{X_T v^*}{\left(|X_S+1|^2 - |X_T|^2\right)\sqrt{Z}} + \frac{X_F^* X_T - X_F(X_S^*+1)}{\left(|X_S+1|^2 - |X_T|^2\right)}$$

$$a = K_f + K_S v - K_T v^*$$

Developing a formulation for the "a" wave in terms of the Current at the port

$$i = \frac{1}{\sqrt{Z}}\left(-X_F + (1-X_S)a - X_T a^*\right)$$

$$i^* = \frac{1}{\sqrt{Z}}\left(-X_F^* + (1-X_S^*)a^* - X_T^* a\right)$$

$$\frac{i\sqrt{Z}}{X_T} = -\frac{X_F}{X_T} - \frac{(1-X_S)}{X_T}a + a^*$$

$$\frac{i^*\sqrt{Z}}{(1-X_S^*)} = \frac{-X_F^*}{(1-X_S^*)} + a^* + \frac{X_T^*}{(1-X_S^*)}a$$

$$\frac{i\sqrt{Z}}{X_T} - \frac{i^*\sqrt{Z}}{(1-X_S^*)} = -\frac{X_F}{X_T} + \frac{X_F^*}{(1-X_S^*)} + \left(\frac{X_T^*}{(1-X_S^*)} - \frac{(1-X_S)}{X_T}\right)a$$

$$i(1-X_S^*)\sqrt{Z} - X_T i^*\sqrt{Z} = X_F^* X_T - X_F(1-X_S^*) + \left(|X_T|^2 - |1-X_S|^2\right)a$$

$$a = \frac{i(1-X_S^*)\sqrt{Z}}{\left(|1-X_S|^2 - |X_T|^2\right)} - \frac{X_T i^*\sqrt{Z}}{\left(|1-X_S|^2 - |X_T|^2\right)} + \frac{X_F^* X_T - X_F(1-X_S^*)}{\left(|1-X_S|^2 - |X_T|^2\right)}$$

$$a = M_f + M_S i - M_T i^*$$

$$a = M_f + M_S i - M_T i^* = K_f + K_S v - K_T v^*$$
$$a^* = M_f{}^* + M_S{}^* i^* - M_T{}^* i = K_f{}^* + K_S{}^* v^* - K_T{}^* v$$
$$\frac{M_f}{M_T} + \frac{M_S}{M_T} i - i^* = \frac{K_f}{M_T} + \frac{K_S}{M_T} v - \frac{K_T}{M_T} v^*$$
$$\frac{M_f{}^*}{M_S{}^*} + i^* - \frac{M_T{}^*}{M_S{}^*} i = \frac{K_f{}^*}{M_S{}^*} + \frac{K_S{}^*}{M_S{}^*} v^* - \frac{K_T{}^*}{M_S{}^*} v$$
$$\frac{M_f}{M_T} + \frac{M_f{}^*}{M_S{}^*} + \left(\frac{M_S}{M_T} - \frac{M_T{}^*}{M_S{}^*}\right) i = \frac{K_f}{M_T} + \frac{K_f{}^*}{M_S{}^*} + \left(\frac{K_S}{M_T} - \frac{K_T{}^*}{M_S{}^*}\right) v + \left(\frac{K_S{}^*}{M_S{}^*} - \frac{K_T}{M_T}\right) v^*$$
$$M_f M_S{}^* + M_f{}^* M_T + \left(|M_S|^2 - |M_T|^2\right) i =$$

$$K_f M_S{}^* + K_f{}^* M_T + \left(K_S M_S{}^* - K_T{}^* M_T\right) v + \left(K_S{}^* M_T - K_T M_S{}^*\right) v^*$$
$$i = \frac{K_f M_S{}^* + K_f{}^* M_T - M_f M_S{}^* - M_f{}^* M_T}{\left(|M_S|^2 - |M_T|^2\right)}$$
$$+ \frac{\left(K_S M_S{}^* - K_T{}^* M_T\right)}{\left(|M_S|^2 - |M_T|^2\right)} v + \frac{\left(K_S{}^* M_T - K_T M_S{}^*\right)}{\left(|M_S|^2 - |M_T|^2\right)} v^*$$

$$i = R_f + R_S v + R_T v^*$$

$$R_f = \frac{K_f M_S{}^* + K_f{}^* M_T - M_f M_S{}^* - M_f{}^* M_T}{\left(|M_S|^2 - |M_T|^2\right)}$$
$$R_f = \frac{\left(X_F{}^* X_T - X_F\left(X_S{}^* + 1\right)\right)\left(1 - X_S\right) + \left(X_F X_T{}^* - X_F{}^*\left(X_S + 1\right)\right) X_T}{\left(|X_S + 1|^2 - |X_T|^2\right)\sqrt{Z}} -$$
$$\frac{\left(X_F{}^* X_T - X_F\left(1 - X_S{}^*\right)\right)\left(1 - X_S\right) + \left(X_F X_T{}^* - X_F{}^*\left(1 - X_S\right)\right) X_T}{\sqrt{Z}\left(|1 - X_S|^2 - |X_T|^2\right)}$$
$$R_S = \frac{\left(K_S M_S{}^* - K_T{}^* M_T\right)}{\left(|M_S|^2 - |M_T|^2\right)}$$
$$R_S = \left(\frac{\left(X_S{}^* + 1\right)\left(1 - X_S\right) - X_T{}^* X_T}{Z\left(|X_S + 1|^2 - |X_T|^2\right)}\right)$$
$$R_T = \frac{\left(K_S{}^* M_T - K_T M_S{}^*\right)}{\left(|M_S|^2 - |M_T|^2\right)}$$
$$R_T = X_T\left(\frac{2\Re(X_S)}{\left(|X_S + 1|^2 - |X_T|^2\right) Z}\right)$$

Matrix Method to Convert Between X-Parameters and voltage, current parameters (A1.5.4)

$$v = \sqrt{Z}(a+b)$$

$$i = \frac{(a-b)}{\sqrt{Z}}$$

$$\begin{bmatrix} b_{2,1} \\ b_{2,1}* \\ b_{2,2} \\ b_{2,2}* \end{bmatrix} = \begin{bmatrix} X^F_{2,1} \\ X^F_{2,1}* \\ X^F_{2,2} \\ X^F_{2,2}* \end{bmatrix} + \begin{bmatrix} X^S_{2,1,2,1} & X^T_{2,1,2,1} & X^S_{2,1,2,2} & X^T_{2,1,2,2} \\ X^T_{2,1,2,1}* & X^S_{2,1,2,1}* & X^T_{2,1,2,2}* & X^S_{2,1,2,2}* \\ X^S_{2,2,2,1} & X^T_{2,1,2,1} & X^S_{2,2,2,2} & X^T_{2,2,2,2} \\ X^T_{2,1,2,1}* & X^S_{2,2,2,1}* & X^T_{2,2,2,2}* & X^S_{2,2,2,2}* \end{bmatrix} \begin{bmatrix} a_{2,1} \\ a_{2,1}* \\ a_{2,2} \\ a_{2,2}* \end{bmatrix}$$

$$\begin{bmatrix} v_{2,1} \\ v_{2,1}* \\ v_{2,2} \\ v_{2,2}* \end{bmatrix} = \sqrt{Z}\left(\begin{bmatrix} a_{2,1} \\ a_{2,1}* \\ a_{2,2} \\ a_{2,2}* \end{bmatrix} + \begin{bmatrix} X^F_{2,1} \\ X^F_{2,1}* \\ X^F_{2,2} \\ X^F_{2,2}* \end{bmatrix} + \begin{bmatrix} X^S_{2,1,2,1} & X^T_{2,1,2,1} & X^S_{2,1,2,2} & X^T_{2,1,2,2} \\ X^T_{2,1,2,1}* & X^S_{2,1,2,1}* & X^T_{2,1,2,2}* & X^S_{2,1,2,2}* \\ X^S_{2,2,2,1} & X^T_{2,1,2,1} & X^S_{2,2,2,2} & X^T_{2,2,2,2} \\ X^T_{2,1,2,1}* & X^S_{2,2,2,1}* & X^T_{2,2,2,2}* & X^S_{2,2,2,2}* \end{bmatrix} \begin{bmatrix} a_{2,1} \\ a_{2,1}* \\ a_{2,2} \\ a_{2,2}* \end{bmatrix} \right)$$

$$\begin{bmatrix} v_{2,1} \\ v_{2,1}* \\ v_{2,2} \\ v_{2,2}* \end{bmatrix} = \sqrt{Z}\left(\begin{bmatrix} X^F_{2,1} \\ X^F_{2,1}* \\ X^F_{2,2} \\ X^F_{2,2}* \end{bmatrix} + \begin{bmatrix} X^S_{2,1,2,1}+1 & X^T_{2,1,2,1} & X^S_{2,1,2,2} & X^T_{2,1,2,2} \\ X^T_{2,1,2,1}* & X^S_{2,1,2,1}*+1 & X^T_{2,1,2,2}* & X^S_{2,1,2,2}* \\ X^S_{2,2,2,1} & X^T_{2,1,2,1} & X^S_{2,2,2,2}+1 & X^T_{2,2,2,2} \\ X^T_{2,1,2,1}* & X^S_{2,2,2,1}* & X^T_{2,2,2,2}* & X^S_{2,2,2,2}*+1 \end{bmatrix} \begin{bmatrix} a_{2,1} \\ a_{2,1}* \\ a_{2,2} \\ a_{2,2}* \end{bmatrix} \right)$$

$$[V] = \sqrt{Z}\left([X^F] + \begin{bmatrix} X^S_{2,1,2,1}+1 & X^T_{2,1,2,1} & X^S_{2,1,2,2} & X^T_{2,1,2,2} \\ X^T_{2,1,2,1}* & X^S_{2,1,2,1}*+1 & X^T_{2,1,2,2}* & X^S_{2,1,2,2}* \\ X^S_{2,2,2,1} & X^T_{2,1,2,1} & X^S_{2,2,2,2}+1 & X^T_{2,2,2,2} \\ X^T_{2,1,2,1}* & X^S_{2,2,2,1}* & X^T_{2,2,2,2}* & X^S_{2,2,2,2}*+1 \end{bmatrix} [A] \right)$$

$$[A] = \begin{bmatrix} X^S_{2,1,2,1}+1 & X^T_{2,1,2,1} & X^S_{2,1,2,2} & X^T_{2,1,2,2} \\ X^T_{2,1,2,1}* & X^S_{2,1,2,1}*+1 & X^T_{2,1,2,2}* & X^S_{2,1,2,2}* \\ X^S_{2,2,2,1} & X^T_{2,1,2,1} & X^S_{2,2,2,2}+1 & X^T_{2,2,2,2} \\ X^T_{2,1,2,1}* & X^S_{2,2,2,1}* & X^T_{2,2,2,2}* & X^S_{2,2,2,2}*+1 \end{bmatrix}^{-1} \left(\frac{1}{\sqrt{Z}}[V] - [X^F] \right)$$

$$[A] = \left([X^{ST}] + [I] \right)^{-1} \left(\frac{1}{\sqrt{Z}}[V] - [X^F] \right)$$

$$\begin{bmatrix} i_{2,1} \\ i_{2,1}* \\ i_{2,2} \\ i_{2,2}* \end{bmatrix} = \frac{-1}{\sqrt{Z}} \left(\begin{bmatrix} X^F_{2,1} \\ X^F_{2,1}* \\ X^F_{2,2} \\ X^F_{2,2}* \end{bmatrix} + \begin{bmatrix} X^S_{2,1,2,1} & X^T_{2,1,2,1} & X^S_{2,1,2,2} & X^T_{2,1,2,2} \\ X^T_{2,1,2,1}* & X^S_{2,1,2,1}* & X^T_{2,1,2,2}* & X^S_{2,1,2,2}* \\ X^S_{2,2,2,1} & X^T_{2,1,2,1} & X^S_{2,2,2,2} & X^T_{2,2,2,2} \\ X^T_{2,1,2,1}* & X^S_{2,2,2,1}* & X^T_{2,2,2,2}* & X^S_{2,2,2,2}* \end{bmatrix} \begin{bmatrix} a_{2,1} \\ a_{2,1}* \\ a_{2,2} \\ a_{2,2}* \end{bmatrix} - \begin{bmatrix} a_{2,1} \\ a_{2,1}* \\ a_{2,2} \\ a_{2,2}* \end{bmatrix} \right)$$

$$[i] = \frac{-1}{\sqrt{Z}} \left([X^F] + \begin{bmatrix} X^S_{2,1,2,1} - 1 & X^T_{2,1,2,1} & X^S_{2,1,2,2} & X^T_{2,1,2,2} \\ X^T_{2,1,2,1}* & X^S_{2,1,2,1}* - 1 & X^T_{2,1,2,2}* & X^S_{2,1,2,2}* \\ X^S_{2,2,2,1} & X^T_{2,1,2,1} & X^S_{2,2,2,2} - 1 & X^T_{2,2,2,2} \\ X^T_{2,1,2,1}* & X^S_{2,2,2,1}* & X^T_{2,2,2,2}* & X^S_{2,2,2,2}* - 1 \end{bmatrix} \begin{bmatrix} a_{2,1} \\ a_{2,1}* \\ a_{2,2} \\ a_{2,2}* \end{bmatrix} \right)$$

$$[i] = \frac{-1}{\sqrt{Z}} \left([X^F] + ([X^{ST}] - [I])[A] \right)$$

$$[A] = ([I] - [X^{ST}])^{-1} \left([X^F] + \sqrt{Z}[i] \right)$$

$$[i] = \frac{1}{\sqrt{Z}} \left(([I] - [X^{ST}])([X^{ST}] + [I])^{-1} \left(\frac{1}{\sqrt{Z}}[V] - [X^F] \right) - [X^F] \right)$$

$$[V] = \sqrt{Z} \left(([X^{ST}] + [I])([I] - [X^{ST}])^{-1} ([X^F] + \sqrt{Z}[i]) + [X^F] \right)$$

The existence of $([X^{ST}] + [I])^{-1}$

and $([I] - [X^{ST}])^{-1}$ **determine whether or not a conversion exists**

Constant power Contour in A2 (A1.5.5)

$$b_2 = X_f + X_s a_2 + X_T a_2^*$$

$$2P = \left| X_f + X_s a_2 + X_T a_2^* \right|^2 - |a_2|^2$$

$$2P = \left(X_f + X_s a_2 + X_T a_2 * \right) \left(X_f * + X_s * a_2 * + X_T * a_2 \right) - |a_2|^2$$

$$2P = \left(\left(X_f + X_s a_2 + X_T a_2 * \right) X_f * + \left(X_f + X_s a_2 + X_T a_2 * \right) X_s * a_2 * + \left(X_f + X_s a_2 + X_T a_2 * \right) X_T * a_2 \right) - |a_2|^2$$

$$2P = X_f * X_f + X_f * X_s a_2 + X_f * X_T a_2 *$$
$$+ X_f X_s * a_2 * + X_s a_2 X_s * a_2 * + X_T a_2 * X_s * a_2 *$$
$$+ X_f X_T * a_2 + X_s a_2 X_T * a_2 + X_T a_2 * X_T * a_2 - |a_2|^2$$

$$2P = |X_f|^2 + X_f * X_s a_2 + \left(X_f * X_s a_2 \right) *$$
$$+ X_s a_2 X_T * a_2 + X_T a_2 * X_s * a_2 *$$
$$+ \left(X_f X_T * a_2 \right) * + X_f X_T * a_2 + X_s X_s * a_2 a_2 * + X_T X_T * a_2 a_2 * - a_2 a_2 *$$

$$2P = \left|X_f\right|^2 + X_f * X_s a_2 + \left(X_f * X_s a_2\right)*$$
$$+ X_s X_T * a_2 a_2 + \left(X_s X_T * a_2 a_2\right)*$$
$$+ X_f X_T * a_2 + \left(X_f X_T * a_2\right)* + \left|X_s\right|^2 \left|a_2\right|^2 + \left|X_T\right|^2 \left|a_2\right|^2 - \left|a_2\right|^2$$
$$2P - \left|X_f\right|^2 = 2\Re(X_f * X_s a_2) + 2\Re(X_f X_T * a_2) + 2\Re(X_s X_T * a_2 a_2) + \left(\left|X_s\right|^2 + \left|X_T\right|^2 - 1\right)\left|a_2\right|^2$$
$$2P - \left|X_f\right|^2 = 2\Re(k_1 a_2) + 2\Re(k_2 a_2) + 2\Re(k_3 a_2 a_2) + k_4 \left|a_2\right|^2$$
$$a_2 = x + jy$$
$$2P - \left|X_f\right|^2 = 2(k_{1R}x - k_{1I}y) + 2(k_{2R}x - k_{2I}y) + 2\Re(k_3 a_2 a_2) + k_4\left(x^2 + y^2\right)$$
$$\Re(k_3 a_2 a_2) = \left(k_{3R} + jk_{3I}\right)(x + jy)^2 = \left(k_{3R} + jk_{3I}\right)\left(x^2 - y^2 + 2jxy\right)$$
$$= \Re\left(k_{3R}\left(x^2 - y^2\right) + j.2xyk_{3R} + jk_{3I}\left(x^2 - y^2\right) - 2k_{3I}xy\right) = k_{3R}\left(x^2 - y^2\right) - 2k_{3I}xy$$
$$2P - \left|X_f\right|^2 = 2(k_{1R}x - k_{1I}y) + 2(k_{2R}x - k_{2I}y) + 2(k_{3R}\left(x^2 - y^2\right) - 2k_{3I}xy) + k_4\left(x^2 + y^2\right)$$
$$2P - \left|X_f\right|^2 = 2(k_{1R}x - k_{1I}y) + 2(k_{2R}x - k_{2I}y) + 2(k_{3R}\left(x^2 - y^2\right) - 2k_{3I}xy) + k_4\left(x^2 + y^2\right)$$
$$0 = \left|X_f\right|^2 - 2P + 2\left(k_{1R} + k_{2R}\right)x - 2\left(k_{1I} + k_{2I}\right)y - 4k_{3I}xy + \left(k_4 + 2k_{3R}\right)x^2 + \left(k_4 - 2k_{3R}\right)y^2$$
$$0 = \left(k_4 + 2k_{3R}\right)x^2 - 4k_{3I}xy + \left(k_4 - 2k_{3R}\right)y^2 + 2\left(k_{1R} + k_{2R}\right)x - 2\left(k_{1I} + k_{2I}\right)y + \left|X_f\right|^2 - 2P$$

Note this equation is an ellipse of form of a general conic section from which is given below on the condition that $\left|X_f\right|^2 - 2P \neq 0$

$$0 = Am^2 + 2Bmp + Cp^2 + Dm + Ep + F$$

Comparing the two equations gives

$$F = \left|X_f\right|^2 - 2P$$
$$A = \left(k_4 + 2k_{3R}\right)$$
$$B = -2k_{3I}$$
$$C = \left(k_4 - 2k_{3R}\right)$$
$$C_1 = 2\left(k_{1R} + k_{2R}\right)$$
$$C_2 = -2\left(k_{1I} + k_{2I}\right)$$
$$K = F - A\alpha^2 - C\beta^2 - 2B\alpha\beta$$
$$k_1 = X_f * X_s$$
$$k_2 = X_f X_T *$$
$$k_3 = X_s X_T *$$
$$k_4 = \left(\left|X_s\right|^2 + \left|X_T\right|^2 - 1\right)$$

$$F = \left|X_f\right|^2 - 2P$$
$$A = \left(\left(\left|X_s\right|^2 + \left|X_T\right|^2 - 1\right) + 2\Re\left(X_s X_T *\right)\right)$$
$$B = -2\Im\left(X_s X_T *\right)$$
$$C = \left(\left(\left|X_s\right|^2 + \left|X_T\right|^2 - 1\right) - 2\Re\left(X_s X_T *\right)\right)$$
$$C_1 = 2\Re\left(X_f * X_s + X_f X_T *\right)$$
$$C_2 = -2\Im\left(X_f * X_s + X_f X_T *\right)$$
$$K = \left|X_f\right|^2 - 2P - A\alpha^2 - C\beta^2 - 2B\alpha\beta$$

$$\beta = \frac{AC_2 - C_1 B}{2\left(B^2 - AC\right)}$$
$$\alpha = \frac{C_1 - 2B\beta}{2A}$$
$$\tan\left(2\theta\right) = \frac{2B}{A - C}$$

Also useful here are

$$rA = \sqrt{\left|\frac{-K}{A\cos^2\left(\theta\right) + C\sin^2\left(\theta\right) + B\sin\left(2\theta\right)}\right|}$$
$$rB = \sqrt{\left|\frac{-K}{A\cos^2\left(\theta\right) + C\sin^2\left(\theta\right) - B\sin\left(2\theta\right)}\right|}$$

Where

$$C_N\left(\phi\right) = C_E + \left(rA\cos\left(\phi\right)\cos\left(\theta\right) + rB\sin\left(\phi\right)\sin\left(\theta\right)\right) + j\left(rA\cos\left(\phi\right)\sin\left(\theta\right) - rB\sin\left(\phi\right)\cos\left(\theta\right)\right)$$

Is a contour of constant power on the a-plane and

$$\Gamma_N\left(\phi\right) = \frac{C_N\left(\phi\right)}{X_f + X_S C_N\left(\phi\right) + X_T C_N\left(\phi\right)*}$$

Is a contour of constant power on the load plane

Reduction of a General conic section to the canonical form of an ellipse (A1.5.6)

The equation of a general conic section is

$$0 = Ax^2 + 2Bxy + Cy^2 + Dx + Ey + F \quad \textbf{(1)}$$

The equation of an ellipse which main axis is rotated away from the x-axis and is centred at (-α,-β)is given by

$$0 = A\left(x - \alpha\right)^2 + 2B\left(x - \alpha\right)\left(y - \beta\right) + C\left(y - \beta\right)^2 + F - A\alpha^2 - C\beta^2 - 2B\alpha\beta$$

Expanding this equation gives

$$0 = Ax^2 - 2A\alpha x + 2Bxy - 2Bx\beta - 2B\alpha y + Cy^2 - 2C\beta y + F$$

Simplifying

$$0 = Ax^2 + 2Bxy + Cy^2 - (2A\alpha + 2B\beta)x - (2B\alpha + 2C\beta)y + F$$

$$0 = Ax^2 + 2Bxy + Cy^2 - C_1 x - C_2 y + F$$

Note A B and C are observed by Directly comparing with (1) then

$$C_1 = (2A\alpha + 2B\beta)$$

$$C_2 = (2B\alpha + 2C\beta)$$

$$\frac{C_1}{2A} = \alpha + \frac{B\beta}{A}$$

$$\frac{C_2}{2B} = \alpha + \frac{C\beta}{B}$$

$$\frac{C_1}{2A} - \frac{C_2}{2B} = \frac{B\beta}{A} - \frac{C\beta}{B}$$

$$\frac{C_1 B - AC_2}{2AB} = \left(\frac{B^2 - AC}{AB}\right)\beta$$

$$\beta = \frac{AC_2 - C_1 B}{2(B^2 - AC)}$$

$$\alpha = \frac{C_1 - 2B\beta}{2A}$$

Note alpha and beta describe the centre of the ellipse as

$$C_E = -\alpha - j\beta$$

$$0 = A(x-\alpha)^2 + 2B(x-\alpha)(y-\beta) + C(y-\beta)^2 + F - A\alpha^2 - C\beta^2 - 2B\alpha\beta$$

$$0 = A(x-\alpha)^2 + 2B(x-\alpha)(y-\beta) + C(y-\beta)^2 + K$$

$$0 = Ax'^2 + 2Bx'y' + Cy'^2 + K$$

Angle of ellipsis main axis is found using

This process is described using rotation matrices

$$\tan(2\theta) = \frac{2B}{A - C}$$

From which it can be shown that the major and minor axis of the canonical ellipse are given by

$$rA = \sqrt{\left|\frac{-K}{A\cos^2(\theta) + C\sin^2(\theta) + B\sin(2\theta)}\right|}$$

$$rB = \sqrt{\left|\frac{-K}{A\cos^2(\theta) + C\sin^2(\theta) - B\sin(2\theta)}\right|}$$

Where

$$1 = \frac{x'^2}{rA^2} + \frac{y'^2}{rB^2}$$

and the term xy has been reduced to zero
The ellipsis can now be described in parametric polar form as

$$C_N(\phi) = C_E + (rA\cos(\phi)\cos(\theta) + rB\sin(\phi)\sin(\theta)) + j(rA\cos(\phi)\sin(\theta) - rB\sin(\phi)\cos(\theta))$$

Which is convenient for drawing the ellipse

Re-normalization of the X-parameter Equation to new base impedance (A1.5.7)

$$v = \sqrt{\Re(Z)}(a+b)$$
$$i = \frac{(a-b)\sqrt{\Re(Z)}}{Z}$$
$$a = \frac{(v+iZ)}{2\sqrt{\Re(Z)}}$$
$$b = \frac{(v-iZ)}{2\sqrt{\Re(Z)}}$$

$$v = \sqrt{\Re(Z)}(X_F + (X_S+1)a + X_T a^*)$$
$$i = \frac{\sqrt{\Re(Z)}}{Z}(-X_F + (1-X_S)a - X_T a^*)$$

Developing a relation ship for the new "a" wave at the port

$$a' = \frac{(v+iZ')}{2\sqrt{\Re(Z')}}$$
$$a' = \frac{\left(\sqrt{\Re(Z)}(X_F + (X_S+1)a + X_T a^*) + \frac{\sqrt{\Re(Z)}}{Z}(-X_F + (1-X_S)a - X_T a^*)Z'\right)}{2\sqrt{\Re(Z')}}$$
$$a' = \frac{\sqrt{\Re(Z)}}{2\sqrt{\Re(Z')}}\left((X_F + (X_S+1)a + X_T a^*) + \frac{Z'}{Z}(-X_F + (1-X_S)a - X_T a^*)\right)$$
$$a' = \frac{\sqrt{\Re(Z)}}{2\sqrt{\Re(Z')}}\left(X_F\left(1-\frac{Z'}{Z}\right) + \left((X_S+1) + \frac{Z'}{Z}(1-X_S)\right)a + X_T\left(1-\frac{Z'}{Z}\right)a^*\right)$$
$$a' = M(k_F + k_S a + k_T a^*)$$

Developing a relation ship for the new "b" wave at the port

$$b' = \frac{(v-iZ')}{2\sqrt{\Re(Z')}}$$
$$b' = \frac{\left(\sqrt{\Re(Z)}(X_F + (X_S+1)a + X_T a^*) - \frac{\sqrt{\Re(Z)}}{Z}(-X_F + (1-X_S)a - X_T a^*)Z'\right)}{2\sqrt{\Re(Z')}}$$

$$b' = \frac{\sqrt{\Re(Z)}}{2\sqrt{\Re(Z')}}\left(\left(X_F + (X_S+1)a + X_T a^*\right) - \frac{Z'}{Z}\left(-X_F + (1-X_S)a - X_T a^*\right)\right)$$

$$b' = \frac{\sqrt{\Re(Z)}}{2\sqrt{\Re(Z')}}\left(X_F\left(1+\frac{Z'}{Z}\right) + \left((X_S+1) + \frac{Z'}{Z}(X_S-1)\right)a + X_T\left(1+\frac{Z'}{Z}\right)a^*\right)$$

$$b' = M\left(R_F + R_S a + R_T a^*\right)$$

Invert the "a" wave relation-ship (as above)

$$a = \frac{k_f^* k_T - k_f k_s^*}{\left(|k_s|^2 - |k_T|^2\right)} + \frac{k_s^*}{M\left(|k_s|^2 - |k_T|^2\right)}a' - \frac{k_T}{M\left(|k_s|^2 - |k_T|^2\right)}a'^*$$

$$b' = M\left(R_F + R_S\left(\frac{k_f^* k_T - k_f k_s^*}{\left(|k_s|^2 - |k_T|^2\right)} + \frac{k_s^*}{M\left(|k_s|^2 - |k_T|^2\right)}a' - \frac{k_T}{M\left(|k_s|^2 - |k_T|^2\right)}a'^*\right)\right)$$

$$+ MR_T\left(\frac{k_f^* k_T - k_f k_s^*}{\left(|k_s|^2 - |k_T|^2\right)} + \frac{k_s^*}{M\left(|k_s|^2 - |k_T|^2\right)}a' - \frac{k_T}{M\left(|k_s|^2 - |k_T|^2\right)}a'^*\right)^*$$

$$b' = \left(MR_F + \frac{MR_S\left(k_f^* k_T - k_f k_s^*\right)}{\left(|k_s|^2 - |k_T|^2\right)} + \frac{R_S k_s^*}{\left(|k_s|^2 - |k_T|^2\right)}a' - \frac{R_S k_T}{\left(|k_s|^2 - |k_T|^2\right)}a'^*\right)$$

$$+ \left(\frac{MR_T^*\left(k_f k_T^* - k_f^* k_s\right)}{\left(|k_s|^2 - |k_T|^2\right)} + \frac{R_T^* k_s}{\left(|k_s|^2 - |k_T|^2\right)}a'^* - \frac{R_T^* k_T^*}{\left(|k_s|^2 - |k_T|^2\right)}a'\right)$$

$$b' = M\left(R_F + \frac{R_S\left(k_f^* k_T - k_f k_s^*\right) + R_T^*\left(k_f k_T^* - k_f^* k_s\right)}{\left(|k_s|^2 - |k_T|^2\right)}\right)$$

$$+ \frac{R_S k_s^* - R_T^* k_T^*}{\left(|k_s|^2 - |k_T|^2\right)}a'$$

$$+ \frac{R_T^* k_s - R_S k_T}{\left(|k_s|^2 - |k_T|^2\right)}a'^*$$

$$b' = X_f' + X_S' a' + X_T' a'^*$$

A2. Supporting Publications

Woodington, S.; Williams, T.; Qi, H.; Williams, D.; Pattison, L.; Patterson, A.; Lees, J.; Benedikt, J.; Tasker, P.J.; , "A novel measurement based method enabling rapid extraction of a RF Waveform Look-Up table based behavioural model," Microwave Symposium Digest, 2008 IEEE MTT-S International , vol., no., pp.1453-1456, 15-20 June 2008
doi: 10.1109/MWSYM.2008.4633053
URL: http://ieeexplore.ieee.org/stamp/stamp.jsp?tp=&arnumber=4633053&isnumber=4632906

Woodington, S.; Saini, R.; Williams, D.; Lees, J.; Benedikt, J.; Tasker, P.J.; , "Behavioural model analysis of active harmonic load-pull measurements," Microwave Symposium Digest (MTT), 2010 IEEE MTT-S International , vol., no., pp.1688-1691, 23-28 May 2010
doi: 10.1109/MWSYM.2010.5517261
URL: http://ieeexplore.ieee.org/stamp/stamp.jsp?tp=&arnumber=5517261&isnumber=5514662

J.Powell, M. Uren, T. Martin, S. Cripps, P. Tasker, J. Benedikt, S.Woodington, A. Mclachlan
"Investigation of high efficiency amplifiers at X-band using GaAs p-HEMT and GaN HFET technologies"
QinetiQ Ltd, Malvern, Cardiff University, Selex Galileo, Edinburgh,
Electro-Magnetic Remote Sensing (EMRS) Defence Technology Centre (DTC), 7th Annual Technical Conference,13th -14th July 2010,Conference Proceedings

J. Horn, S. Woodington, R. Saini, J. Benedikt, P.J. Tasker, D.E. Root, "Harmonic Load Tuning Predictions from X-parameters,"
Agilent Technologies, Santa Rosa, CA, USA; Cardiff University, Cardiff, UK
http://pasymposium.ucsd.edu/papers2009_2/2009_PA_Symp_Final_Program.htm

Saini, R.S.; Woodington, S.; Lees, J.; Benedikt, J.; Tasker, P.J.; , "An intelligence driven active loadpull system," *Microwave Measurements Conference (ARFTG), 2010 75th ARFTG* , vol., no., pp.1-4, 28-28 May 2010
doi: 10.1109/ARFTG.2010.5496327
URL: http://ieeexplore.ieee.org/stamp/stamp.jsp?tp=&arnumber=5496327&isnumber=5496310

A Novel Measurement Based Method Enabling Rapid Extraction of a RF Waveform Look-up Table Based Behavioral Model

S. Woodington[1], T. Williams[1], H. Qi[1], D.Williams[2], L. Pattison[2], A. Patterson[2],

J. Lees[1], J. Benedikt[1], P. J. Tasker[1,]

[1]School of Engineering, Cardiff University, Cardiff, UK, CF24 3TF
Tel +44 2920 876347 email: woodingtonsp@cf.ac.uk
[2]Mimix Europe, Woodchester House, Newforge lane, Belfast, BT9 5NW
email: dwilliams@mimixbroadband.com

***Abstract* — A solution allowing for the rapid, cost effective and accurate extraction of nonlinear Direct Waveform Look-Up table (DWLU) based behavioral models is presented in this paper. The behavioral model extracted is a reformulation of the PHD model, now defined about a non 50-Ohm reference impedance, enabling it to accurately predict load-pull contours. The technique exploits a simple active and passive load-pull architecture enabling a numerical integration solution for model coefficient extraction that necessitates only varying the phase of the input stimulus during measurement. This solution dramatically speeds up the behavioral model coefficient extraction process, enabling 'real time' access to critical device behavior. It ensures that only a minimum, optimized set of load-pull measurements are performed. The technique is demonstrated on a Mimix Broadband Gas 8x2x30um 0.5W HBT.**

***Index Terms* — Poly Harmonic Distortion Model, , non-linear device modeling, microwave measurements, power amplifiers.**

I. Introduction

In the RF Power Amplifier (PA) design cycle, it is important to be able to rapidly prototype complex nonlinear circuits and concepts. In order for this to be successfully achieved using modern CAD tools, rather than experimental prototyping, the nonlinear behavior of active devices needs to be accurately modeled for use within CAD design environments. However, this requires the rapid availability of nonlinear models as new device technologies emerge. Also as the complexity of RF systems has increased the requirements for model accuracy and convergence speeds have also increased. This has led to a move away from physics based models towards behavioral modeling approaches.

Recently, a behavioral modeling approach [1] based on Direct Waveform Look-Up (DWLU), using measured large signal RF I-V waveforms has been developed. This exploits the ability of modern CAD tools to use both data storage look-up and to interpolate between measurement points. This DWLU behavioral model provides for the rapid availability of accurate, load-pull contour and waveform data, thus enabling reliable CAD based RF Power Amplifier design with emerging device technologies to be immediately undertaken. A further development involved formulating the DWLU approach to utilize behavioral model coefficients tables [2], the goal being to further improve load-pull contour prediction and increase simulation convergence speeds. The resulting DWLU behavioral model, defined about a non 50-ohm reference impedance, is a reformulation of the Poly-Harmonic Distortion (PHD) model introduced by Verspect and Root [3].

One of the significant constraints in generating these accurate data based nonlinear behavioral models is the need for relevant, large signal waveform measurement datasets. In [2], the DWLU behavioral model was extracted from measured RF waveforms resulting from conventional load-pull measurement sequences: swept input power and load impedance.

This paper presents novel measurement based hardware, together with an extraction methodology, that optimizes the measurement procedure and population requirements for this DWLU behavioral model solution. It will be shown how the approach dramatically reduces the time spent measuring the necessary large signal datasets, and overcomes the previously mentioned barriers for model generation. This allows for the rapid, near-real-time generation of DWLU based behavioral models.

II. Model Extraction

Fundamentally, the nonlinear large-signal reflected traveling wave response (b_1 and b_2) of a device is mathematically related to the incident traveling wave stimulus (a_1 and a_2). The measured behavioral model data coefficient tables must quantify this generic relationship;

$$b_1 = f(a_1,a_2),\ b_2 = g(a_1,a_2) \qquad (1)$$

The DWLU behavioral model used in this paper, introduced by Qi et al. [2], was specifically formulated to provide accurate load-pull contour prediction. In this case, the behavior of the fundamental wave components can be

quantified in terms of the following describing functions shown in (2)

$$b_1 = S_{11}.a_1 + T_{11}.a_1^*.Q^2 + S_{12}.a_2 + T_{12}.a_2^*.P^2$$
$$b_2 = S_{21}.a_1 + T_{21}.a_1^*.Q^2 + S_{22}.a_2 + T_{22}.a_2^*.P^2 \quad (2)$$

Where Q and P are the respective fundamental input and output a-wave phase operators, given by

$$P = a_1/|a_1|,\ Q = a_2/|a_2| \quad (3)$$

Note that in this case, the model *S* and *T* coefficients are functions only of the magnitudes of the stimulus a-wave (a_1 and a_2) fundamental components. Fundamental phase is accounted for directly in the formulation. Thus, DWLU behavioral model population simply reduces to the extraction of the respective *S* and *T* coefficient look-up tables as a function of $|a_1|$ and $|a_2|$ directly from an appropriate sequence of large signal RF waveform load-pull measurements. To help understand the optimum load-pull measurement sequence required and the coefficient extraction procedure developed, reformulate (2) as shown below.

$$b_1 = S_{11}.|a_1|.P + T_{12}.|a_2|.P.\frac{P}{Q} + S_{12}.|a_2|.Q + T_{11}.|a_1|.Q.\frac{Q}{P}$$
$$b_2 = S_{21}.|a_1|.P + T_{22}.|a_2|.P.\frac{P}{Q} + S_{22}.|a_2|.Q + T_{21}.|a_1|.Q.\frac{Q}{P} \quad (4)$$

This clearly highlights that each *S* and *T* coefficient has a unique phase operator. Thus, if large-signal RF waveform measurements are performed on a load-pull locus of constant $|a_1|$ and $|a_2|$, but with swept relative phase θ (P/Q or Q/P), then each *S* and *T* coefficient can be extracted independently by simply numerically integrating the measured respective b-waves after dividing by the associated coefficient phase operators, as follows

$$S_{11}.|a_1| = \frac{1}{n}\sum b_1.1/P,\quad T_{11}.|a_1| = \frac{1}{n}\sum b_1.P/Q^2$$
$$S_{12}.|a_2| = \frac{1}{n}\sum b_1.1/Q,\quad T_{12}.|a_2| = \frac{1}{n}\sum b_1.Q/P^2 \quad (5)$$

$$S_{21}.|a_1| = \frac{1}{n}\sum b_2.1/P,\quad T_{21}.|a_1| = \frac{1}{n}\sum b_2.P/Q^2$$
$$S_{22}.|a_2| = \frac{1}{n}\sum b_2.1/Q,\quad T_{22}.|a_2| = \frac{1}{n}\sum b_2.Q/P^2 \quad (6)$$

Where n is the number of measured equal phase steps from 0 to 2π.

The required load-pull locus can be achieved by simply terminating the device into a matched signal source. However, it was also demonstrated in [2] that renormalization of the a_n and b_n traveling waves can improve significantly the accuracy of the generated models.

Thus we need to work with renormalized a'_n and b'_n traveling waves. At the output plane the new normalizing impedance is selected to be at or near the device optimum output impedance Z_{opt} for maximum power. For the input, it is set equal to the actual measurement system input impedance. Note, the *S* and *T* coefficients are now formulated in terms of the renormalized a'_n and b'_n parameters, thus the swept relative phase (θ), large signal RF waveform measurements actually need to be performed on a load-pull locus of constant $|a'_1|$ and $|a'_2|$. The load termination required to achieve this load-pull locus, relative to the calibrated system impedance, is a signal source with a impedance equal to $Z'_2 (= Z_{opt})$. Note that once the measured data is renormalized, such a load termination will become a matched signal source; hence a circular a'_2 locus. The corresponding flow diagrams are shown in Fig 1.

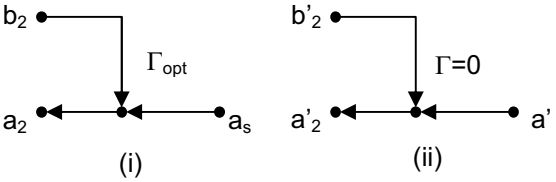

Fig 1. Flow diagrams of the required load; (i) referenced to calibrated system impedance Z_o and (ii) after renormalized to Z_{opt}

Hence, in the renormalized a'_2 plane the value of a'_2 is given by;

$$a'_2 = a'_s \quad (7)$$

and is thus, as required, independent of b'_2. Hence, simple direct extraction of *S* and *T* coefficients requires the following sequence of load-pull locus measurements; fixed, magnitude and phase, a'_s output stimulus for constant magnitude $|a'_1|$ but swept phase (i.e. P from 0 to 2π) input stimulus. In other words, measuring RF large-signal waveform performance under swept power conditions into appropriately engineered load-pull loci impedances. The required load-pull loci must satisfy the following equation;

$$a_2 = b_2.\Gamma_{opt} + a_s \quad (8)$$

III. MEASUREMENT SOLUTIONS FOR THE COLLECTION OF THE MODEL DATA

Standard load-pull measurements can be utilized to collect the relevant data sets for *S* and *T* coefficient extraction. This approach generally requires the collection of a large number of data points in order to use 2-D interpolation to determine the

values of the b-waves on the required load-pull loci. It would be more appropriate, if possible, to configure the load-pull hardware to only measure on the relevant load-pull loci.

Consider the integration of a passive load-pull and signal source achieved by insertion of a directional coupler between the load-pull tuner and the device under test, as shown in Fig 2. This architecture directly replicates the desired load; a signal source with a user defined non 50 ohm impedance. Firstly, the passive tuner is adjusted to set the Γ_{opt} seen by the DUT to the desired renormalizing impedance value $Z'_2(= Z_{opt})$; typically the optimum for output power. The load-pull locus required for extracting *S* and *T* coefficients is simply realized by setting the output signal a'_s source to a fixed power level while stepping the input phase P (0 to 2π); thus providing the required values of a'_2. These load-pull locus sweeps can be repeated for different output signal source $|a'_s|$ and/or input signal source $|a'_1|$ power levels.

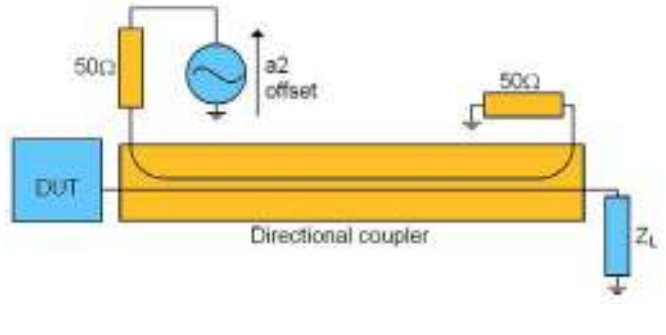

Fig 2. Architecture for generating the required load-pull loci by integrating an active source with a passive load-pull system

The resulting measured b-waves on each load-pull locus sweep can be simply divided by the respective phase operator and integrated to extract the *S* and *T* coefficient data table as a function of $|a'_1|$ and $|a'_2|$, using the equations given in (5) and (6). This allows for rapid population of the *S* and *T* look-up data tables.

IV. Application of the Measurement Method to an HBT Device

The technique outlined in this paper was applied to a GaAs 8x2x30um 0.5W HBT Device supplied by Mimix broadband. During the RF waveform measurements at each input drive level (fixed $|a_1'|$), a load-pull loci consisting of a sequence of n=64 uniformly stepped source phase points P (0 to 2π) for a sequence of 11 constant $|a_2'$ values$|$ were measured. The measurement time for these measurements is only dependent on the level of averaging used at each measurement point, as the method requires no iterations to converge on to specific load impedance. The resulting load-pull loci are shown in Fig 3. The corresponding computed output power load-pull contours from these measurements shows that the load-pull loci cover a 3dB output power range.

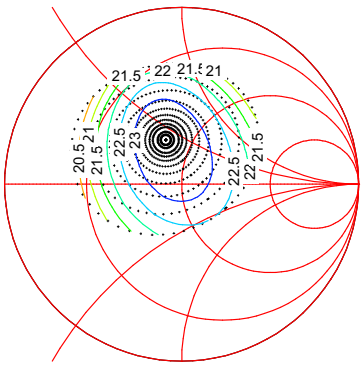

Fig 3. Shows the measured load-pull loci and the associated output power contours.

The corresponding stimulus a_1 and a_2 and response b_1 and b_2 traveling wave are shown in figure 4. The observed behavior of b_2 clearly indicating that the device is exhibiting non-linear behavior. These transform to the required set, for model extraction, of simple fixed a_1', circular a_2' contours, as shown in Fig 5,after renormalization.

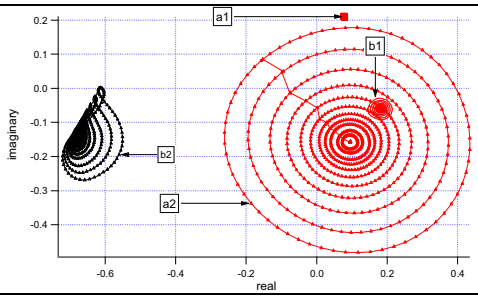

Fig 4. Shows the measured a and b traveling wave on the sequence of load-pull loci, referenced to the system impedance.

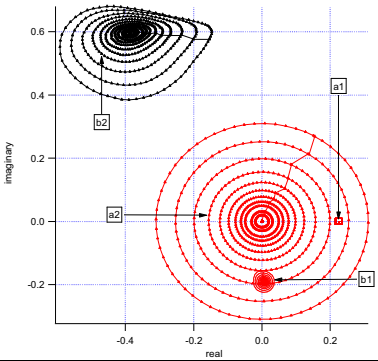

Fig 5. Shows the measured a and b traveling wave on the sequence of load-pull loci, once renormalized.

Fig 6 compares the corresponding b_2' measured and computed values using equation 4. The results clearly indicate that for small values of a'_2 about the optimum load impedance the model can accurately predict b'_2, hence the load-pull

contours. However, for larger values of a'_2 model prediction of b'_2 degrades.

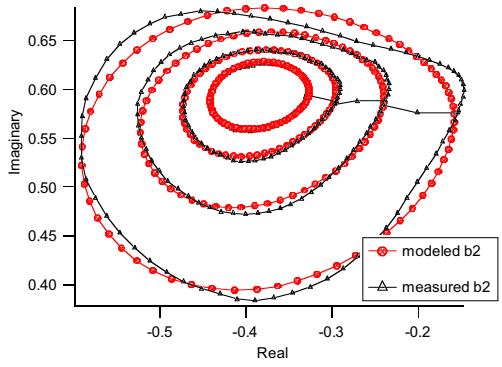

Fig 6. Comparison the measured and modeled b_2' traveling wave using the S and T parameter DWLU behavioral model.

This weakness is consistent with the fact that the S and T model as formulated only accounts for non-linear behavior, a_1, a_2 mixing, up to 3rd order. This is clearly adequate for small values of a'_2 but as a'_2 increases higher orders mixing terms must be considered.

V. Extraction of Models Based Around Higher Order Distortion Terms

The *S* and *T* model formulation shown in equations (4) can be consider as a polynomial function of the a_1, a_2 mixing phase operators $(P/Q)^n.P$ and $(Q/P)^n.Q$ for values of n up 1 (accounts for 3rd order mixing). Increasing n, as shown in Fig 7, up to 3 (accounts for 7th order mixing) provides for a formulation of the DWLU behavioral model that can now more accurately predicts b'_2, hence the load pull-contours. Fig 8 compares the output power load-pull contours computed from both the measured b_2 response and the modeled b_2 performance. For the power contours shown power prediction is within 0.1dB

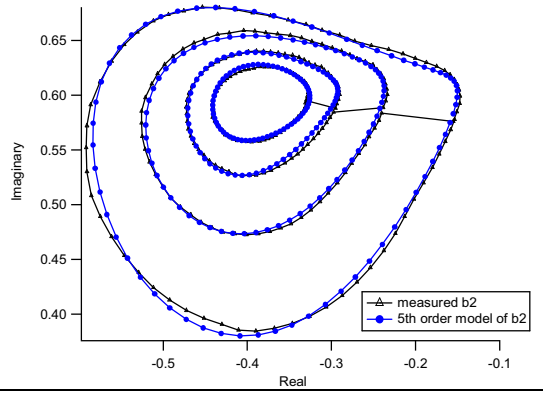

Fig 7. Comparison the measured and modeled b_2' traveling wave using the higher order DWLU behavioral model.

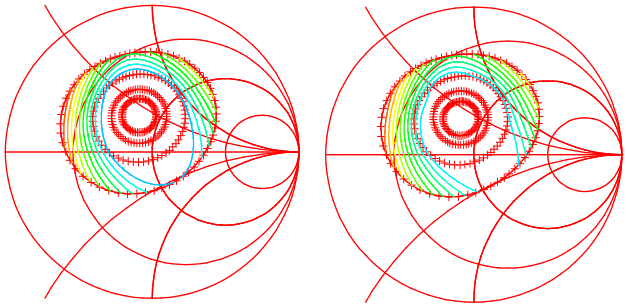

Fig 8. Comparison of modeled (right) and measured (left) output load-pull contours.

VI. Conclusion

A novel measurement configuration has been presented that enables the rapid extraction of a non-linear Direct Waveform Look-Up table (DWLU) formulated behavioral model. The technique exploits both a combined active and passive load-pull architecture and a numerical integration based parameter extraction concept that requires only measurements involving varying the phase of the input source. This solution allows for the rapid, cost effective, accurate extraction of nonlinear behavioral models required for accurate load-pull contour prediction. The approach ensures only the optimum, hence minimum; load-pull measurements are necessary for behavioral model extraction.

Acknowledgement

The authors wish to acknowledge the assistance and support of Mimix Broadband

References

[1] H. Qi, J. Bendikt P J Tasker, "A Novel Approach for Effective import of Nonlinear Device Characteristics into CAD for Large Signal Power Amplifier Design " *IEEE MTT-S International Microwave Symposium, 2006*

[2] Hao Qi, Johannes Benedikt P. J. Tasker, "Novel Nonlinear Model for Rapid Waveform-based Extraction Enabling Accurate High Power PA Design" *IEEE MTT-S International Microwave Symposium, 2007*

[3] Jan Verspecht, David E. Root, "Poly Harmonic Distortion Modeling" *Microwave Magazine, IEEE Volume 7, Issue 3 IEEE June 2006Page(s):44-57*

Behavioral Model Analysis of Active Harmonic Load-pull Measurements

S. Woodington[1], R. Saini[1], D. Williams[2], J. Lees[1], J. Benedikt[1], P. J. Tasker[1]

[1]School of Engineering, Cardiff University, Cardiff, UK, CF24 3TF
Tel +44 2920 876347 email: woodingtonsp@cf.ac.uk
[2]Mimix Europe, Woodchester House, Newforge lane, Belfast, BT9 5NW
email: dwilliams@mimixbroadband.com

***Abstract* — This paper outlines the formulation of a mixing based behavioral model, capable of capturing the nonlinear response of microwave transistors to fundamental and harmonic load pull effects for use in Computer Aided Design tools. The key to the model formulation was the experimental identification of the dominating mixing terms. The model is able to accurately compute the voltage and current waveforms present at a Transistors Terminals. The formulation lends itself to economical use of measured data, reducing data storage required within the CAD environment. In this paper the modeling approach has been demonstrated on a 10x75µm GaAs HEMT operating at 9 GHz.**

***Index Terms* — behavioral modeling, S parameters, Load-Pull, power amplifiers.**

I. Introduction

A number of behavioral modeling approaches have been proposed for High frequency Transistors [1-3], based on the exploitation of measurement data collected under representative system conditions. These methods utilize extensive databases of RF measurements describing the device behavior over a range of operating conditions. Such databases can be used directly in a lookup table approach [1], be condensed into descriptive functions using a modeling framework [1-3] or a combination of both X-parameters can be utilized [4].

The Poly-Harmonic Distortion (PHD) model [3], which uses third order nonlinear mixing equations to describe the behavior of devices to different stimuli and conditions, has been shown to provide a very appropriate descriptive framework. The PHD model has been used very successfully to describe nonlinear device behavior locally to the operating conditions about which they were extracted. To overcome this limitation the concept can be extended, for example, by measuring PHD datasets as function of another parameter, for i.e. interpolating between various measured fundamental load impedances. Alternatively, previous work [5] has shown that by considering higher order mixing terms a model can be developed which does not require the simulator to interpolate between data sets for different fundamental load impedance measurements.

In this paper it will be shown that the behavioral modeling framework based on nonlinear mixing can be further extended to accurately represent device behavior over full range of both fundamental and harmonic terminations. This is an important requirement if behavioral models are to be successfully utilized in the design of RF power amplifiers, since harmonic source and load terminations are crucial in predicting accurate power levels and achieving high efficiencies; for example the design of Class-B,-E, -F & -J power amplifiers.

II. Mixing Based Device Model for Single Tone Stimuli

A linear network can be fully described by the use of S-parameters [6], which are made up of the ratios of incident and scattered voltage traveling waves at a single frequency. The response of nonlinear networks cannot be fully described by S-parameters. Instead the mapping of incident travelling waves to all scattered frequencies must be considered – hence the mixing model approach. To develop an understanding of the mixing model and its nomenclature, a two port network will be considered as in Fig. 1.

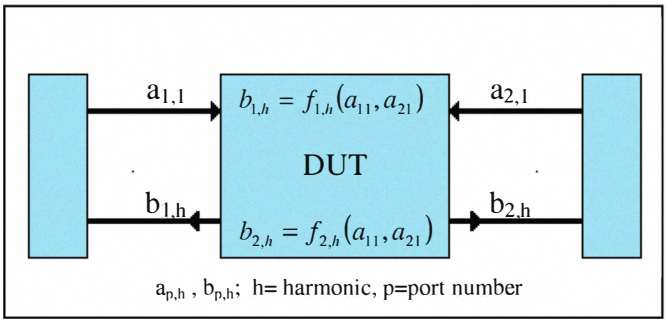

Fig. 1. Relationship of travelling waves to a two port network

The mixing model for the single tone case is formulated using describing functions to capture the behavior of a device when subjected to fundamental stimuli at each port. Under these conditions, it can be shown that the device responds only to the magnitudes of the signals applied to the device and the relative phase difference between the signals at the device ports.

The formulation is simplified by referencing all phases to the phase of the input signal at the fundamental frequency, allowing the removal of absolute phase from the describing function. This algebraic step is shown in (1) - (2) and in [3]

$$b_{p,h} = f_{p,h}(a_{1,1}, a_{2,1}) = e^{jh\angle a_{1,1}} g_{p,h}\left(|a_{1,1}|, |a_{2,1}|, e^{j(\angle a_{2,1} - \angle a_{1,1})}\right) \quad (1)$$

$$b_{p,h} = P_1^h g_{p,h}\left(|a_{1,1}|, |a_{2,1}|, \left(Q_1 / P_1\right)\right) \quad (2)$$

With $a_{1,1} = |a_{1,1}| e^{j\angle a_{1,1}} = |a_{1,1}| P_1$, $a_{2,1} = |a_{2,1}| e^{j\angle a_{2,1}} = |a_{2,1}| Q_1$

Importantly, the resulting equation (2) shows a separation between the relative phase and the magnitudes of the stimuli signals. This is useful as it allows the consideration of phase effects independently of the magnitudes.

The separation of phase and magnitude simplifies the measurements required to populate the model coefficients. To capture the entire phase response at a given power level, the measurement technique can be reduced to a pair of constant magnitude tones injected at both ports with their relative phase swept through 360 degrees.

It is important to account for the physical impedance of the measurement system in order to accurately view the measured phase response. This is achieved by renormalizing the travelling waves to the measured port impedances of the system at all frequencies of interest [5].

Examination of the results of this measurement technique lead to an expanded version of (2) that allows all orders of phase non-linearity in the system to be described by a set of coefficients. This representation is given in (3).

$$\sqrt{\Re(Z)} b_{p,h} = V_{p,h}^{+} = P_1^h \sum_{n=-(N-1)/2}^{(N+1)/2} \left\{ R_{p,h,n}\left(|a_{1,1}|, |a_{2,1}|\right) \left(\frac{Q_1}{P_1}\right)^n \right\} \quad (3)$$

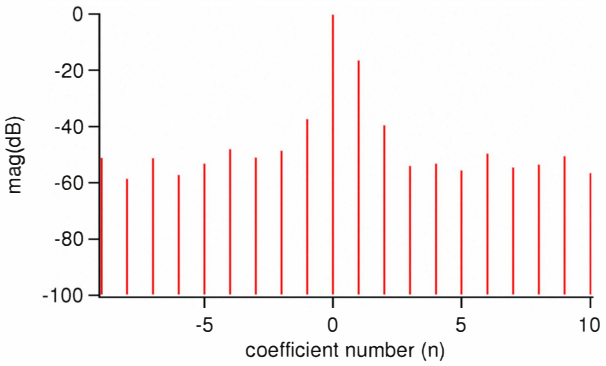

Fig. 2. Coefficient spectrum for $R_{2,1,n}$ for a 10x75µm GaAs HEMT

The $R_{p,h,n}$ parameters in (3) are the coefficients of the Fourier transform of the device under test (DUT) output response. Fig. 2 shows in a spectral plot the result of extracting these coefficients from a measured dataset, in this case a 10x75µm GaAs HEMT. This dataset shows a clearly defined measurement noise floor around -50 dB. This noise floor can be used to determine the maximum order to which any model could be accurately extracted. In this case the optimum model order would be between 5th and 7th order. Applying this concept to different levels of stimuli causes the respective coefficients $R_{p,h,n}$ to be seen as functions of $|a_{1,1}|$ and $|a_{2,1}|$ which can be represented by polynomials with an order no larger than the order identified using (3).

III. A Model Frame Work For The Analysis of Harmonic Interactions

The model discussed in the previous section describes how changes such as load impedance at the fundamental frequency affects harmonically related frequencies. Any changes to terminations at frequencies other than the fundamental frequency are unaccounted for leading to degradation in the accuracy of the model. However, it is well known that harmonic terminations are important when considering the efficiency and the linearity of RF Power Amplifiers; hence their effects should be included in the formulation.

Extending the model to include the effects of harmonic terminations, other phase vectors need to be considered. Keeping the framework in line with the model presented in section II, all phase vectors are formed with reference to the phase of the fundamental stimulus at port 1 (P_1). Thus to be able to consider a second harmonic termination at port 2, two other signals need to be accounted for, namely $b_{2,2}$ and $a_{2,2}$. Here $a_{2,2}$ is a stimulus signal resulting in one new phase vector (Q_2/P_1^2). This phase vector can become part of the coefficient set generated from (3) and is shown in (4)

$$R_{p,h,n} = G_{p,h,n}\left(|a_{1,1}|, |a_{2,1}|, |a_{2,2}|, \frac{Q_2}{P_1^2}\right) \quad (4)$$

In a measurement, to extract these additional coefficients, the phase vector (Q_2/P_1^2) should be rotated around 360°. The resulting coefficients would then be expected to produce periodic changes in the coefficients with respect to the phase vector (Q_2/P_1^2). These effects can be captured by (5)

$$R_{p,h,n} = \sum_r \left\{ G_{p,h,n,r}\left(|a_{1,1}|, |a_{2,1}|, |a_{2,2}|\right) \left(\frac{Q_2}{P_1^2}\right)^r \right\} \quad (5)$$

$$b_{p,h} = P_1^h \sum_n \sum_r \left\{ G_{p,h,n,r}\left(|a_{1,1}|, |a_{2,1}|, |a_{2,2}|\right) \left(\frac{Q_i}{P_1}\right)^n \left(\frac{Q_2}{P_1^2}\right)^r \right\} \quad (6)$$

Substituting the coefficients from (5) into (3) forms (6). The coefficients in this equation are only functions of the stimuli magnitudes and are independent of their phases. It can also be noted that the phase difference between the two signals at the output are accounted for by the cross product terms in this equation, i.e. the terms that are related to Q_1Q_2 and Q_1/Q_2.

In order to extract these coefficients two conditions must be met. Firstly, datasets containing sweeps of the phase component of the fundamental phase vector are required. Secondly, datasets containing sweeps of the phase component of the second harmonic phase vector are required where the fundamental phase vector is held constant.

IV. Measurement of Model Specific Data Sets

To demonstrate the necessary measurement approach, results were taken for a 10x75µm GaAs HEMT device, operating at 9GHz using the waveform measurement system developed at Cardiff University [6]. The measurement strategy followed included spinning the second harmonic phase vector around 360 degrees in 18-degree steps whilst holding the fundamental phase vector constant. This was repeated as the fundamental phase vector was spun around 360 degrees, with points distributed every 18 degrees. Finally, the entire process was carried out with varying magnitudes of the fundamental and second harmonic stimuli at port 2 ($|a_{2,1}|$ and $|a_{2,2}|$).

This dataset was renormalized to the measured system impedances and the fundamental phase at port 1 was removed. The complex values of $a_{2,1}$, $a_{2,2}$, $b_{2,1}$ and $b_{2,2}$ for a subset of these measurements have been plotted in Figure 4. Examining this data importantly shows that the perturbations of the fundamental $b_{2,1}$ at the output of the device due to the phase of $a_{2,1}$ and $a_{2,2}$ produce closed forms in $b_{2,2}$ and $b_{2,1}$. This allows the separation of fundamental and harmonic functions when coefficients are extracted.

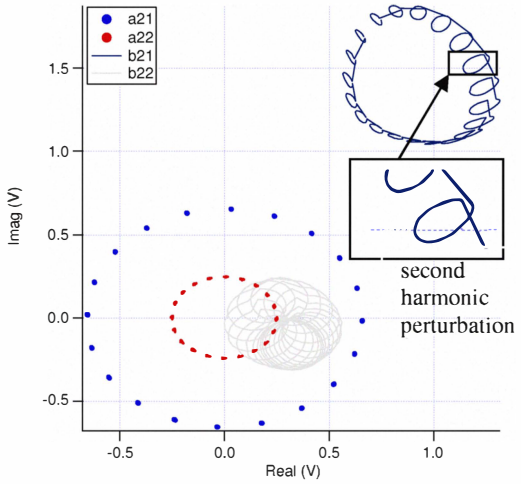

Fig. 4. Sample of the recorded traveling waves during the measurement Sequence

V. Model Extraction and Validation

The extraction process can be demonstrated by sampling a dataset whereby one magnitude point in each of the sets of $a_{2,1}$ and $a_{2,2}$ are used to extract the model coefficients. Based on the formulation of (6), there are two approaches to this process. Firstly, if the magnitude functions are not included, Eqn. 6 can be regarded as a 2-Dimensional Fourier transform. Alternatively, the coefficients in Eqn. 6 can be extracted using the Polynomial Least Mean Squares Method (LMS). It has to be noted that the Fourier transform provides the best method due to the fact that all the model coefficients can be extracted in one process, without over-fitting the data. However, this technique suffers when it is presented with data that does not include ideal sample points, thereby causing leakage into other sample bins. This effect can be overcome by interpolation onto the nearest ideal sample point. The LMS algorithm avoids the leakage problem by allowing measured points to be used as independent data.

In order to illustrate the complexity of the coefficient space required, the dataset presented in Fig. 4 was overlaid with a dataset produced by a 5th order model and analyzed using two different cases.

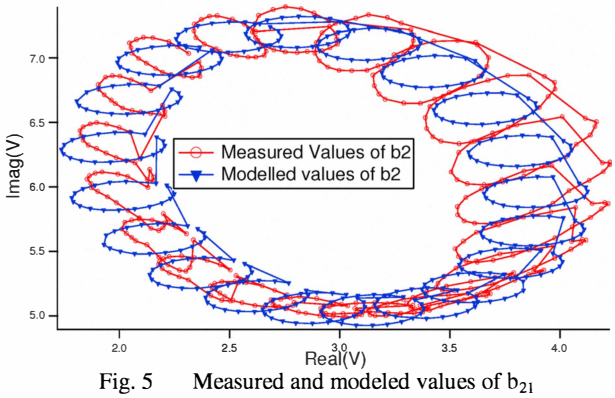

Fig. 5 Measured and modeled values of b_{21}

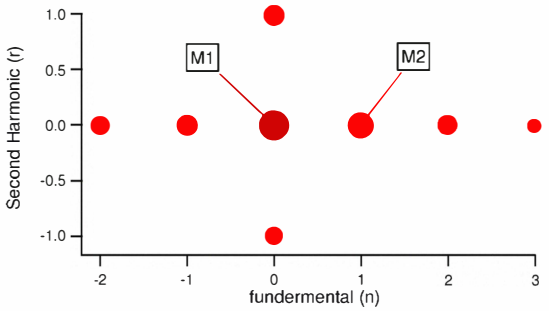

Fig. 6. Extracted coefficients plotted where the size of the point represents the logarithmic magnitude of the coefficient

In the first case (Fig. 5 and Fig. 6), the 5th order model is represented by the coefficient space as shown in Fig 6. In this figure, the magnitude of each coefficient is represented by the size of its data point. The largest point, indicated by "m1" is the most dominant term in the extraction process and is equivalent to $S_{21}|a_{1,1}|$. "m2" is equivalent to $S_{22}|a_{2,1}|$ and this term is the second most dominant in the coefficient set.

Figures 5 and 6 indicate that this model is able to reproduce most of the form of the perturbation only due to the mixing of the fundamental phase with the input stimuli ($a_{1,1}$); however it is unable to model the interactions of the second harmonic signal ($a_{2,2}$) with the input fundamental signal ($a_{1,1}$). This is due to the mixing between the injected second harmonic signal at the output ($a_{2,2}$) and the injected fundamental signal at the output ($a_{2,1}$). The average error produced in this extraction was 1.8% although the peak error was much larger.

In the second case (Fig. 7 and Fig. 8) the optimum number of coefficients which includes cross product terms has been added to enable capturing of the output mixing behavior. This allows the model to properly track changes in the second harmonic's perturbation around all phases of the fundamental

value of $b_{2,1}$. The average error resulting from this extraction was 0.25%.

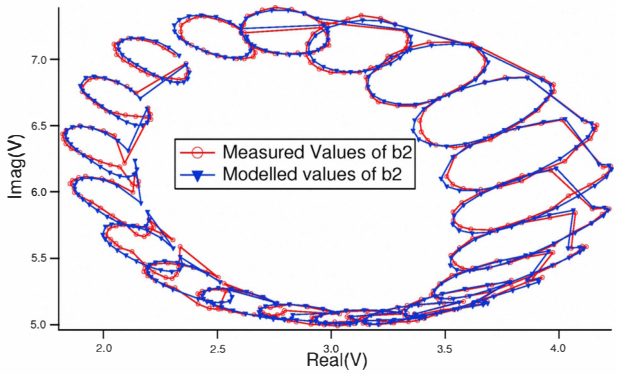

Fig. 7. Measured and modeled values of $b_{2,1}$

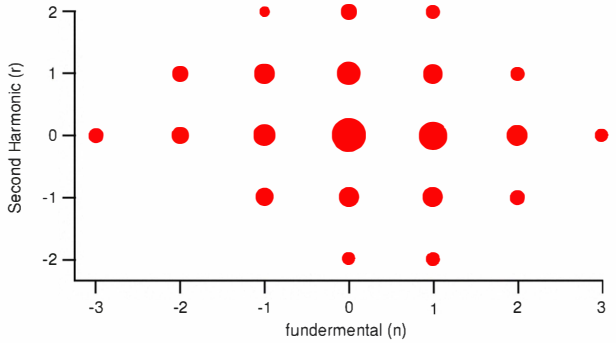

Fig. 8. Extracted coefficients plotted where the size of the Point represents the logarithmic magnitude of the coefficient

VI. Use of the Model Within Computer Aided Design Software

The discussed model can be structured within Computer Aided design software utilizing a Frequency domain Defined Device (FDD). The FDD enables computation of the incident travelling waves at the device ports, which are then used to compute new spectral voltages at these ports. The process discussed in this paper is repeated on all valid harmonics within the system at each device port to enable this functionality. An illustration of this has been conducted on an example data point, with measured and modeled voltage and current waveforms shown in Fig 9, 10.

VII. Conclusion

A behavioral modeling framework based on mixing theory has been demonstrated, capable of taking into account the changes of load impedance at the fundamental and second harmonic frequencies. It was identified that in order to correctly the track changes resulting from second harmonic perturbation for all phases of the output fundamental signal it was necessary to include cross product terms that accounted for output mixing. The resulting model is capable of modeling the device-plane I-V waveforms.

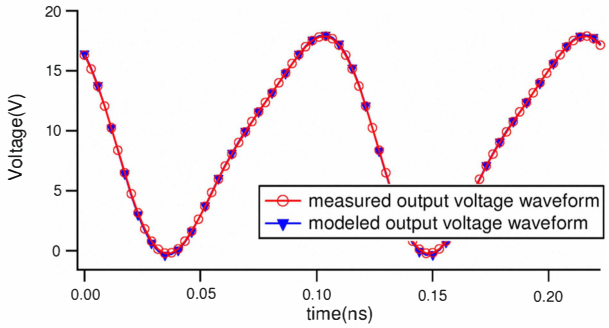

Fig. 9. Measured and modeled output voltage waveforms

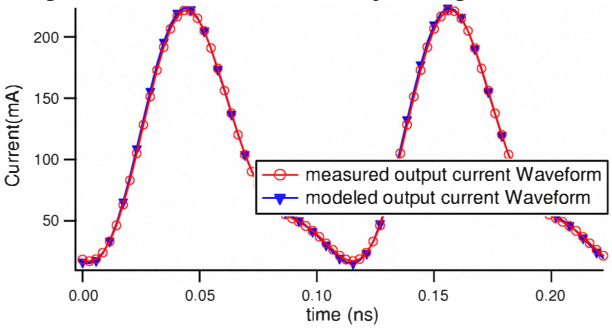

Fig. 10. Measured and modeled output current waveforms

Acknowledgement

The Authors wish to acknowledge the assistance and support of Mimix Broadband, ERMS-DTC and Agilent Technologies Foundation. Also, the support of Mr Christopher Roff who helped with the editing of this paper.

References

[1] Hao Qi, Johannes Benedikt, Paul Tasker, *"A Novel Approach for Effective Import of Nonlinear Device Characteristics into CAD for Large Signal Power Amplifier Design"*, IEEE MTT-S International, Page(s) 2019-2022,3-8 June 2007

[2] J. Verspecht et al. *"Hot S-ParameterTechniques6=4+2"*, 66th IEEE ARFTG Conference Digest, January 2008

[3] Jan Verspecht, David E. Root, *"Poly-harmonic Distortion Modeling"*, IEEE microwave magazine 1527-3342/06, June 2006.

[4] Jason Horn, Daniel Gunyan, Loren Betts, Chad Gillease, Jan Verspect, David E. Root, *"Measurement-Based Large-Signal Simulation of Active Components from Automated Nonlinear Vector Network Analyzer Data via X-Parameters"* ,COMCAS 2008,13-14 May 2008 Page(s):1 - 6, IEEE

[5] S. Woodington, T. Williams, H. Qi, D.Williams, L. Pattison, A. Patterson, J. Lees, J. Benedikt, P. J. Tasker, *"A Novel measurement based method enabling rapid extraction of a RF waveform look-up table based behavioral model"* Microwave Symposium Digest IEEE MTT-S International, Page(s) 1453-1456, 15-20 June 2008

[6] Tasker. P.J *"Practical Waveform Engineering"*, Microwave Magazine, IEEE Volume 10, Issue 7, pp 65-67, December 2009

An Intelligence Driven Active Loadpull System

R. S. Saini, S. Woodington, J. Lees, J. Benedikt and P. J. Tasker

School of Engineering, Cardiff University, Cardiff, UK, CF24 3TF
Tel +44 2920 876347 email: SainiR4@Cardiff.ac.uk

***Abstract* — This paper describes how the application of the PHD model can add intelligence to an open loop active loadpull system. This intelligence driven approach by providing for an improved prediction of the operating conditions required to emulate a specified load speeds up the load emulation convergence process by minimizing the number of iterations to predict the injected signal, therefore making more efficient use of a measurement system.**

The results were validated by carrying out loadpull measurements on the fundamental tone of a 10x75um GaAs HEMT, operating at 3 GHz.

***Index Terms* — active loadpull, X-parameters, device non-linear models.**

I. Introduction

Load and Source-pull measurements are widely used in the design of power amplifiers to deduce optimum efficiency, gain, linearity and power, providing a clear understanding of the various modes of amplifier operation. This paper is based around measurements carried out using the Open Loop Active Loadpull system, developed in Cardiff University and described in [1] and [2], with phase coherent Signal Generators. The architecture of the single-tone (continuous wave) setup is illustrated in Fig 1 and is based on the Tektronix DSA 8200 four-channel oscilloscope as a receiver [3].

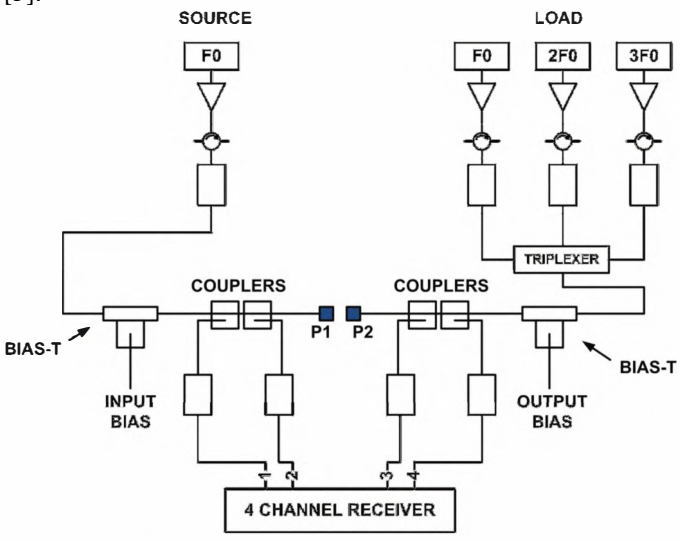

Fig 1 Schematic of measurement system

Such a setup reduces losses faced by most passive tuning systems by actively injecting the desired signals to realize the required reflection coefficient. The system is also less prone to RF oscillations noticed in closed loop systems [4].

Load emulation is achieved in this system by solving (1) for A_{2h}, with h indicating the harmonic index.

$$A_{2h} - \Gamma_h . B_{2,h}\left(A_{2,1}, A_{2,2}, \ldots, A_{2,h}\right) = 0 \qquad (1)$$

Therefore, if we have no prior knowledge of the function $B_{2,h}(.)$, the solution to (1) is found using a numerical technique. This process is iterative and can take up to 5-10 iterations to converge to a solution for the fundamental harmonic tone. If harmonic loadpull is required, the iterations are further increased due to a change in the fundamental tone causing distortion in higher harmonics. This problem is further compounded by the fact that the numerical techniques utilized present their own disadvantages such as multiple roots and numerical oscillations [5].

Recent advancements in device behavioral modeling have seen the introduction of the Poly Harmonic Distortion Modeling (PHD) framework [6]-[8]. As well as containing magnitude and phase relating to the spectral components of the input signal, this framework introduces harmonic cross product information. These products give us the relationships between harmonic frequencies for a given drive level and frequency and could therefore be beneficial in an Open Loop Active Loadpull measurement scenario, since a locally derived model can be used to assist in calculating the required injection signals to simultaneously perform both fundamental and harmonic loadpull emulation [9] when solving (1).

The motivation of this paper is to demonstrate how the behavioral modeling framework, based on non linear mixing terms can be used to aid prediction of the desired injection signals necessary in an Open Loop Active Harmonic Loadpull system to provide a desired load impedance.

II. Theory and Design of a Model Based Algorithm

The technique explained in [6] (see (2) with h indicating the harmonic index) provides a mathematical framework for describing the response, $B_{2,h}$ of a non-linear system as a function of the respective injection signals. Combining this with (1) thus allows for the formulation of a new open loop loadpull algorithm with improved load emulation capability.

978-1-4244-6366-4/10/$26.00 ©2010 IEEE

This algorithm therefore provides us with a singular approximation to the solution of (1), which is valid in the region that it is determined.

$$B_{2h} = S_{21}(|A_{11}|)|A_{11}| + \sum_h S_{22}(|A_{11}|)A_{2h} + \sum_h T_{22,h}(|A_{11}|)(A_{2h}^*) \quad (2)$$

This formulation can be modified as illustrated in [8] by describing P and Q as input and output a-wave harmonic phase operators, as shown in (3)-(4). This expression, a third order model, can be generalized to give the formulation shown in (5)-(6).

$$B_{2h} = S_{21}.|A_{11}|.\left(\frac{Q}{P}\right)^0.P + \sum_h S_{22}.|A_{2h}|.\left(\frac{Q}{P}\right)^1.P + \sum_h T_{22}.|A_{2h}|.\left(\frac{Q}{P}\right)^{-1}.P \quad (3)$$

$$P = A_{11}/|A_{11}| \qquad Q = A_{21}/|A_{21}| \quad (4)$$

$$B_{2,h} = P\sum_{n=-1}^{n=1}\left\{R_{2,h,n}.\left(\frac{Q}{P}\right)^n\right\} \quad (5)$$

$$R_{2,h,n} = G_{h,n}(|A_{1,1}|,|A_{2,1}|,\ldots) \quad (6)$$

Adapting this generalized formulation and assuming that the magnitude of the input signal ($|A_{11}|$) during this process is held constant; we can simplify it to (7) by considering only the linear third order mixing terms. This is analogous to "X-parameter" formulation described in [7].

$$B_{2h} = \underline{G_{2,0,h}} + \underline{G_{2,1,h}.|A_{2h}|.\left(\frac{Q}{P}\right)} + \underline{G_{2,-1,h}.|A_{2h}|.\left(\frac{P}{Q}\right)} \quad (7)$$

In a measurement scenario, $G_{2,0}$ can be deduced from the output response of $|A_{11}|$ at the harmonic being load-pulled. Parameters $G_{2,1}$ and $G_{2,-1}$ are extracted by applying a perturbation signal to the incident A_{21} wave, first of all with a zero degree phase and then followed by the same signal with a 90 degree shift, keeping $|A_{11}|$ constant in both cases [6]. By utilizing the measured values of A_{2h} and B_{2h} at the center and the offset points (indicated by subscripts 0, 1 and 2), we can then calculate the G parameters using the equation set (8)-(11).

$$\Delta_1 = A_{2h,1} - A_{2h,0} \qquad \Delta_2 = A_{2h,2} - A_{2h,0} \quad (8)$$

$$G_{2,1,h} = \frac{(\Delta_2^*)(B_{2h,1} - B_{2h,0}) - (\Delta_1^*)(B_{2h,2} - B_{2h,0})}{(\Delta_1)(\Delta_2^*) - (\Delta_1^*)(\Delta_2)} \quad (9)$$

$$G_{2,-1} = \frac{B_{2h,1} - B_{2h,0} - G_{2,1,h}(\Delta_1)}{(\Delta_1^*)} \quad (10)$$

$$G_{2,0,h} = B_{2h,0} - G_{2,1,h}(A_{2h,0}) - G_{2,-1,h}(A_{2h,0}^*) \quad (11)$$

If we consider Γ_h as the target reflection coefficient in (1), the computed value of A_{2h}; the desired injection signal to achieve the desired load emulation can now be analytically computed. If the resulting load accuracy is not sufficient, the process can be repeated.

III. Implementation of the Algorithm

In order to implement the algorithm for the measurement system described in the introduction, we have to include the following practical considerations.

Firstly, the predicted signal computed using (1) does not take into account the non-ideal behaviors of the Open Loop loadpull realization. This is best described by the error model shown in Fig. 2; whereby $T_{s,h}$ accounts for the insertion gain/loss of the loadpull amplifiers and couplers, etc., while $\Gamma_{L,h}$ accounts for the load match of the measurement system, both of which can be dependent on $A_{2set,h}$. It is therefore imperative to re-adjust the calculated signal ($A_{2,h}$) to the compensated value ($A_{2set,h}$) to account for the physical state of the system. To achieve this, the characterized system impedance at the harmonic being load-pulled ($\Gamma_{L,h}$) and amplifier gain ($T_{s,h}$) is incorporated into (1), as shown in Fig. 2 and (12).

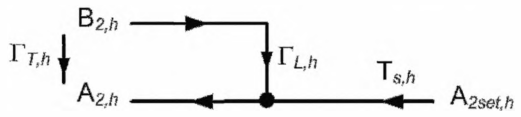

Fig 2 Flow graph showing the losses in the system and amplifier gain

$$A_{2set,h} = \frac{B_{2,h}(\Gamma_{T,h} - \Gamma_{L,h})}{T_{s,h}} \quad (12)$$

As two distinct measurements are required to compute the local model, an optimization is necessary to maximize the use of an existing set of G parameters, provided the input drive ($|A_{11}|$) or biasing conditions have remained unchanged. If the new load position is found to be within the acceptable tolerance of the target load, the existing model would have converged without requiring an update; this is beneficial during load pull of an impedance grid. The efficiency of this

algorithm can therefore be calculated by comparing the number of useful to redundant measurements.

Finally, as described in the introduction, any adjustments in the fundamental injection signal (A_{21}) distorts higher harmonic components, thereby requiring additional iterations, if they were of interest. This effect can be compensated-for by utilizing harmonic cross-product information from the local model generated by the fundamental tone. For example, during loadpull of the fundamental, the second harmonic may be required to stay at constant impedance.

In this case, the measured output response of the second harmonic (B_{22}) can be used to calculate the adjustments required in the injection signal (A_{22}) to achieve a constant impedance using the process described above and the equation set (8)-(11).

The flow chart in Fig. 3 summarizes the implementation of the algorithm, including the optimization and adjustment steps.

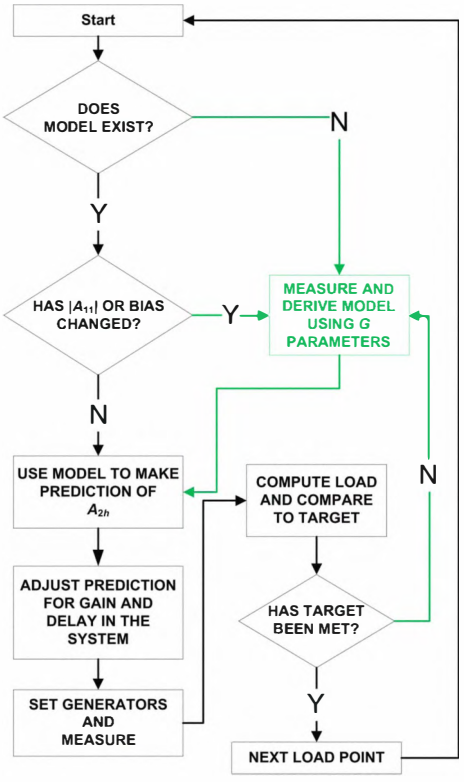

Fig 3 Flow chart of the implementation

IV. Testing and Validation

In order to illustrate how the target load is attained, a single target was considered. This was followed by carrying out measurements to attain multiple targets using two types of grid. The measurements were carried out on a 10x75µm GaAs HEMT, operating at 3 GHz with Class-B biasing conditions. Figure 4 illustrates the path taken by the algorithm to achieve the target impedance.

At the starting point (-0.2 + 0i), two perturbations are made to the $A_{2,\,1}$ injection signal; thereby creating the two offset points (indicated by green square-shaped markers) which allow the calculation of a local model. The local model is then used to compute a value of $A_{2set,\,h}$ which moves the load to a new position (-0.08+0.65i), which in this case is not within the tolerance range (set at 5%) of the algorithm. The algorithm therefore requires the model to update itself at this stage, hence the additional set of offset points. The position of the load now obtained (-0.003+0.61i) is within 1% of the target (0+0.6i); implying the algorithm has now converged to a solution.

Fig. 5 shows the convergence results on a 5x5 square grid of target impedances. In Fig. 6, a 25 point impedance-shaped grid is utilized. In both cases, the points at which the algorithm required the model to be updated are highlighted.

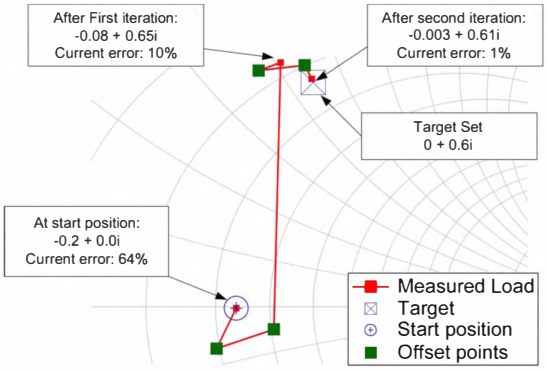

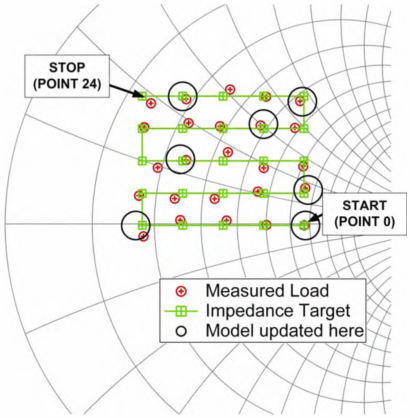

Fig 7-8 show the cumulative number of measurements required in the convergence of each load point in both cases and percentage error between the target and attained values of load. In both cases, the points at which the algorithm required the model to be updated are highlighted.

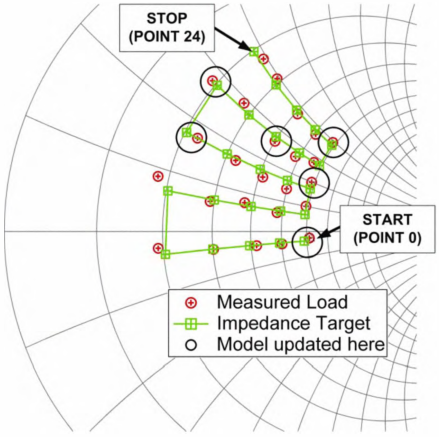

Fig 6 25 point impedance-shaped grid of targets

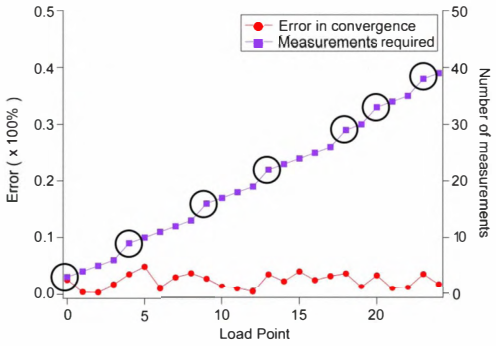

Fig 7 Cumulative measurements and convergence error from the square grid

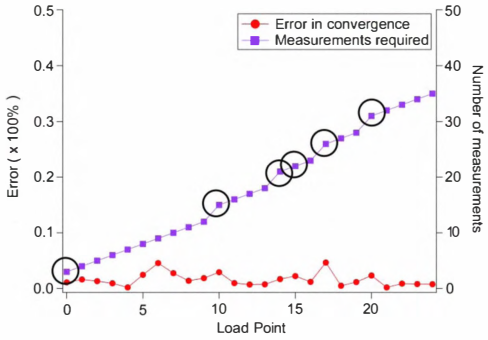

Fig 8 Cumulative measurements and convergence error from the impedance-shaped grid

The performance of the algorithm can be quantified in terms of its efficient use of the measurement system. An ideal system 100% efficient would require only one measurement per load point. The efficiency of the algorithm to converge to a solution is 44% for the square-shaped grid (averaging 2.26 measurements per point) and 62% for the impedance-shaped grid (averaging 1.56 measurements per point), compared to a typical value previously of only 5% to 10%. The average error in convergence for both grids is less than 3% of the target value required.

VII. Conclusion

The PHD model has shown to be capable of adding intelligence to an open loop active loadpull system. This approach enabled a significant improvement in the system's ability to provide the desired load emulation. The algorithm was also optimized to maximize use of locally generated parameters. Hence the measurement system utilization efficiency for realization of the desired load conditions, with less than 3% error in the achieved load-impedances on a multi-point load grid was significantly improved since PHD model generation was not necessary for each load point.

Acknowledgement

The authors would like to acknowledge the support provided by Agilent Technologies, Mimix Broadband and the EMRS DTC.

References

[1] D.J. Williams, P.J. Tasker, "An Automated Active Source and Load Pull Measurement System", *Proceedings of 6th IEEE High Frequency Postgraduate Colloquium, Cardiff, UK*, pp. 7-12, September 9th-10th 2001.

[2] Tasker, P.J, "Practical Waveform Engineering", *Microwave Magazine, IEEE, Volume 10, Issue 7*, pp 65-76, December 2009

[3] D. Williams, P. Hale, K. A. Remley, "The sampling oscilloscope as a microwave instrument," *IEEE Microwave Mag., vol. 8, no. 4*, pp.59–68, Aug. 2007

[4] T. Williams, J. Benedikt and P. J. Tasker, "Experimental Evaluation of an Active Envelope Load-Pull Architecture for High Speed Device Characterization", *IEEE MTT-S International Microwave Symposium 2005*

[5] Chapra, Steven C., "Numerical methods for Engineers", pp 73-75, 5-ed, 2002

[6] Jan Verspecht, David E. Root, "Poly-harmonic Distortion Modeling", *IEEE microwave magazine 1527-3342/06,* June 2006

[7] Jason Horn, Daniel Gunyan, Loren Betts, Chad Gillease, Jan Verspect, David E. Root, "Measurement-Based Large-Signal Simulation of Active Components from Automated Nonlinear Vector Network Analyzer Data via X-Parameters", *COMCAS 2008,*13-14 May 2008 Page(s):1 - 6, IEEE

[8] S. Woodington, T. Williams, H. Qi and P.J. Tasker, "A novel measurement based method enabling rapid extraction of a RF Waveform Look-Up table based behavioral model", *Microwave Symposium Digest, 2008 IEEE MTT-S 2008,* June 2008 Page(s): 1453 – 145

[9] J. Horn, S. Woodington, R. Saini, J. Benedikt, P.J. Tasker, D.E. Root, "Harmonic Load Tuning Predictions from X-parameters", *Fall 2009 IEEE Power Amplifier Symposium*, September 2008.